Physicochemical and biological characterisation of novel immunomodulators

Madlen Hubert

A thesis submitted to the University of Otago in fulfilment of the requirements for the degree of Doctor of Philosophy in the School of Pharmacy

Dunedin, New Zealand

October 2012



Abstract

Native phosphatidylinositol mannosides (PIMs) isolated from the cell wall of mycobacteria, and synthetic analogues, have been reported to have the ability to both suppress and stimulate the immune system. These immunomodulating properties have resulted in PIMs being utilised for the treatment of atopic diseases and as adjuvants to improve the efficacy of vaccines. While numerous studies have examined the biological activity of these molecules, little data is available on the behaviour of these compounds at a molecular level. The aim of this thesis was to assess the physicochemical properties of a series of synthetic PIM analogues and to attempt to correlate these characteristics with immunological activity.

To accomplish this, the flexibility and lipophilicity of synthetic PIM_2 was varied by changing the polar head group (inositol versus glycerol) and the length of the fatty acid residues (C0, C10, C16 and C18). A series of six phosphatidylinositol dimannoside (PIM_2) and phosphatidylglycerol dimannoside (PGM_2) compounds was synthesised and characterised. Examination of their behaviour at an air/water interface using a Langmuir trough technique, showed that surface pressure-area (π-A) isotherms were significantly influenced by the length of lipid acyl chains and by the nature of the head group. Stronger hydrophobic attractive forces between the longer fatty acid chains enabled a closer packing in the pure monolayers. Furthermore, the more flexible glycerol head group led to more tightly arranged molecules at the air/water interface. In aqueous solution acylated PIM_2 and PGM_2 were observed to self-assemble into spherical aggregates, as confirmed by dynamic light scattering (DLS) and transmission electron microscopy (TEM). The length of the fatty acid chains affected the size of the formed aggregates. In a mouse model of allergic asthma all compounds showed modest immunosuppressive

activity. Replacement of the inositol core with the three carbon glycerol unit maintained biological activity. The deacylated PGM_2, which did not show self-organisation, had no effect on the eosinophil numbers but did impact on the expansion of OVA-specific $CD4^+$ T cells. In order to investigate adjuvant activities, the phosphoglycolipids were incorporated into liposome-based delivery systems prepared using phosphatidylcholine (PC). To obtain insight into bilayer interactions and incorporation of the phosphoglycolipids into PC bilayers, binary Langmuir monolayers were investigated. In mixed films the phosphoglycolipids were found to be miscible with PC based on evaluation of collapse pressures and deviations of experimental molecular areas from calculated ideal values. ConA agglutination assays confirmed the surface display of the mannosyl residues. However, using murine bone marrow-derived dendritic cells (BMDC), no significant adjuvant activity or effect on vaccine uptake was detected *in vitro*. Investigations of the immunostimulatory activities *in vivo* revealed that modified liposomes were unable to elicit an improved antigen-specific humoral or cellular immune response, as compared to unmodified PC liposomes. The fact that inclusion of mannosylated phosphoglycolipids into liposomal bilayers did not enhance immune responses may reflect the complexity of mannose recognition and signalling. The findings may indicate that the conformation of the mannose moieties when presented in the prepared liposomes was not optimal for receptor binding.

In conclusion, physicochemical properties of the investigated compounds were determined and data gained may help to elucidate the requirements for receptor interactions of synthetic PIM_2 and PGM_2. With regards to biological effects, the impact of structural variations was less pronounced. Varied lipophilicity did not necessarily correlate with immunological activities and no conclusive structure-function relationship could be established.

to my parents

Acknowledgement

It all started in 2008 when I first came to New Zealand as part my training to become a pharmacist. The experience of doing a project at Otago University gave me a first glimpse of research and I was highly inspired. However, I realised that doing a PhD was a whole different story. Undertaking this PhD has been a truly life-changing experience for me and it would not have been possible to do without the support and guidance that I received from many people.

Foremost, I am extremely grateful to my supervisors Professor Sarah Hook and Professor Thomas Rades for their continuous support, patience and invaluable advices over the last three years. I always appreciated the super-fast corrections of chapters and manuscripts which had to be read over again. Thank you for always enlightening data etc. when I did not to see the wood for the trees. I am astonished on how much I learned and experienced.

I have been very fortunate to work with Associate Professor David Larsen. I still remember the day when he showed me around the lab and we went straight to perform our (rather my) first column chromatography - my head was spinning!! The joy and enthusiasm he has for his research was contagious and motivational for me. And I could eventually be convinced that organic chemistry is fun! I had an unforgettable time working in his lab and I really appreciate his immense knowledge and patience.

My thanks also goes to Katie Young for all her help during the animal experiments and for her willingness to answer all my questions about antibiotics and FACSing. I am also very grateful to my fellow PhD students Mo and Silke for helping me out and making long hours during cull days more

bearable. Special thanks to Silke for our great discussions, the “open ear” and your constant friendly support. Thanks for putting up with me especially in the last six months.

I would like to acknowledge the support received through the collaborative work undertaken with the Carbohydrate Chemistry Team from Industrial Research Limited, Lower Hutt. Thanks is also owed to the Foundation for Research, Science and Technology for the financial support. I am grateful to the administrative and technician staff in the School of Pharmacy and the Department of Chemistry for their support and help. Furthermore, the technical assistance from Richard Easingwood at the Otago Centre for Electron Microscopy is also gratefully acknowledged.

I have been lucky to come across many very good friends, without whom life would be bleak. John proofread this thesis and I thank him for his careful attention and for filling many gaps with commas! I wouldn’t have seen the light at the end of the tunnel without my sport buddies Sara, Karen, Mathias and Amanda. Getting chased up Ross Creek or hill reps up Mt. Cargill kept me sane, I’m sure! Big thanks to Juan, with whom I enjoyed talking about everything but work, and anyone who jumped straight in when there was need for an emergency coffee break deserves many thanks! I also wish to thank everyone for some very enjoyable festivities and for your skill in spreading happiness on those scientifically dark days. All my friends back home, particularly Ulrike, Gumpi, Tilmann, Vicky, Claudia, Chrissi and Britta, deserve massive thanks for not giving up on me as someone who responds to emails with a huge delay.

And most of all Moodie, who has been on my side throughout this PhD, living and sometimes suffering every single minute of it. It has been tough from time

to time, with both of us working hard, but we managed to always put a smile onto each other's face. Thank you so much for your immense support - you are amazing!

Abschliessend, möchte ich mich ganz herzlich bei meinen Eltern fuer die Liebe und Unterstützung bedanken, die Ihr mir gegeben habt. Ich weiss, dass es fuer Euch nicht einfach war, dass es mich bis an das andere Ende der Welt gezogen hat. Danke, dass Ihr immer an mich geglaubt habt!

Madlen

Publications arising from this thesis

Refereed journal articles

Hubert M. , Larsen D. S. , Hayman C. M., Painter G. F., Rades T. and Hook S. Physicochemical and biological characterisation of synthetic phosphatidyl-inositol mannosides and analogues. *Manuscript submitted to Molecular Pharmaceutics*

Hubert M. , Larsen D. S. , Hayman C. M., Painter G. F., Rades T. and Hook S. Physical characterisation of PIM_2 and PGM_2 molecules in binary systems with PC and immunostimulatory evaluations. *Manuscript in preparation for Journal of Pharmaceutical Sciences*

Conference contributions

Oral presentations

Hubert M., Hook S., Larsen D. S., Hayman C. M., Painter G. F., Rendle P. and Rades T. Synthesis and Physical Characterisation of PIM mimetics as Novel Immunomodulating Agents. *Australasian Pharmaceutical Science Association (APSA)*, Brisbane, Australia, December 2010.

Hubert M., Hook S., Larsen D. S., Hayman C. M., Painter G. F., Rendle P. and Rades T. Monolayer Study of PIM mimetics - Novel Immunomodulating Agents. *Formulation and Delivery of Bioactives (FDB) Conference*, Dunedin, New Zealand, February 2011.

Hubert M., Rades T., Larsen D. S., Hayman C. M., Compton B. J. and Hook S. Physicochemical and Biological Characterisation of PIM mimetics - Novel Immune Modulating Agents. *New Zealand Australasian Society for Immunology (NZASI)*, Dunedin, New Zealand, June 2012.

Poster presentations

Hubert M., Hook S., Rades T., Hayman C. M., Painter G. F., Rendle P. and Larsen D. S. Formulation and immunological characterisation of novel carbohydrate containing immuno-pharmaceuticals. *Formulation and Delivery of Bioactives (FDB) Conference*, Dunedin, New Zealand, February 2010.

Hubert M., Hook S., Larsen D. S., Hayman C. M., Painter G. F., Rendle P. and Rades T. Investigating the interfacial behaviour of novel PIM mimetics in pure and mixed monolayers using the Langmuir-trough technique. *American Association of Pharmaceutical Scientists (AAPS) Annual Meeting and Exposition*, Washington, DC, USA, October 2011.

Hubert M., Hook S., Larsen D. S., Hayman C. M., Painter G. F., Rendle P. and Rades T. Investigating the interfacial behaviour of novel PIM mimetics in pure and mixed monolayers using the Langmuir-trough technique. *Formulation and Delivery of Bioactives (FDB) Conference*, Dunedin, New Zealand, February 2012.

Hubert M., Rades T., Larsen D. S., Hayman C. M., Compton B. J. and Hook S. Physicochemical and Biological Characterisation of PIM mimetics - Novel Immune Modulating Agents. 8th World Meeting on Pharmaceutics, Biopharmaceutics and Pharmaceutical Technology (PBP), Istanbul, Turkey, March 2012.

Table of content

Abstract ii

Acknowledgement v

Publications arising from this thesis viii

Table of content x

List of tables xv

List of figures xvii

List of schemes xxiv

List of abbreviations xxv

1 General Introduction 2

1.1 Mycobacterium 2

1.1.1 Immunology of mycobacterial infection 3

1.1.2 Subversion of immune response 6

1.1.3 Mycobacterial cell wall 8

1.1.4 Role of cell wall components in modulation of immune responses 11

1.2 Phosphatidylinositol mannosides 13

1.2.1 Structure of PIMs 13

1.2.2 Immunomodulatory properties 16

1.3 Atopy and allergic responses 19

1.3.1 Strategies for treatment of allergic diseases 20

1.3.1.1 Allergen-specific immunotherapy 21

1.3.1.2 Cytokine-based immunotherapy 22

1.3.1.3 DNA vaccines 22

1.3.1.4 Bacterial extracts 23

1.4 Vaccines 24

1.4.1 Types of vaccines 24

1.4.2 Developments in tuberculosis vaccines 26

1.5 Adjuvants 27

1.5.1 Licensed adjuvants 30

1.5.1.1 Mineral salts 30

1.5.1.2 Emulsions 31

1.5.1.3 MPL 32

1.5.1.4 Liposomes 34
1.5.2 Adjuvants in clinical development 39
1.5.3 Emerging adjuvants 41
1.6 Thesis aim 43
2 Synthesis of a PIM_2 analogue 46
2.1 Introduction 46
2.2 Chapter aim 51
2.3 Experimental section 51
2.3.1 General experimental 51
2.3.1.1 Nuclear magnetic resonance spectroscopy 51
2.3.1.2 Mass spectrometry 52
2.3.1.3 Chromatography 52
2.3.1.4 Infrared spectroscopy 53
2.3.1.5 Solvents 53
2.3.1.6 Polarimetry 53
2.3.2 Experimental protocol 54
2.4 Synthetic strategy 68
2.4.1 Preparation of alcohol 21 69
2.4.2 Preparation of phosphoramidite 28 77
2.4.3 Preparation of target PGM_2 analogue 2c 81
3 Investigation of physicochemical properties and immunosuppressive activity of PIM_2 and PGM_2 compounds 87
3.1 Introduction 87
3.1.1 Langmuir monolayers 87
3.1.1.1 Langmuir trough technique 89
3.1.1.2 Surface pressure-area (π-A) isotherm 91
3.1.2 Amphiphilic compounds and self-assembly in aqueous media 95
3.1.3 PIMs as immunosuppressive agents 97
3.2 Chapter aims 100
3.3 Experimental section 101
3.3.1 Materials 101
3.3.2 Physicochemical characterisation 102
3.3.2.1 Langmuir trough technique and monolayer conditions 102
3.3.2.2 Analysis of surface pressure-area isotherm 103

3.3.2.3 Size and zeta potential measurements 103
3.3.2.4 Transmission electron microscopy 103
3.3.3 Investigation of inhibitory activity (*in vivo*) 104
3.3.3.1 Experimental mice 104
3.3.3.2 Testing of transgenic mice 104
3.3.3.3 Adoptive T cell transfer 105
3.3.3.4 *In vivo* airway inflammation model 106
3.3.3.4.1 Immunisation and airway challenge with ovalbumin 106
3.3.3.4.2 Treatment with PIM_2 and PGM_2 compounds 106
3.3.3.5 Bronchoalveolar lavage 106
3.3.3.6 Harvesting cells from treated mice 107
3.3.3.7 *In vitro* T cell restimulation 107
3.3.3.8 Cytokine production 108
3.3.3.9 Cell staining and flow cytometry analysis 109
3.3.4 Statistical analysis 110

3.4 Results 110

3.4.1 Optimisation of the Langmuir trough technique using a model phospholipid 110
3.4.2 Behaviour of PIM_2 and PGM_2 lipids at the air/water interface 112
3.4.2.1 Effect of acyl chain length on monolayer formation 112
3.4.2.2 Effect of polar head group on monolayer formation 117
3.4.3 Self-aggregation in aqueous solution 118
3.4.4 Suppression of airway eosinophilia 122
3.4.5 Expansion of transgenic $CD4^+$ and $CD8^+$ T cells 125
3.4.6 T cell proliferation after *in vitro* restimulation with OVA 128
3.4.7 OVA-specific production of cytokines 129

3.5 Discussion 131

4 Physical characterisation of PIM_2/PGM_2 and PC in binary systems and immunostimulatory investigations 138

4.1 Introduction 138

4.1.1 Mixed monolayers 139
4.1.2 Mixed monolayers and their relationship to lipid bilayers 142
4.1.3 Liposomes as vaccine delivery systems 144
4.1.4 Thermotropic behaviour of lipid bilayer 146
4.1.5 PIMs as immunostimulatory agents 147

4.2 Chapter aims 150

4.3 Experimental section 151

4.3.1 Materials 151

4.3.1.1 Preparation of fluorescently-labelled ovalbumin 152

4.3.2 Langmuir trough technique and mixed monolayer conditions 152

4.3.2.1 Analysis of π-A isotherm for binary systems 153

4.3.2.2 Ideal areas of binary systems 153

4.3.3 Determination of phase transition temperature 154

4.3.4 Preparation of liposomes by the thin film method 154

4.3.5 Physicochemical characterisation of liposomes 155

4.3.5.1 Vesicle size and zeta potential measurements 155

4.3.5.2 Lectin binding assay 156

4.3.5.3 Determination of FITC-OVA entrapment efficiency 156

4.3.5.4 Liposome stability 157

4.3.6 Experimental mice 157

4.3.7 Testing of transgenic mice 157

4.3.8 *In vitro* immunological methods 157

4.3.8.1 Preparation of murine bone marrow-derived dendritic cells 157

4.3.8.2 Dendritic cell activation 158

4.3.9 *In vivo* vaccine model 159

4.3.9.1 Preparation of liposome formulations for immunological investigations 159

4.3.9.2 Adoptive T cell transfer 159

4.3.9.3 Immunisation protocol 160

4.3.9.4 Harvesting cells from vaccinated mice 160

4.3.9.5 *In vitro* T cell restimulation 161

4.3.9.6 Cytokine production 161

4.3.9.7 OVA IgG enzyme-linked immunosorbent assay 161

4.3.10 Cell staining and flow cytometry analysis 162

4.3.11 Statistical analysis 163

4.4 Results 163

4.4.1 Interfacial behaviour in mixed monolayers 163

4.4.2 Thermal phase behaviour of PIM_2 and PGM_2 lipids 170

4.4.3 Characterisation of liposome formulations 171

4.4.3.1 Vesicle size and zeta potential 171

4.4.3.2 ConA agglutination assay 173

4.4.3.3 Entrapment of FITC-OVA and membrane stability 174
4.4.4 *In vitro* liposome immunogenicity- Formulation uptake and DC activation 176
4.4.5 *In vivo* vaccine model 179
4.4.5.1 Expansion of transgenic $CD4^+$ and $CD8^+$ T cells 179
4.4.5.2 T cell proliferation after *in vitro* restimulation with OVA 182
4.4.5.3 OVA-specific production of cytokines 184
4.4.5.4 Production of OVA-specific antibody 185
4.5 Discussion 186
5 General discussion and future directions 202
6 References 214
7 Appendices 239
7.1 Appendix A 239
7.2 Appendix B 243
7.3 Appendix C 249

List of tables

Table 1-1. Outline of various adjuvant systems including their corresponding mode of action and the type of immune response activated. For more details see text below. Table modified from Mbow *et al.*[156], O'Hagan and De Gregorio[140], Pulendran and Ahmed[150], and Reed *et al.*[158].....**29**

Table 3-1. Limiting area per molecule A_0 (Å^2) and collapse pressure π_{coll} (mN m^{-1}) of DSPG monolayers at the air/liquid interface at 25°C.....**112**

Table 3-2. Limiting area per molecule A_0 (Å^2), collapse pressure π_{coll} (mN m^{-1}) and maximum elastic compressibility modulus $C_s^{-1}{}_{max}$ (mN m^{-1}) at the corresponding surface pressure π_{comp} (mN m^{-1}) of pure monolayers of PIM_2 and PGM_2 at 24°C (mean ± SD, n=3). **113**

Table 3-3. Zeta potential measurements (ZP in mV) of PIM_2 and PGM_2 compounds in PBS at a concentration of 0.4 mg mL^{-1}. Measurements were carried out at 25°C (mean ± SD, n=3). **121**

Table 4-1. Various liposome formulations used for the vaccination of mice and the amount of FITC-OVA (μg) delivered in a total volume of 200 μL on day 0 and 14. Data is shown as mean ± SD for three independent vaccine studies. **160**

Table 4-2. Monolayer characteristics of PC and PIM_2 lipids mixed at various ratios (mol%): Experimental average area per molecule (A_{exp}, Å^2), ideal average area per molecule (A_{ideal}, Å^2), deviation from ideality (Dev, %) and collapse pressure (π_{coll}, mN m^{-1}). Results are displayed as mean ± SD of three independent measurements, * denotes $p \leq 0.05$ relative to PC.....**166**

Table 4-3. Monolayer characteristics of PC and PGM_2 lipids mixed at various ratios (mol%): Experimental average area per molecule (A_{exp}, Å^2), ideal average area per molecule (A_{ideal}, Å^2), deviation from ideality (Dev, %) and collapse pressure (π_{coll}, mN m^{-1}). Results are displayed as mean ± SD of three measurements, * denotes $p \leq 0.05$, ** $p \leq 0.01$ and *** describes $p \leq 0.001$ relative to PC. **169**

Table 4-4. Phase transition temperatures (T_ms) of various lipids, T_ms as onset temperatures (mean ± SD, n=3). **171**

Table 4-5. Physical characterisation of liposome formulations. Average particle size shown as z-average (d.nm), polydispersity index (PDI) and zeta potential (mV) of PC liposomes ± 2% (w/w) of different incorporated

phosphoglycolipids. Results are displayed as mean ± SD of three independent formulations. **172**

Table 4-6. Entrapment of fluorescently-labelled OVA in liposome formulations. Amount of protein incorporated (mg mL^{-1}) on day 0 and after 21 days following storage at 4°C in PBS (pH 7.5). Results are shown for PC liposomes ± 2% of different phosphoglycolipids incorporated. Values represent mean ± SD of three independent formulations. **175**

List of figures

Figure 1-1. Illustration of *M. tuberculosis* infection and key features of the host immune response. Following inhalation of aerosols containing *M. tuberculosis* by the host, pathogens generally settle within the lung. Local macrophages and dendritic cells (APCs) phagocytose the pathogens and trigger a pro-inflammatory response including cytokine production and recruitment of cells of the innate immune system. APCs migrate to the draining lymph nodes and stimulate $CD8^+$ and $CD4^+$ cells, via major histocompatibility complex (MHC) class I and II receptors, respectively. These activated T cells attract further cells, which eventually results in the formation of a granuloma containing various immune cells such as monocytes, lymphocytes and foamy macrophages. Figure was adopted from Harding *et al.*[22]. **4**

Figure 1-2. Schematic presentation of the mycobacterial cell wall. The characteristic lipoglycan lipomannans (LMs) and lipoarabinomannans (LAMs) are dispersed throughout the lower and upper layer of the cell wall structure. Phosphatidylinositol mannosides (PIMs) represent anchor motifs for attachment to the plasma membrane. Adopted from Park and Bendelac[25]..... **9**

Figure 1-3. Schematic illustration of the glycolipids found in the mycobacterial cell envelope. Figure was modified from Jozefowski *et al.*[57]. **10**

Figure 1-4. General structure of phosphatidylinositol mannosides (PIMs). PIMs can have two acyl residues (R) at the phosphatidyl moiety which in nature are palmitatoyl, tuberculostearoyl or stearoyl residues. The structure can be further acylated, indicated as R', at the mannosyl group attached to the C-2 position of the inositol ring (Ac_1PIMs) and at the C-3 position of inositol (Ac_2PIMs) (R' = R or H). **14**

Figure 1-5. Common acyl residues identified in extracts from various mycobacterial strains. **15**

Figure 1-6. Pathogenesis of allergic immune responses. A crucial feature of allergic reactions is the polarisation of the immune response towards the Th2–type, as indicated by the red triangle. Subsequently, Th2-associated cytokines are released which recruit eosinophils into the airways. This cascade results in the typical allergic reaction and airway inflammation. Figure was modified from Wills-Karp *et al.*[112]..... **19**

Figure 1-7. Chemical structure of *Salmonella minnesota* MPL..... **33**

Figure 1-8. Liposomes and their versatile structures. Details are described in the text below. Figure was adapted from Henriksen-Lacey *et al.*[190].....**35**
Figure 2-1. Series of PIM compounds investigated in this thesis: structures of phosphatidylinositol dimannoside (PIM_2) **1a**, **1b** and phosphatidylglycerol dimannosides (PGM_2) **2a** - **2d**. **46**
Figure 2-2. Structure of *myo*-inositol core of PIMs. **47**
Figure 2-3. Glycerol core structure of phosphatidylglycerol mannosides (PGMs) (highlighted in red). The removal of the C-3, -4 and -5 unit from the *myo*-inositol core gave a symmetrical phosphatidylglycerol mannoside containing a three-carbon glycerol centre.....**50**
Figure 2-4. Proposed series of phosphatidylglycerol dimannosides (PGM_2) **2a** - **2d**. **50**
Figure 2-5. Mechanism of formation of the α-allyl mannoside **13**. **71**
Figure 2-6. The principle of a chemical glycosylation reaction. Figure modified from Galonic *et al.*[240]. **75**
Figure 2-7. 125 MHz ^{13}C NMR shifts of anomeric carbons and corresponding one-bond coupling constants $^1J_{C\text{-}H}$ (Hz) of key intermediate **21**. *Inset*: ^{13}C-NMR spectrum, expansion of the anomeric region showing the ^1H-decoupled spectrum (lower panel) and ^1H-coupled spectrum (upper panel).....**77**
Figure 2-8. 500 MHz ^1H NMR spectrum of phophoramidite **28**. **81**
Figure 2-9. 500 MHz ^1H NMR spectrum of PGM_2 (10:10) (**2c**). The spectrum was recorded in 2:1 $CDCl_3$:CD_3OD and solvent peaks are assigned in the spectrum. **84**
Figure 2-10. Analysis of PGM_2 (10:10) (**2c**) by HPLC, with an indicated purity of 95%. A blank was subtracted from the sample trace to give a flat baseline. 85
Figure 3-1. General structure of a phospholipid **(A)**. The glycerol residue includes two fatty acid residues (R_1 and R_2) which can vary in chain length and degree of saturation. The structure comprises a phosphate group with the common head groups (R) as shown in **(B)**. **88**
Figure 3-2. Set-up of the Langmuir trough.....**90**
Figure 3-3. Typical surface pressure-area (π-A) isotherm for a phospholipid. The monolayer undergoes various phases during compression such as gaseous (G), liquid-expanded (LE), liquid-condensed (LC) and solid (S). LE-LC denotes the phase transition from liquid-expanded to liquid-condensed. Extrapolation of the part of the isotherm with the highest

slope to zero surface pressure gives the limiting area per molecule A_0 (Å^2). The collapse pressure π_{coll} (mN m^{-1}) of the monolayer can be assigned to the highest pressure to which the film can be compressed without any abrupt changes. Figure was modified from Erbil[254].....**93**

Figure 3-4. The shape of the assemblies depends on the geometry of the molecules and can be described the packing parameter P. Figure modified from Erbil[254]. **96**

Figure 3-5. General structure of PIMs. PIMs can have two acyl residues (R) at the phosphatidyl moiety naturally occurring as palmitatoyl, tuberculostearoyl or stearoyl residues. Further acylation is indicated as R' (R' = R or H). **99**

Figure 3-6. Structure of distearoylphosphatidylglycerol (DSPG). **110**

Figure 3-7. Monolayer compression of phosphatidylinositol dimannosides (PIM_2) at the air/water interface: surface pressure-molecular area (π-A)-isotherms of PIM_2 (16:16) (**---**) and PIM_2 (18:18) (**---**), respectively. Arrows indicate: (a) collapse of PIM_2 (16:16) monolayer, (b) collapse of PIM_2 (18:18) monolayer. *Inset*: Compressibility modulus plot versus molecular area as a function of molecular area. The curves are each a representative of three independent experiments. **114**

Figure 3-8. Monolayer compression of phosphatidylglycerol dimannosides (PGM_2) at the air/water interface: surface pressure-molecular area (π-A)-isotherms of PGM_2 (10:10) (**---**), PGM_2 (16:16) (**---**) and PGM_2 (18:18) (**---**), respectively. Arrows indicate: (a) collapse of PGM_2 (16:16) monolayer, (b) collapse of PGM_2 (18:18) monolayer, (c) LE-LC phase transition of PGM_2 (18:18) monolayer. *Inset*: Compressibility modulus plot versus molecular area as a function of molecular area. The curves are each a representative of three independent experiments. **116**

Figure 3-9. Effect of head group on monolayer formation: π-A isotherms of PIM_2 (18:18) (**---**) and PGM_2 (18:18) (**---**) at the air/water interface. The curves are each a representative of three independent experiments...**117**

Figure 3-10. Transmission electron micrographs along with a representative histogram of volume-based particle size distribution of PIM_2 compounds in PBS at 0.4 mg mL^{-1}. TEM samples were prepared by negative staining with 1% PTA. **(A)** PIM_2 (16:16) (scale bar= 100 nm), **(B)** PIM_2 (18:18) (scale bar= 500 nm). **119**

Figure 3-11. Transmission electron micrographs along with a representative histogram of volume-based particle size distribution of PGM_2 compounds in PBS at 0.4 mg mL^{-1}. TEM samples were prepared by negative staining with 1% PTA. **(A)** PGM_2 (0:0) (scale bar= 500 nm) **(B)** PGM_2 (10:10) (scale bar= 100 nm), **(C)** PGM_2 (16:16) (scale bar= 500 nm), **(D)** PGM_2 (18:18) (scale bar= 500 nm). **120**

Figure 3-12. Cytospin samples for mice treated with **(A)** PGM_2 (16:16), **(B)** PBS and **(C)** dexamethasone. On day 11 of the study bronchoalveolar lavages (BALs) were performed and BAL cells spun onto slides. Following staining, the percentages of different cell types were determined microscopically. Arrows indicate different cell types: (a) eosinophils, (b) macrophages, (c) lymphocytes and (d) neutrophils... **123**

Figure 3-13. Airway eosinophilia in OVA-sensitised mice. **(A)** Percent **(B)** total number of airway eosinophils in BAL fluid. C57BL/6 mice were immunised i.p. with OVA/alum on day 0. On day 6 mice were treated i.n. with various PIM_2 and PGM_2 in 50 μL of PBS or PBS alone. Mice were challenged intranasally with OVA on day 7. Four days post-OVA challenge lungs were flushed and differential cell count performed on stained cytospins. Bars depict mean + SE from n=3 mice per group from four independent experiments. * denotes $p \leq 0.05$, ** $p \leq 0.01$, and *** describes $p \leq 0.001$ relative to PBS group. **124**

Figure 3-14. OVA-specific expansion of Vα2Vβ5 T cells. **(A)** Percent and **(B)** total number of $CD4^+$ (striped bars) and $CD8^+$ (black bars) Vα2Vβ5 T cells in the mediastinal lymph nodes. Graphs depict mean + SE from n=3 mice per group from four independent experiments, * denotes $p \leq 0.05$, ** $p \leq 0.01$, and *** describes $p \leq 0.001$ relative to PBS treatment group. **126**

Figure 3-15. OVA-specific expansion of Vα2Vβ5 T cells. **(A)** Percent and **(B)** total number of $CD4^+$ (striped bar) and $CD8^+$ (black bar) Vα2Vβ5 T cells in spleens. Spleens were pooled within each treatment group. Graphs depict mean + SE from n=3 mice per group from four independent experiments, **denotes $p \leq 0.01$ relative to PBS treatment group. **127**

Figure 3-16. Proliferation of T cells isolated from mediastinal lymph nodes (striped bars) and spleens (black bars) of each study group after in vitro restimulation with OVA and media. Results are expressed as stimulation indices (SI= OVA/media). Bars depict mean + SE from n=3 mice per group from three independent experiments. **128**

Figure 3-17. Production of **(A)** IFN-γ and **(B)** IL-13 by T-cells isolated from mediastinal lymph nodes of each study group. Titres of cytokine responses were determined after *in vitro* restimulation with OVA (black bars) or medium (white bars, negative control). Bars depict mean + SE from n=3 mice per group from four independent experiments. * denotes $p \leq 0.02$, while ** denotes $p \leq 0.002$ relative to PBS treatment group. **130**

Figure 4-1. Schematic illustration of the relationship between monolayers, bilayer structures and bilayer vesicles (liposomes). Following spreading onto water, surface active agents orientate at the air/water interface. Amphiphilic molecules such as phospholipids spontaneously associate into bilayers upon dispersion in aqueous media which bend round to form closed compartment vesicles termed liposomes. The orientation of the phospholipid molecules allows for incorporation of hydrophilic and lipophilic molecules in the aqueous core and lipid bilayer, respectively. **143**

Figure 4-2. Chemical structures of **(A)** PC whereby R can be a mixture of palmitic, stearic, oleic and linoleic acid, **(B)** C32 monomycoloyl glycerol analogue (MMG), **(C)** dimethyldioctadecylammonium bromide (DDA) and **(D)** trehalose-6,6-dibehenate (TDB). **145**

Figure 4-3. Monolayer compression at the air/water interface: π-A isotherms for mixtures of PC (**---**) with 2 (**—**), 25 (**---**), 50 (**-··**) and 100 mol% **(A)** PIM_2 (16:16) (**---**) and **(B)** PIM_2 (18:18) (**---**). **165**

Figure 4-4. Monolayer compression at the air/water interface: π-A isotherms for mixtures of PC (**---**) with 2 (**—**), 25 (**---**), 50 (**-··**) and 100 mol% **(A)** PGM_2 (10:10) (**---**), **(B)** PGM_2 (16:16) (**---**) and **(C)** PGM_2 (18:18) (**---**). **168**

Figure 4-5. DSC scans of PIM_2 and PGM_2 lipids. The measurements of the dry samples were performed at a heating rate of 10 K min^{-1}. **170**

Figure 4-6. ConA-induced agglutination of liposome formulation PC PIM_2 (16:16) (□), PC PIM_2 (18:18) (►), PC PGM_2 (0:0) (○), PC PGM_2 (10:10) (▲), PC PGM_2 (16:16) (Δ), PC PGM_2 (18:18) (◄) and PC (■). The aggregation was monitored by measuring the particle size every 5 min. Addition of the ConA solution is indicated by the arrow. Values are expressed as mean + SD (n=2). **173**

Figure 4-7. Effect of storage on average particle size (z-average) of liposome formulations PC PIM_2 (16:16) (□), PC PIM_2 (18:18) (►), PC PGM_2 (0:0) (○), PC PGM_2 (10:10) (▲), PC PGM_2 (16:16) (Δ), PC PGM_2 (18:18) (◄)

and PC (■). Liposomes were stored at 4°C in PBS (pH 7.5). Results are shown as mean + SD of three independent experiments. **176**

Figure 4-8. Uptake of FITC-OVA containing liposome formulations by BMDC in vitro. BMDC were pulsed at 37°C for 48 hours with different amounts of total lipid of PC PIM_2 (16:16) (□), PC PIM_2 (18:18) (►), PC PGM_2 (0:0) (○), PC PGM_2 (10:10) (▲), PC PGM_2 (16:16) (Δ), PC PGM_2 (18:18) (◄) and PC (■). Results are expressed as fold increase of CD11c-positive cells incubated with liposomes over CD11c-positive cells pulsed with media (background). The data is shown for one experiment. The results of two other replicates are shown in **Appendix C**. **177**

Figure 4-9. Expression of BMDC surface activation marker CD86 following in vitro incubation with various formulations at 37°C for 48 hours. **(A)** BMDC were incubated with FITC-OVA containing liposome formulations (250 μg mL^{-1} total lipid). **(B)** BMDC were pulsed with FITC-OVA containing liposome formulations (250 μg mL^{-1} total lipid) + MPL (10 ng mL^{-1}) and MPL (10 ng mL^{-1}). Results are expressed as fold increase of CD11c-positive cells incubated with various formulations over CD11c-positive cells pulsed with media (background). Data represent mean of three independent experiments + SD. **178**

Figure 4-10. OVA-specific expansion of Vα2Vβ5 T cells. **(A)** Percent and **(B)** total number of $CD4^+$ Vα2Vβ5 T cells in lymph nodes of each vaccination group. Bars depict mean + SE from n=3 mice per group from three independent experiments, * describes $p \leq 0.05$ and *** $p \leq 0.001$ relative to PC vaccination group. **180**

Figure 4-11. OVA-specific expansion of Vα2Vβ5 T cells. **(A)** Percent and **(B)** total number of $CD8^+$ Vα2Vβ5 T cells in lymph nodes. Bars depict mean + SE from n=3 mice per group from three independent experiments, * denotes $p \leq 0.05$ and *** $p \leq 0.001$ relative to PC vaccination group.....**182**

Figure 4-12. Proliferation of T cells isolated from **(A)** lymph nodes and **(B)** spleens of each study group after in vitro restimulation with OVA and media. Results are expressed as stimulation indices (SI= OVA/media). Bars depict mean + SE from n=3 mice per group from three independent experiments, * denotes $p \leq 0.05$ relative to PC group, ‡ denotes $p \leq 0.05$, ‡‡ $p \leq 0.01$ relative to alum vaccination group. **184**

Figure 4-13. Production of IFN-γ by T-cells isolated from lymph nodes of each study group. Titres of cytokine responses were determined after *in vitro*

restimulation with OVA (black bars) or medium (white bars, negative control). Bars depict mean + SE from n=3 mice per group from three independent experiments.....**185**

Figure 4-14. Production of OVA-specific IgG antibody as determined by ELISA. The circles depict results from individual mice, whereas red bars represent the mean values within a vaccination group. Data is presented for two independent experiments, with each experiment consisting of n = 3 mice per group. **186**

Figure 5-1. General structure of phosphatidylinositol mannosides (PIMs). Possible structural modifications are described in the left panels. PIMs can have two acyl residues (R) at the phosphatidyl moiety and can be further acylated, indicated as R'. Potential carbohydrates could be used to create a new PIM scaffold, e.g. α-galactose or α,α-trehalose. **210**

List of schemes

Scheme 2-1. Synthesis of *myo*-inositol derivative by Elie *et al.*[230]. For clarity only one enantiomer is presented for (±)-**3**. **48**
Scheme 2-2. Preparation of chiral *myo*-inositol derivative **9** via a method described by Pietrusiewicz *et al*.[231]. **48**
Scheme 2-3. Synthesis of an enantiomerically pure *myo*-inositol derivative by Bender *et al.*[234]. **49**
Scheme 2-4. Key intermediate **21** and synthetic approach for the preparation of target molecule PGM_2 **2c**. **68**
Scheme 2-5. Retrosynthesis of alcohol **21**. **69**
Scheme 2-6. Preparation of the allyl glycoside **13.** **70**
Scheme 2-7. Synthesis of **14**. **71**
Scheme 2-8. Synthesis of the benzylated allyl mannoside **15**. **72**
Scheme 2-9. Synthesis of the glycerol mannoside **16**. **72**
Scheme 2-10. Synthesis of the 2-*O*-benzoyl glyceryl glycoside **17**. **73**
Scheme 2-11. Synthesis of the mannosyl donor **19**. **74**
Scheme 2-12. Mannosylation of the benzoylated glycerol mannoside **20**. **75**
Scheme 2-13. Synthesis of the α,α-dimannoside **21**. **76**
Scheme 2-14. Retrosynthesis of target **2c**. **78**
Scheme 2-15. Synthesis of the glycerol diester **26**. **79**
Scheme 2-16. Synthesis of phosphoramidite **28**. **80**
Scheme 2-17. Formation of fully benzyl-protected target molecule **29**. **82**
Scheme 2-18. Final deprotection to prepare the target PGM_2 **2c** (sodium salt). **83**
Scheme 5-1. Modified approach for the preparation of the PGM_2 head group **32**. **204**

List of abbreviations

α-GalCer	α-galactosylceramide
AIDS	acquired immunodeficiency syndrome
AM	alveolar macrophages
APC	antigen presenting cell
AraLAM	uncapped LAM
BAL	bronchoalveolar lavage
BCG	**b**acillus Calmette-Guérin
BMDC	bone marrow-derived dendritic cells
CD	cluster of differentiation
cIMDM	complete Iscove's Modified Dulbecco's Medium
CFA	Complete Freund's adjuvant
CpG ODN	unmethylated sequences of DNA
ConA	concanavalin A
c.p.m.	counts per minute
CRD	carbohydrate recognition domain
CTL	cytotoxic T lymphocyte
DC	dendritic cell
DC-Chol	3β-[N-(N',N'-dimethylaminoethane)-carbomyl] cholesterol
DC-SIGN	dendritic cell-specific intercellular adhesion molecule 3-grabbing non-integrin
DDA	dimethyldioctadecylammonium
DLS	dynamic light scattering
DOPE	dioleoylphosphatidylethanolamine
DOTAP	dioleoyl-3-trimethylammonium-propane
DPPC	dipalmitoylphosphatidylcholine
DPPE	dipalmitoylphosphatidylethanolamine
DSC	differential scanning calorimetry
DSPC	distearoylphosphatidylcholine
DSPG	distearoylphosphatidylglycerol
DT	diphtheria and tetanus
ELISA	enzyme-linked immunosorbent assay
FAB-MS	fast atom bombardment-mass spectrometry
FACS	fluorescence activated cell sorting
FITC	fluorescein isothiocyanate
FITC-OVA	fluorescein isothiocyanate conjugated ovalbumin

FCS	foetal calf serum
GM-CSF	granulocyte macrophage colony stimulating factor
HAV	hepatitis A virus
HBV	hepatitis B virus
HEPES	4-(2-hydroxyethyl)-1-piperazineethanesulfonic acid
HIV	human immune deficiency virus
HPLC	high-performance liquid chromatography
HPV	human papilloma virus
IFA	Incomplete Freund's adjuvant
IFN-γ	interferon-γ
Ig	immunoglobulin
IL	interleukin
IR	infrared
LAM	lipoarabinomannan
LM	lipomannan
LPS	lipopolysaccharide
ManLAM	mannose-capped lipoarabinomannan
MFI	mean fluorescence intensity
MHC	major histocompatibility
MMG	monomycoloyl glycerol
MoDC	monocyte-derived dendritic cells
MPL	monophosphoryl lipid A
MR	mannose receptor
MS	mass spectrometry
MTP-PE	muramyl tripeptide phosphatidylethanolamine
NF-κB	nuclear factor-kappaB
NK T cell	natural killer T cell
NMR	nuclear magnetic resonance
NO	nitric oxide
ODN	oligodeoxynucleotide
OVA	ovalbumin
PAMP	pathogen associated molecular pattern
PBS	phosphate buffered saline
PC	phosphatidylcholine
PDI	polydispersity index
PGM_2	phosphatidylglycerol dimannoside
PI	phosphatidylinositol

PILAM	lipoarabinomannan with phosphoinositol caps
PIM_2	phosphatidylinositol dimannoside
PRR	pattern recognition receptor
Tb	tuberculosis
T_m	phase transition temperature
TCR	T cell receptor
TDB	trehalose-6,6-dibehenate
TDM	trehalose-6,6-dimycolate
TEM	transmission electron microscopy
Th1	T helper 1 cell
Th2	T helper 2 cell
TLR	Toll-like receptor
TNF-α	tumour necrosis factor-α
Treg	regulatory T cells
VLP	virus-like particle
WHO	World Health Organisation
ZP	zeta potential

Chapter One

General Introduction

1 General Introduction

1.1 Mycobacterium

Background

Pulmonary tuberculosis (Tb) is caused by *Mycobacterium tuberculosis* (*M. tuberculosis*) and can result in a severe respiratory disability[1]. A symptomatic infection is characterised by cough, night sweats, fever and weight loss[2]. At present, Tb is one of the most common infectious diseases worldwide with about 9 million new infections and 1.4 million deaths annually[3]. Reports concerning tuberculosis infections have been traced back to as far as 2400 BC, the time of the Egyptians[4]. In the late 19th century, the bacterium was identified by Robert Koch, a German scientist who was also the first to visualise the bacteria following the development of a staining technique[4]. Following this milestone, Calmette and Guérin developed the first tuberculosis vaccine (Bacillus Calmette-Guérin (BCG) vaccine) from an attenuated strain of *M. bovis* which was first tested in humans in 1921[5]. *M. bovis* is the causative agent of bovine tuberculosis in cattle[6]. The availability of a vaccine was a major breakthrough in the fight against tuberculosis and made the disease controllable worldwide. However, the vaccine has been shown to have a low efficacy in certain populations[7,8] and development of drug-resistant mycobacterial strains[9] has been reported. Moreover, due to problems such as poverty and crowded conditions in developing countries and also an increasing incidence of HIV positive co-infections[10-12], the threat of the disease has reappeared. In 2005, the World Health Organisation (WHO) classified tuberculosis an emergency in Africa[13]. Unfortunately, despite many continuing studies, the pathogenesis of tuberculosis is not yet fully understood. An understanding of the complex interactions between pathogen and host during

infection is crucial for developing new vaccines. Current research focusses on novel vaccine formulations comprising mycobacterial proteins and peptides, recombinant BCG strains and DNA[14-16]; this is discussed further in **Section 1.4.2**.

Mycobacterial species

Different species of mycobacteria such as *M. bovis* and *M. africanum* can cause tuberculosis. However, most human infections are caused by *M. tuberculosis*. While Tb is controlled in industrialised countries, it is a health hazard in developing countries such as Africa, particularly due to the transmission from animal to human, with potential infections deriving from consumption of unpasteurised milk and close physical contact between humans and infected animals[6]. Other pathogenic species include *M. avium*, *M. leprae* (causative agent of leprosy) and *M. kansasii*. A particularly virulent strain of *M. tuberculosis*, the Beijing/W strain, has been associated with large outbreaks of multidrug resistant extra-pulmonary tuberculosis[17]. Strains frequently used to investigate immunological responses to mycobacterial infections in various models (animal models and cell cultures) are *M. bovis* BCG, *M. tuberculosis*[18] and *M. tuberculosis* H37Rv[19-21]. *M. marinum* is used as a model pathogen for studies in zebrafish embryos or in the amoeba *Dictyostelium*[18].

1.1.1 Immunology of mycobacterial infection

Innate and adaptive immune response

Tuberculosis is transmitted via inhalation of droplets containing the bacteria. Due to its high pathogenicity, a mycobacterial infection can result after exposure to low levels of the pathogen. Bacteria reside in the pulmonary tract

and encounter local antigen-presenting cells (APCs), such as alveolar macrophages (AMs) and dendritic cells (DCs) (**Figure 1-1**). As part of the innate immune defence, their function is to eradicate pathogens. APCs express cell surface receptors (pathogen recognition receptors, PRRs) which enable them to identify specific structures within the mycobacterial cell envelope.

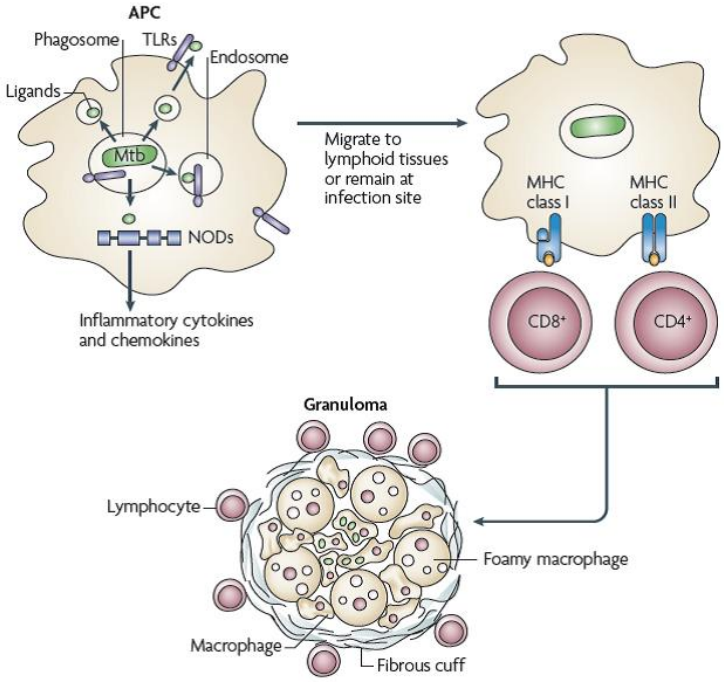


Figure 1-1. Illustration of *M. tuberculosis* infection and key features of the host immune response. Following inhalation of aerosols containing *M. tuberculosis* by the host, pathogens generally settle within the lung. Local macrophages and dendritic cells (APCs) phagocytose the pathogens and trigger a pro-inflammatory response including cytokine production and recruitment of cells of the innate immune system. APCs migrate to the draining lymph nodes and stimulate $CD8^+$ and $CD4^+$ cells, via major histocompatibility complex (MHC) class I and II receptors, respectively. These activated T cells attract further cells, which eventually results in the formation of a granuloma containing various immune cells such as monocytes, lymphocytes and foamy macrophages. Figure was adopted from Harding *et al.*[22].

These receptors include toll-like receptors (TLRs)[23], complement receptor (CR) 3[24], CD1 (cluster of differentiation 1) surface receptors[25], and C-type lectins such as the mannose receptor (MR) and dendritic cell-specific intercellular adhesion molecule 3-grabbing non-integrin (DC-SIGN)[26-28]. Following receptor binding,

bacteria are internalised via phagocytosis. Subsequent bacterial degradation inside the APCs can only occur through fusion of the phagosome and the lysosome. Once digested, bacterial antigens are loaded onto the cell surface for presentation. As a result of successful pathogen processing, DCs upregulate co-stimulatory surface molecules including CD80, CD86 and CD40 and undergo maturation. Both the matured DCs and partially activated AMs produce cytokines such as interleukin (IL)-12 and tumour necrosis factor (TNF)-α. Secretion of these pro-inflammatory cytokines and other chemokines generates local inflammatory stimuli. These in turn attract other immune cells such as monocytes, DCs, natural killer cells (NK cells), neutrophils and T cells to the site of infection.

Approximately 15 days post infection, the adaptive immune response is activated. Mature DCs migrate to draining lymph nodes and activate $CD8^+$ and $CD4^+$ T cells via the major histocompatibility complex (MHC) class I and II receptors, respectively. Macrophages can additionally activate $CD4^+$ cells, whereas APCs with CD1 surface receptors are able to stimulate NK T cells expressing $\alpha\beta$ T cell receptors (TCRs), by presenting glycolipid antigens from bacterial cell wall[29]. These cells help to control mycobacterial infections by producing IFN-γ and exerting a cytotoxic activity[22]. Activated $CD8^+$ and $CD4^+$ T cells proliferate and migrate to the lung and stimulate a large number of AMs and DCs. As a result of the cellular invasion, an aggregate containing various immune cells such as monocytes, lymphocytes and foamy macrophages is formed[30]. This distinctive feature of tuberculosis is called granuloma or tubercle. Until recently, the granuloma was thought to be protective to the host and a way to control the infection. However, recent studies suggested that the granuloma may serve as a reservoir for bacteria, playing a key role in retaining a latent infection[30,31].

To exert an appropriate immune response, mediators such as TNF-α[32,33] and IL-12[34] are fundamental. The crucial role of IL-12 has been established in IL-12 deficient (IL-12 p40$^{-/-}$) mice, which have an inability to limit bacterial proliferation following *M. tuberculosis* infection[34]. These findings were later reinforced by a study conducted in tuberculosis patients, where mutations in genes encoding for IL-12 were found to result in an increased susceptibility to infection[35]. The essential function of IL-12 is its role in the development of a protective Th1 immune response, which is required to eradicate intracellular pathogens such as *Mycobacterium*[1,36]. As a consequence of Th1 stimulation, pro-inflammatory cytokines including INF-γ are produced, mainly by CD4$^+$ T cells as compared to CD8$^+$ T cells and NK cells[1,36]. This has been well studied *in vitro*[37] and in patients[38,39]. INF-γ activates infected macrophages and upregulates MHC class II expression, which in turn increases antigen presentation to T cells. *In vivo* models using knockout mice demonstrated the essential role of INF-γ-mediated immunity in the control of mycobacteria[40]. Other mechanisms for killing pathogens include the secretion of microbicidal molecules such as superoxides by phagocytic cells[41,42].

Several studies have also shown high levels of regulatory T cells (Tregs) in tuberculosis patients[43,44]. Interestingly, Tregs are beneficial to mycobacteria by modifying immune responses of the host and so help generate a chronic infection[45]. Tregs have been shown to decrease macrophage activity by secreting anti-inflammatory cytokines including IL-10[46] and also to negatively regulate pathogen-specific IFN-γ production[43,44].

1.1.2 Subversion of immune response

Innate immunity plays an important role for protection against mycobacterial infection. If activated appropriately, T cell immunity is protective in more than

90% of infected individuals[47]. However, mycobacteria have developed mechanisms to subvert elimination allowing them to replicate and remain concealed. It has been shown that once internalised by macrophages, mycobacteria can suppress fusion of the phagosome with lysosomes by altering the acidic environment within the phagosome[41]. Therefore, bacteria can circumvent phagocytic degradation within the phagolysosome in order to survive and grow intracellularly. Macrophages are the primary host cells for mycobacteria. However, *in vivo* studies have shown that DCs can also support replication[48]. Furthermore, findings from *in vitro* experiments with human and murine macrophages, have suggested that mycobacteria may escape eradication by macrophages by preventing INF-γ-mediated signalling. A 19-kDa lipoprotein found in the mycobacterial cell wall inhibited macrophage responses to INF-γ, as well as MHC class II expression and antigen presentation via TLR-2[49-51]. A similar activity has been reported for cell wall glycolipids. The corresponding underlying mechanism is further discussed in **Section 1.2.2**. As a result of decreased antigen processing, DC migration and subsequent antigen presentation to lymphocytes are reduced. Consequently, the control of the infection is diminished[48].

Another study found that mycobacterial oxygenated mycolic acids activate the differentiation of macrophages to foamy macrophages[30]. These cells are contained in the granuloma structure and are filled with lipid droplets[52]. Results suggested that bacteria change to a non-replicating persistent phase once internalised by foamy macrophages[30]. Concealed inside the granuloma, the host is unable to recognize pathogens and persistent mycobacteria are maintained.

Interactions between pathogens and the host immune system are complex. A distinct role in modulating immune responses has been attributed to the bacterial cell wall with its highly complex structure and varied composition. Therefore, the effect of specific components, particularly focussing on phosphatidylinositol mannosides (PIMs), in manipulating the immune response is discussed in detail below.

1.1.3 Mycobacterial cell wall

As illustrated in **Figure 1-2,** the mycobacterial cell wall is a complex network of lipids, proteins and polysaccharides. It is generally composed of two layers, the outer region of which comprises free surface glycolipids varying in their fatty acid chains. Located underneath is the cell wall core known as the mycolyl arabinogalactan–peptidoglycan (mAGP) complex. Within this complex are mycolic acids, consisting of long and short-chained fatty acids, linked to arabinogalactans which are further covalently bound to peptidoglycan[53]. Additionally distributed throughout the cell wall are proteins and lipoglycans including lipoarabinomannans (LAMs), lipomannans (LMs) and phosphatidylinositol mannosides (PIMs) (**Figure 1-2**).

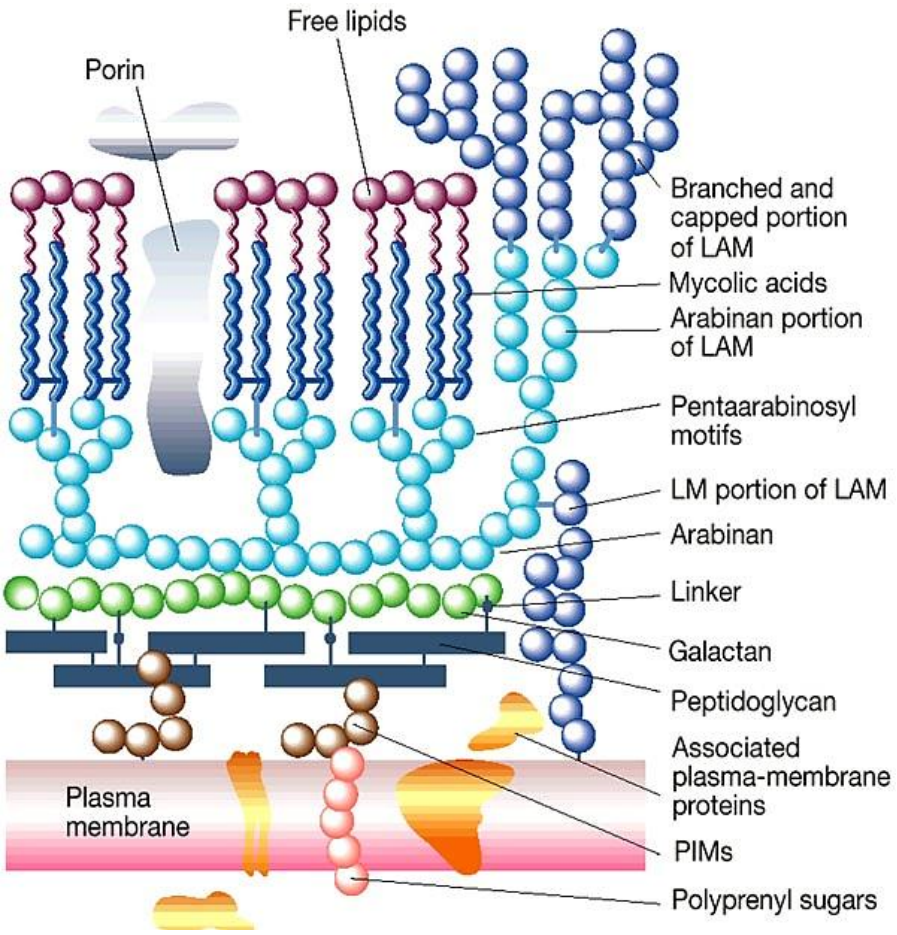


Figure 1-2. Schematic presentation of the mycobacterial cell wall. The characteristic lipoglycan lipomannans (LMs) and lipoarabinomannans (LAMs) are dispersed throughout the lower and upper layer of the cell wall structure. Phosphatidylinositol mannosides (PIMs) represent anchor motifs for attachment to the plasma membrane. Adopted from Park and Bendelac[25].

Phosphatidylinositols (PI) are the anchor structures that insert into the plasma membrane bilayer[53]. The lipoglycans are structurally related and are derived from the same biosynthetic pathway, with PIMs acting as precursors for the more complex LAM and LM[54,55] (**Figure 1-3**). Generally PIMs consist of an inositol core linked to mannose residues and a phosphatidyl moiety with fatty acids. Additional mannosylation of PIMs with 1,6-α-D-linked mannopyranosides generates LMs. In the case of LAMs, the mannan backbone structure is further extended with branched arabinan domains[55,56] (**Figure 1-3**).

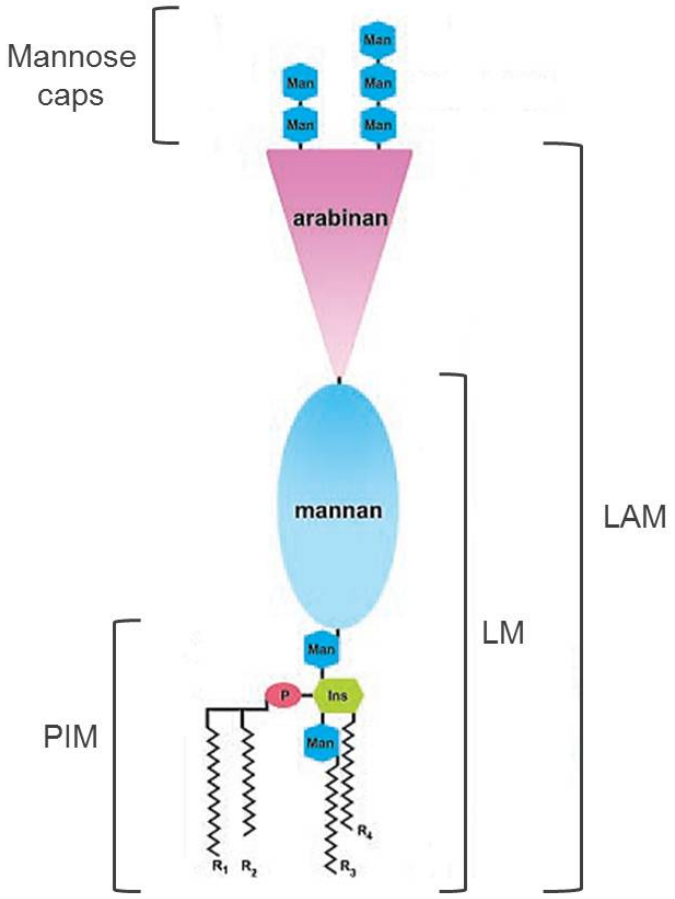


Figure 1-3. Schematic illustration of the glycolipids found in the mycobacterial cell envelope. Figure was modified from Jozefowski *et al.*[57].

Different forms of LAM are mainly due to variations in capping motifs and variations in anchor structure (nature, degree and location of fatty acids). Additional capping of LAM with one, two or three mannose residues (ManLAM) is characteristic for virulent slow-growing mycobacterial species such as *M. tuberculosis*, *M. avium*, *M. leprae* and *M. kansasii* and *M. bovis* BCG[58]. Fast growing non-virulent species, including *M. smegmatis*, have phosphoinositol caps (PILAM), while other species like *M. chelonae* lack the terminal capping (AraLAM)[57]. Pioneering work in the early 1980's by several groups clarified the specific structural features of these crucial cell components which allowed for the establishment of structure-function relationships[54,56,59].

1.1.4 Role of cell wall components in modulation of immune responses

Over the past decade, research efforts have found that particular cell wall lipids play an important role in the virulence of mycobacteria. Several studies have reported mechanistic data on how these components contribute to controlling the function, and activity of immune cells such as macrophages and DCs. Importantly, outcomes from these studies supported the proposition that glycolipids exert different immunomodulatory activity profiles due to varied structural compositions[60]. For instance, PILAMs have been found to evoke secretion of pro-inflammatory molecules such as IL-12 and TNF-α from murine macrophages *in vitro*[19,61-63]. This was mediated via TLR-2 receptor binding and subsequent activation of immune cells[64]. It is worth mentioning that the inability of this mycobacterial species to survive inside macrophages, has been attributed to this stimulation of the host's immune system[60].

In contrast to this, the pathogenicity of *M. tuberculosis* and *M. bovis* BCG and the ability to persist within host cells, was reported to be associated with the presence of ManLAMs in the bacterial cell envelope[60]. ManLAMs inhibit production of IL-12 and TNF-α *in vitro* via binding to MRs[65] and DC-SIGN[26,28,66]. MRs comprise eight carbohydrate recognition domains (CRDs) which interact to bind multi-valent ligands with high affinity[67]. Mannose-capping of LAM facilitated binding to MRs. However, affinity assays revealed a dependency on the degree of acylation[65], and ManLAMs from various *M. tuberculosis* strains differed in their MR binding affinity[68]. At least two fatty acids were required to exhibit inhibitory effects. This was attributed to the clustering behaviour of acylated ManLAM in water[65,69]. These assembled supramolecular structures may have enhanced MR binding resulting in increased MR signalling, and subsequent negative regulation of pro-inflammatory agents[65,69].

In addition to ManLAMs, other mycobacterial ligands to DC-SIGN have been proposed[26,70]. Indeed, the fact that a number of diverse mycobacterial glycolipids are able to bind to different C-type lectins, including MR, DC-SIGN and Dectin 1[71] creates a great complexity in this area. As well as generating anti-inflammatory activity by signalling through these receptors, studies also reported the stimulation of inflammatory responses[72,73]. Furthermore, mycobacterial lipid interactions with C-type lectins have been shown to induce a signalling cascade that inhibits TLR-mediated IL-12 production[28,66,74]. The concurrent interaction of mycobacterial components with C-type lectins and TLRs, may shift the immune responses from protective Th1 to Th2, resulting in the ability of the pathogen to circumvent elimination[75]. This again highlights how crucial receptor interactions are for determining immunomodulatory activity of mycobacterial components.

LMs and LAMs on the other hand, exert a very different activity profile as compared to ManLAM, with studies showing interactions with TLRs rather than C-type lectins due to distinctive structural features[23,76]. Numerous studies have reported LM and LAMs exerting both pro-inflammatory and anti-inflammatory activity[19,23,76-79]. Conflicting data is likely due to diverse models (cell lines, different concentrations of active agents, timing of delivery of agents), and different bacterial strains used as the source of these compounds[22,55]. Nevertheless, acylation was found to play a significant role in determining the bioactivity of the immunomodulatory components. Along with a 19-kDa lipoprotein, LAM and LMs were identified as agonists of TLR-2 and, to a lesser extent TLR-4[78]. In particular, tri-and tetra-acylated LM showed high receptor binding, while mono- and di-acylated LM were inactive[70]. The inactivity of mono- and di-acylated LMs may be due to the fact that signalling through TLR-2 is modulated via dimerisation with other TLRs. Thus, it is

believed that tri- and tetra-acylated forms offer optimal structural requirements[78]. The inhibitory effect of di-acylated and tri-acylated LMs on LPS-induced TNF-α secretion has yet to be fully elucidated, as this was found to be independent of TLR-2 signalling[70,76]. However, in good agreement with other structure-function relationship of ManLAMs[65], was that at least two fatty acids were necessary for suppressive activity *in vitro*[70].

1.2 Phosphatidylinositol mannosides

1.2.1 Structure of PIMs

The discovery of *myo*-inositol structures in mycobacterial extracts was first described in 1930 by Anderson[80]. Following on from the work of Anderson, Ballou *et al.* examined a series of PIMs in chloroform–methanol extracts from *M. bovis* BCG[81], *M. tuberculosis* and *M. phlei*[82]. They characterised the chemical structures of isolates as the phosphatidylinositol di-, tri-, tetra-, penta- and hexamannosides (PIM_2 to PIM_6) using degradation reactions and paper chromatography[81,82]. The structures of these compounds were later confirmed by nuclear magnetic resonance (NMR) analysis[83]. For example PIM_1 compromises a 1-D-*myo*-inositol core with a glyceryl phosphate residue at the C-1 position and a α-D-mannopyranosyl unit at C-2[83] (**Figure 1-4**).

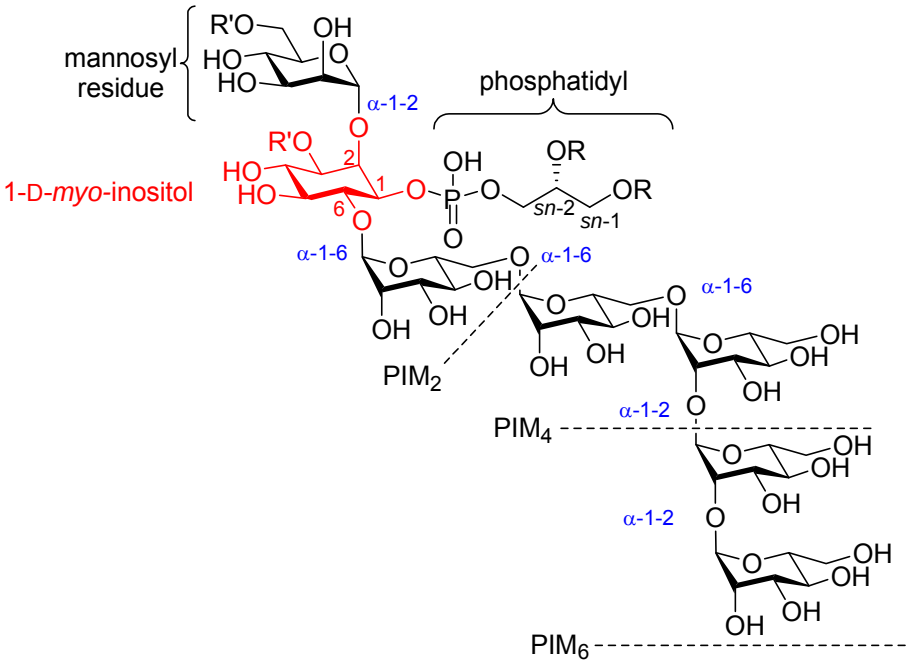


Figure 1-4. General structure of phosphatidylinositol mannosides (PIMs). PIMs can have two acyl residues (R) at the phosphatidyl moiety which in nature are palmitatoyl, tuberculostearoyl or stearoyl residues. The structure can be further acylated, indicated as R', at the mannosyl group attached to the C-2 position of the inositol ring (Ac_1PIMs) and at the C-3 position of inositol (Ac_2PIMs) (R' = R or H).

PIMs are generally classified according to their structure, whereby in PIM_y, y denotes the number of mannosyl residues, while x in Ac_xPIM refers to the number of additional acyl chains, excluding the ones linked to the phosphatidyl moiety (Ac_1PIM_y and Ac_2PIM_y are tri-and tetra-acylated, respectively). With regard to the structure of PIM_1, another mannosyl residue at C-6 would give PIM_2. Structures of PIM_3 and PIM_4 correspond to additional *α*-1-6-mannosylation while PIM_5 and PIM_6 are generated by further elongation of the oligosaccharide side chain via *α*-1-2-mannosylation[81-83]. Severn *et al.*[84] characterised the core structures of deacylated forms of PIM_2 and PIM_6 in extracts from *M. bovis* and *M. smegmatis*, using advanced technologies such as two-dimensional NMR studies and mass spectrometry (MS).

In the late 1980's, research was refocused on the resolution of the PIM structures due to increasing interest in the immunomodulatory capacity of these components. Initial investigations confirmed the presence of multi-acylated forms of PIMs in the mycobacterial cell wall, which varied in the number, location and type of acyl residues[85,86]. However, these studies lacked details about the nature of the acyl residues and their location within the PIM structure. It was then shown that palmitate and tuberculostearate were the major fatty acids, with small amounts of stearic acid in purified extracts from *M. leprae* and *M. tuberculosis*[59] (**Figure 1-5**). In 1995, Khoo *et al.*[87] clarified the acylation status of PIM_2 and PIM_6 in *M. leprae* and *M. tuberculosis* using fast atom bombardment-MS (FAB-MS). The two fatty acids attached to C-1 and C-2 of the glycerol unit were demonstrated to be palmitate and tuberculostearate[87]. An additional position of fatty acid attachment at O-6 of the mannosyl residue linked to C-2 of the *myo*-inositol core in PIM_2 was also identified[87]. FAB-MS was used to successfully describe the structure of an $AcPIM_3$[88].

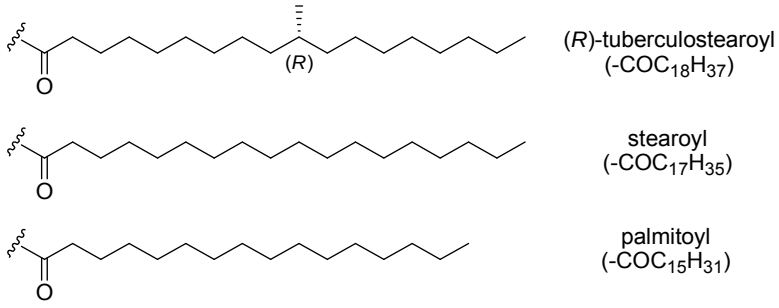


Figure 1-5. Common acyl residues identified in extracts from various mycobacterial strains.

A limitation of this analytical approach was the requirement for chemical modification of molecules, as well as the purification steps of acyl forms for investigation. Further technical improvements in recent studies enabled clarification of acylation sites in PIM_2[89,90] and PIM_6[21], using NMR and matrix-assisted laser desorption/ionization (MALDI)-MS, to identify position and

nature respectively. Gilleron and colleagues[21,89,90] reported mono- to tetra-acylation and established a fourth site of acylation at the C-3 of the *myo*-inositol core. Fatty acid residues described, were consistent with those reported by Khoo *et al.*[87].

1.2.2 Immunomodulatory properties

PIMs are essential biosynthetic precursors of the hypermannosylated cell wall components LM and LAM, and occur naturally in the predominant forms PIM_2 and PIM_6. Numerous studies have shown how these low molecular weight molecules elicit a variety of immune responses. They have provided strong evidence for a key role in mycobacteria-mediated immune responses.

Several studies reported the ability of mycobacterial PIM_2 and PIM_6 to stimulate macrophages in a TLR-2 dependent manner[21,91]. This potent pro-inflammatory activity led to increased production of TNF-α and was not affected by the acylation state[21]. This is surprising as the binding efficacy of mycobacterial LMs was found to be dependent on the degree of acylation with fatty acids[78]. However, the mannosyl residue was shown to have a great impact on binding to TLR-2[92]. It was shown that signalling through TLR-2 of PIM_2 was considerably reduced when compared to LMs[92]. Thus, the potency at TLR-2 receptors may not be restricted by number of acyl residues but the length of the oligosaccharide chain. Specific mechanisms by which PIMs modulate immune responses are still under investigation. Until recently, these mycobacterial molecules were believed to indirectly modulate the function and response of T cells via interactions with APCs. While pro-inflammatory signalling through TLR-2 leads to production of TNF-α and IL-12, prolonged TLR-2 stimulation inhibited MHC class II expression and antigen processing[93,94]. This results in inhibited $CD4^+$ T cell activation. As mentioned earlier, following cellular

uptake, microbes live persistently inside macrophages. Studies have shown that PIMs are actively trafficked out of the phagosome[93,94] where they can exit the cell in membrane vesicles and so interact with TLR-2 on the cell surface[95]. Moreover, mycobacterial PIM_2 and PIM_6 provoked anti-inflammatory effects via TLR-4 receptors which were independent of TLR-2 in a model of LPS-activated macrophages[96].

More recent work has also shown that mycobacterial compounds can directly affect $CD4^+$ T cells. They can inhibit cytokine secretion and T cell proliferation independent of APCs through interaction with VLA-5 ($\alpha_5\beta_1$) on $CD4^+$ T cells[97,98]. Synthetic PIM analogues maintained biological activity and showed similar potency *in vitro* to their natural counterparts[96,99].

To elucidate interactions with MRs, Torrelles *et al.*[27] extracted various PIMs from *M.tuberculosis* H37Rv and further fractionated them according to their mannose content and degree of acylation. Binding efficacy for MRs on human monocyte-derived macrophages, using a bead model, was increased for the higher-order PIMs such as Ac_1PIM_6 and Ac_1PIM_5. While the binding of PIMs to the MR was affected by the degree of mannosylation, recognition by DC-SIGN was independent of the number of the mannosyl residues. The researchers attributed this phenomenon to the different orientations of the carbohydrate recognition domains in the different receptors, affecting mannose recognition. These findings differ from results reported by other groups[100,101], where DC-SIGN demonstrated a high affinity for PIM_6 and a lower affinity for the less mannosylated PIM_2 and PIM_4. This may be due to different *in vitro* binding assay conditions resulting in varied receptor specificities. The number of acyl residues also impacted on receptor interactions, with Ac_2PIM_6 being less effective in binding to the MR than Ac_1PIM_6[27]. This was in good agreement with

studies on the interaction between ManLAM and C-type lectins. In particular, the presence of the fourth fatty acid in Ac_2PIM_6 was suggested to alter the conformation of the mannosyl cap, thus modifying attachment to the MR. The high content of ManLAM and highly mannosylated PIMs in the cell wall of *M. tuberculosis* may enable increased phagocytosis by macrophages mediated through MRs[67]. Subsequently PIMs may also inhibit phagosome fusion with lysosomes and contribute to virulence by promoting survival inside macrophages[27].

Mycobacteria-infected cells can be detected and eliminated by CD1-restricted NK T cells[102]. CD1 molecules, which are structurally related to MHC class I, present non-protein antigens such as glycolipids to T cells. They can be divided into two groups, where group 1 (CD1a, CD1b, CD1c and CD1e) is mainly present in humans, while the group 2 molecule CD1d is found in mice and humans[103]. Crystal structure analysis revealed a hydrophobic binding groove in CD1[104] and presentation of mycobacterial PIMs by CD1b and CD1d has been reported[105-107]. PIM_6 from *M. leprae* and *M. tuberculosis* was recognized by human $\alpha\beta$ TCR-expressing T cells when presented via CD1b[105]. In addition PIM_2 was shown to interact with CD1b molecules independently of acyl chain length[106]. In a study by Fischer *et al.*[107], the recognition of mycobacterial PIM_4 by $\alpha\beta$ NK T cells, was mediated through CD1d resulting in increased INF-γ production and cytotoxicity. Binding to CD1d was constrained by the degree and location of acyl chains with the optimal affinity being found with two acyl chains.

Of the families of mycobacterial glycolipids found in the cell envelope, the structurally less complex PIMs offer a variety of immunomodulating activities. This diversity makes PIMs excellent compounds for the development of novel

immunosuppressive agents, for treatment of atopic diseases or as adjuvants to improve the efficacy of vaccines. The ability of PIMs to suppress and activate immune responses is discussed in more depth in **Chapters Three** and **Four**.

1.3 Atopy and allergic responses

The number of individuals developing atopic diseases is steadily rising worldwide[108]. Epidemiologic studies in industrialised countries suggest that more than 25% of the population suffer from allergic hypersensitivity conditions[109]. This includes allergic asthma, a chronic respiratory disease typified by altered airway reactivity, inflammation and narrowing of the airways[110]. The development of asthma is effected by many factors such as genetic predisposition, environmental stimuli and impairment of the immune system[111]. In asthmatic individuals the immune response to inhaled environmental allergens is characterised by a strong, predominantly $CD4^+$ Th2 response (**Figure 1-6**).

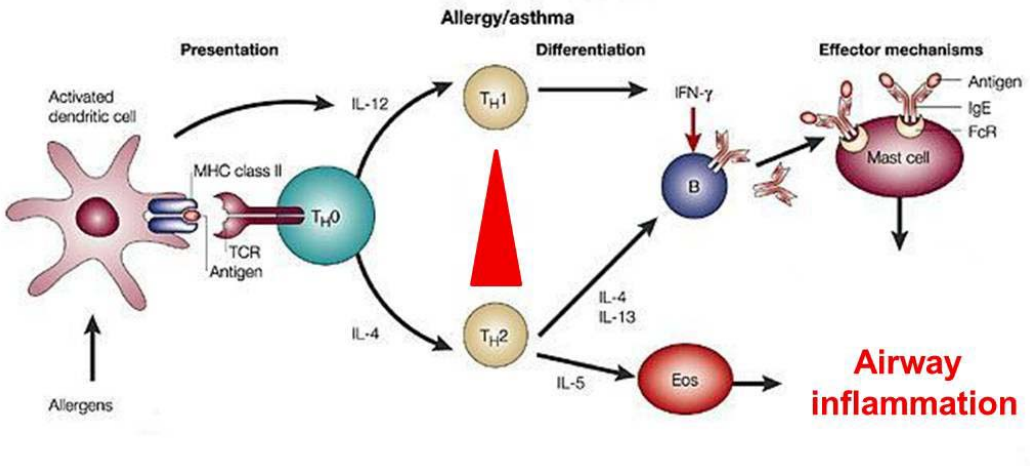


Figure 1-6. Pathogenesis of allergic immune responses. A crucial feature of allergic reactions is the polarisation of the immune response towards the Th2–type, as indicated by the red triangle. Subsequently, Th2-associated cytokines are released which recruit eosinophils into the airways. This cascade results in the typical allergic reaction and airway inflammation. Figure was modified from Wills-Karp *et al.*[112]

Following activation by APCs, $CD4^+$ Th2 cells migrate into the lung and secrete the cytokines IL-4, IL-5 and IL-13. The crucial functions of these cytokines in mediating the immune response have been assessed in humans and murine models. IL-4 triggers differentiation of naïve T cells into Th2 cells[113]. Both IL-4 and IL-13 stimulate B cells to produce IgE, the main antibody associated with allergic diseases[112]. Secretion of IL-13 also stimulates chemokines to activate and recruit inflammatory cells into the airways[112,114]. IL-5 induces eosinophil differentiation in the bone marrow and activates an eosinophil influx into the lung[115]. Lung infiltration of eosinophils and other inflammatory cells such as mast cells and basophils is thought to be a key feature of asthma, resulting in local inflammation and airway hyperresponsiveness.

The increased occurrence of allergic diseases, particularly asthma, may be associated with less contact to bacteria and/or viruses[112,116]. This is known as the "hygiene hypothesis", whereby infections during early childhood are thought to bias the cytokine profile towards Th1 and so reduce the risk for the development of Th2-dependent allergies[116]. Shifting the immune response to Th1 promotes the production of IL-2 and INF-γ. The latter is highly potent in suppressing Th2-dependent inflammation and inhibition of Th2 type T cells. A promising approach for the treatment of allergic diseases is to redirect immune responses from Th2 to Th1 in order to restore the Th1/Th2 balance[109,117]. Interestingly, mycobacteria are known to be effective stimulators of Th1 immune responses.

1.3.1 Strategies for treatment of allergic diseases

Conventional strategies to treat allergic reactions include various medications such as antihistamines, (H_1 antagonists), β2-receptor agonists (bronchodilators), adrenaline, corticosteroids and immunosuppressive agents including

cyclosporine A[117]. For successful therapies, treatment plans require long-term daily medication use. However, these drugs (especially corticosteroids) are known to cause severe side effects particularly if prescribed at high doses over prolonged time. These can include thrush, osteoporosis, skin thinning and bruising, cataracts and glaucoma[118]. The aim of most conventional treatments is to improve symptoms rather than treating the underlying disease mechanism. As a consequence, there is a need for novel immunoregulatory compounds to treat asthma. Currently, a number of different strategies such as allergen-specific and cytokine-based immunotherapy, DNA vaccines and bacterial extracts are being tested for their therapeutic potential in both mouse models and human allergic patients.

1.3.1.1 Allergen-specific immunotherapy

As a preventive approach, individuals can be desensitised to particular disease-causing allergens. This is generally performed by exposing patients to increasing doses of allergen extracts over a prolonged period of time in order to promote immunological tolerance[117]. However, problems related to the crude allergen extracts often used in these therapies such as variable efficacy, instabilities of active agents and impurities can cause undesired side effects. To avoid this and to improve patient safety, recombinant allergens and hybrid variations with defined immunological properties have been developed. Examples of allergens for which modified versions have been developed and which are undergoing clinical studies are birch pollen[119,120] and grass pollen[119,121]. These allergens are hypoallergenic but still sufficiently immunogenic to elicit an appropriate immune response[117,119].

1.3.1.2 Cytokine-based immunotherapy

Cytokines represent promising targets for immunotherapy of asthma since their crucial role in the pathogenesis of allergic asthma has been established. There are different approaches on how to modulate cytokines and the associated immune responses. Blocking monoclonal antibodies, which have been designed to bind particular molecules, can inhibit the effects of the Th2-related cytokines IL-4, IL-5 and IL-13[117]. Other investigations have been directed towards the use of recombinant cytokines, including INF-γ and IL-12. It has been shown that INF-γ[122] and IL-12[123] can decrease levels of Th2-associated cytokines and the number of eosinophils, respectively when tested in patients. However, the effect of IL-12 was limited to early stage allergic symptoms and administration also induced arrhythmia and liver side effects[123].

1.3.1.3 DNA vaccines

Alternative approaches to prevent and treat allergic diseases are based on shifting the immune response from Th2 to Th1 responses via TLR stimulation. TLRs identify pathogen associated molecular patterns (PAMPs) derived from bacteria and viruses. Subsequently, APCs are stimulated to produce cytokines which polarise towards a Th1-type immune response. Dinucleotide sequences such as CpG DNA are known TLR-9 ligands[124] and coupling of allergens with CpG DNA has been proved effective in allergic patients[125-127]. For instance, the application of the immune complex containing the ragweed allergen Amb a 1 and CpG DNA, elicited strong allergen-specific Th1 responses in comparison to the placebo control groups[125,126]. Patients showed increased production of INF-γ, decreased Th2 cytokine production and eosinophilia[125,126] and reduced levels of IgE antibodies[127]. Following these promising outcomes, a recent study reported the evaluation of CpG DNA in patients with allergic rhinitis[128]. By

using allergen-free vaccines, potentially occurring allergic reactions can be diminished. CpG DNA was incorporated into virus-like particles (VLP) to provide protection from rapid degradation and ensure delivery to APCs. Allergen-induced symptoms (nasal blockage, eye reddening, sneezing etc.) were significantly improved in patients treated with CpG DNA-VLPs in contrast to the placebo group[128].

1.3.1.4 Bacterial extracts

The fact that various bacteria and bacteria-derived compounds show immunomodulating activities makes them considerable as potential vaccine components. The ability of mycobacterial extracts to prevent asthma was initially demonstrated in Japanese children[129]. Despite the findings by Shirikawa *et al.*[129], the inverse correlation between exposure to mycobacteria and incidence of allergic diseases could not be confirmed in a Swedish population[130]. However, several studies using murine models have shown that mycobacterial infections can modulate Th2-driven immune responses[131-136]. BCG immunisation 14 days prior to allergen (OVA)-sensitisation resulted in elevated INF-γ titres, decreased production of IL-4 and IL-5 in lungs and less eosinophils infiltrating airways[132]. Similar results were observed when allergen-sensitised mice were treated with either live attenuated[131] or killed[134-136] mycobacterial strains. Moreover, components of the mycobacterial cell wall have been shown to modulate the immune responses. **Chapter Three** focuses particularly on suppressive activities exerted by PIMs. Similar immunomodulating activities were found for the Gram-positive *Listeria monocytogenes*[137] and the Gram-negative bacteria *Francisella tularensis*[138]. In allergen-sensitised mice, live-attenuated vaccines derived from *F. tularensis* and bacterial extracts suppressed eosinophil influx and dampened airway inflammation[138]. This was mediated by correcting the Th1/Th2 immune

response. Due to these encouraging *in vivo* results, bacterial-based vaccines may be useful candidates to prevent allergic diseases.

1.4 Vaccines

Vaccines have contributed immensely to human health status since their worldwide introduction in the beginning of the 20th century. A milestone in the history of immunisation can be attributed to Edward Jenner and his successful attempt to immunise a boy against smallpox in 1796[139]. Inoculation of the child with infectious material from a cowpox patient resulted in protection against later exposure to smallpox. Following on from the success of this first vaccination, Louis Pasteur greatly advanced the understanding of immunisation and developed both anthrax and rabies vaccines during the 1880's[139]. Since the late 1920's a great number of vaccines has been introduced. These included vaccines against diseases with high incidence and lethality such as polio, measles, mumps, rubella, diphtheria, tetanus and pertussis. Many diseases have been able to be controlled worldwide due to vaccination campaigns. While there are many examples in which vaccines were successfully employed to control or even eradicate diseases, such as smallpox in 1979[139], there are still a number of diseases for which no vaccine is yet available. There is an obvious need for vaccine research to develop prophylactic vaccines for diseases such as tuberculosis, HIV, malaria. There is also a need for therapeutic vaccines to treat non-communicable conditions, such as Alzheimer's disease, allergy and cancer[140].

1.4.1 Types of vaccines

The general aim of prophylactic vaccination is to initiate effective antigen-specific immune responses and establish long-term protection. This requires

activation of humoral as well as cell-mediated responses associated with the induction of effector T cells, antibody and memory T cells. Conventional vaccines can be categorised into inactivated pathogens, live attenuated pathogens, inactivated toxins produced by these organisms, and subunit vaccines. The class of inactivated vaccines is characterised by chemically or heat killed pathogens. Such vaccines have been used to protect against pertussis, polio and influenza. As these vaccines are non-replicating, protection is short-lived and boosting with multiple dosages is required to maintain immunity. Further, inactivated vaccines vary in efficacy and cellular responses are not necessarily stimulated.

Live attenuated vaccines (for example the measles, mumps, rubella (MMR) vaccine and the tuberculosis vaccine) contain pathogenic organisms which have been weakened and have reduced virulence. Attenuation can occur through selective *in vitro* culture or by targeted genetic mutation. However, with attenuated vaccines there is a risk of reversion to virulence and even an attenuated vaccine may cause disease in immunocompromised individuals.

Furthermore, toxoid-based vaccines can be used to provide protection if morbidity and mortality are caused by a toxin. This is the case for instance with diphtheria and tetanus and corresponding vaccines contain inactivated bacterial toxins. A major drawback associated with toxoids is the potential presence of impurities. Despite their ability to induce protective immunity, a disadvantage of using vaccines based on whole pathogens is the adverse effects which vary in severity from a headache and fever, to encephalitis, anaphylaxis and neurological complications[141]. Due to these safety issues, a major focus in vaccine research has been towards the development of subunit vaccines containing antigenic motifs (peptides, proteins or DNA) from pathogens. In

1981 the first subunit vaccine, the Hepatitis B surface antigen vaccine[142], was licenced. Other examples of vaccines licensed since then include typhoid and influenza vaccines. An advantage of these vaccines is their safety and low reactogenicity as the subunit antigens can be produced at high purity and quantity by chemical and recombinant synthesis. The use of essential epitopes as an alternative of whole organisms reduces the chances of adverse reaction and improves antigen specificity[143]. However, one of the drawbacks of subunit vaccines is their low immunogenicity, consequently insufficient protection may be provided[143].

1.4.2 Developments in tuberculosis vaccines

The only tuberculosis vaccine currently licensed in humans is the live attenuated BCG vaccine. BCG is a well-established vaccine that has been used for more than 80 years with reports of severe adverse events being extremely rare[14]. It is thought to induce a strong protective Th1 immune response against mycobacteria[15]. However, BCG has proven ineffective in preventing pulmonary tuberculosis in adults[15]. Due to serious side effects caused by BCG vaccination in immunocompromised HIV individuals, it is now contraindicated in this population[144]. Efforts are increasing to develop more potent and efficient subunit Tb vaccines which are able to elicit protective immunity and can also be given to immunosuppressed individuals. Twelve vaccine candidates are currently undergoing evaluation in clinical trials[16]. New strategies involve either modifications of the current BCG vaccine designed to improve efficacy or the introduction of new vaccines which can be used as booster vaccines following an initial BCG immunisation[14]. Moreover, therapeutic vaccines are being developed for combination with conventional treatments such as chemotherapy[14].

1.5 Adjuvants

As discussed above, progress in vaccine research has led to the development of new vaccine candidates based on antigenic epitopes derived from pathogenic organisms. Due to their highly purified structures, subunit vaccines lack features associated with live pathogens and do not provide danger signals to initiate immune system activation. In order to improve their immunogenicity and trigger appropriate immune responses *in vivo*, co-administration of the sub-unit antigen with adjuvants has become common. The term adjuvant is derived from Latin word "*adjuvare*" meaning to help or aid. Adjuvants include a broad variety of compounds such as mineral salts[140,145], emulsions[146,147], microbial products[148-150] and particulate systems[151,152] each of which exert diverse modes of action. Until 2009 alum (aluminum salt–based adjuvant) was the only adjuvant contained in vaccines for human use in the United States. Only in 1997 was the first non-aluminium adjuvant, MF59 (Fluad®), available. Many reasons account for the slow progress in adjuvant development, including concerns related to biocompatibility, as well as short and long-term safety in humans[140]. Many adjuvants such as complete Freund's adjuvant (CFA)[153] or lipopolysaccharides (LPSs)[148] have been evaluated in animal models. However, their application in humans is limited due to their toxicity[154]. Accessibility and origin of adjuvant components plays an important role, as they need to be available in a pure and reproducible form. Strategies have been developed to obtain these compounds via chemical synthesis. However, this applies only to a limited number of molecules including the synthetic molecule E6020 which mimics the structure of a LPS[155]. Progress has been further delayed by the lack of scalable manufacturing techniques and problems associated with the stability of antigens/adjuvant combinations[140,156]. **Table 1-1** gives an overview of currently licenced adjuvants and those undergoing clinical investigations or preclinical evaluations.

The diversity of adjuvant types, mode of action and specific implications on the immune response complicates their classification. According to earlier reports, adjuvants can be categorized by their mode of action into immunopotentiators and delivery systems[157]. However, new studies reveal that their activity cannot always be ascribed to a single pathway, but is rather the interplay of different actions. In addition, combinations of delivery systems and immunostimulatory agents are commonly being developed. These improve the immunogenicity of specific antigens and activate both humoral and cellular immune responses. A number of adjuvants relevant to the thesis are discussed in more detail in the following section. **Table 1-1** gives a summary of these examples categorised by their current development status.

Table 1-1. Outline of various adjuvant systems including their corresponding mode of action and the type of immune response activated. For more details see text below. Table modified from Mbow *et al.*[156], O'Hagan and De Gregorio[140], Pulendran and Ahmed[150], and Reed *et al.*[158].

Development status	Adjuvant	Mode of action	Type of immune response
Licensed	▪ Alum	Depot effect, antigen delivery	Th2
	▪ MF59 (o/w emulsion)	Local inflammation at injection site, no depot effect, enhances AG uptake	Th2
	▪ AS03 (o/w emulsion)	Local inflammation at injection site, no depot effect, enhances AG uptake	Th2
	▪ AS04 (MPL + alum)	TLR-4 agonist (MPL)	Th1 and Th2
	▪ Liposomes	Depot effect, antigen delivery	Th1
Clinical trials	▪ Montanides	Depot effect, antigen delivery	Th1
	▪ Saponins	Poorly understood, proposed mechanism: mediate delivery of AG directly into cytosol of APC (lytic capacity)	Th1
	▪ Immunostimula-tory nucleic acids	TLR-9 agonist	Th1
	▪ AS02 (o/w emulsion + MPL + QS-21)	Poorly understood, proposed mechanism: Synergistic effect of TLR and non-TLR dependent adjuvants	Th1/Th2
	▪ AS01 (Liposomes + MPL + QS21)	Poorly understood, TLR-4 agonist (MPL)	Th1
	▪ CFA01 (DDA/TDB liposomes)	Local inflammation, enhance uptake via interaction with APCs (surface charge)	Th1
Emerging adjuvants	▪ TLR agonists	TLR-2/4, TLR-7/8 agonists	Th1
	▪ Monomycoloyl-glycerol	Unknown TLR-independent pathway	Th1

1.5.1 Licensed adjuvants

1.5.1.1 Mineral salts

Different aluminium mineral salts such as aluminium hydroxide, aluminium phosphate and aluminium potassium sulphate are collectively called alum. First reported in 1926[159], they are until now the most commonly used adjuvants in human vaccine formulations. Alum-adjuvanted vaccines include the hepatitis A virus (HAV), hepatitis B virus (HBV), human papillomavirus (HPV), diphtheria and tetanus (DT) vaccines. The extensive use of alum is due to its well-established safety profile[140]. It is known that alum aggregates act as delivery systems for an antigen by adsorbing the antigen onto its surface. Alum prolongs antigen stability at the injection site and thus lengthens the contact between APCs and antigens which results in increased uptake[145]. It further evokes nonspecific local inflammation and thereby enhances the recruitment of immune cells[145]. Alum has been demonstrated to induce immune responses biased towards Th2-type responses, typified by the production of cytokines such as IL-4, IL-5 and IL-13 and high levels of antibodies such as IgE and IgG1[145]. A major drawback arises from the production of IgE; an antibody known to cause local allergic reactions such as erythema, swelling and nodule formation[160]. Further, the Th2 polarisation and its inability to induce cellular immune responses (Th1 and cytolytic T cells), make alum unsuitable for intracellular pathogens such as tuberculosis, malaria, leishmaniasis, leprosy and AIDS. However, current advances have partly overcome these issues and combinations of alum with Th1 stimulators such as MPL (AS04) are now available.

In addition, there are reports suggesting the role of alum as immunostimulatory agent[161,162]. Results by several research groups have

suggested that Nalp3 (NODlike receptor, pyrin domain containing 3), a component of the inflammasome complex, may be involved in the immune response to alum. For instance, *in vitro* models revealed alum signalling through Nalp3, with increased production of the pro-inflammatory cytokines IL-1β and IL-18 by macrophages[161-164].

1.5.1.2 Emulsions

Emulsions have long been known to enhance immune responses since their introduction by Freund *et al.*[165] in 1937. The use of water in oil (w/o) emulsions based on mineral oils (paraffin) is well established with examples being complete Freund's adjuvant (CFA) and incomplete Freund's adjuvant (IFA)[166]. CFA contains heat killed mycobacteria which limits its application to laboratory research[153]. Its toxicity and side effects which include acute inflammation and granuloma formation, do not allow for administration in humans[153]. IFA, which lacks mycobacterial components, had been commercially used as part of influenza vaccines. During the 1960's approximately 900 000 individuals received IFA-adjuvanted vaccines[167]. It was withdrawn due to occasional severe local reactions and is only used in a small number of veterinary vaccines today[153,168].

MF59 was the first oil in water (o/w) adjuvant to be licensed in Europe in 1997 (Fluad®). MF59 is an microfluidised o/w emulsion of squalene, a biodegradable and biocompatible natural compound, mixed with the surfactants polyoxyethylene sorbitan monooleate (Tween 80) and sorbitan trioleate (Span 85)[143,147]. Interestingly, the licensing of MF59 as an adjuvant in humans was not always certain. The originally introduced emulsion included a synthetic immune potentiator muramyl tripeptide phosphatidylethanolamine (MTP-PE) which appeared to be reactiogenic for use in humans[169,170]. Clinical studies

revealed that MTP-PE was not necessary for MF59 to show adjuvant activity[140,171]. Once administered MF59 has been shown to induce the production of cytokines and chemokines, to attract immune cells to the site of infection and to enhance the maturation and subsequent migration of DCs[172,173]. Studies have also suggested increased antigen uptake[173,174]. Similar to MF59, is the novel multi-component adjuvant system AS03[146]. As part of the 'Adjuvant System' introduced by GlaxoSmithKline (GSK), this squalene-based o/w emulsion additionally contains α-tocopherol and was licensed in Europe for the pandemic flu vaccine Prepandrix® in 2008[140].

Montanides are a new generation emulsion-type adjuvant system and were developed following the safety issues of IFA[175,176]. Montanide®ISA51 and Montanide®ISA720 are currently undergoing clinical trials for use in humans (**Table 1-1**) and details concerning mechanism of action are briefly described in **Section 1.5.2**.

1.5.1.3 MPL

MPL (3-*O*-desacyl-4′-monophosphoryl lipid A) is a detoxified derivative of *Salmonella minnesota* lipopolysaccharides (LPS)[148], an endotoxin typically found in the cell wall of Gram-negative bacteria. **Figure 1-7** shows the chemical structure of MPL which is a β-1′-6-linked diglucosamine bearing seven fatty acids[177].

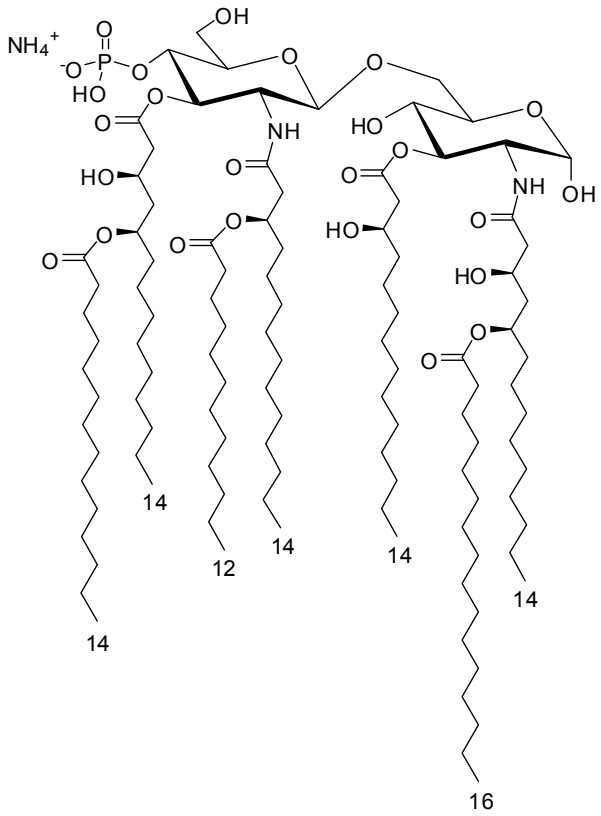


Figure 1-7. Chemical structure of *Salmonella minnesota* MPL.

The inflammatory activity of LPS is mediated through TLR-4 binding[178,179]. Similarly, reports suggested that MPL induces immunostimulation by signalling through TLR-4[148,180]. Studies have shown that MPL polarises towards Th1-type immune responses by enhancing associated INF-γ production[180]. MPL has been formulated in combination with liposomes (AS01), in an o/w emulsion (AS02), and in combination with a QS21, a purified component of Quil A, and alum (AS04). AS04 has recently been approved in Europe and the USA for use in vaccines against human papilloma virus (Cervarix®)[181] and hepatitis B (Fendrix®)[182]. Although a synergistic effect was thought to be the result from the adsorption of MPL onto alum particles, it was shown that alum improved the adjuvanticity of MPL by physically stabilising MPL in the vaccine formulation and by retaining MPL and the antigen at the injection site[180].

1.5.1.4 Liposomes

Liposomes were first described by Bangham *et al.*[183] and have been extensively studied as drug[184] and vaccine delivery systems[151] since their discovery in 1965. Liposomes are colloidal structures which form upon dispersion of amphiphilic substances (that have a polar head group and non-polar hydrocarbon chains) in excess aqueous solution[185]. The assemblies can consist of single or multiple lipid bilayers alternating with aqueous compartments enclosing an aqueous core (**Figure 1-8**). Depending on their size and structural properties, liposomes can be generally divided into small unilamellar vesicles (SUV), multilamellar vesicles (MLV) and large unilamellar vesicles (LUV)[186]. Typically, they are prepared from phospholipids such as phosphatidylcholine, 1,2-distearoylphosphatidylcholine (DSPC), 1,2-dioleoylphosphatidylethanol-amine (DOPE) or dimethyldioctadecylammonium (DDA)[186]. Their ability to entrap hydrophilic and lipophilic drugs within the aqueous structures or lipid compartments, respectively make them extremely versatile as delivery systems[187]. Furthermore, based on electrostatic interactions, molecules such as negatively charged proteins or nucleic acid may be adsorbed onto the surface of cationic liposomes.

The composition of the liposomal bilayer plays an important role with regard to physicochemical properties such as vesicle stability and the retention of encapsulated drugs. The membrane stability is greatly influenced by the temperature at which the amphiphiles used, change from the tightly ordered crystalline gel structure to the liquid-crystalline phase[188]. This temperature is referred to as the main phase transition temperature T_m. The hydrocarbon chains are randomly oriented and fluid above the T_m and molecules show a greater movement[185]. Amphiphiles with higher T_m which are associated with increased hydrocarbon length and higher chain saturation, may be selected in

order to design liposomes with an improved membrane rigidity[185,189] The thermotropic behaviour of lipids is further discussed in **Section 4.1.4.**

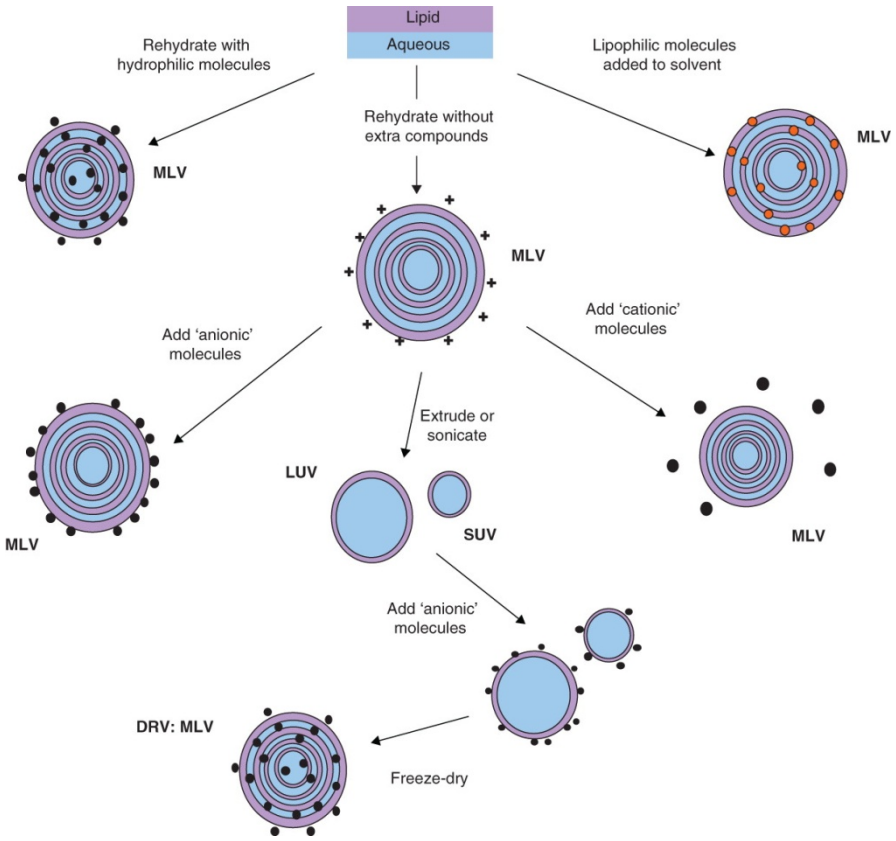


Figure 1-8. Liposomes and their versatile structures. Details are described in the text below. Figure was adapted from Henriksen-Lacey *et al.*[190].

The inclusion of cholesterol at low concentrations (< 30 mol%) into lipid bilayers further enhances membrane stability and fluidity[186,188] and has been shown to reduce membrane permeability *in vitro* and *in vivo*[191]. Cholesterol can be accommodated into spaces formed between the phospholipid molecules and subsequently improves lipid packing[192,193]. Steric repulsion can also improve liposome stability and is achieved by insertion of charged lipids into the bilayer[194]. Numerous studies have investigated the fate of liposome formulations *in vivo* post administration. Following systemic application, the blood circulation and *in vivo* clearance are affected by liposome size and surface charge[186,195,196]. Hence, these properties also determine interactions with immune

cells and the pharmacokinetics of entrapped drugs[196-198]. Generally, removal from blood circulation increases with increased vesicle size. Larger vesicles may be cleared rapidly by opsoninization and subsequent phagocytosis, by cells of the reticuloendothelial system (RES)[196]. Interactions with plasma proteins and enzymes result in relatively fast degradation of lipid bilayers. This destabilisation also leads to leakage of the encapsulated therapeutic agents[196,198].

With respect to delivery of active agents, **Chapter Four** further discusses the physical characterisation and stability of modified PC-based liposomes.

Preparation of liposomes

Various approaches are available for the preparation of liposomes. These can be categorised based on methods where liposomes are prepared by forming new bilayer structures or by altering existing bilayers[186]. The thin film method of Bangham *et al*.[183] was used in this thesis to produce liposomes and fits into the first category. A lipid film is deposited onto the inner surface of a glass flask from an organic phase using solvent evaporation. MLVs are generated by rehydration of the lipid film with an aqueous solution under agitation. Due to a passive loading process during liposome formation, only relatively low drug entrapment is achieved with this technique[199]. However, the amount of encapsulated hydrophilic drug can be increased by using methods such as freeze-thawing, where the liposome suspensions are subjected to consecutive cycles of freezing and thawing[200]. The formed ice crystals induce rupture of the liposomal membranes and subsequently the vesicles reassemble upon thawing. Freeze-thawing may improve incorporation of hydrophilic drugs, by forcing apart closely associated lipid bilayers and expanding the aqueous compartment [200]. Using other techniques such as reverse-phase evaporation (REV)[201], bilayers

are prepared by combining an aqueous solution of the drug with an organic phase containing the drug. Solvent removal from the resultant emulsion produces LUVs with moderate entrapment[199]. Liposomes prepared by these methods are large, and heterogeneous in size and lamellarity. Repeated extrusion of liposomes suspensions, through polycarbonate membranes under high pressure, is commonly used to produce liposomes with a homogeneous particle size distribution and reduced lamellarity[202]. By using well-defined pore sizes (80-800 nm) specific sizes of liposomes can be achieved. Further techniques for size reduction are sonication, microfluidization and high-pressure homogenisation[199].

Methods for producing liposomes by altering existing bilayers include the preparation of SUVs from MLV using sonication. This disrupts the bilayer structures and generates smaller vesicles. Liposomes prepared by this method show low drug encapsulation. Higher entrapments can be achieved using dehydration–rehydration vesicles (DRV), whereby a suspension of ''empty'' SUV is mixed with an aqueous solution containing the drug to be entrapped[203]. Subsequent freeze-drying and hydration induces encapsulation of the drug into the formed MLVs.

An approach for active loading of liposomes uses ion gradients across the lipid bilayer. A drug is added to empty preformed liposomes and passively diffuses into the aqueous core. Once inside the liposomes, trapping of the drug can occur either through the drug becoming charged due to the internal liposomal pH, or through a change in solubility resulting in drug precipitation[199].

Liposomal adjuvants

Besides being a drug and antigen delivery system, liposomes can also exert specific adjuvant activities. Allison and Gregoriadis[151] first reported that antigens when entrapped in liposomes were able to stimulate increased antibody titres, compared to free antigens, in a murine model. Incorporation into vesicles may provide protection of the antigen from enzymatic degradation following administration. Thus, liposomes indirectly potentiate immune responses, by efficiently delivering antigens to APCs and enhancing interactions between antigens and these immune cells[157]. However, a result of using mainly naturally-derived phospholipids for liposomes preparation is that the vesicles are non-toxic and biocompatible, exerting a low immunogenicity[204]. Fortunately, their extremely flexible structure allows for incorporation of immunostimulatory components for the purpose of exerting appropriate immune responses to liposome-associated antigens[187]. Studies have further indicated that specific cells can be targeted by modification of the liposome surface[205,206]. As mentioned above, DCs express PRRs to recognise pathogen-associated molecular patterns (PAMP). Therefore, liposomes offer the potential to target designated cell types, by incorporating specific ligands which mimic pathogen-related structures. Different ligands such as peptides, oligonucleotides or carbohydrates may be displayed on the surface of liposomes to further enhance the resulting immune response[205,207]. For instance, the inclusion of mannosylated dipalmitoylphosphatidylethanolamine (DPPE) into the bilayer of PC-based liposomes (20%, w/w), significantly increased the uptake by monocyte derived dendritic cells (Mo-DC) *in vitro*[206]. This was thought to be mediated through an increased affinity for the mannose receptors (MRs) expressed on these cells.

Currently, lipid vesicle-based vaccines against and influenza (Inflexal® V) and HAV (Epaxal®) have been licensed in Europe which were developed by Crucell (The Netherlands)[140,156]. Both adjuvants are composed of purified viral antigens intercalated within the phospholipid bilayer, forming so-called virosomes[208].

Studies have shown that cationic liposomes are more potent in stimulating the immune response then anionic and neutral liposomes[196,209]. Due to their positive charge, they can interact with negatively charged membranes and deliver the antigen to APCs. Additionally they cause cell damage at site of injection[209]. Various cationic systems have been evaluated for vaccine delivery, including 1,2-dioleoyl-3-trimethylammonium-propane (DOTAP) and DDA. A combination of DDA and synthetic mycobacterial cord factor (TDB) was found to be an effective immunopotentiator. Cellular and humoral immune responses could be induced *in vivo*, as well as high levels of INF-γ and IgG2[149,210,211]. CFA01, composed of DDA/TDB (5:1 w/w) liposomes, is currently being tested in phase I clinical trials against tuberculosis[190].

1.5.2 Adjuvants in clinical development

Montanides

Montanides are w/o emulsions stabilised by the surfactant mannide-monooleate. Adjuvant formulations derived from this type of emulsion include Montanide®ISA51, based on a mineral oil, and Montanide®ISA720, which contains vegetable-based oil (Seppic, Paris, France). Both systems are currently undergoing evaluations in clinical studies for use in malaria, HIV and cancer vaccines[158] (**Table 1-1**). Montanides act as adjuvant via sustained release of antigens from the oily deposit at the injection site, which is not achieved with o/w emulsion types such as MF59[175,176]. The mechanism of action of montanides

has further been attributed to recruitment of immune cells, and enhanced antigen uptake through interactions between the surfactant and cell membranes. High levels of Th1–type antibodies as well as cytotoxic immune response are stimulated[175].

Saponins

Saponins are triterpene glycosides found in plants, including in the bark of *Quillaja saponaria* Molina, a tree native to Chile. Saponins have been long known to be immunostimulatory and saponin-based adjuvants such as Quil A and its semi-purified component QS-21 have been assessed in several immunisation studies[212,213]. Partially purified fractions of Quil A combine different saponins varying in their cytotoxicity and adjuvanticity. Major drawbacks arise from their surfactant activity, which may cause lysis of cell membranes (haemolytic effect). However, reports suggested that this pore-forming ability may be involved in the mechanism of action, by promoting the antigen uptake into APCs, and subsequent induction of high antibody titres and cell-mediated immune responses. Due to its bias towards a Th1 immune response, it can be used for intracellular pathogens. Quil A as well as QS21 (in combinations AS01 and AS02, **Table 1-1**) have been investigated in vaccine formulations for viral infections, leishmaniasis, HIV, malaria and therapeutic cancer vaccines[213].

Quil A is also a component of immune-stimulating complexes (ISCOMs). The idea of combining a particulate system with the Quil A adjuvant was originally reported in 1982. These complexes are formed spontaneously when cholesterol, phospholipid and Quil A are mixed in a certain ratio[152]. Due to high content of Quil A in these mixtures, the lipid bilayer structures are ruptured and open,

cage-like structures with a highly negative surface charge are formed. Studies demonstrated that ISCOMs increased both Th1- and Th2-mediated immune responses[214]. However, a drawback associated with this adjuvant system is that antigens need to be incorporated into the lipid network and thus antigen modifications may be necessary[157].

Immunostimulatory nucleic acids

Unmethylated CpG oligodeoxynucleotide sequences (ODN) derived from bacterial DNA or synthetic analogues, elicit Th1-dominated immune responses[150]. They stimulate B cells and DCs in a TLR-9 dependent pathway, leading to secretion of pro-inflammatory cytokines (TNF-α, IL-1 and IL-6) as well as Th1-type associated INF-γ[124]. ODNs have limited biological stability. However, methods have been developed to overcome this issue and enhance bioavailability, for instance via combination with cationic peptides. The promising adjuvant system IC31® consists of antimicrobial cationic peptide $KLKL_5KLK$ and ODN1a[215]. Immunostimulating properties are attributed to both components, whereby $KLKL_5KLK$ induces a Th2 immune response[216] and the TLR-9 ligand ODN1a generates a cellular and humoral Th1 immune response[217]. An advantage is that with the combination of these synthetic compounds reactogenicity is reduced. IC31® is currently being evaluated in clinical studies with the mycobacterial fusion protein Ag85B-ESAT-6[218,219].

1.5.3 Emerging adjuvants

The adjuvant activity exerted by *Mycobacterium* was originally demonstrated with complete Freund's adjuvant (CFA), though due to toxicity issues it is not suitable for use in humans. However, a number of purified components from the mycobacterial cell wall have been shown to induce potent immune

responses. The glycolipid trehalose-6,6-dimycolate (TDM, also known as cord factor) and its synthetic analogue trehalose-6,6-dibehenate (TDB) are strong Th1 adjuvants[149,211]. As mentioned above, TDB is being assessed as a component of DDA liposomes. Interestingly, the immune stimulation induced by this formulation was independent of TLR signalling. A possible signalling through the Syk–Card9 pathway was proposed, resulting in high levels of Th17[209,220]. Comparable to the activity of TDB, was that of native monomycoloyl glycerol (MMG), isolated from *M. bovis* BCG[221]. Delivered as liposome-based vaccine formulations, MMG and its synthetic analogues enhanced Th1-type immune responses *in vivo*[221-223].

Signalling through TLR-2 and TLR-4 has been suggested for certain mycobacterial glycolipids. For instance, native and synthetic PIMs such as PIM_2 and PIM_4 were found to stimulate cytokines and induce inflammatory response *in vitro* and *in vivo*, in a TLR-dependent manner[21,79,90,224,225]. A synthetic PIM_2 combined with the model antigen Ag85B-ESAT-6, decreased numbers of bacteria in the lung when assessed in a bovine tuberculosis model. Furthermore, the treatment induced high levels of INF-γ and other cytokines (TNF-α, IL-2, IL-6) indicative of a Th1 response[226].

Other TLR ligands include imiquimod and resiquimod, which were identified to signal through the endosome TLRs (TLR-7 and TL-7/TLR-8, respectively), provoking polarised Th1 activity. These small molecules are currently being assessed in pre-clinical studies[156].

Taken together, on-going research has revealed a large variety of different adjuvants. However, only a few novel adjuvants have been licensed for use in humans. Acceptability and safety of potential candidates still need to be proven

in clinical and preclinical studies. Particularly interesting are potential mycobacterial TLR agonists. As part of this thesis the immunostimulatory potential of synthetic PIMs in liposomal formulations was investigated (**Chapter Four**).

1.6 Thesis aim

PIMs have attracted great research interest in recent years due to their significant immunomodulatory activity. Numerous studies have examined their biological activities in both *in vitro* and *in vivo* assays and investigated their potential use for the treatment of atopic diseases or as adjuvants to improve the efficacy of vaccines. However, despite extensive research on their bioactivity, current literature provides limited information on molecular characteristics and pharmaceutical properties of PIMs.

Therefore, the aim of this thesis was to investigate how the physical properties of PIMs are impacted by structural modifications, and how this affects biological activity. The main focus was to investigate the influence of varied lipophilicity and head group characteristics on the structure-function relationship. To do this, a library of six related PIMs was produced. The lipophilic nature of these synthetic compounds was varied, by changing the length of the acyl chains of the fatty acid residues (C0, C10, C16 and C18) and the polar head group (inositol versus glycerol based core structure). The impact of these changes on the interfacial behaviour between two dissimilar phases (air/water) was studied in one-component and binary systems. In order to evaluate the structure-function relationship, the suppressive activity of the compounds in a mouse model of allergic asthma was investigated *in vivo*. Furthermore, liposomal delivery systems were developed and a thorough physical characterisation of the particulate formulations was carried out. These

systems were assayed for their ability to activate dendritic cells *in vitro*, followed by an *in vivo* vaccine model, to assess their potential to elicit cell-mediated and humoral immune responses.

Chapter Two

Synthesis of a PIM_2 analogue

2 Synthesis of a PIM_2 analogue

2.1 Introduction

The series of PIMs investigated in this thesis was designed to produce a range of related compounds with varied lipophilicities (**Figure 2-1**). Due to their structural diversity, native PIMs are difficult to isolate in pure form from mycobacterial cell wall extracts. Fortunately, their relatively low molecular weights make them accessible by chemical synthesis. Synthetic strategies have been developed to prepare PIMs based on the structure of the natural components found in the mycobacterial cell wall[224,227-229].

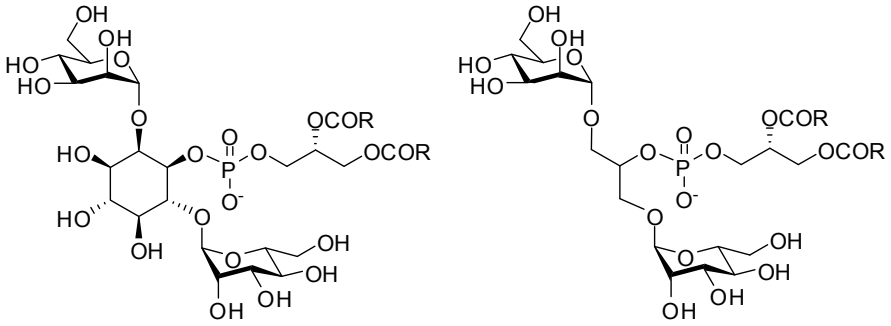


Figure 2-1. Series of PIM compounds investigated in this thesis: structures of phosphatidylinositol dimannoside (PIM_2) **1a**, **1b** and phosphatidylglycerol dimannosides (PGM_2) **2a** - **2d**.

As part of the proposed compound library to be explored, phosphatidylinositol dimannosides (PIM_2) **1a** and **1b** were prepared by members of the Carbohydrate Team at Industrial Research Limited (IRL, Lower Hutt, New Zealand) using previously described methods[224,227]. The ability of compound **1a** to suppress eosinophilia in an allergic airway disease model of asthma had been assessed in an earlier study[227]. Similarly compound **1b**, varying in the fatty

acid residues, was available as it had been studied by Ainge *et al.*[224] for its immunostimulatory activity.

Despite the development of strategies to prepare PIMs, the synthetic routes are difficult and mainly impeded by controlling the stereochemical centres of the *myo*-inositol core of PIMs. As shown in **Figure 2-2**, *myo*-inositol is a *meso* compound with an internal plane of symmetry along the C-2 to C-5 axis. As a result of this symmetry, the hydroxyl groups attached to C-1 and C-3 are identical and cannot be differentiated. The same principle applies to those attached to C-4 and C-6. Functionalization at any of the *O*-1, *O*-3, *O*-4 and *O*-6 positions would result in loss of the plane of symmetry and the formation of pairs of stereoisomers. In the case of an achiral derivatising agent, pairs of enantiomers are produced. Enantiomers are extremely difficult to separate due to the fact that their physical properties are identical in achiral environments.

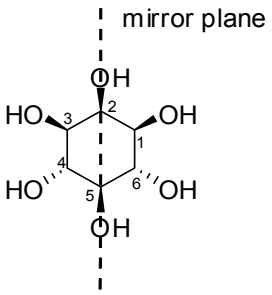
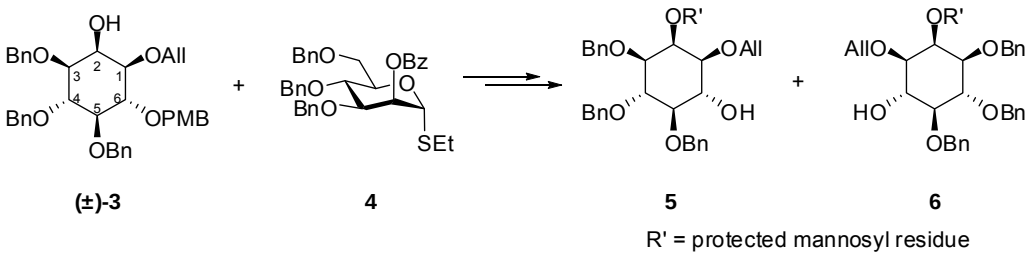


Figure 2-2. Structure of *myo*-inositol core of PIMs.

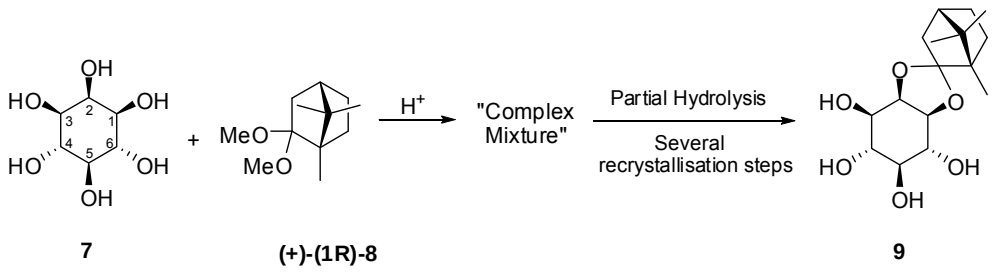
However, several methods have been developed to provide stereoisomerically pure *myo*-inositol derivatives by attaching chiral residues. These methods result in pairs of diastereoisomers which would be more amenable to separation techniques. Elie and colleagues[230] prepared pure diastereoisomers of a *myo*-inositol mannoside as shown in **Scheme 2-1**. Firstly, *myo*-inositol was desymmetrised with achiral reagents to obtain the racemic inositol derivative

(±)-**3**. Subsequent reaction with enantiomerically pure D-mannose **4** afforded a 1:1 mixture of inositol mannosides **5** and **6**. The two diastereoisomers **5** and **6** could be isolated by column chromatography. Unfortunately, the maximum theoretical yield of the desired stereoisomer **5**, which would further be converted into PIM, was 50%[230]. The unwanted isomer **6** was discarded.



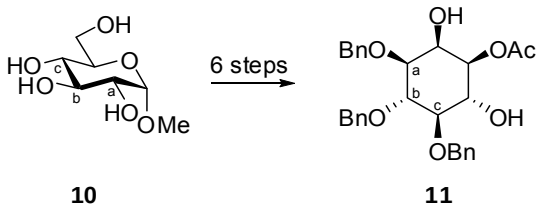
Scheme 2-1. Synthesis of *myo*-inositol derivative by Elie *et al.*[230]. For clarity only one enantiomer is presented for (±)-**3**.

In a desymmetrisation method described by Pietrusiewicz *et al.*[231], L-camphor dimethyl acetal (**8**) was employed to provide the chiral *myo*-inositol derivative **9** (**Scheme 2-2**). Following partial hydrolysis and several recrystallisation steps, **9** was obtained in desired configuration in slightly higher yield compared to the method above[230]. Unfortunately, this procedure was found to give inconsistent results when applied by other research groups[232,233].



Scheme 2-2. Preparation of chiral *myo*-inositol derivative **9** via a method described by Pietrusiewicz *et al.*[231].

An alternative synthetic strategy utilising an enantiomerically pure starting material was developed by Bender *et al.*[234]. This method afforded the chiral *myo*-inositol derivative **11,** via a lengthy synthetic route from commercially available methyl α-D-glucopyranoside **10**[234] (**Scheme 2-3**).



10 **11**

Scheme 2-3. Synthesis of an enantiomerically pure *myo*-inositol derivative by Bender *et al.*[234].

Although this approach demonstrated an effective way of preparing *myo*-inositol derivatives, it required multi-step synthetic sequences to make the chiral inositol starting material available for PIM synthesis.

In order to produce a range of closely related compounds where incremental changes have been made, a series of PIM analogues in which the inositol ring had been replaced by a glycerol unit was proposed for the current study (**Figure 2-3**). These compounds have been referred to as "cutaway PIMs" or phosphatidylglycerol mannosides (PGMs). The replacement of the naturally occurring *myo*-inositol core by a three-carbon glycerol structure, aids the preparation of those compounds, by overcoming the stereochemical issues associated with the *myo*-inositol core. The absence of asymmetric centres in the cutaway core structure of PGMs facilitates their syntheses.

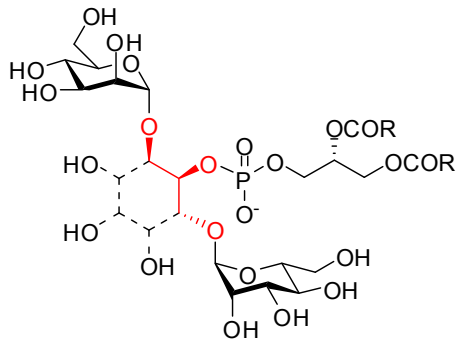
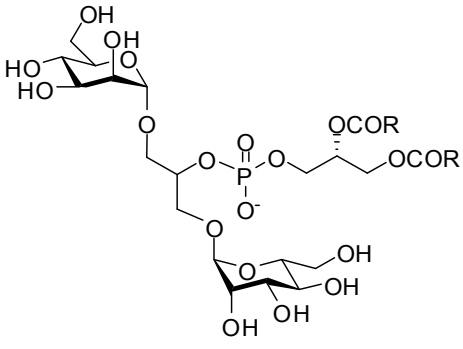


Figure 2-3. Glycerol core structure of phosphatidylglycerol mannosides (PGMs) (highlighted in red). The removal of the C-3, -4 and -5 unit from the *myo*-inositol core gave a symmetrical phosphatidylglycerol mannoside containing a three-carbon glycerol centre.

In earlier work, Singh-Gill *et al.*[235] designed and synthesised PGM_2 **2a**, a structure possessing stearate (C18) fatty acid esters (**Figure 2-4**). This compound maintained immunological activity when tested in an allergic airway disease mouse model[235], comparable to that observed for the bistearate PIM_2 (**1a**). Those findings indicated that the *myo*-inositol core was dispensable for activity, while it is known from other studies that fatty acid residues, along with mannosyl-moieties are essential structural features for biological activity[227,236].



2a PGM_2 (18:18) R= $COC_{17}H_{35}$
2b PGM_2 (16:16) R= $COC_{15}H_{31}$
2c PGM_2 (10:10) R= COC_9H_{19}
2d PGM_2 (0:0) R= H

Figure 2-4. Proposed series of phosphatidylglycerol dimannosides (PGM_2) **2a** - **2d**.

More recently, those results have been verified by Doz and colleagues[96], who reported an elegant way of synthesising a similar molecule, containing a glycerol core which differed only in the fatty acid residues.

2.2 Chapter aim

The phosphatidylglycerol dimannoside (PGM_2) analogues **2a** - **d** (**Figure 2-4**) required for the current study only differ in the acyl residues attached to the phosphatidyl group. PGM_2 **2a** containing two C18 fatty acid residues was available from the study mentioned above[235]. Compounds PGM_2 (0:0) (**2b**) and PGM_2 (16:16) (**2d**) were prepared by modification of this synthetic strategy (Carbohydrate Team, IRL). As part of this project the synthesis of the corresponding PGM_2 (10:10) analogue **2c** was the object of this chapter. The synthetic chemistry used is described in detail below.

2.3 Experimental section

2.3.1 General experimental

2.3.1.1 Nuclear magnetic resonance spectroscopy

^{1}H (400 MHz), ^{13}C (100 MHz), ^{31}P (162 MHz) NMR spectra were recorded on a Varian 400 MR spectrometer in chloroform-d_1 ($CDCl_3$), deuterated water (D_2O) or a mixture of methanol-d_4 and chloroform-d_1 (CD_3OD:$CDCl_3$) standardised against the residual solvent peak (7.26 ppm). ^{1}H (500 MHz), ^{13}C (125 MHz), ^{31}P (202 MHz) NMR spectra were recorded on a Varian 500 MHz Premium Shielded spectrometer in chloroform-d_1 ($CDCl_3$), deuterated water (D_2O) or a mixture of methanol-d_4 and chloroform-d_1 (CD_3OD:$CDCl_3$) standardised against the residual solvent peak (77.08 ppm). Spectra are reported according to

the convention: chemical shift, integrated area, multiplicity, coupling constant, assignment. Proton multiplicities are reported according to appearance as s (singlet), d (doublet), dd (double doublet), ddd (double double doublet), t (triplet), dt (double triplet), ddt (double double triplet), quin (quintet), m (multiplet). Assignments of the proton signals are designated by the attached carbon.

2.3.1.2 Mass spectrometry

High resolution mass spectrometry (HRMS) experiments were conducted using a Bruker microTOFQ (Bruker Daltronics, Bremen, Germany) with an electrospray ionization (ESI) source in either positive or negative mode. Samples are introduced using direct infusion at 180 μL hr^{-1}, Capillary voltage -4500 V, employing a dry gas of N_2 at 180°C, 5 L min^{-1}. Acetonitrile or methanol was utilised as the mobile phase for ESI.

2.3.1.3 Chromatography

Thin layer chromatography (TLC) was performed on Merck TLC aluminum foil coated with a thickness of 0.2 mm silica gel 60 F_{254}. Components were detected using ultraviolet light, acidic vanillin dip, phosphomolybdic acid dip or aqueous phosphomolybdic dip, with subsequent heating.

Column chromatography was accomplished using Merck silica gel 60 (230-400 mesh), which was packed by the slurry method. Solvent systems are expressed as ratios (vol:vol).

High-performance liquid chromatography (HPLC) analyses were carried out on an Agilent 1100 quaternary pump system. Following dilution in water, a

sample volume of 8 μL was injected onto a Phenomenex Synergi Fusion-RP reversed phase column (4 μm, 80 Å pore size, 4.6 x 250 mm). The compounds were eluted using a gradient: solvent A water; solvent B 1:1 MeOH/water containing 50 mM NH_4OAc (pH 5); solvent C MeOH; Program 0-20 min 0-10% B, 70 to 90% C; 20-28 min hold; 30-32 min return to 100% A; 32-40 min equilibrate at 100% A. The flow rate was 1 min mL^{-1} and compounds were detected with an ESA Corona Charged Aerosol detector.

2.3.1.4 Infrared spectroscopy

Infrared spectra were acquired on a Bruker alpha-P FTIR spectrometer for liquid and solid samples. No sample preparation was required. Spectra were recorded against a background of air.

2.3.1.5 Solvents

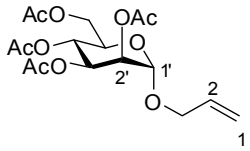
Dry dichloromethane (CH_2Cl_2), diethylether and tetrahydrofuran (THF) were dried using the PURE SOLV MD-6 solvent purification system. Analytical grade methanol (MeOH) was used without purification (Fisher Scientific). All other laboratory grade solvents were used as received.

2.3.1.6 Polarimetry

Optical rotations (specific rotation $[\alpha]_D^T$) were recorded at room temperature (described by T in $[\alpha]_D^T$) on a Jasco DIP-1000 Digital polarimeter using a 100 mm cell with a 3.5 mm aperture at 589 nm (sodium filter). Samples were prepared at the concentration (g 100 mL^{-1}) in the solvent indicated.

2.3.2 Experimental protocol

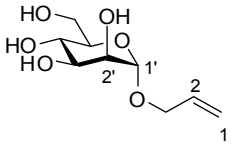
Allyl 2,3,4,6-tetra-*O*-acetyl-α-D-mannopyranoside (13)[235].



13

Penta-*O*-acetyl-D-mannopyranose **12** (5.00 g, 12.81 mmol) was dissolved in dry CH_2Cl_2 (75 mL). Allyl alcohol (4.36 mL, 64.0 mmol) and boron trifluoride diethyl etherate (8.12 mL, 64.0 mmol) were added. The reaction mixture was stirred overnight at RT. The reaction mixture was washed with water, the organic phase dried (anh. $MgSO_4$), filtered and the solvent removed. The residue was purified on silica gel (2:3 EtOAc/PE) to give the title compound **13** (2.5 g, 50%) as a dark orange syrup, which was spectroscopically identical to that reported in the literature[235]. ^{1}H NMR (400 MHz, $CDCl_3$) δ 1.99 (3 H, s), 2.04 (3 H, s), 2.11 (3 H, s), 2.15 (3 H, s), 3.98-4.07 (2 H, m), 4.11 (1 H, dd, *J* = 12.2, 2.3 Hz), 4.18 (1 H, d, *J* = 5.2 Hz), 4.29 (1 H, dd, *J* = 12.2, 5.3 Hz), 4.87 (1 H, s, H-1'), 5.22-5.30 (3 H, m), 5.32 (1 H, d, *J* = 8.2 Hz), 5.38 (1 H, dd, *J* = 10.0, 3.4 Hz), 5.90 (1 H, ddt, *J* = 16.9, 11.4, 5.8 Hz, H-2).

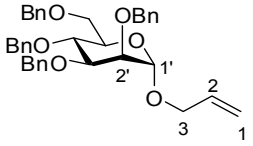
Allyl α-D-mannopyranoside (14)[235].



14

Compound **13** (2.50 g, 6.44 mmol) was dissolved in methanol (50 mL). Sodium carbonate (1.7 g, 16.09 mmol) was added to the solution and the reaction was stirred overnight at RT. The mixture was filtered and the solvent removed under reduced pressure to give title compound **14** (1.84 g, 89%). The spectroscopic data found for compound **14** was identical to earlier reports[235]. ^{1}H NMR (400 MHz, D_2O) δ 3.66-3.71 (2 H, m), 3.79-3.87 (2 H, m), 3.92 (1 H, d, *J* = 12.2 Hz), 3.98 (1 H, dd, *J* = 3.4, 1.8 Hz), 4.11 (1 H, dd, *J* = 12.7, 6.3 Hz), 4.27 (1 H, ddd, *J* = 5.4, 4.9, 1.5 Hz), 4.95 (1 H, dd, *J* = 2.1, 0.7 Hz, H-1'), 5.28-5.44 (2 H, m, H-1), 5.94-6.09 (2 H, m, H-2)

Allyl 2,3,4,6-tetra-*O*-benzyl-α-D-mannopyranoside (15)[235].

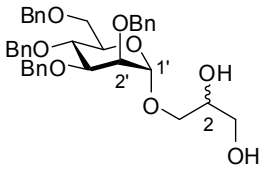


15

Sodium hydride (7.4 g, 154 mmol, 50% by weight) was slowly added to a solution of **14** (5.65 g, 25.7 mmol) in dry DMF (30 mL). The solution was cooled to 0°C under nitrogen and stirred until bubbling stopped. Benzyl bromide (15.5

mL, 128 mmol) was carefully added. The reaction mixture was stirred overnight at RT and then quenched by the addition of water (5 mL). The mixture was diluted with water (300 mL) and extracted into EtOAc. The organic phase was washed with water, brine and dried (anh. $MgSO_4$). Evaporation of the solvent gave a crude material which was purified on silica gel (2:3 PE/CH_2Cl_2 to CH_2Cl_2) to afford title compound **15** (5.9 g, 40%) as a pale yellow syrup. The spectroscopic data for compound **15** was consistent with that reported in literature[235]. ^1H NMR (400 MHz, $CDCl_3$) δ 3.69-3.82 (4 H, m), 3.90-4.03 (3 H, m), 4.12-4.19 (1 H, m, H-1), 4.47-4.79 (7 H, m), 4.88 (1 H, d, *J* = 10.7 Hz), 4.92 (1 H, d, *J* = 1.7 Hz, H-1'), 5.12-5.24 (2 H, m, H-3), 5.84 (1 H, ddd, *J* = 15.5, 10.7, 5.5 Hz, H-2), 7.13-7.41 (20 H, m, Ar-H).

1-*O*-(2,3,4,6-Tetra-*O*-benzyl-*α*-D-mannopyranosyl)glycerol (16)[235].

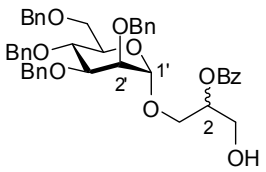


16

Pyranoside **15** (1.00 g, 1.7 mmol) and *N*-methylmorpholine *N*-oxide (0.030 g, 2.58 mmol) were dissolved in mixture of water-acetone (1:9, 40 mL) and 1% aqueous osmium tetroxide solution (1.5 mL) was added. The reaction mixture was stirred overnight at RT, then poured into 10% sodium thiosulfate solution (20 mL) and then extracted with CH_2Cl_2 (40 mL). The organic layer was washed with water and dried (anh. $MgSO_4$). The solvent was removed under reduced pressure and the residue was purified on silica gel (2:3 PE/CH_2Cl_2) to give the title compound **16** (0.800 g, 76%) as a pale yellow oil, which was

spectroscopically identical to that reported in the literature[235]. ^{1}H NMR (500 MHz, $CDCl_3$) δ 3.44-3.55 (1 H, m), 3.56-3.93 (10 H, m), 4.46-4.65 (5 H, m), 4.68-4.78 (2 H, m), 4.82-4.88 (1 H, m), 7.12-7.40 (20 H, m, Ar-H); HRMS-ESI $[MNa]^+$ calculated for $C_{37}H_{42}NaO_8^+$: 637.2772. Found: 637.2825.

2-*O*-Benzoyl-3-*O*-(2,3,4,6-tetra-*O*-benzyl-*α*-D-mannopyranosyl)glycerol (17)[235].

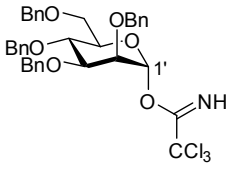


17

The glycerol mannoside **16** (2.44 g, 3.97 mmol) and trityl chloride (2.21 g, 7.93 mmol) were dissolved in dry pyridine (40 mL) then heated at 100°C for 4 hours. The mixture was cooled to 0°C and a solution of benzoyl chloride (1.84 mL, 15.86 mmol) was added. The reaction was allowed to warm up to RT and stirred overnight. The solvent was removed and the residue dissolved in CH_2Cl_2 (100 mL), washed with HCl (2 x 40 mL), water (50 mL) and brine (50 mL). The organic layer was dried over anh. $MgSO_4$, filtered and the solvent removed under reduced pressure. The residue was again dissolved in CH_2Cl_2/MeOH (7:3, 100 mL) and *p*-toluenesulfonic acid (*p*-TSA) (150 mg) was added and stirred for 24 hours at RT. The reaction washed with saturated bicarbonate solution (50 mL), brine, dried (anh. $MgSO_4$) and the solvent removed under reduced pressure. The residue was purified on silica gel firstly using CH_2Cl_2 as eluent until trityl alcohol was removed. The eluent was then changed to 1:9-1:4 EtOAc/CH_2Cl_2 to give the title compound **17** (1.14 g, 47%) as

a yellow syrup, which was spectroscopically identical to that reported in the literature[235]. The polarity of the eluent was increased to EtOAc to regain glycerol glycoside **16** (0.33 g, 14%) as starting material. Data for **17**: ^{1}H NMR (500 MHz, $CDCl_3$) δ 3.62-4.01 (11H , m), 4.45-4.75 (7H , m, $PhCH_2$), 4.93 (0.5 H, d, *J* = 2.0, H-1'), 4.89 (0.5 H, d, *J* = 2.0, H-1'), 5.22 and 5.27 (each 0.5 H, quin, *J* = 5.0, H-2), 7.11-7.37 (20H, m, Ar-H), 7.54 (1H, ddd, *J* = 2.2, 1.7, 1.1 Hz, H-4'' of Bz), 8.01-8.04 (2H, m, H-2'',6'' of Bz); HRMS-ESI $[MNa]^+$ calculated for $C_{44}H_{46}NaO_9^+$: 741.3034. Found: 741.3081.

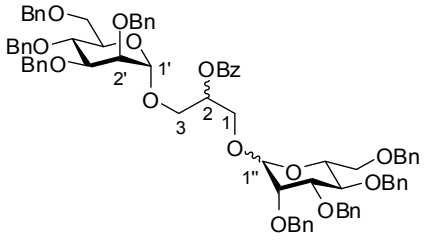
2,3,4,6-Tetra-*O*-benzyl-α-D-mannopyranosyl trichloroacetimidate (19)[237].



19

2,3,4,6-Tetra-*O*-benzyl-*D*-mannopyranose **18** (0.536 g, 0.991 mmol) was dissolved in dry CH_2Cl_2 (20 mL) and cooled to 0°C under nitrogen atmosphere. Trichloroacetonitrile (994 μL, 9.91 mmol) and diazabicycloundecene (DBU) (150 μL, 0.991 mmol) were added and the reaction stirred for 60 min. The solvent was removed and the residue was purified on silica gel (1:2 EtOAc/PE) to give title compound **19** (0.669 g, 99%). The spectroscopic data for compound **19** was consistent with earlier reports[237]. ^{1}H NMR (400 MHz, $CDCl_3$) δ 3.73 (1 H, dd, *J* = 11.2, 1.8 Hz), 3.79-4.01 (4 H, m), 4.14 (1 H, dd, *J* = 11.7, 4.4 Hz), 4.50-4.71 (5 H, m), 4.77 (1 H, s), 6.37 (1 H, d, *J* = 2.0 Hz, H-1'), 7.17-7.44 (20 H, m, Ar-H), 8.52 (1 H, s, NH).

2-*O*-Benzoyl-1,3-*bis*-*O*-(2,3,4,6-tetra-*O*-benzyl-D-mannopyranosyl) glycerol (20)[235].

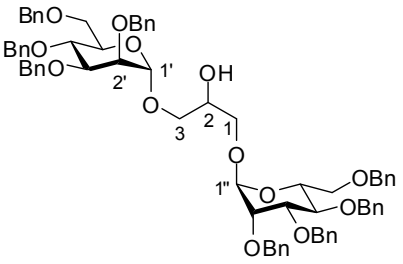


20

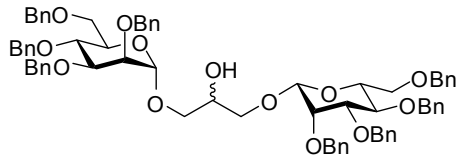
TMSOTf (15.00 μL, 0.083 mmol) was added drop wise to a stirred solution of glycerol **17** (600 mg, 0.835 mmol) and trichloroacetimidite **19** (740 mg, 1.08 mmol) in dry ether (30 mL) cooled to -42°C. The reaction mixture was stirred and allowed to warm up to 0°C. The reaction was monitored regularly by silica TLC (1:2 EtOAc/PE) after it had warmed up to -10°C. Following stirring overnight at RT the reaction was quenched with Et_3N (700 μL, 4.99 mmol). The mixture was filtered through Celite and the filter cake further washed with ether. The solvent was evaporated under reduced pressure and the obtained crude material was purified on silica gel (4:1-3:1-2:1 EtOAc/PE) to afford the title compound **20** (0.800 g, 78%, 4:1 mixture of α,α and α,β-diastereoisomers) as a yellow syrup. The spectroscopic data found for compound **20** was identical to earlier reports[235]. Data for **20**: ^{1}H NMR (500 MHz, $CDCl_3$) δ 3.50–4.13 (16H, m), 4.42–4.52 (4H, m), 4.55–4.65 (4H, m), 4.69 (2H, d, *J* = 12.5 Hz, PhCH2), 4.72 (2H, d, *J* = 12.5 Hz, PhCH2), 4.82 (2H, d, *J* = 11 Hz, PhCH2), 4.86 (2H, d, *J* =11 Hz, PhCH2), 4.91 (1H, d, *J* = 2 Hz), 4.96 (1H, d, *J* = 2 Hz), 5.33–5.38 and 5.41–5.53 (1H, 2 x m, H-2'), 7.08–7.38 (42H, m, Ar-H), 7.55 (1H, t, *J* = 7.7 Hz), 8.00 (2H, d, *J* = 7.7); ^{13}C NMR (125 MHz, $CDCl_3$) δ 65.5, 65.9, 69.1, 69.2, 71.4, 72.2, 72.3, 72.4, 72.65, 72.68, 73.38, 73.42, 74.7, 74.8, 74.9, 75.0, 75.1, 79.9, 80.0, 97.7,

98.4, 127.52, 127.60, 127.63, 127.73, 127.76, 127.78, 127.81, 127.87, 127.92, 128.03, 128.29, 128.33, 128.35, 128.41, 128.5, 129.8, 130.0, 133.2, 138.35 138.42, 138.43, 138.5, 138.5, 138.6, 165.9; HRMS-ESI (+ve) $[MNa]^+$ calculated for $C_{78}H_{80}NaO_{14}^+$: 1263.5440. Found: 1263.5363.

1,3-Bis-*O*-(2,3,4,6-tetra-*O*-benzyl-*α*-D-mannopyranosyl)glycerol (21)[235].



21



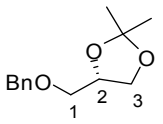
22

The dimannoside **20** (800 mg, 0.644 mmol) was dissolved in 1 M sodium methoxide (80 mL) (2.3 g of Na metal dissolved in 100 mL methanol). Additionally CH_2Cl_2 (20 mL) was added to enhance the solubility of **20**. The reaction was stirred overnight at RT. The solvent was reduced to one third of the initial volume, diluted into water and extracted with CH_2Cl_2. The aqueous phase was back extracted several times. The combined organic phases were washed with 1M HCl (80 mL), water (80 mL) and dried over anh. $MgSO_4$. The solvent was evaporated under reduced pressure and the residue purified on

silica gel (3:1-2:1-3:2 EtOAc/PE) to give the title compound **21** (0.328 g, 45%) and **22** (0.091 g, 12%), both as a colorless syrup. The spectroscopic data for compound **21 and 22** were consistent with earlier reports[235]. Data for **21** (α,α isomer): $[\alpha]_D^{20}$ +22 (c 0.21, CH_2Cl_2); ν_{max}cm^{-1} 3438 *br* (OH stretch); ^{1}H NMR (500 MHz, $CDCl_3$) δ 2.79 (1 H, d, *J* = 4.2 Hz, OH), 3.44 (1 H, dd, *J* = 10.6, 7.1 Hz), 3.51 (1 H, dd, *J* = 10.9, 4.1 Hz), 3.56 (1 H, dd, *J* = 10.9, 5.9 Hz), 3.60 (1 H, dd, *J* = 10.6, 4.3 Hz), 3.67-3.80 (8 H, m), 3.85 (2 H, dt, *J* = 9.2, 3.2 Hz), 3.86-3.91 (1 H, m, H-2), 3.94 (1 H, d, *J* = 9.4 Hz), 3.98 (1 H, d, *J* = 9.4 Hz), 4.46-4.53 (4 H, m), 4.57-4.65 (6 H, m), 4.69 (2 H, d, *J* = 12.4 Hz, H-1'), 4.74 (2 H, d, *J* = 12.4 Hz, H-1''), 4.82-4.88 (4H, m), 7.12-7.39 (43 H, m, Ar-H); ^{13}C NMR (125 MHz, $CDCl_3$) δ 69.20, 69.22, 69.41, 69.60, 69.98, 72.22, 72.24, 72.31, 72.35, 72.74, 73.40, 73.42, 74.90, 74.95, 75.06, 75.12, 80.02, 80.06, 98.73, 98.89, 127.53, 127.56, 127.65, 127.66, 127.67, 127.70, 127.81, 128.03, 128.34, 128.35, 128.37, 128.39, 138.32, 138.42, 138.49; HRMS-ESI (+ve) $[MNa]^+$ calculated for $C_{17}H_{76}NaO_{13}$: 1159.5178. Found: 1159.5228.

Data for **22** (α,β isomer): ^{1}H NMR (500 MHz, $CDCl_3$) δ 3.58-3.42 (1H, m), 4.00-3.64 (16H, m), 4.76-4.44 (15H, m), 4.92-4.83 (2H, m), 5.04 (1H, d, *J* = 2 Hz, H-1'), 7.34-7.16 (40H, m, Ar-H); ^{13}C NMR (125 MHz, $CDCl_3$) δ 61.69, 67.03, 69.29, 72.23, 72.36, 72.38, 72.40, 72.71, 72.78, 73.46, 74.88, 74.92, 74.96, 75.11, 75.17, 79.95, 80.14, 97.7, 98.6, 98.6, 127.55, 127.59, 127.66, 127.69, 127.76, 127.84, 127.92, 127.97, 128.06, 128.08, 128.14, 128.18, 128.22, 128.37, 128.40, 138.23, 138.26, 138.30, 138.36, 138.42, 138.50, 138.53; HRMS-ESI (+ve) $[MNa]^+$ calculated for $C_{17}H_{76}NaO_{13}$: 1159.5178. Found: 1159.5101.

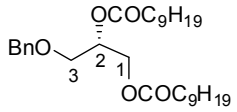
3-*O*-Benzyl-1,2-*O*-isopropylidene-*sn*-glycerol (24)[238].



24

(*S*)-(+)-1,2-*O*-isopropylidene-*sn*-glycerol **23** (5.123 g, 38.8 mmol) was dissolved in dry DMF (50 mL) under argon at RT. The flask was immersed in a water bath at RT and NaH (2.89 g, 50% dispersion in oil, 60.2 mmol) was added portion wise. Benzyl bromide (BnBr) was added (6.75 mL, 56.8 mmol), the water bath removed after 5 min and the reaction stirred for 72 hours. The reaction was quenched with the addition of 2 M NaOH (10 mL) and diluted into ether (200 mL) and water (300 mL). The aqueous phase was back extracted with ether (100 mL) and the combined ether phases were washed with water (3 x 150 mL). The organic phase was dried over anh. $MgSO_4$ and the solvent removed under reduced pressure. The residue was purified on silica gel (initially PE, followed by 1:19-1:9-1:4-2:3 EtOAc/PE) to give title compound **24** (8.290 g, 96%), which was spectroscopically identical to that reported in the literature[238]. ^{1}H NMR (500 MHz, $CDCl_3$) δ 1.37 (3 H, d, *J* = 0.5 Hz, CH_3), 1.42 (3 H, d, *J* = 0.5 Hz, CH_3), 3.48 (1 H, dd, *J* = 9.8, 5.6 Hz, H-1), 3.56 (1 H, dd, *J* = 9.8, 5.7 Hz, H-1), 3.75 (1 H, dd, *J* = 8.3, 6.3 Hz, H-3), 4.06 (1 H, dd, *J* = 8.3, 6.4 Hz, H-3), 4.27-4.34 (1H, m, H-2), 4.56 (1 H, d, *J* = 12.1 Hz), 4.60 (1 H, d, *J* = 12.1 Hz), 7.23-7.38 (5 H, m, AR-H); ^{13}C NMR (125 MHz, $CDCl_3$) δ 25.46, 26.84, 66.95, 71.16, 73.59, 74.81, 109.47, 127.78, 127.80, 128.46, 138.03.

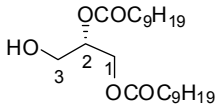
3-*O*-Benzyl-1,2-di-*O*-decanoyl-*sn*-glycerol (25).



25

A mixture of **24** (2.008 g, 9.03 mmol), decanoic acid (3.141 g, 18.23 mmol) and *p*-toluenesulfonic acid monohydrate (0.15 g, 0.789 mmol) was heated at 120°C (oil bath) for 3 hours. The reaction flask was left uncovered to evaporate water and acetone formed in the reaction. The residue was dissolved in CH_2Cl_2 and purified on silica gel (0.5:9.5-1:9 EtOAc/PE) to give title compound **25** (2.478 g, 66%); $[\alpha]_D^{22}$ +5.1 (c 1.63, CH_2Cl_2); $\nu_{max}cm^{-1}$ 1739 (ester CO); 2853, 2922 (CH stretch); ^{1}H NMR (400 MHz, $CDCl_3$) δ 0.88 (6H, t, *J* = 6.9 Hz, 2 x CH_3), 1.25-1.30 (24 H, m), 1.54-1.67 (4 H, m), 2.25-2.34 (4 H, m), 3.59 (2 H, dd, *J* = 5.2, 1.1 Hz, H-3), 4.19 (1 H, dd, *J* = 11.9, 6.4 Hz, H-1), 4.34 (1 H, dd, *J* = 11.9, 3.8 Hz, H-1), 4.52 (1 H, d, *J* = 12.1 Hz), 4.56 (1 H, d, *J* = 12.1 Hz), 5.21-5.27 (1 H, m, H-2), 7.23-7.38 (5 H, m, Ar-H); ^{13}C NMR (100 MHz, $CDCl_3$) δ 14.06, 22.64, 24.84, 24.86, 24.88, 24.93, 29.03, 29.06, 29.08, 29.09, 29.24, 29.25, 29.26, 29.36, 29.41, 31.84, 34.01, 34.07, 34.17, 34.20, 34.29, 62.05, 62.15, 62.61, 62.87, 68.24, 68.87, 69.99, 73.26, 127.52, 127.57, 127.61, 127.71, 128.36, 128.40, 129.53, 129.66, 133.19, 137.71, 165.91, 172.76, 172.81, 172.99, 173.16, 173.19, 173.28; HRMS-ESI (+ve) $[MNa]^+$ calculated for $C_{30}H_{50}NaO_5$: 513.3550. Found: 513.3546.

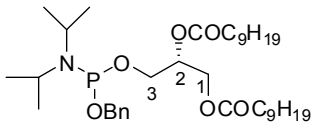
1,2-Di-*O*-decanoyl-*sn*-glycerol (26).



26

Compound **25** was suspended in HOAc/EtOH 1:10 (25 mL). Pd/C (10%, 0.171 g) was added and the reaction mixture was stirred under an atmosphere of hydrogen for 3 hours at RT. The hydrogen atmosphere was removed, the mixture was filtered through Celite and the solvent was removed. The residue was purified on silica gel (2:8 EtOAc/PE) to give title compound **26** (0.420 g; 85%) as a white solid; $[\alpha]_D^{20}$ -2.6 (c 0.15, CH_2Cl_2); $\nu_{max}cm^{-1}$ 1739 (ester CO); 2853, 2922, 2954 (CH stretch), 3504 *br* (OH stetch); ^{1}H NMR (400 MHz, $CDCl_3$) δ 0.84-0.89 (6 H, m, 2 x CH_3), 1.26 (24 H, m), 1.60 (4 H, dt, *J* = 13.4, 6.5 Hz), 2.31 (4 H, dt, *J* = 8.9, 4.3 Hz), 3.71 (2 H, d, *J* = 4.8 Hz, H-3), 4.21 (1 H, ddd, *J* = 12.0, 5.8, 1.9 Hz, H-1), 4.31 (1 H,dd, *J* = 11.9, 4.4 Hz, H-1), 5.07 (1 H, quin, *J* = 5.0 Hz, H-2); ^{13}C NMR (100 MHz, $CDCl_3$) δ 14.17, 22.74, 24.97, 25.02, 29.16, 29.19, 29.34, 29.50, 31.93, 34.19, 34.37, 61.67, 62.05, 72.19, 173.50, 173.86; HRMS-ESI (+ve) $[MNa]^+$ calculated for $C_{23}H_{44}NaO_5$: 423.3081. Found: 423.3098.

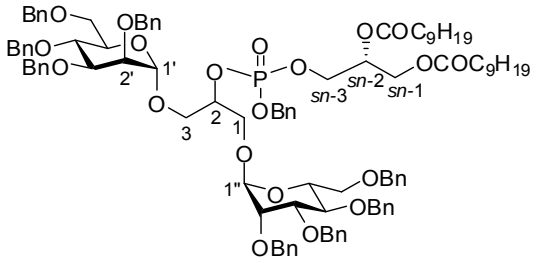
Benzyl 1,2-di-*O*-decanoyl-*sn*-glycero-diisopropylphosphoramidite (28).



28

4,5-Dicyanoimidazole (0.116 g, 0.982 mmol) was added to a stirred solution of compound **26** and benzyloxy-bis-(diisopropylamino)phosphine **27** (0.628 g, 1.855 mmol) in dry CH_2Cl_2 (10 mL). After stirring at RT for 1.5 hours the solvent was removed and the residue purified on silica gel (1:19 Et_3N/PE) to give title compound **28** (0.541 g, 91%) as a colorless oil; $\nu_{max}cm^{-1}$ 1738 (ester CO); 2854, 2924, 2960 (CH stretch); ^1H NMR (500 MHz, $CDCl_3$) δ 0.89 (6 H, t, *J* = 6.9 Hz, 2 x CH_3), 1.18-1.21 (12 H, m), 1.25-1.33 (27 H, m), 1.58-1.65 (5 H, m), 2.30 (4 H, td, *J* = 7.7, 2.0 Hz), 3.59-3.83 (4 H, m), 4.15-4.22 (1 H, m), 4.30-4.39 (1 H, m), 4.63-4.78 (2 H, m), 5.18-5.23 (1 H, m, H-2), 7.25-7.38 (5 H, m, Ar-H); ^{13}C NMR (125MHz, $CDCl_3$) δ 11.03, 14.11, 14.16, 22.73, 23.05, 23.82, 24.58, 24.60, 24.63, 24.66, 24.69, 24.75, 24.97, 24.99, 29.00, 29.18, 29.20, 29.35, 29.50, 30.44, 31.93, 3421, 34.41, 38.81, 43.10, 43.11, 43.19, 43.21, 61.55, 61.68, 61.73, 61.86, 62.55, 62.59, 65.36, 65.39, 65.50, 65.54, 58.22, 70.82, 70.86, 70.88, 70.92, 127.00, 127.34, 127.35, 128.31, 128.32, 128.53, 128.86, 130.93, 173.07, 173.45; ^{31}P NMR (162 MHz, $CDCl_3$) δ 148.70, 148.85; HRMS-ESI (+ve) $[MNa]^+$ calculated for $C_{36}H_{64}NNaO_6P$: 660.4363. Found: 660.4369.

2-*O*-(Benzyl-1,2-di-*O*-decanoyl-*sn*-glycero-3-phosphoryl)-1,3-*bis*-*O*-(2,3,4,6-tetra-*O*-benzyl-α-D-mannopyranosyl)glycerol (29).

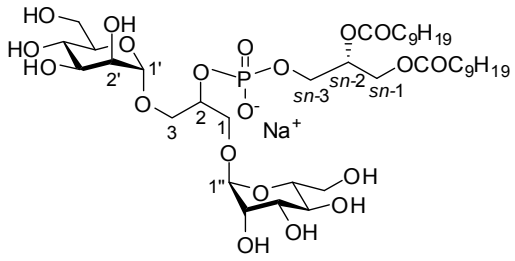


29

Compound **21** (0.033 g, 0.029 mmol) and phosphoramidite **28** (0.116 g, 0.181 mmol) were stripped down together from dry CH_2Cl_2 and evaporated under high vacuum for 90 min. The mixture was dissolved in dry CH_2Cl_2 (5 mL) stored over 4Å molecular sieves at RT and then cooled down in a water/ice-bath. After addition of 4,5-dicyanoimidazole (0.011 g, 0.097 mmol) the cooling bath was immediately removed. The disappearance of **21** and **28** was monitored by TLC (3:7 EtOAc/PE) and after 3 hours a dried (anh. $MgSO_4$) solution of 3-chloroperoxybenzoic acid (50%, 0.053 g, 0.154 mmol) in dry CH_2Cl_2 (~10 mL) was added. After stirring for 30 min, the reaction was diluted with ether (25 mL) and washed with 10% $Na_2S_2O_3$ (25 mL). The aqueous phase was back extracted with ether (25 mL). The combined organic phases were washed with saturated $NaHCO_3$ (3 x 25 mL) and dried over anh. $MgSO_4$. The solvent was removed under reduced pressure and the residue purified on silica gel (1:3-1:2-2:3 EtOAc/PE) to afford the title compound **29** (0.048 g, 56%) as a white solid; $\nu_{max}cm^{-1}$ 1496 (C=C), 1739 (ester CO); 2854, 2923 (CH stretch), 3030 (Ar-CH stretch); ^1H NMR (500 MHz, $CDCl_3$) δ 0.83-0.92 (6 H, m, 2 x CH_3), 0.17-035 (24 H, m), 1.45-1.60 (4 H, m), 2.15-2.27 (4 H, m), 3.50-3.90 (12 H, m), 3.95-4.35 (8 H, m), 4.45-4.80 (12 H, m), 4.82-5.05 (6 H, m), 5.05-5.15 (2 H, m),

6.88-7.58 (45 H, m, Ar-H); ^{13}C NMR (125 MHz, $CDCl_3$) δ 14.16, 22.72, 24.85, 29.12, 29.17, 29.34, 29.49, 29.76, 31.92, 34.00, 34.11, 61.71, 61.75, 69.17, 69.41, 72.06, 72.13, 72.24, 72.27, 72.30, 72.36, 72.41, 72.65, 72.71, 72.73, 72.75, 73.37, 73.42, 74.40, 74.76, 74.88, 75.12, 80.16, 98.63, 127.50, 127.50, 127.57, 127.61, 127.64, 127.65, 127.66, 127.71, 127.74, 127.76, 127.78, 127.82, 128.00, 128.03, 128.07, 128.29, 128.30, 128.32, 128.34, 128.36, 128.37, 128.38,128.67, 128.69, 138.40, 138.41, 138.50, 138.53, 138.56, 172.95; ^{31}P NMR (162 MHz, $CDCl_3$) δ -1.65 (s), -1.39 (s); HRMS-ESI (+ve) $[MNa]^+$ calculated for $C_{101}H_{125}NaO_{20}P$: 1711.8394. Found: 1711.8414.

2-*O*-(1,2-D-*O*-decanoyl-*sn*-glycero-3-phosphoryl)-1,3-bis-*O*-(α-D-mannopyranosyl)glycerol (2c).



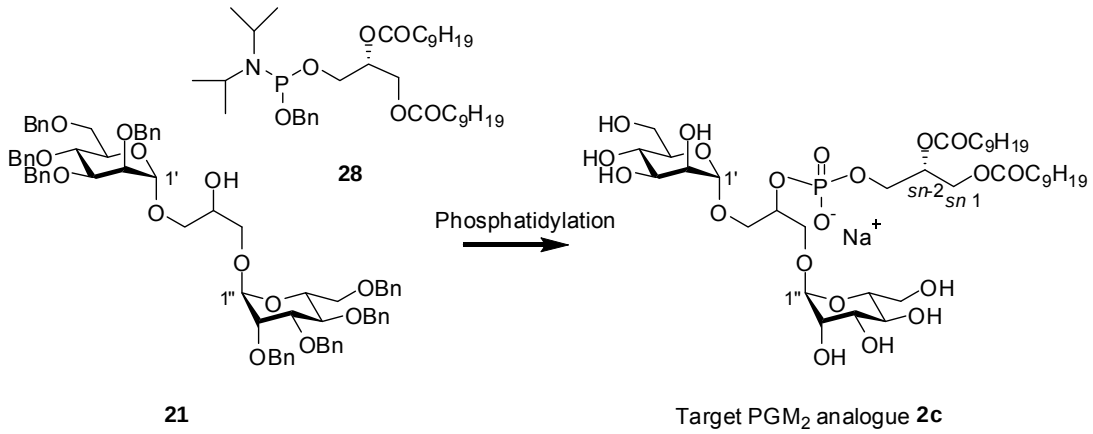
2c

$Pd(OH)_2$/C (20%, 86 mg) was added to a solution of compound **29** (120 mg, 0.071 mmol) in dry THF/MeOH (2:3, 10 mL). The mixture was stirred under hydrogen atmosphere for 4 hours at RT. After removing the hydrogen atmosphere the mixture was filtered through Celite that had been prewashed with dry THF/MeOH (2:3, 100 mL) and the solvent removed. The residue was purified on silica gel (9:1:0–8:2:0–2:1:0.05–2:1:0.1 $CHCl_3$/MeOH/water) to afford the title compound **2c** (45.0 mg, 72%) as a white solid; ν_{max}cm^{-1} 1737 (ester CO); 2852, 2922 (CH stretch), 3315 *br* (OH); ^{1}H NMR (500 MHz, 2:1 $CDCl_3$:CD_3OD)

δ 0.84 (6 H, t, *J* = 6.8 Hz, 2 x CH_3), 1.28 (24 H, m), 1.55 (4 H, s), 2.28 (4 H, dt, *J* = 15.1, 7.5 Hz), 3.50-3.99 (18 H, m), 4.06-4.20 (3 H, m), 4.32-4.46 (3 H, m), 4.85 (2 H, d, *J* = 15.7, 1-H′ and 1-H′′), 5.20 (1 H, s, 2-H); ^{13}C NMR (125 MHz, 2:1 $CDCl_3$:CD_3OD) δ 14.34, 23.06, 25.28, 25.37, 29.57, 29.60, 29.72, 29.75, 29.81, 29.90, 29.93, 30.07, 32.30, 34.51, 34.66, 61.86, 63.23, 64.14, 66.99, 67.80, 70.84, 71.57, 73.16, 73.70, 100.47, 174.3; HRMS-ESI (-ve) $[M-H]^-$ calculated for $C_{38}H_{70}O_{20}P$: 877.4204. Found: 877.4142. The product was stirred with DOWEX 50X8-100 in the sodium form to afford the product as the sodium salt; $[\alpha]_D^{20}$ +38.4 (c 0.12, 70:40:6 $CHCl_3$/MeOH/water); HRMS-ESI (-ve) $[M-Na]^-$ calculated for $C_{38}H_{70}O_{20}P$: 877.4204. Found: 877.4187.

2.4 Synthetic strategy

The proposed synthetic strategy for target molecule PGM_2 (10:10) **2c** included the phosphatidylation of alcohol **21** with phosphoramidite **28** as shown in **Scheme 2-4**. Subsequent global debenzylation of the protected PGM_2 intermediate would provide the desired target **2c**.

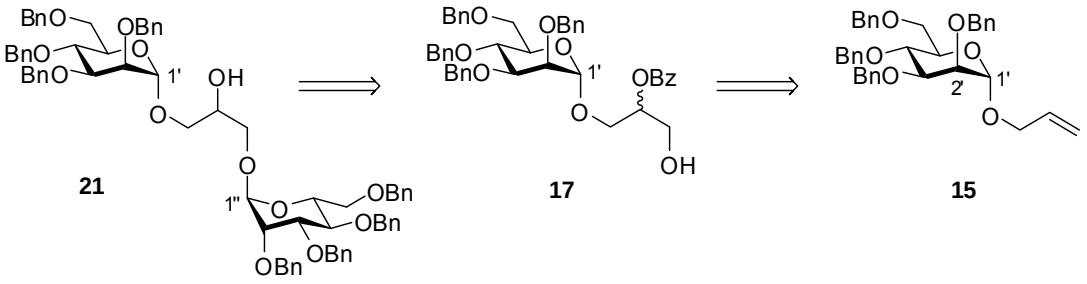


Scheme 2-4. Key intermediate **21** and synthetic approach for the preparation of target molecule PGM_2 **2c**.

Alcohol **21** could serve as a common intermediate for the preparation of various PGM_2 molecules by reaction with glyceryl phosphoramidites containing different fatty acids. The described chemistry had previously been employed by Singh-Gill *et al.*[235] for the synthesis of PGM_2 (18:18). Thus, the initial focus of the synthetic study presented in this chapter was to prepare the two key intermediates, alcohol **21** and phosphoramidite **28**.

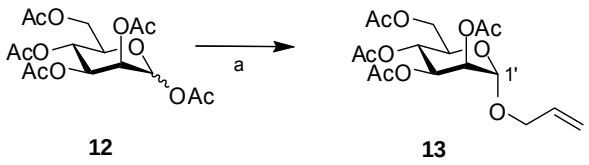
2.4.1 Preparation of alcohol 21

Retrosynthetic analysis revealed that alcohol **21** could be obtained by glycosylation of the protected mannosyl glycerol **17,** followed by debenzoylation (**Scheme 2-5**). Mannosyl glycerol **17** would be attainable from allyl mannoside **15**, by dihydroxylation of the allyl group and selective benzoylation of the secondary alcohol.



Scheme 2-5. Retrosynthesis of alcohol **21**.

The synthesis began with the preparation of acetylated allyl mannoside **13** (**Scheme 2-6**). The readily available per-acetylated mannosyl donor **12** was reacted with allyl alcohol and boron trifluoride diethyl etherate (BF_3Et_2O) to give allyl glycoside **13** in 50% yield.



12 **13**

Reagents and conditions: (a) Allyl alcohol, BF_3Et_2O, CH_2Cl_2 (50%).

Scheme 2-6. Preparation of the allyl glycoside **13.**

^{1}H NMR analysis of the product obtained after purification by column chromatography, revealed four three-proton singlets between δ 1.99-2.15, confirming the presence of four acetyl methyl groups. Furthermore, a one-proton signal typical for a vinylic proton was found at δ 5.90, verifying the successful introduction of the allyl group at the anomeric carbon C-1′. ^{1}H NMR data of **13** was identical to those previously reported in literature, confirming the α-configuration of the newly formed linkage[235]. Formation of 1,2-trans-α-linkages was essential as naturally occurring PIMs incorporate α-D-mannopyranosyl residues. The anomeric stereochemistry of product **13** was controlled by the participating ester group on the mannosyl donor **12**. Protecting groups such as an acetate at C-2′ block the attack of the acceptor molecule from the β-face of the ring, thus favouring the formation of the desired α-configuration (**Figure 2-5**). After loss of the protecting group, a reactive oxocarbenium-ion intermediate (**A**) is formed, which interacts with the acetate at the adjacent C-2′ carbon, to form the stabilised cyclic oxocarbenium ion **B**. Attack of the allyl alcohol preferentially occurs from the least hindered α-face.

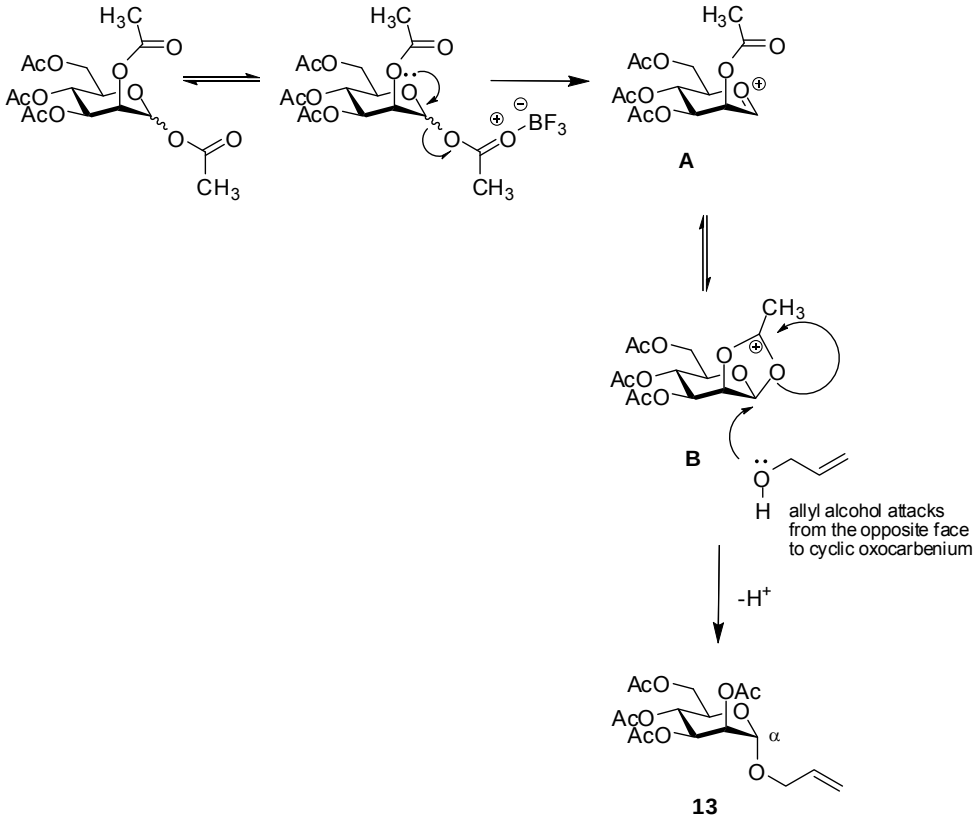
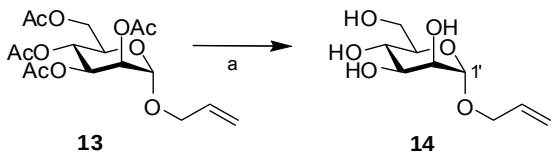


Figure 2-5. Mechanism of formation of the α-allyl mannoside **13**.

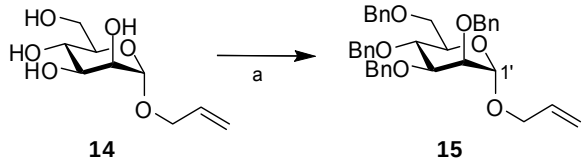
The next step in the synthesis required the removal of the acetate groups of **13**. This was undertaken by reaction with methoxide, produced *in situ* by sodium carbonate suspended in methanol (**Scheme 2-7**). The success of the reaction was confirmed by the ^{1}H NMR analysis of the reaction product **14,** wherein no signals characteristic for acetate groups were detected. The spectroscopic data was identical to those previously reported[235].



Reagents and conditions: (a) Na_2CO_3, MeOH (89%).

Scheme 2-7. Synthesis of **14**.

Following deacetylation, the free hydroxyl groups were benzylated under standard conditions to afford the protected allyl mannoside **15** in 40% yield (**Scheme 2-8**). The ^{1}H NMR spectrum for compound **15** exhibited a 20-proton multiplet at δ 7.13-7.41, indicating the presence of four benzyl groups. All the other signals found were consistent with data reported earlier[235].

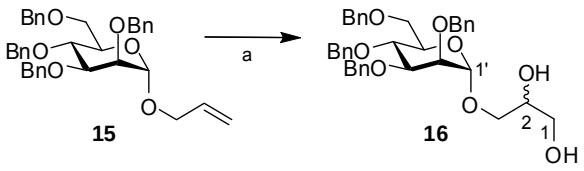


14 **15**

Reagents and conditions: (a) NaH, BnBr, DMF (40%).

Scheme 2-8. Synthesis of the benzylated allyl mannoside **15**.

With the benzylated allyl mannoside **15** completed, the allyl moiety was subsequently converted into a glycerol group in order to produce the core structure of the target **21**. This was accomplished by dihydroxylation of the allyl group in **15,** as shown in **Scheme 2-9**. Allyl mannoside **15** was reacted with a catalytic amount of osmium tetroxide, using *N*-methylmorpholine *N*-oxide as a reoxidant. The glycerol mannoside **16** was obtained in 76% yield as a 1:1 mixture of diastereoisomers about the C-2 carbon.



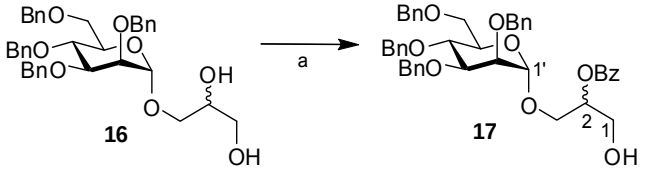
15 **16**

Reagents and conditions: (a) 1% aqueous OsO_4, *N*-methylmorpholine *N*-oxide, 1:9 water/acetone (76%).

Scheme 2-9. Synthesis of the glycerol mannoside **16**.

The high resolution mass spectrum of compound **16** showed a $[MNa]^+$ peak at 637.2825 confirming the molecular formula as $C_{37}H_{42}O_8$. ^1H NMR analysis clearly indicated the absence of the distinctive signals for the allyl unit.

The synthesis of the desired compound **21** required the incorporation of a second mannosyl residue. To ensure the correct regioselectivity during the mannosylation, the secondary alcohol in **16** needed to be protected, leaving the primary alcohol free for reaction with mannosyl donor **19**. This was achieved by tritylation of the primary alcohol with trityl chloride, followed by benzoylating the secondary alcohol using benzoyl chloride (**Scheme 2-10**). Mild acid hydrolysis removed the trityl group giving compound **17** in 47% yield.



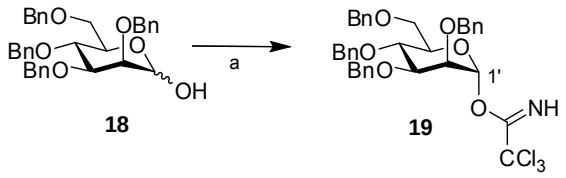
Reagents and conditions: (a) (i) TrCl, pyridine, 100°C, (ii) BzCl, pyridine, (iii) *p*-TSA, 7:3 CH_2Cl_2/MeOH (47%).

Scheme 2-10. Synthesis of the 2-*O*-benzoyl glyceryl glycoside **17**.

HRMS data of the purified product confirmed the molecular formula as $C_{44}H_{46}O_9$. The ^1H NMR spectrum showed the expected signals for the anomeric C-1' protons for both diastereoisomers (δ 4.93 and 4.89), as well as two one-proton signals at δ 5.22 and 5.27, which corresponded to H-2, deshielded by the benzoyloxy group, for each diastereoisomer. Notably evident, was the presence of characteristic peaks of the benzoyl group at δ 7.54 and 8.01-8.04.

The described synthetic route required the preparation of *O*-glycosyl trichloroacetimidate **19**, a well-known and commonly used mannosyl donor[239].

Accordingly, the free anomeric hydroxyl of **18** was reacted with trichloroacetonitrile (Cl_3CCN) in the presence of catalytic DBU[237] to generate the mannosyl donor **19** in 99% yield (**Scheme 2-11**). The one-proton singlet at δ 8.52 in the ^1H NMR spectrum of the purified product was assigned to the proton of the acetimidate group and supported the formation of **19**. Further support was apparent from the absence of the doublet peak at δ 2.48, attributed to the hydroxyl group in starting material **18**.



Reagents and conditions: (a) Cl_3CCN, DBU, CH_2Cl_2 (99%).

Scheme 2-11. Synthesis of the mannosyl donor **19**.

Following the preparation of mannoside **17** and mannosyl donor **19**, glycosylation of the partners could be explored. In general, a glycosylation is performed by coupling an activated glycosyl donor with a glycosyl acceptor (**Figure 2-6**). Sugars with a suitable leaving group (LG) at the anomeric centre can act as glycosyl donor. Activation with an electrophilic agent (E^+, e.g. Lewis acid) promotes the loss of leaving group and results in the electrophilic anomeric carbon. This allows for a nucleophilic attack by the glycosyl acceptor (Nu-H). The facial selectivity (α or β) of the glycosyl acceptor can be modulated by the orientation of protecting groups at C-1′ and C-2′ position of the donor[240].

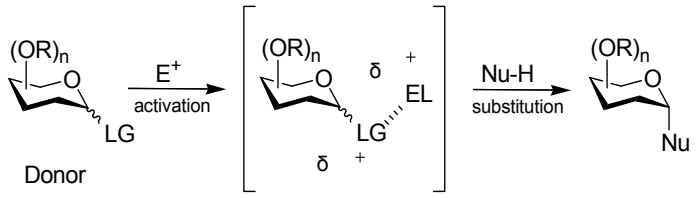
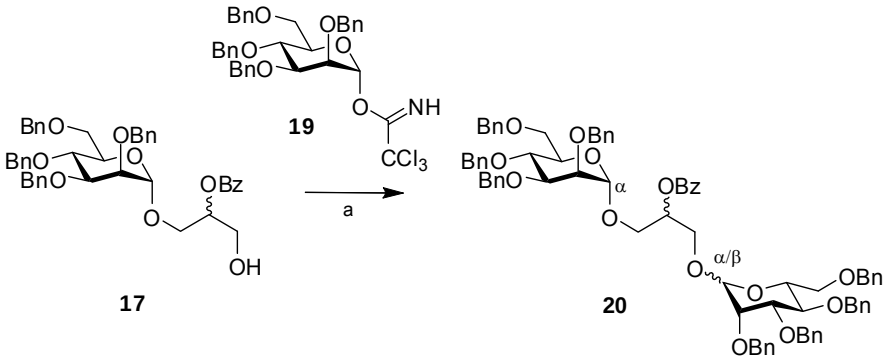


Figure 2-6. The principle of a chemical glycosylation reaction. Figure modified from Galonic *et al*.[240].

Glycosylation of the protected mannosyl glycerol **17** was mediated by trichloroacetimidite **19** (**Scheme 2-12**). Thus, compound **17** was reacted with an excess of *O*-mannosyl trichloroacetimidite **19**, in the presence of catalytic amounts of TMSOTf as the activating agent. The corresponding glycerol mannoside **20** was obtained as a 4:1 inseparable mixture of α,α and α,β-anomers (78% yield).

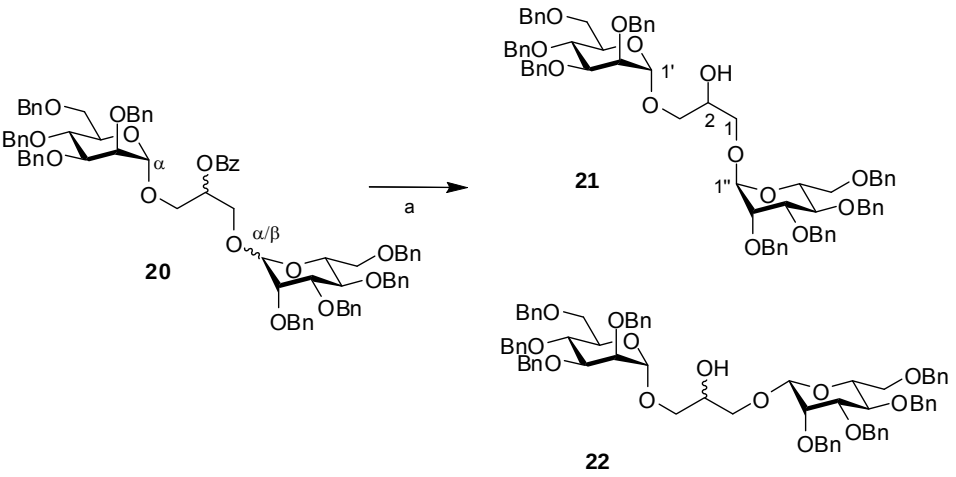


Reagents and conditions: (a) TMSOTf, ether, -42 °C (78%).

Scheme 2-12. Mannosylation of the benzoylated glycerol mannoside **20**.

The high resolution mass spectrum of product **20** showed an ion consistent with the molecular formula of $C_{78}H_{80}O_{14}$. The successful introduction of the mannosyl residue was also confirmed by a 40-proton multiplet at δ 7.08-7.38, which was assigned to the phenyl protons of the eight benzyl protecting groups.

In order to allow separation of the diastereomeric mixture, the benzoyl group of compound **20** was removed (**Scheme 2-13**). Deprotection of **20** with sodium methoxide afforded the chromatographically separable α,α-dimannoside **21**, plus α,β-dimannoside **22** in 45% and 12% yield, respectively. A high resolution mass spectrum of the purified compounds **21** and **22** confirmed both as having the molecular formula of $C_{17}H_{76}O_{13}$.



Reagents and conditions: (a) 1 M $NaOCH_3$, CH_2Cl_2 (45% for **21**, 12% for **22**).

Scheme 2-13. Synthesis of the α,α-dimannoside **21**.

The ^{1}H NMR spectrum of **21** displayed a broad doublet at δ 2.79, which was attributed to the proton of the hydroxyl group. The proton at C-2 of the glycerol unit resonated as a broad multiplet at δ 3.86-3.91. The resonances of the anomeric protons at C-1′ and C-1′′ were difficult to identify due to overlapping with other signals. These were found at δ 4.82-4.88, according to data received from HQSC (heteronuclear single quantum correlation) spectroscopy. The two anomeric carbon resonances of **21** appeared at δ 98.73 and 98.89 (**Figure 2-7**). The ^{1}H-coupled spectrum showed that C-1′ and C-1′′ each had a coupling constant $^1J_{C\text{-}H}$ of approximately 170 Hz, confirming that the new anomeric linkage of compound **21** possessed the α-configuration[241]

(**Figure 2-7**). Comparatively, β-mannosyl linkages have coupling constants $^{1}J_{C\text{-}H}$ of 160 Hz. The optical rotation obtained of the purified product **21** was in agreement with the literature value[235].

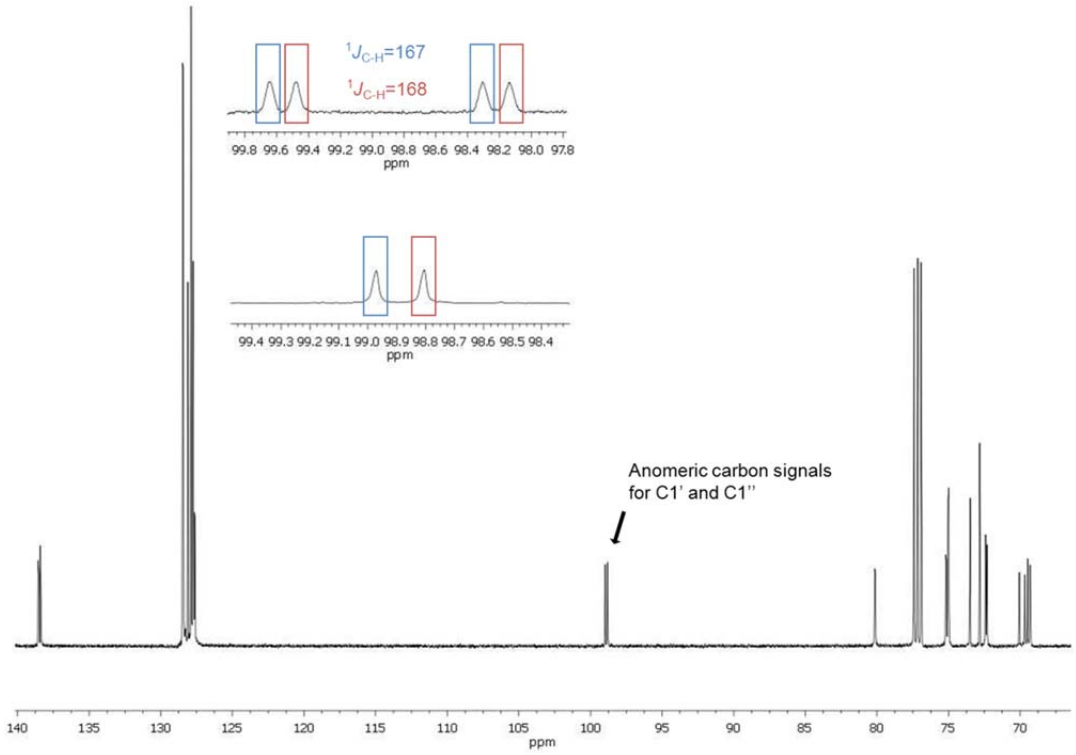
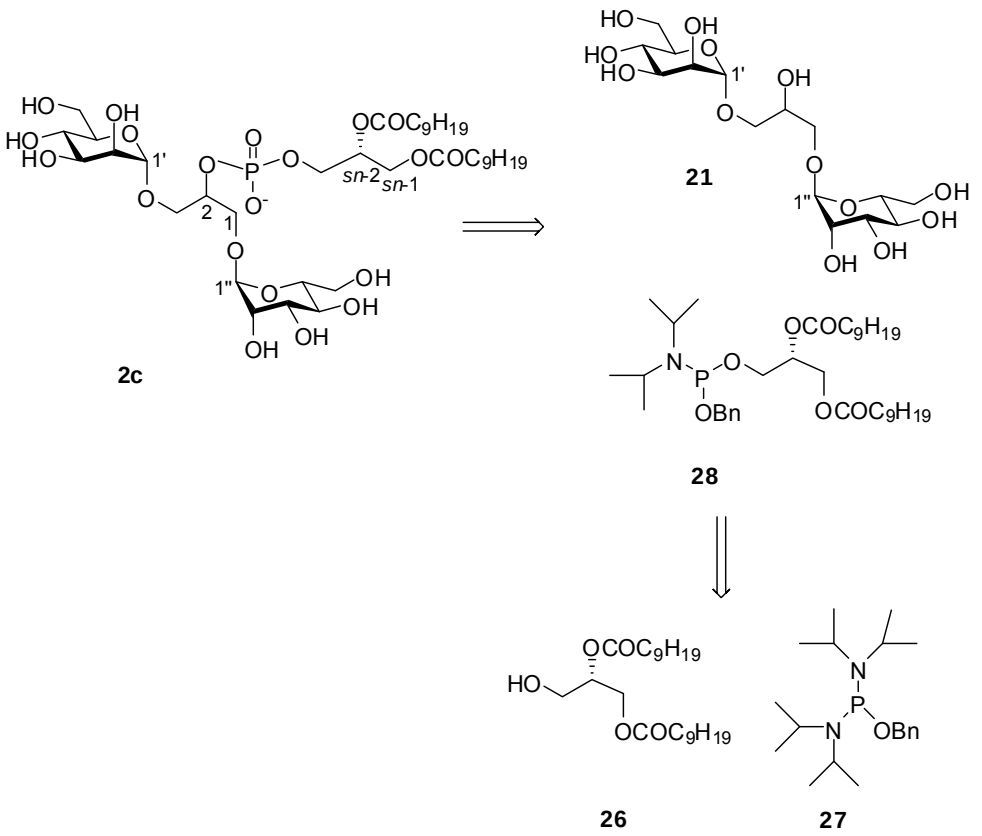


Figure 2-7. 125 MHz ^{13}C NMR shifts of anomeric carbons and corresponding one-bond coupling constants $^{1}J_{C\text{-}H}$ (Hz) of key intermediate **21**. *Inset:* ^{13}C-NMR spectrum, expansion of the anomeric region showing the ^{1}H-decoupled spectrum (lower panel) and ^{1}H-coupled spectrum (upper panel).

2.4.2 Preparation of phosphoramidite 28

The proposed synthesis required the construction of the phosphodiester linkage between alcohol **21** and glycerol diester **26** via phosphoramidite coupling. It was envisaged that phosphoramidite **28** could be accessed from glycerol diester **26** via coupling with the phosphatidylating reagent **27** (**Scheme 2-14**).

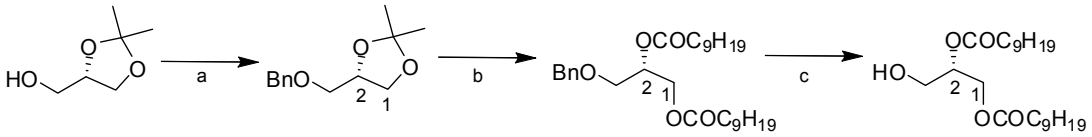


Scheme 2-14. Retrosynthesis of target **2c**.

The commercially available (*S*)-(+)-1,2-*O*-isopropylidene-*sn*-glycerol **23** was benzylated under standard conditions, to afford compound **24** in a yield of 96% (**Scheme 2-15**)[238]. Following purification by column chromatography, ^{1}H NMR spectroscopy revealed characteristic resonances of the benzylic CH_2 groups at δ 3.48 and 3.56, as well as a five-proton multiplet at δ 7.23-7.38 verifying the benzene ring. A multiplet at δ 4.27-4.34 was assigned to the proton at stereogenic C-2.

In order to attach lipid residues, the acetal was hydrolysed with a catalytic amount of *p*-toluenesulfonic acid, and the unisolated intermediate subsequently acylated with decanoic acid, under conditions similar to those reported by Nifantyev *et al.*[242]. The glycerol diester **25** was obtained after

purification by column chromatography on silica gel in a moderate yield of 66%.



23 **24** **25** **26**

Reagents and conditions: (a) NaH, BnBr, DMF (96%); (b) decanoic acid, *p*-toluenesulfonic acid monohydrate (66%); (c) Pd/C (10%), H_2 (85%).

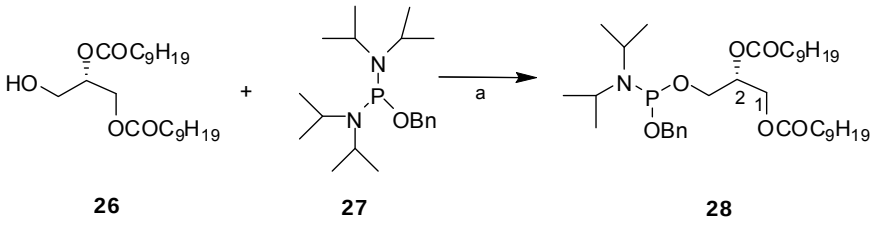
Scheme 2-15. Synthesis of the glycerol diester **26**.

A high resolution mass spectrum of the pure compound **25** confirmed the molecular formula as $C_{30}H_{50}O_5$. The presence of the fatty chains was supported by an IR band at 1739 cm^{-1}, indicative of an ester carbonyl stretching mode. ^1H NMR analysis revealed characteristic peaks for two C10 acyl chains. A triplet at δ 0.88 integrated for 6 protons was assigned to the CH_3-groups. The two carbons of the acyl chain, vicinal to the carbonyl group, resonated each as a four-proton multiplet at δ 2.30 and 1.60. A 24-proton multiplet at δ 1.25-1.30, related to the remaining protons of CH_2-chains. The distinct H-2 signal was shifted downfield and appeared as a one-proton multiplet at δ 5.21-5.27.

To enable the attachment the phosphorus coupling agent **27** to the glycerol unit, compound **25** was debenzylated by hydrogenolysis over a palladium catalyst, under hydrogen atmosphere, to give the glycerol diester **26** in 85% yield (**Scheme 2-15**). The molecular formula obtained by HRMS showed the loss of the benzyl group ($C_{23}H_{44}O_5$). The presence of hydroxyl group at C-3 was further confirmed by a broad peak in the IR spectrum at 3504 cm^{-1}. In the ^1H NMR spectrum the proton at the stereogenic C-2 centre gave a resonance at δ 5.07. Also evident was the optical rotation of -2.6 (c 0.15, CH_2Cl_2) which is

approximate to the optical rotation of -2.3 (c 1.00, $CHCl_3$) measured for a similar compound containing two C16 acyl chains[243].

Finally, the target phosphoramidite **28** was prepared from alcohol **26** by 4,5-dicyanoimidazole (DCI) activated phosphatidylation, with benzyloxy-bis(diisopropylamino)phosphine **27**. Purification by column chromatography on silica gel afforded phosphoramidite **28** in 91% yield (**Scheme 2-16**)[244-246].



26 **27** **28**

Reagents and conditions: (a) 4,5-dicyanoimidazole (DCI), CH_2Cl_2 (91%).

Scheme 2-16. Synthesis of phosphoramidite **28**.

The phosphine **27** used in this reaction was kindly provided by Carbohydrate Research Team from Industrial Research Limited (Lower Hutt, New Zealand). The data acquired by high resolution mass spectroscopy revealed a combined ion $[MNa]^+$ consistent with the molecular formula $C_{36}H_{64}NO_6P$. Evidence for the successful reaction were characteristic peaks at δ 148.70 and 148.85 in the ^{31}P NMR spectrum related to the two diastereomeric forms of **28**. As shown in **Figure 2-8** the ^1H NMR spectrum showed a five-proton multiplet at δ 7.25-7.38, assigned to the phenyl group and characteristic peaks for the stearyl residue between δ 0.89-2.30. The ^{13}C NMR spectrum clearly showed carbonyl functionality signals at δ 173.07 and 173.45.

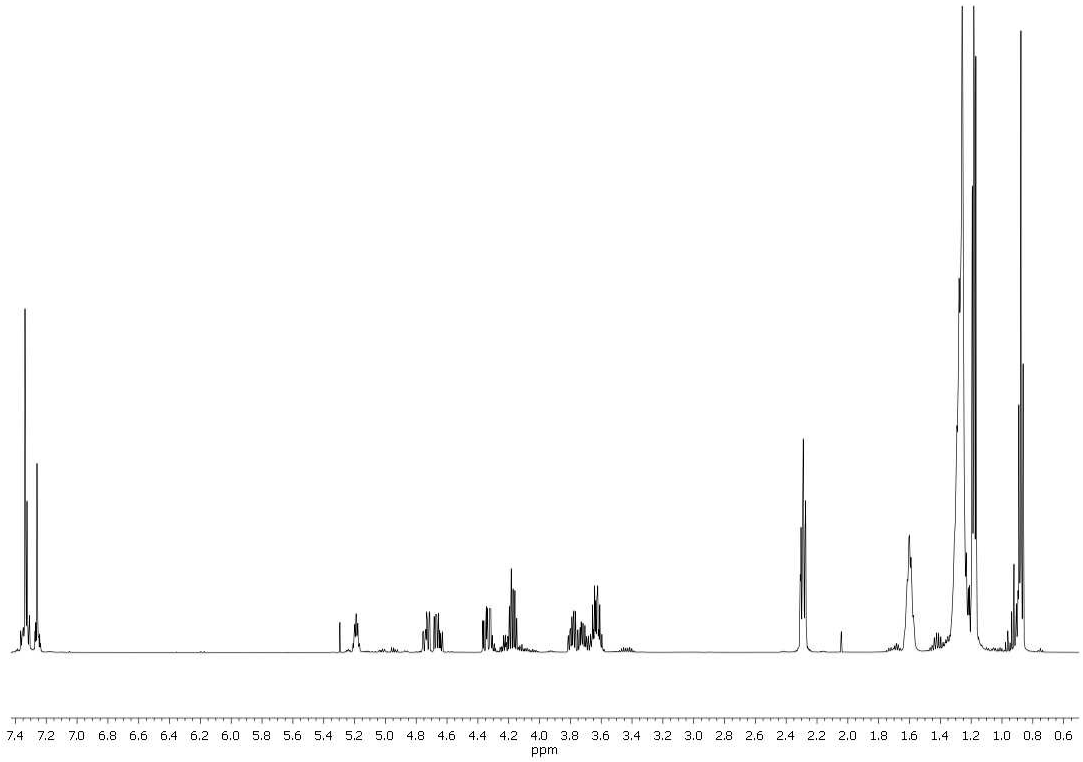
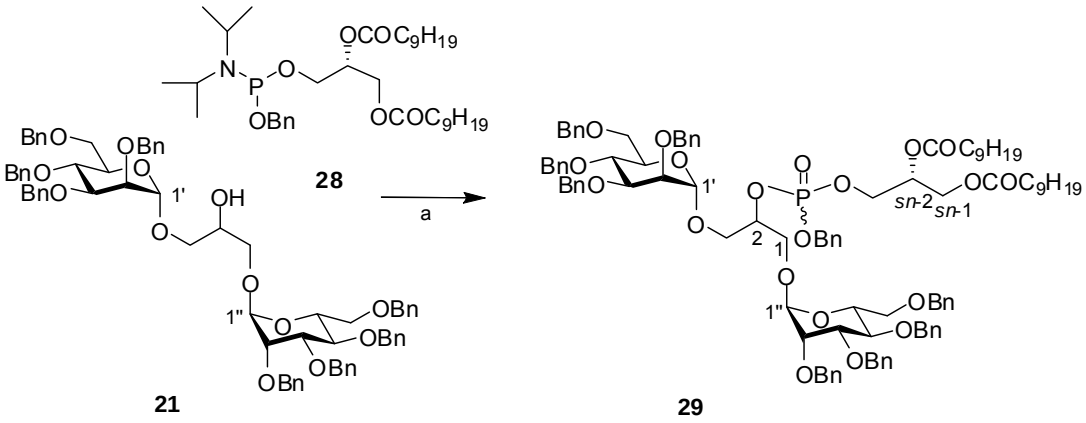


Figure 2-8. 500 MHz ^{1}H NMR spectrum of phophoramidite **28**.

2.4.3 Preparation of target PGM_2 analogue 2c

The converging synthetic strategy towards **2c** required the phosphatidylation of α,α-bismannoside **21** with phosphoramidite **28**[247]. Thus, the phosphodiester linkage in target molecule **2c** was achieved by reacting the 4,5-dicyanoimidazole (DCI) activated alcohol **21,** with an excess of phosphoramidite **28,** followed by oxidation of the intermediate phosphite with *m*-chloroperoxybenzoic acid (**Scheme 2-17**). The formation of the benzyl protected target **29** was performed under strictly anhydrous conditions, and a reasonable yield of 56% was obtained after purification by column chromatography. High resolution mass spectroscopy data of the purified product was consistent with the proposed molecular formula $C_{101}H_{125}O_{20}P$. The IR spectrum showed the expected ester carbonyl stretch at 1739 cm^{-1}, as well as the typical C-H stretch bands at 2854 and 2923 cm^{-1} due to the fatty acid chain.

Aromatic bands at 1496 cm^{-1} refer to the presence of benzyl protecting group in the product.

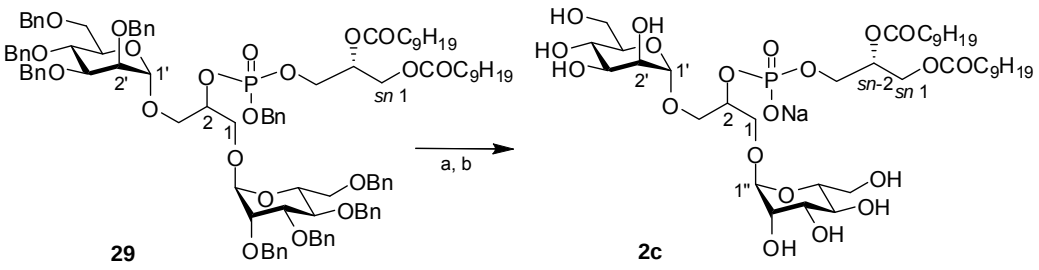


Reagents and conditions (a) 4,5-dicyanoimidazole (4,5-DCI), mCPBA (56%).

Scheme 2-17. Formation of fully benzyl-protected target molecule **29**.

The ^{1}H NMR spectrum of compound **29** was difficult to analyse as many of the proton signals overlapped. Nevertheless, the spectrum showed characteristic signals for the aromatic protons of the nine benzyl groups (δ 6.88-7.58), and resonances of the fatty acid chains were consistent with those of compound **28**. The two-proton multiplet at δ 5.05-5.15 was assigned to the stereogenic proton at the *sn*-2 position. The ^{13}C NMR spectrum displayed the expected peaks for the anomeric carbon C-1′ at δ 98.63, as well as carbonyl resonances at δ 172.95. Additionally the formation of the phosphate was verified by ^{31}P NMR spectroscopy. The resonances of the phosphorus ester shifted upfield and gave signals at δ -1.65 and -1.39.

The final step in the synthesis of the desired target **2c** is presented in **Scheme 2-18** and involved removal of benzyl groups by catalytic hydrogenolysis under a hydrogen atmosphere.



Reagents and conditions (a) $Pd(OH)_2/C$, H_2 (72%); (b) DOWEX 50X8-100 as Na-salt.

Scheme 2-18. Final deprotection to prepare the target PGM_2 **2c** (sodium salt).

Purification by silica gel using a gradient eluent system of $CHCl_3$/MeOH/water gave **2c** in 72% yield. The IR spectrum of the purified product showed bands at 1737 (ester CO), 2852 and 2922 cm^{-1} due to the C-H stretch of the fatty acid, which were consistent with the bands found for **29**. The broad band at 3315 cm^{-1} consistent with an O-H vibration indicated the successful removal of the protecting groups. This was supported by HRMS analysis (-ve) which gave a signal corresponding to the $[M-Na]^-$ ion at 877.4187 in comparison to 1711.8414 found for the starting material **29**.

^1H NMR data reinforced the proposed structure and showed no signals in the aromatic region (**Figure 2-9**). Among the typical signals for the fatty acid chain, consistent with those found for **29**, the spectrum displayed a doublet at δ 4.85, attributed to the two anomeric protons and a singlet at δ 5.20, caused by the deshielded glycerol *sn*-2 proton.

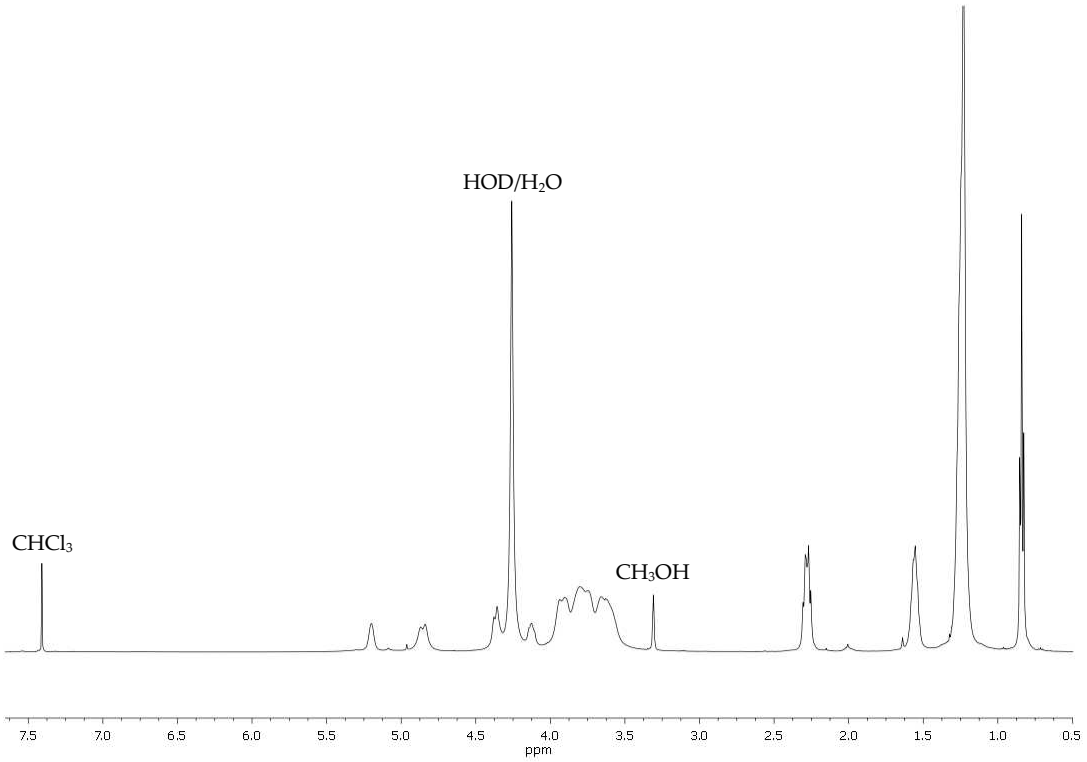
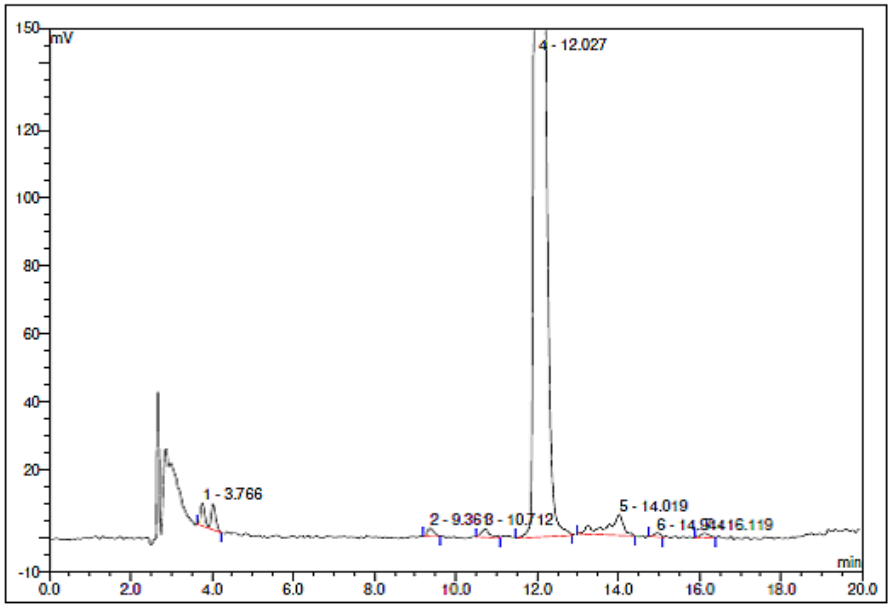


Figure 2-9. 500 MHz ^{1}H NMR spectrum of PGM_2 (10:10) (**2c**). Solvent peaks are assigned in the spectrum.

Compound **2c** was converted into its sodium salt by stirring with DOWEX 50X8-100 resin (sodium form). Also evident was the optical rotation of **2c** as sodium salt of +38.4 (c 0.12, 6:40:70 water/MeOH/$CHCl_3$) which is comparable to the optical rotation of +37 (c 1.4, 0.17:1:2 water/MeOH/$CHCl_3$) reported for a similar PGM_2 compound[248]. Purity of the target **2c** (95%) was verified by analytical high-performance liquid chromatography (HPLC) (**Figure 2-10**).



No.	Ret.Time min	Peak Name	Height mV	Area mV*min	Rel.Area %	Amount	Type
1	3.77	n.a.	6.703	1.740	1.37	n.a.	BMB*
2	9.36	n.a.	2.412	0.444	0.35	n.a.	BMB*
3	10.71	n.a.	2.591	0.586	0.46	n.a.	BMB
4	12.03	n.a.	493.099	120.926	95.13	n.a.	BMB
5	14.02	n.a.	6.044	2.869	2.26	n.a.	BMB*
6	14.94	n.a.	1.185	0.207	0.16	n.a.	BMB*
7	16.12	n.a.	1.364	0.349	0.27	n.a.	BMB*
Total:			513.398	127.120	100.00	0.000	

Figure 2-10. Analysis of PGM_2 (10:10) (**2c**) by HPLC, with an indicated purity of 95%. A blank was subtracted from the sample trace to give a flat baseline.

In summary, PGM_2 (10:10) (**2c**) was successfully prepared by the synthetic strategy presented in this chapter. Phosphoramidite **28** could be effectively coupled with the α,α-bismannoside **21** and subsequent total deprotection gave the desired target **2c**.

The following chapters describe studies on the physicochemical characteristics of the presented series of synthetic PIM compounds. The main purpose is to determine the effect of the structural variations on physicochemical properties and establish correlations in these qualities to their bioactivity.

Chapter Three

Investigation of physicochemical properties and immunosuppressive activity of PIM_2 and PGM_2 compounds

3 Investigation of physicochemical properties and immunosuppressive activity of PIM_2 and PGM_2 compounds

3.1 Introduction

The focus of this chapter was on investigating the pharmaceutical properties of a series of synthetic PIM compounds with the aim of understanding the impact of the chemical composition on the behaviour at an air/water interface, using the Langmuir trough technique, as well as in an aqueous environment. To further evaluate the structure-function relationship, the bioactivity of these compounds was assessed *in vivo*.

3.1.1 Langmuir monolayers

The principle of spreading oil on water surfaces goes back to the eighteenth century BC, when it was used for the art of prophecy. For this purpose Babylonians observed the oil spreading on a water surface. The first scientific record concerning the particular effects of oil on water surfaces was made by Benjamin Franklin in 1774[249]. In his Clapham pond experiment, Franklin was able to show that one teaspoon of oil had a calming effect on half an acre of choppy water. Following numerous studies, including initial film compression experiments using barriers by Agnes Pockels[250], Lord Rayleigh postulated a dense packing of oil molecules at a certain compression stage[251]. This theory was later supported by Irving Langmuir in 1917[252]. He also greatly expanded knowledge in this area by elucidating the orientation of the molecules in the interface and their arrangement as a mono-molecular film. Langmuir advanced the experimental concepts by performing the first monolayer measurements with pure substances. Nowadays these insoluble monolayers are referred to as Langmuir monolayers.

Molecules possessing both hydrophilic and hydrophobic groups exhibit characteristic surface adsorption behaviour. In general the chemical structures of these amphiphiles comprise non-polar tail groups and polar head groups. Due to these different features within one chemical structure, molecules can orientate at air/water interfaces and form mono-molecular layers between a liquid and gaseous phase. These stable films are usually prepared from compounds dissolved in an organic solvent (chloroform is commonly used) and deposited onto the water surface. Organic substances such as phospholipids and glycolipids are well-known water-insoluble amphiphiles. At the interface these molecules orientate with their hydrophilic group immersed in the water (attracted to the polar phase), while their hydrophobic tails are directed towards the air[253]. Organisation and packing of these monolayers is affected by the geometries of the head group and hydrophobic tail. Typical head groups of phospholipids are phosphatidylglycerols, phosphatidylcholine, phosphatidyl-serine, phosphatidylethanolamine and phosphatidylinositol (**Figure 3-1**).

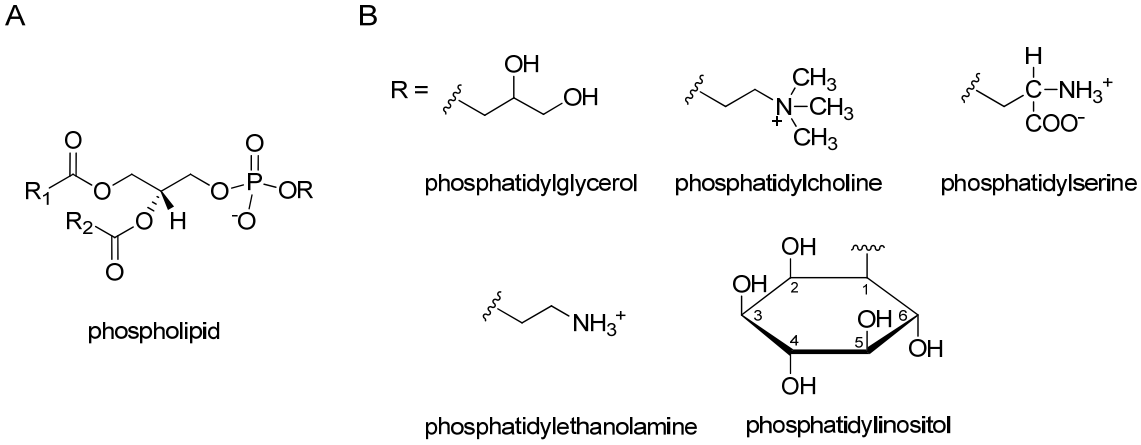


Figure 3-1. General structure of a phospholipid **(A)**. The glycerol residue includes two fatty acid residues (R_1 and R_2) which can vary in chain length and degree of saturation. The structure comprises a phosphate group with the common head groups (R) as shown in **(B)**.

The head groups have a great impact on the orientation of the molecules in the interface due to characteristics such as size, polarity, hydrophilic interactions and steric hindrance[253]. A balance between the hydrophobic and hydrophilic moieties is essential to be able to form monolayers. For instance, reduced hydrophilicity may lead to evaporation of volatile molecules during film preparation. Crystallization at the surface can occur if the tail groups are too long[254]. In contrast, if the 'tail' is not sufficiently long, the molecules dissolve into the water phase and form a soluble monolayer[255]. Phospholipids commonly possess two acyl chains varying in their number of carbons (6-24 carbons) and the degree of saturation. Two-dimensional Langmuir monolayers of phospholipids have been extensively studied as useful models of cell membranes[256]. By being essentially half a bilayer, a phospholipid monolayer provides a convenient model for understanding bilayer structures[193]. Insight into fundamental processes within bilayers can be obtained by mimicking the bilayer structure in physical monolayer. These studies enable investigations of mutual interactions between molecules and a variety of monolayer properties relevant to biological processes[257-259].

3.1.1.1 Langmuir trough technique

Langmuir monolayer studies can be conducted with a Langmuir trough which provides a convenient method to prepare and investigate phospholipid monolayers at an air/liquid interface. The experiments described in this thesis were performed on a traditional computer-controlled Langmuir trough. This consists of a chemically inert Teflon trough (holding the aqueous sub-phase) a surface tensiometer and movable barriers (**Figure 3-2**) between which the test molecules are added. Moving the barriers at a set rate across the surface of the sub-phase compresses the monolayer in a controlled fashion.

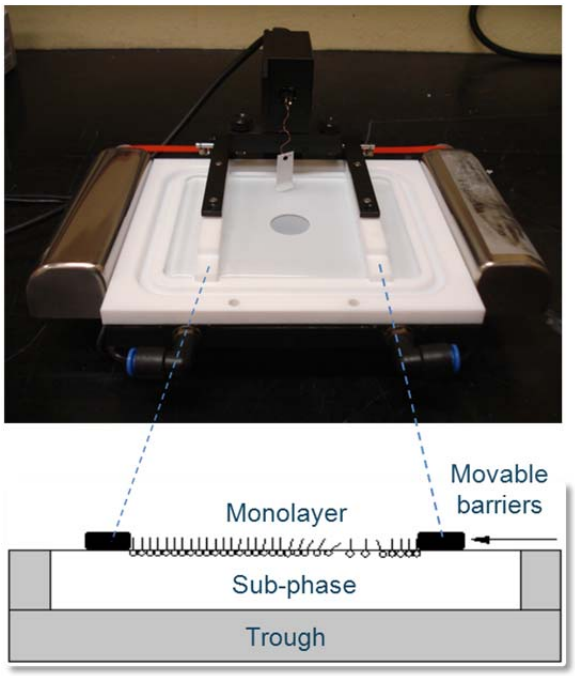


Figure 3-2. Set-up of the Langmuir trough.

When the molecules are deposited onto a large surface area sub-phase and the organic solvent is evaporated, the molecules freely diffuse and the effect on the surface tension of the sub-phase is minimal. However, upon compression, the available surface area per molecule is decreased and molecules start to interact as the intermolecular distance is reduced. Molecules accumulate at the interface and the surface tension of the sub-phase is reduced. The reduction in surface tension is equal to the surface pressure (π) and is described by **Equation 3-1**, where γ_0 and γ_1 are the surface tension of the sub-phase alone and in the presence of a mono-molecular film respectively:

$$\pi = \gamma_0 - \gamma_1 \qquad \textbf{Equation 3-1}$$

This experimental method for probing the organisation of molecules on the water surface has been used in numerous studies to investigate amphiphilic lipids or membrane components[193,260-262]. For instance, phosphatidylinositol (PI)

plays a major role in cellular functions and is an important precursor of key cell wall components. The behaviour of PI with synthetic lipids in monolayers was investigated to obtain information about membrane distribution and the role of PI in cellular processes[263-266]. Furthermore, the surface behaviour of mycolic acids, fatty acids found in the mycobacterial cell wall, has been extensively studied. Mycolic acids isolated from several species of *Mycobacterium* have been analysed to understand correlations between chemical structures and monolayer properties and packing[267-271]. Other studies have demonstrated that monolayer investigations can also be useful to establish pharmaceutical properties such as stability of liposomes[272] and drug-lipid interactions in liposomal bilayers[223].

The Langmuir monolayer technique has the added advantage of a relatively simple experimental set-up and the fact that tests can be conducted in a controlled manner under customized conditions (temperature, monolayer composition, sub-phase)[257]. Recently, the application of the Langmuir method has been broadened to investigate less conventional amphiphilic substances such as polymers[273], peptides[274-277], amphiphilic dendrimers[278] and organometallic compounds[279].

3.1.1.2 Surface pressure-area (π-A) isotherm

There are different methods available to measure changes in surface tension[253]. In the experiments presented in this thesis the Wilhelmy method was utilised, in which a filter paper is suspended from a balance so that it is partially immersed into the sub-phase. The water phase exerts a downwards force F on the paper which can be described by the equation, $F = \gamma L \cos \theta$, where L is the perimeter of the paper and θ the contact angle of the liquid to the paper. In the

case of a filter paper, the contact angle θ is zero (cos θ = 1) and the surface tension is therefore given by[254]:

$$\gamma = \frac{F}{L} \qquad \textbf{Equation 3-2}$$

As mentioned above, the surface pressure π is the reduction in surface tension γ (**Equation 3-2**) which is determined by measuring the change in F acting on the filter paper.

Monitoring the surface pressure as a function of area occupied by each molecule (molecular area in $Å^2$) at constant temperature, gives the surface pressure-area (π-A) isotherm (**Figure 3-3**). During film compression, the molecules may undergo various phase changes and the isotherm provides a useful method to elucidate the phase behaviour of the monolayer. After initial deposition of the amphiphilic substance onto the sub-phase, the molecules spread over the available area and if there is no external pressure applied to the monolayer, the behaviour of the molecules can be defined as a two-dimensional gas:

$$\pi A = K T \qquad \textbf{Equation 3-3}$$

Where A is the molecular area, K the Boltzmann constant and T is the thermodynamic temperature[255]. Upon compression molecules begin to interact and orientate at the interface. The monolayer progresses through different phases, similar to those in a three-dimensional system (gaseous (G), liquid (L) and solid (S)) (**Figure 3-3**). Eventually, after reaching a certain pressure at which the molecules are compressed to their maximum density, the film collapses (collapse pressure π_{coll}).

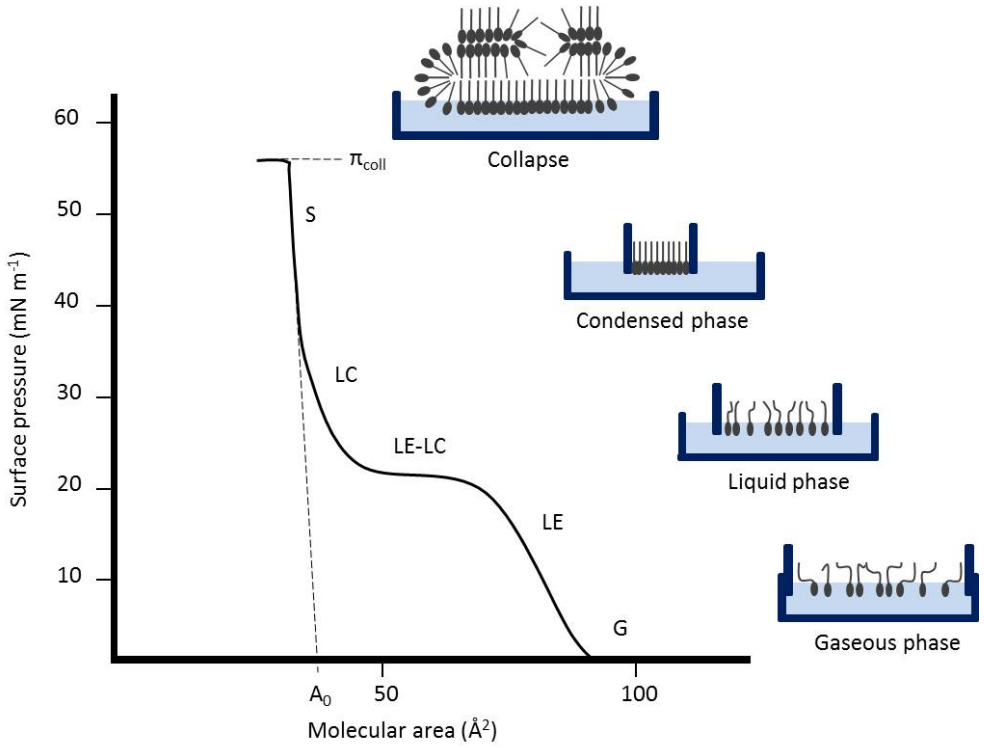


Figure 3-3. Typical surface pressure-area (π-A) isotherm for a phospholipid. The monolayer undergoes various phases during compression such as gaseous (G), liquid-expanded (LE), liquid-condensed (LC) and solid (S). LE-LC denotes the phase transition from liquid-expanded to liquid-condensed. Extrapolation of the part of the isotherm with the highest slope to zero surface pressure gives the limiting area per molecule A_0 (Å^2). The collapse pressure π_{coll} (mN m^{-1}) of the monolayer can be assigned to the highest pressure to which the film can be compressed without any abrupt changes. Figure was modified from Erbil[254].

Several parameters determine the shape of the π-A isotherm including temperature and the chemical composition of the amphiphiles. In general, to be able to form stable monolayers, hydrocarbon chains require a minimum of 12 carbon atoms[255]. Weak interactions occurring between short hydrocarbon chains result in a steady increase in surface pressure; as shown in studies on *N*-dodecanoic acid[253] or 1,2-dioctanoyl-*sn*-glycerol-3-phosphocholine[280] and the formation of expanded monolayers. Lengthening the hydrocarbon chains increases intermolecular interactions such as hydrophobic forces and Van der Waals contacts between the adjacent chains[280,281]. Due to these stronger interactions the chains appear to be more ordered compared to shorter chains and

a transition from the liquid-expanded (LE) to the liquid-condensed (LC) phase can occur[253,281]. This can be seen as a plateau region in the isotherm where molecules arrange in ordered monolayers. The degree of hydrocarbon saturation has been reported to have a large effect on the phase behaviour. Double or triple bonds restrict rotation and can prevent lipid chain ordering and close packing at the interface[253]. The presence of unsaturation also increases the total volume occupied by the hydrocarbon chain and thus generates a less condensed film[282]. The polar head group also plays a significant role in interfacial organisation of monolayers (and therefore on the π-A isotherm)[283,284]. Thus, the π-A isotherm of the film and lipid packing can be affected by the dimension and polarity of the head groups as well as hydrophilic interactions and steric hindrance between these[283,284].

While the π-A isotherm is widely used to provide information on phase states and transitions in monolayers and monolayer stability[193], important information can also be gained from *in-situ* imaging techniques such as fluorescence microscopy[285]. This optical approach enables analysis of the complexity of lipid monolayers larger than 1 μm. Further developments with atomic force microscopy (AFM)[286,287], allowing nano-scale imaging, provided additional information on miscibility of the components and enabled researchers to detect domains of lipids within the monolayer. This can be done *in-situ*[283] or following the transfer of the monolayer onto a substrate (e.g. glass slide) using a dipping technique[267]. Besides AFM, Brewster angle microscopy (BAM)[288,289] has been established to visualise the morphology of lipid monolayers and additional information on the interfacial properties of the film (miscibility and complex formation) can be obtained.

3.1.2 Amphiphilic compounds and self-assembly in aqueous media

Findings obtained from monolayer studies can help to understand and predict the aggregation behaviour of amphiphilic molecules. Self-assembly is a concentration-dependent spontaneous process which occurs when amphiphilic molecules are exposed to polar environments. At low concentrations the molecules occur in a monomeric state in solution and all molecules interact in the same way with their surroundings. Molecules orientate at an interface due to the tendency of the non-polar tail groups to avoid the water and to reduce the free energy of the system. With an increasing number of molecules the solution surface becomes completely occupied. To further reduce the free energy the molecules associate in the bulk-phase. The concentration at which aggregation begins is called the critical aggregation concentration or critical micelle concentration. If more molecules are added to this phase, they will form aggregates[290] such as micelles. The principle of this self-association is similar to the formation of Langmuir monolayers and leads to well-defined and thermodynamically stable structures[254]. In order to minimize the surface free energy the molecules orientate in a way that the polar and non-polar groups can interact with their favoured environments. An aggregate is formed in which the hydrophobic groups are isolated from the aqueous environment and water is in contact only with the hydrophilic groups. This is known as the hydrophobic effect[291].

The morphology of the aggregates varies and depends on solution properties and the shape and composition of the amphiphilic molecules. The geometry of the molecules and the packing morphology have been correlated by Israelachvili *et al.*[292] in the critical packing parameter:

$$P = \frac{v_t}{a_o} l_c \qquad \textbf{Equation 3-4}$$

Where v_t and l_c describe the volume and critical length of the hydrocarbon chain respectively and a_o is the optimal surface area of the head group. The assembly of aggregates is not only dependent on length and volume of the tail group of the amphiphilic molecule but also factors which determine the optimal head group area such as ionic and steric repulsions[290]. The packing parameter is used to describe the most favoured curvature of the lipids and subsequent structure. Some common assemblies and their respective approximate packing parameters are shown in **Figure 3-4**. Typically spherical micelles are formed by single chained amphiphiles with large head group areas, whereas double-chained lipids with large head group areas assemble into vesicles.

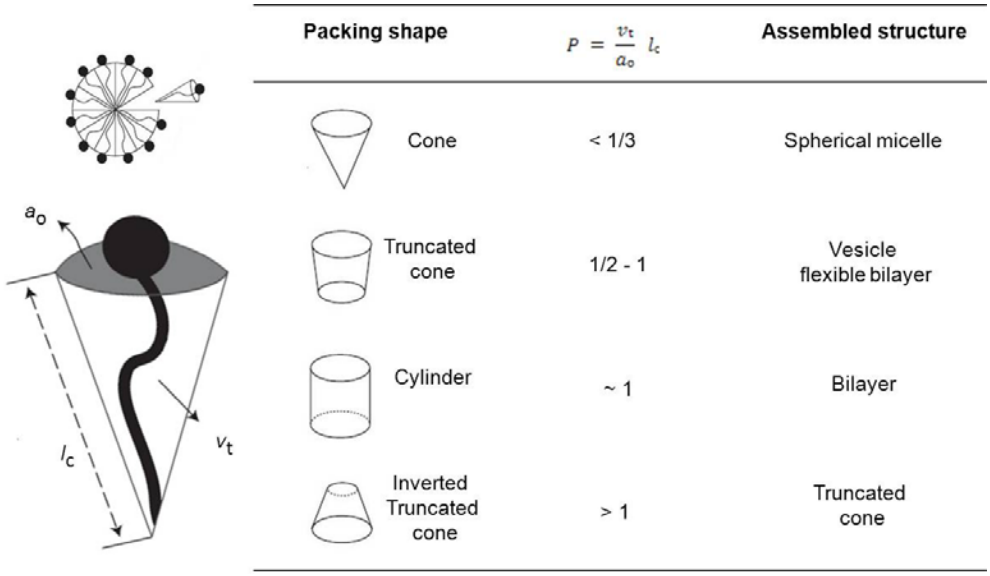


Figure 3-4. The shape of the assemblies depends on the geometry of the molecules and can be described the packing parameter *P*. Figure modified from Erbil[254].

Several components of the mycobacterial cell wall have been described to self-associate in aqueous media. Nigou *et al.*[65] reported a clustering of total fractioned mannosylated lipoarabinomannan (tManLAM, *M. bovis* BCG) in water. The aggregation depended on the presence of fatty acid residues and

was demonstrated by a broad peak seen in the ^{31}P NMR spectrum. It was later shown that purified ManLAM from *M. bovis* BCG aggregated spontaneously after dispersion in water to form micelles with a relatively homogenous size distribution around 30 nm[69]. Several studies demonstrated the ability of PIMs extracted from *M. bovis* (BCG) to form vesicular systems. Liposomes could be prepared from native PIMs substituted with a varying number of sugar residues, in combination with cholesterol[293,294] and phospholipids[294]. While Sprott and colleagues[225] reported the formation of liposomes from the total polar lipid fraction of *M. bovis* BCG, comprising different phosphoglycolipids and phospholipids. Biological investigation of these systems has revealed a cell specific delivery towards macrophages[293,294] and it has been suggested that self-aggregation may play a key role in recognition and receptor-mediated uptake by immune cells[65,69]. There have been no published studies examining the phase behaviour of pure synthetic PIMs, either on their own or in combination with other amphiphilic lipids.

3.1.3 PIMs as immunosuppressive agents

As described in **Chapter One**, various components of the mycobacterial cell wall such as phosphatidylinositol mannosides (PIMs) and their hypermannosylated products lipoarabinomannans (LAMs), lipomannans (LMs) and mannose-capped lipoarabinomannans (ManLAMs) have been found to induce a wide range of immune responses[19,55,295,296]. In particular, the relatively small phosphoglycoplipids, known as PIMs, have attracted great research interest in recent years due to their significant immunomodulatory activity[21,90,227,236]. Native PIMs, isolated from the mycobacterial cell wall, and synthetic PIM analogues have been reported to exert immunosuppressive activity. PIM molecules are recognized by macrophages and dendritic cells through a number of pattern recognition receptors (PRRs), including TLR-2

and TLR-4[96,297], CD1d[107] and C-type lectins such as MR and DC-SIGN[26,27]. However, data linking specific molecular interaction(s) to biological activity is conflicting and strongly depends on the source of these compounds, whether they are purified from extracts or synthetically prepared. Consideration must also be given to the mycobacterial species, as previous studies demonstrated different anti-inflammatory profiles for PIM extracts from *M. smegmatis* or *M. bovis*[236]. Similarly, the experimental model used to determine biological function appears to play a significant role. *In vitro* studies are approximations of biological processes conducted in a controlled, artificial environment. Thus, results may not reflect the complex circumstances occurring in a living organism. Whereas *in vivo* approaches observe the overall effects of an experiment on a living subject, in which many parameters may influence the fate of biologically active compounds.

In mouse models of OVA-induced allergic asthma, intranasal administration of natural and synthetic PIMs and a PIM_2 mimetic was shown to suppress the accumulation of eosinophils in the lung[227,236,248]. Furthermore, the cytokine profile implied that this was not mediated by inducing a Th1 response which suppressed the Th2 mediated eosinophilia, but through the production of IL-10 in the spleen and lymph node suggesting regulatory T cell (Treg)-mediated immune suppression[236]. Tregs are essential immune cells for controlling the immune response. It has been shown that mycobacterial pathogens subvert immune response via Treg activation and subsequently down-regulate the immune system[43-45,298]. This proposed mechanism was supported by other studies[136,299] where splenocytes isolated from OVA-sensitised mice showed a higher production of IL-10, while there was no difference in INF-γ levels as compared to the control group[136].

Using a similar airway model, synthetic PIM_1 and a PIM_2 mimetic were shown to suppress endotoxin (LPS)-induced airway inflammation[96]. Co-administration of synthetic compounds suppressed infiltration of neutrophils into the lungs, and reduced local levels of and chemokines and the pro-inflammatory cytokine TNF *in vivo*.

Important structural features for immunosuppressive activity have been identified by several research groups[96,99,227,236,248]. The general structure of PIMs is presented in **Figure 3-5**.

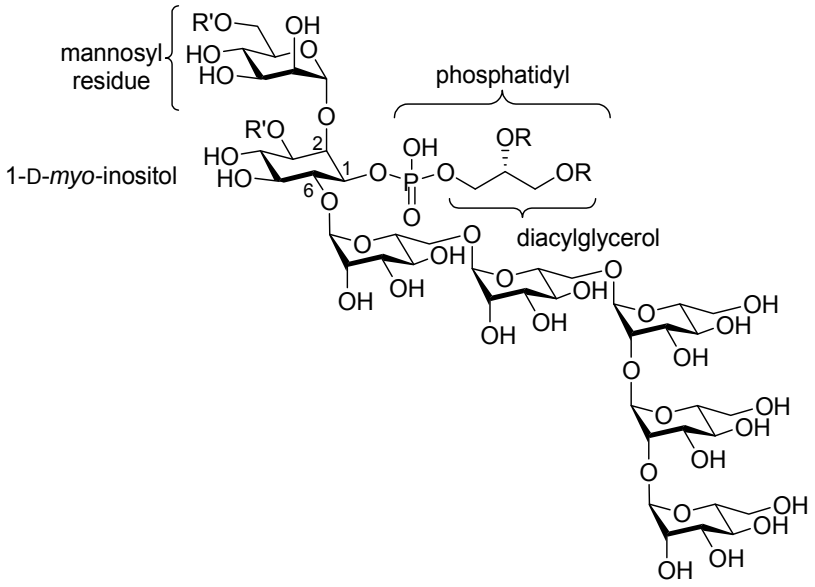


Figure 3-5. General structure of PIMs. PIMs can have two acyl residues (R) at the phosphatidyl moiety naturally occurring as palmitatoyl, tuberculostearoyl or stearoyl residues. Further acylation is indicated as R' (R' = R or H).

The biological activity was found to be dependent on the presence of at least one mannosyl-residue, fatty acid residues and the phosphodiester linkage[96,99,227,236,248]. Studies showed that the *myo*-inositol core was dispensable for anti-inflammatory activity. Various reports reviewing the replacement of the inositol core by a three-carbon glycerol structure[96,226,248] or acyclic or heterocyclic core structures[300] verified that biological activities were

maintained. However, modifications in the diacylglycerol unit such as the replacement of the fatty acid ester unit with ether or amide linkages attenuated immunosuppressive activity *in vitro*[99].

Following LPS-activation, mycobacterial-purified fractions of PIM_6 and PIM_2 (*M. bovis* BCG) inhibited activation of primary bone marrow-derived macrophages and subsequent release of cytokine TNF, IL-12 and IL-10[96]. The inhibitory activity was found to be dependent on the degree of acylation, as less or no efficacy could be detected for PIM_6 containing four or one acyl residues, respectively[96]. Synthetic analogues exerted similar abilities to suppress activated macrophages and cytokine release[96,99]. Contrary to findings by Doz *et al.*[96], Sayers *et al.*[236] found that fractionated PIM from *M. bovis* BCG induced high levels of IL-10 in an *in vivo* asthma model. These differences highlight again the importance of the model and extract type.

Despite diverse findings, individual members of the PIM family exhibit inherent and versatile biological activities; properties which make them useful tools to assess structure-activity relationships in defined models.

3.2 Chapter aims

Results of biological studies investigating the activity of PIM compounds are likely to be confounded by the different sources of the PIMs (natural extract or synthetic compound), variation in PIM composition (number, location, type of the acyl residues and degree of mannosylation), and the type of delivery and presentation *in vitro* and *in vivo*. However, even if the chemical structures of PIMs are well characterised and biological activities of PIMs are extensively studied, little data is available on the behaviour of pure PIM compounds at a

molecular level and specific structure-function relationships remain poorly understood. The assessment of physicochemical properties of these synthetic PIM_2 analogues and correlation between these characteristics and their bioactivity could promote the understanding of particular mechanisms involved in their immunological activity.

Thus, the work presented in this chapter investigated the physicochemical properties of a series of synthetic PIM_2 and analogues with a main focus on the impact of the chemical modifications on the physical behaviour of the molecules at the air/water interface and on the processes of self-aggregation in aqueous solution. Furthermore, to evaluate the influence of lipophilicity on the structure-function relationship, the suppressive activity of the compounds was investigated in a mouse model of allergic asthma *in vivo*.

3.3 Experimental section

3.3.1 Materials

Chloroform (purity 99-99.4%) and methanol (purity > 99.8%) were purchased from Merck (Darmstadt, Germany). The sub-phase used for the Langmuir trough experiment consisted of water which was distilled, de-ionized, purified with a Milli-Q Continental Water System (Millipore, Bedford, MA, USA) and had a resistivity of 18.2 MΩcm. Distearoylphosphatidylglycerol (DSPG) was purchased from Avanti Polar Lipids, Inc. (Alabama, USA) as its sodium salt. The following PIM_2 and PGM_2 compounds were synthesised and supplied by Industrial Research Limited (Lower Hutt, New Zealand): PIM_2 (16:16), PIM_2 (18:18), PGM_2 (0:0), PGM_2 (16:16) and PGM_2 (18:18). The synthesis of PGM_2 (10:10) was described in **Chapter Two**.

Phosphate buffered saline (PBS, DulbeccoA, Oxoid, UK) was prepared in Milli-Q water with a pH of 7.5.

Antibodies (anti-CD16/CD32, primary antibodies, secondary reagents) and propidium iodide (PI) used for flow cytometry were all supplied by BD Pharmingen (Franklin Lakes, NJ, USA).

3.3.2 Physicochemical characterisation

3.3.2.1 Langmuir trough technique and monolayer conditions

The monolayer studies were performed using a method described earlier with modifications[301]. For the one-component monolayer studies, lipid stock solutions of either PIM_2 or PGM_2 compounds were prepared at a concentration of 0.5 mg mL^{-1} in chloroform/methanol (4:1, v/v). The Langmuir trough and the pressure sensor used were acquired from NIMA technology Ltd (UK). The surface pressure was recorded according to the Wilhelmy plate principle using Whatman's No.1 chromatography paper (1.0 cm x 2.4 cm, ATA Scientific Pty Ltd, Australia, accuracy of 0.1 mN m^{-1}) and the NIMA A-TR516 software. The trough provided a total area of 90 cm^2 (volume of 50 mL) and was placed on a vibration-free table. Milli-Q water was used as sub-phase in all experiments. Before each experiment, the Teflon trough and barriers were thoroughly cleaned using Kimwipes® (surfactant-free tissue; Kimberly-Clark) and dichloromethane, followed by several purges with Milli-Q. In addition, when the barriers were closed the sub-phase was cleaned by suction of the interface using an aspirator. Before each experiment, contamination of the sub-phase was checked by repeated compression without lipids and monitoring the surface pressure. An increase in surface pressure at the end of the compression stage indicated the presence of contaminants in the sub-phase. Cleaning was

repeated until the surface pressure increase was less than 0.2 mN m^{-1}, at which point the surface was considered clean. The lipid solutions (25 μL) were spread onto the surface using a Hamilton micro-syringe. After allowing the solvent to evaporate for 10 min, the monolayer was compressed at a constant rate of 5 cm^2 min^{-1} and the π-A isotherm was continuously recorded. All experiments were carried out at ambient temperature of 24 ± 1°C and repeated three times.

3.3.2.2 Analysis of surface pressure-area isotherm

The NIMA A-TR516 software provided by NIMA technology Ltd was used for π-A isotherm analysis. Extrapolation of the part of the isotherm with the highest slope to zero surface pressure gave the limiting area per molecule A_0 in $Å^2$. The collapse pressure of the monolayer was assigned to the highest pressure (π_{coll}) the film could be compressed to without any abrupt changes[302].

3.3.2.3 Size and zeta potential measurements

Stock solutions (0.4 mg mL^{-1} in sterile phosphate buffered saline, pH 7.5) of PIM_2 or PGM_2 were prepared. Particle diameters were measured by dynamic light scattering (DLS) with a Zetasizer NanoZS (Malvern Instruments) at 25°C. Results were presented as a volume-based distribution. Particle surface charge was investigated by zeta potential measured at 25°C applying the Smoluchowski equation[303] and using the same instrument.

3.3.2.4 Transmission electron microscopy

Samples were prepared using the negative staining technique. Briefly, 10 μL of sample solution were placed onto a carbon coated grid. After 60 seconds, the grid was blotted with filter paper and negatively stained with 10 μL of 1%

phosphotungstic acid (PTA; pH 6.8). The staining solution was immediately removed by blotting and the grid dried completely. The images were viewed using a Philips CM100 transmission electron microscope at an accelerating voltage of 100kV (Philips Electron Optics, Eindhoven, Netherlands). Images were captured using a MegaView 3 digital camera (Soft imaging System GmBH, Münster, Germany).

3.3.3 Investigation of inhibitory activity (*in vivo*)

3.3.3.1 Experimental mice

Male C57BL/6, OT-I and OT-II mice aged between 6 and 8 weeks were obtained from the HTRU, University of Otago. Transgenic OT-I and OT-II mice are genetically modified to express T cell receptors specific for the CD8 epitope (OT-I) and the CD4 epitope (OT-II) of OVA[304,305]. All mice were bred and maintained under specific-pathogen free conditions and had free access to food and water. All experiments were performed with the approval of the University of Otago Animal Ethics Committee (AEC D46/11).

3.3.3.2 Testing of transgenic mice

A blood sample (4 - 5 drops) was collected from each mouse by tail bleeding into a tube containing 1 mL Alseviers solution (**Appendix A**). Blood samples were spun down at 1200 rpm for 5 min, the supernatant discarded and the tubes flicked to resuspend the cells. To lyse the red blood cells 1 mL sterile lysis buffer (**Appendix A**) was added to each tube and incubated at room temperature for 10 min. The cells were washed with fluorescence-activated cell sorting (FACS) buffer (**Appendix A**) and spun down (1200 rpm, 5 min). After discarding the supernatant and resuspension, the cells were stained for FACS

analysis. For detection of OT-I and OT-II cells, anti-CD8-PE-Cy7 (53-6.7) and anti-CD4-V500 (RM 4-5) were added to tubes in combination with specific transgenic T cell markers Vα2-PE (B20.1) and Vβ5.1-biotin (MR9-4). Antibodies were diluted to 1:200 in FACS buffer at a final volume of 100 µL per tube. The secondary reagent streptavidin-APC-Cy7 in FACS buffer (1:200 dilution) was added to visualise Vβ5.1. Flow cytometry analysis was performed as described in **Section 3.3.3.9**.

3.3.3.3 Adoptive T cell transfer

Adoptive transfer of OT-I ($CD8^+$) and OT-II ($CD4^+$) transgenic T cells into C57BL/6 mice was carried out on day -1. The mesenteric, brachial, axial, cervical and inguinal lymph nodes and spleens from OT-I and OT-II transgenic mice and stored on ice in complete Iscove's Modified Dulbecco's Media (cIMDM, **Appendix A**). Subsequently, single cell suspensions were prepared from lymph nodes and spleens, while OT-I and OT-II transgenic cells were processed separately. The suspensions were washed and centrifuged at 1100 rpm for 8 min. To lyse red blood cells, spleen samples were treated with sterile lysis buffer (**Appendix A**) at room temperature for 10 min. All four suspensions were washed before combining lymphatic and spleen cells, OT-I and OT-II cells, respectively. Following further washing steps, the cells were resuspended in cIMDM and the OT-I and OT-II transgenic cell numbers were determined. Each single cell suspension was diluted with trypan blue dye (1:10 dilution) in order to facilitate live cell counting using phase-contrast microscopy and the total cell numbers were calculated. To achieve the final cell concentration (8×10^6 cells mL^{-1}), single cell suspensions were diluted with sterile PBS and OT-I cells were combined with OT-II (1:1). Filtration through a cell strainer was conducted to remove aggregated cells. A volume of 500 µL of mixed OT-I and OT-II cell suspensions in PBS was injected via the tail vein into C57Bl/6 mice.

3.3.3.4 *In vivo* airway inflammation model

3.3.3.4.1 Immunisation and airway challenge with ovalbumin

On day -1, transgenic T cells (OT-I and OT-II) were adoptively transferred into experimental mice (see **Section 3.3.3.3**). The utilised airway model is a variation of an earlier protocol[306]. Mice were sensitised intraperitoneally (i.p.) with 100 μg of ovalbumin (OVA) (Sigma Aldrich, St. Louis, MO, USA) in 200 μL of alum adjuvant (Serva Electrophoresis GmbH, Heidelberg, Germany) on day 0. On day 7 mice were anaesthetised with a mixture of ketamine (100 mg mL^{-1}, Phoenix Pharm Distributors Ltd, New Zealand), xylazine (15 mg mL^{-1}) and atropine (77 mg mL^{-1}). 10 μL of anaesthetic per body weight were administered via the intraperitoneal route. Subsequently, the mice were given an intranasal (i.n.) challenge of 100 μg OVA. Four days later mice were sacrificed with a lethal dose of anaesthetic (volume of 1 mL i.p.) containing ketamine (10 mg mL^{-1}) and xylazine (300 μg mL^{-1}). The trachea was cannulated and a bronchoalveolar lavage (BAL) was performed with three washes of 1 mL PBS. The mediastinal lymph nodes and spleen were harvested from each mouse.

3.3.3.4.2 Treatment with PIM_2 and PGM_2 compounds

On day 6 mice were anaesthetised with ketamine (100 mg mL^{-1})/xylazine (15 mg mL^{-1})/atropine (77 mg mL^{-1}). PIM_2 and PGM_2 compounds (20 μg in 50 μL PBS) were administered i.n. Control mice were given PBS or dexamethasone (Dex, 4 mg mL^{-1}, Hospira, Australia) i.n.

3.3.3.5 Bronchoalveolar lavage

The bronchoalveolar lavage (BAL) cells were counted, spun onto slides (Shandon CytoSpin II, Shandon Southern Products Ltd., Runcorn, UK) and stained (Diff-Quick, Siemens, Newark, USA). The percentages of different cell

types (eosinophils, lymphocytes, macrophages, neutrophils) were determined microscopically using standard histological criteria, by a single investigator blinded to the treatment groups. A total of 200 cells from each slide was counted.

3.3.3.6 Harvesting cells from treated mice

The mediastinal lymph nodes and spleens were harvested and stored on ice in cIMDM. Mediastinal lymph nodes were analysed individually for each mouse, whilst harvested spleens were pooled for each treatment group. A single cell suspension was prepared as described in **Section 3.3.3.3**. After resuspension in cIMDM the total cell numbers were determined using phase-contrast microscopy. Cells were then resuspended at 8×10^6 cells mL^{-1} in cIMDM for subsequent processing.

3.3.3.7 *In vitro* T cell restimulation

Prior to cultivation of harvested cells in a 96 well round-bottomed tissue culture plates, wells were coated with α-CD3 in triplicate with a 50 µL aliquot of anti-CD3 antibody (10 µg mL^{-1}) in coating buffer (**Appendix A**) and incubated overnight at 4°C. Following the removal of excess anti-CD3, the wells were washed three times with cIMDM. A volume of 100 µL of IL-2 (10 IU mL^{-1}) in cIMDM was added to these wells and to a further three wells to act as a media control. A 100 µL volume of OVA (200 µg mL^{-1}) and IL-2 (10 IU mL^{-1}) was plated into another three wells. The single-cell suspensions prepared from collected tissue (2×10^6 cells mL^{-1}) were added to the plates into wells containing either α-CD3, OVA or media; each in conjunction with IL-2. Plates were incubated at 37°C with 5% CO_2 for 72 hours (HERAcell incubator, Heraeus, Hanau, Germany).

After three days, 100 μL of supernatant was removed from each sample well and transferred to wells of flat-bottomed 96 well plates for analysis of cytokine production. The plates were sealed and stored at -20°C. A volume of 100 μL of [^{3}H] thymidine (6.7 Ci/mmol; PerkinElmer, Boston, MA, USA) at a 1:20 dilution in cIMDM was added back to the wells for the last 8 hours of culture. To determine the extent of T cell proliferation, the amount of [^{3}H] thymidine which was taken up by dividing T cells was measured. To do this, an automated cell harvester (Harvester 96® Mach III M, Tomtec, CT, USA) was used to harvest cells onto glass fibre filter mats (Wallac, Turku, Finland). Scintillation fluid was added and cellular incorporation of [^{3}H] thymidine was then assessed using a 1450 MicroBeta Plus Liquid Scintillation Counter (Wallac, Turku, Finland). Results were expressed in counts per minute (c.p.m.).

3.3.3.8 Cytokine production

Culture supernatants were collected (see **Section 3.3.3.7**) and IFN-γ, IL-4, IL-5 and IL-13 levels measured using BD CBA Mouse Flex Set (BD Biosciences) specific for each cytokine. A CBA Mouse/Rat Soluble Protein Master Buffer Kit (BD Biosciences) was utilised as the buffer system during sample preparation. Samples were analysed on BD FACSCanto II (Becton Dickinson, Franklin Lakes, NJ, USA). Cytokine concentrations of IFN-γ, IL-4, IL-5 and IL-13 were calculated against standards using FCAP Array software (v1.0, Soft Flow) with lowest level of detection of 9.71 pg mL^{-1}, 10.20 pg mL^{-1}, 5.43 pg mL^{-1} and 19.09 pg mL^{-1}, respectively. Experiments in which the cytokine level of background medium was greater than 10% of the level of OVA-specific restimulation were excluded from further analysis.

3.3.3.9 Cell staining and flow cytometry analysis

To analyse the frequency of specific surface markers on T cells, flow cytometry, also known as fluorescence-activated cell sorting (FACS), was performed.

Samples of lymph node and spleen cell suspensions (see **Section 3.3.3.3**) were washed with FACS buffer (**Appendix A**) by centrifugation at 1200 rpm for 5 min. The supernatants were discarded and the cell pellets resuspended by flicking the tube and gentle vortexing. The cells were then incubated with anti-CD16/CD32 (2.4G2 Fc Block; 0.5 mg mL^{-1}) at a 1:400 dilution in FACS buffer (according to manufacturer's instructions) for 10 min on ice in the dark. This was undertaken in order to block non-specific binding. Cells were subsequently diluted to stop the binding and washed with FACS buffer (2 mL) by centrifugation (1200 rpm, 5 min) to remove unbound antibody. Supernatants were discarded and cells resuspended by flicking and vortexing. Further cell staining was conducted with 100 μL of a cocktail of anti-CD8-PE-Cy7 (53-6.7), anti-CD4-V500 (RM 4-5), Vα2-PE (B20.1) and Vβ5.1-biotin (MR9-4), all diluted at 1:200. After 10 min incubation on ice in the dark, FACS buffer (2 mL) was added and samples were centrifuged to remove excess antibodies. After the supernatants were discarded and the cells resuspended, 100 μL of streptavidin-APC-Cy7 in FACS buffer (1:200 dilution) was added. Again samples were incubated for 10 min on ice in the dark. The cells were washed, supernatants decanted and cells resuspended in 100 μL of FACS buffer containing propidium iodide (PI, 50 μg mL^{-1}). Flow cytometry was performed on a BD FACSCanto II (Becton Dickinson) and data analysed using FlowJo software (version 9.2; TreeStar, Inc., Ashland, Oregon, USA).

3.3.4 Statistical analysis

Where applicable, results are expressed as mean ± standard deviation (SD) unless otherwise stated. Statistical analyses were carried out using an unpaired Student's t-test (two-tailed) or one-way analysis of variance (ANOVA) followed by post hoc analysis using Tukey's pairwise comparison, as appropriate. In all instances, statistical analyses were conducted using IBM SPSS Statistics 20 (SPSS Inc., Chicago, IL, USA).

3.4 Results

3.4.1 Optimisation of the Langmuir trough technique using a model phospholipid

Experimental conditions to characterise lipid monolayers at air/water interfaces were established using distearoylphosphatidylglycerol (DSPG) as a model lipid. DSPG is a well-studied phospholipid[301,307] with structural similarities (number and length (C18) of fatty acid residues, presence of a phosphatidyl moiety and negatively charged polar head group) to the molecules investigated as part of this study (**Figure 3-6**).

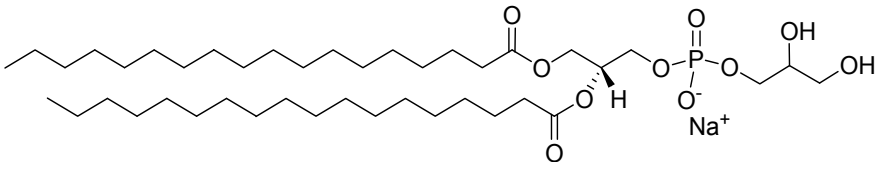


Figure 3-6. Structure of distearoylphosphatidylglycerol (DSPG).

The aim was to prepare DSPG monolayers and to demonstrate the validity and reliability of the Langmuir trough technique. In order to do this, the limiting area per molecule A_0 and collapse pressure π_{coll} of the DSPG film were determined and compared to that previously published[301,307].

The effect of experimental parameters such as lipid concentration, choice of solvent system and sub-phase, compression rate and the reproducibility of measurements were investigated (**Appendix B**). The optimal lipid concentration was found to be 0.5 mg mL^{-1}, as previously published[301], with 25 μL of sample being applied to the sub-phase (**Appendix B**, **Figure B-1**). While in previous reports DSPG stock solutions were prepared in chloroform, due to the low solubility of PIM_2 and PGM_2 a mixture of chloroform and methanol was used to prepare the stock DSPG solution. No differences in π-A isotherms were detected using chloroform or chloroform/methanol (4:1, v/v) (**Appendix B**, **Figure B-2**). In all experiments the lipid monolayers were compressed at a constant barrier speed of 5 cm^2 min^{-1} although there were no differences between the isotherm obtained after compression at 5 or 10 cm^2 min^{-1} (**Appendix B**, **Figure B-3**). Compression at both rates gave similar limiting area per molecule (A_0) and collapse pressures (π_{coll}). Furthermore, the composition of the sub-phase did not affect monolayer formation and similar isotherms were found using Milli-Q water and PBS buffer (pH 7.5) (**Appendix B**, **Figure B-4**). Repeated experiments under the evaluated conditions gave limiting area per molecule (A_0) and collapse pressures (π_{coll}) values in good agreement with those reported in the literature[301,307] (**Table 3-1** and **Appendix B**, **Figure B-5**).

Table 3-1. Limiting area per molecule A_0 (Å^2) and collapse pressure π_{coll} (mN m^{-1}) of DSPG monolayers at the air/liquid interface at 25°C.

	Experimental[#]	**Literature**
A_0	41.4 ± 5.3	45 ± 0.3 *
π_{coll}	53.1 ± 1.2	50 **

[#] Values are presented as mean ± SD of three independent experiments.
* A_0 was determined from monolayer formed on water sub-phase[301].
** π_{coll} was obtained from a lipid film formed on aqueous sub-phase containing 1.0 x 10^{-2} M $CaCl_2$, pH = 6 [307].

3.4.2 Behaviour of PIM_2 and PGM_2 lipids at the air/water interface

3.4.2.1 Effect of acyl chain length on monolayer formation

The π-A isotherms obtained for PIM_2 and PGM_2 compounds are shown in **Figure 3-7** and **Figure 3-8**, respectively along with the corresponding elastic compressibility moduli (C_s^{-1}) as a function of molecular area (inset). The degree of packing and stability of the monolayer films were quantified by the limiting area per molecule A_0 and the collapse pressure π_{coll} (**Table 3-2**). The compressibility of the monolayer can be assessed by C_s^{-1} values which are described by **Equation 3-5**:

$$C_s^{-1} = -A_\pi \left(\frac{\partial \pi}{\partial A}\right)_\pi \qquad \textbf{Equation 3-5}$$

where A is the molecular area at the corresponding surface pressure π[308]. A C_s^{-1} value is a first derivative function multiplied by the molecular area and can be directly calculated from the π-A data recorded for each compound. This parameter gives additional information on the physical state of the monolayer during compression: the higher the value, the more condensed the

monolayer[282,309]. The maximum C_s^{-1} values ($C_s^{-1}_{max}$) for each monolayer and the corresponding surface pressure π_{comp} are summarised in **Table 3-2**.

Table 3-2. Limiting area per molecule A_0 (Å^2), collapse pressure π_{coll} (mN m^{-1}) and maximum elastic compressibility modulus $C_s^{-1}_{max}$ (mN m^{-1}) at the corresponding surface pressure π_{comp} (mN m^{-1}) of pure monolayers of PIM_2 and PGM_2 at 24°C (mean ± SD, n=3).

Lipid	Acyl chain length	A_0	π_{coll}	$C_s^{-1}_{max}$*	π_{comp}
PIM_2	16:16	81.0 ± 3.2	43.7 ± 1.0	73.1 ± 1.5	27.7 ± 0.4
PIM_2	18:18	69.6 ± 3.0	55.3 ± 0.7	92.5 ± 7.0	43.3 ± 2.3
PGM_2	0:0	-	-	-	-
PGM_2	10:10	-	-	22.9 ± 1.1	6.0 ± 0.5
PGM_2	16:16	79.5 ± 1.4	52.7 ± 1.0	61.1 ± 3.3	43.9 ± 2.3
PGM_2	18:18	63.2 ± 2.2	60.7 ± 2.1	119.4 ± 17.2	46.4 ± 7.5

*calculation from π-A isotherm using **Equation 3-5**

PIM_2 (16:16) and PIM_2 (18:18) displayed typical π-A isotherms, similar to profiles of phospholipid monolayers[280,301,310] (**Figure 3-7**). At the start of the compression stage PIM_2 (16:16) was in a gaseous phase (G) as evidenced by the decreasing molecular area (120 – 100 Å^2), but stable surface pressure. Upon further compression, the surface pressure increased and molecules orientated in the liquid-expanded state (LE). The C_s^{-1} values (**Figure 3-7**, inset) for PIM_2 (16:16) rose steadily to a maximum of 73.1 ± 1.5 mN m^{-1}, a value that defines an expanded state[308]. The collapse point of the film occurred at 43.7 ± 1.0 mN m^{-1}. In contrast to PIM_2 (16:16), the C_s^{-1} values for PIM_2 (18:18) increased initially and exhibited a small decrease in elastic compressibility moduli, before continuing to increase (**Figure 3-7**, inset). This minimum in C_s^{-1} values signifies an additional ordering of the molecules, most likely occurring due to increased

intermolecular Van der Waals attractive forces between the longer hydrocarbon chains[284,310,311]. The steeper slope of the isotherm and the smaller limiting area per molecule of 69.6 ± 3.0 Å^2 suggested a closer packing of the PIM_2 (18:18) molecules compared to the PIM_2 (16:16) molecules ($p \leq 0.01$). The result of the tighter monolayer organisation was increased stability of the PIM_2 (18:18) monolayer, evidenced by a significantly higher collapse pressure compared to PIM_2 (16:16) (55.3 ± 0.7 mN m^{-1} compared to 43.7 ± 1.0 mN m^{-1}, $p \leq 0.001$).

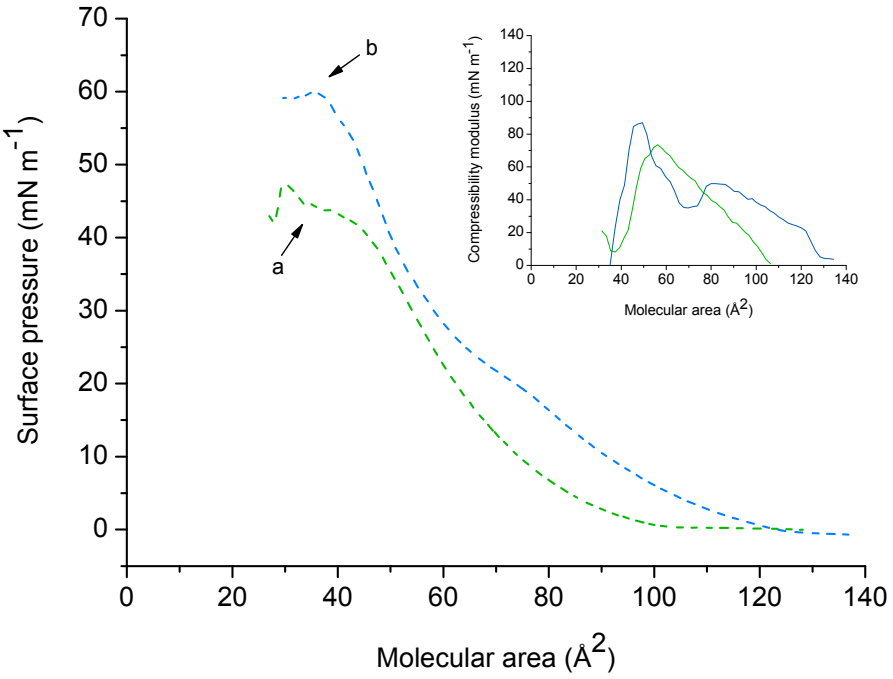


Figure 3-7. Monolayer compression of phosphatidylinositol dimannosides (PIM_2) at the air/water interface: surface pressure-molecular area (π-A)-isotherms of PIM_2 (16:16) (---) and PIM_2 (18:18) (---), respectively. Arrows indicate: (a) collapse of PIM_2 (16:16) monolayer, (b) collapse of PIM_2 (18:18) monolayer. *Inset:* Compressibility modulus plot versus molecular area as a function of molecular area. The curves are each a representative of three independent experiments.

No increase in surface pressure was detected for the PGM_2 (0:0) under the applied experimental conditions and thus no isotherm could be recorded. The lack of fatty acids attached to the phosphatidyl moiety increased the

hydrophilicity of the compound allowing for solubilisation into the aqueous sub-phase. Upon compression of PGM_2 (10:10), surface pressure increased slowly up to 23.3 ± 0.2 mN m^{-1} (**Figure 3-8**). The isotherm showed no abrupt change at the end of interface compression, which would indicate the collapse of the film. Also, no phase transition could be detected upon compression suggesting the monolayer remained in the LE state. The low $C_s^{-1}{}_{max}$ value (22.9 ± 1.1 mN m^{-1}) similarly indicated the presence of a LE layer[308] (**Table 3-2**). These findings suggest that unstable monolayers were formed whereby PGM_2 (10:10) molecules were progressively released into the bulk phase upon compression.

PGM_2 (16:16) and PGM_2 (18:18) molecules were sufficiently water-insoluble to form stable monolayers (**Figure 3-8**). The immediate increase in pressure suggested that the molecules orientated in the expanded state. With progressive compression the surface pressure rose to a maximum of 52.7 ± 1.0 mN m^{-1}, at which point the film collapsed. The limiting area for PGM_2 (16:16) monolayer was found to be 79.5 ± 1.4 $Å^2$. The recorded isotherm and C_s^{-1} plot suggested an additional ordering PGM_2 (16:16) monolayer at 60 $Å^2$. However, the $C_s^{-1}{}_{max}$ value of 61.1 ± 3.3 mN m^{-1} implied a LE phase at point of collapse[308]. The PGM_2 (18:18) monolayer underwent a transition to a more condensed phase at approximately 10 mN m^{-1}. The coexistence of an LE and LC phase is demonstrated by the plateau region in the isotherm and the dramatic decline in C_s^{-1} values beginning at a molecular area of 90 $Å^2$ (**Figure 3-8**, inset)[284,310,311].

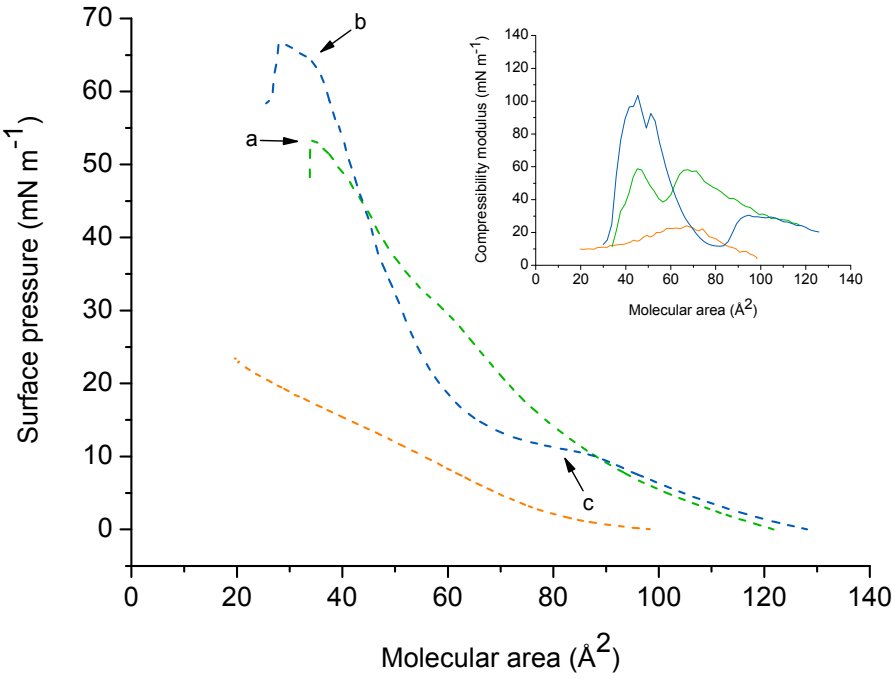


Figure 3-8. Monolayer compression of phosphatidylglycerol dimannosides (PGM_2) at the air/water interface: surface pressure-molecular area (π-A)-isotherms of PGM_2 (10:10) (---), PGM_2 (16:16) (---) and PGM_2 (18:18) (---), respectively. Arrows indicate: (a) collapse of PGM_2 (16:16) monolayer, (b) collapse of PGM_2 (18:18) monolayer, (c) LE-LC phase transition of PGM_2 (18:18) monolayer. *Inset*: Compressibility modulus plot versus molecular area as a function of molecular area. The curves are each a representative of three independent experiments.

Upon further compression, the PGM_2 (18:18) isotherm slope showed a steep increase and the molecules became even more densely packed. The isotherm reached a maximum pressure of 60.7 ± 2.1 mN m^{-1} before collapsing, significantly higher than the collapse pressure detected for PGM_2 (16:16) ($p \leq 0.001$). Moreover, the PGM_2 (18:18) monolayer had a smaller A_0 compared to PGM_2 (16:16) (63.2 ± 2.2 mN m^{-1} compared to 79.5 ± 1.4 mN m^{-1}, $p \leq 0.001$). These measurements confirm the ability of the acylated PGM_2 to form monolayers with stabilities depending on the length of acyl chains.

3.4.2.2 Effect of polar head group on monolayer formation

Polar head groups have a great impact on the orientation of the hydrocarbon chains in the interface and affect the isotherm[253]. This study particularly focused on how monolayer formation is influenced by the presence of the inositol or glycerol head groups found in PIM_2 and PGM_2. For ease of comparison the isotherms recorded for PIM_2 (18:18) and PGM_2 (18:18) are plotted in **Figure 3-9**. Although these two compounds have an identical number of total carbons in their acyl chains, their film configuration revealed significant differences.

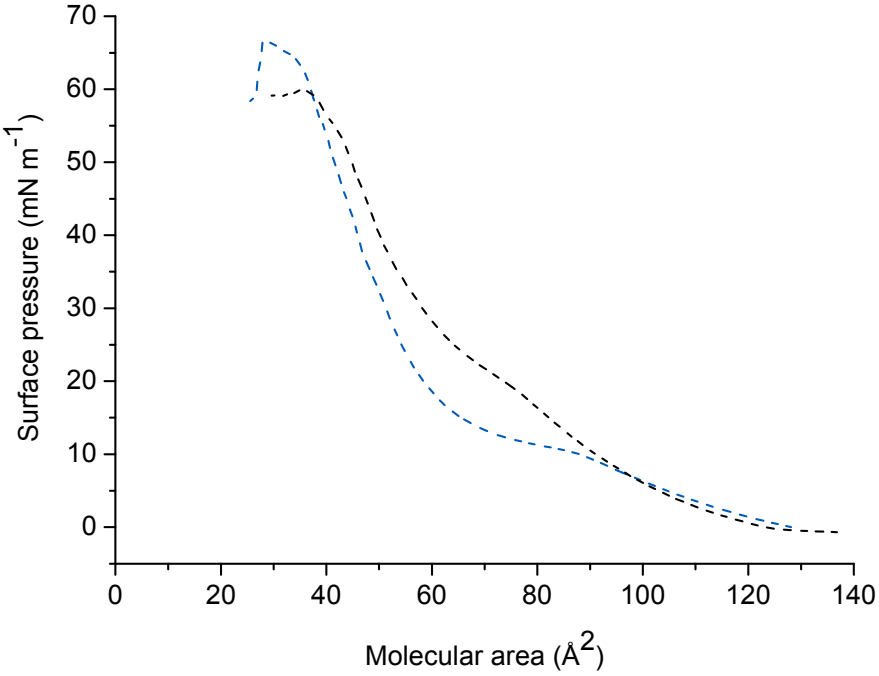


Figure 3-9. Effect of head group on monolayer formation: π-A isotherms of PIM_2 (18:18) (**---**) and PGM_2 (18:18) (**---**) at the air/water interface. The curves are each a representative of three independent experiments.

While both monolayers underwent chain ordering, the PGM_2 (18:18) isotherm showed a transition from an expanded to a more condensed state (LE-LC

transition) at low surface pressures. The molecules became tightly packed in the interface, causing a steep rise of the isotherm. The film collapsed at a significantly higher surface pressure than that one recorded for PIM_2 (18:18) (60.7 ± 2.1 mN m^{-1} compared to 55.3 ± 0.7 mN m^{-1}, $p \leq 0.01$).

The formation of a condensed PGM_2 (18:18) monolayer is further suggested by a maximum compressibility modulus which exceeded 100 mN m^{-1}, indicating an LC film. In contrast, the PIM_2 (18:18) monolayer remained in the LE state. The likely explanation for these results is that the steric hindrance of the inositol group prevented a compact arrangement of the PIM_2 (18:18) molecules in the interface, leading to a larger area occupied by the molecules and a less stable film. Similar results were found for monolayers of PIM_2 (16:16) and PGM_2 (16:16) (**Appendix B**).

3.4.3 Self-aggregation in aqueous solution

The aggregation behaviour of PIM_2 and PGM_2 compounds in the aqueous phase was investigated by dynamic light scattering (DLS), zeta potential measurement and transmission electron microscopy (TEM). Volume-based size distribution analysis for PIM_2 (16:16) found three populations of particles, one main population (89.4 ± 0.9%) with a diameter of approximately 13.21 ± 0.56 nm and two minor populations with diameters of approximately 79.82 ± 4.98 nm and 1476 ± 137.39 nm (**Figure 3-10 A**).

Evidence supporting the formation of spherical aggregates was provided by TEM. The micrographs show spherical objects with diameters mainly between 15 and 20 nm, which showed good agreement with the DLS data. The two other populations are likely to be aggregates of small particles. Light scattering

measurements of PIM_2 (18:18) revealed a large population (98.5 ± 1.3% of the sample) with an average size of 1410.33 ± 197.0 nm (**Figure 3-10 B**). The distribution width of the peak (386.3 ± 205.5 nm) suggested this was a heterogeneous population. Particles were found to be spherical or oval in shape under the transmission electron microscope. A particle population sized between 200-300 nm observed by TEM was detected by DLS with a low abundance of 1.7 ± 0.4%.

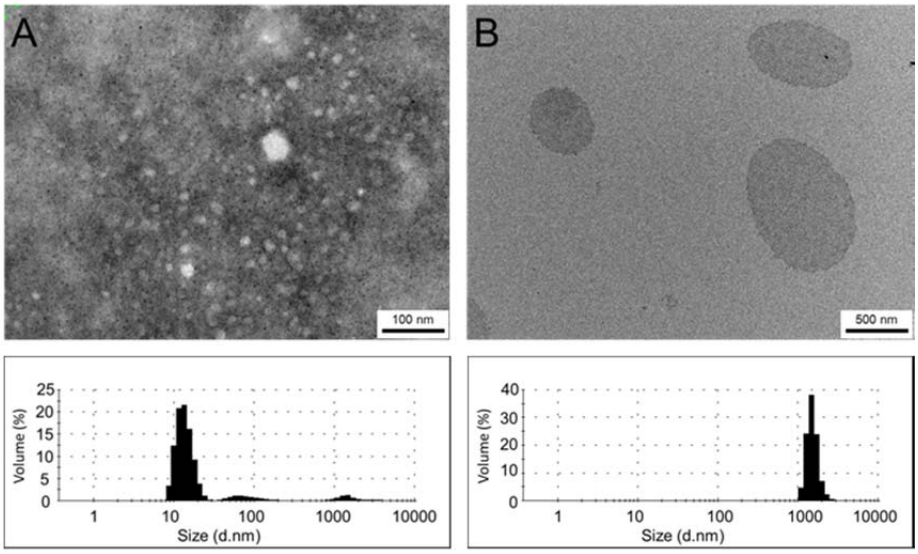


Figure 3-10. Transmission electron micrographs along with a representative histogram of volume-based particle size distribution of PIM_2 compounds in PBS at 0.4 mg mL^{-1}. TEM samples were prepared by negative staining with 1% PTA. **(A)** PIM_2 (16:16) (scale bar= 100 nm), **(B)** PIM_2 (18:18) (scale bar= 500 nm).

For PGM_2 (0:0), the deacylated analogue, no light scattering particles could be recorded and no particles were visualised by TEM despite examination of different grid preparations (**Figure 3-11 A**). This suggested that self-aggregation is dependent on the presence of fatty acids bound to the phosphatidyl moiety. Of particular interest was the behaviour of PGM_2 (10:10) since the monolayer study suggested that a soluble lipid film was formed at the air/water interface.

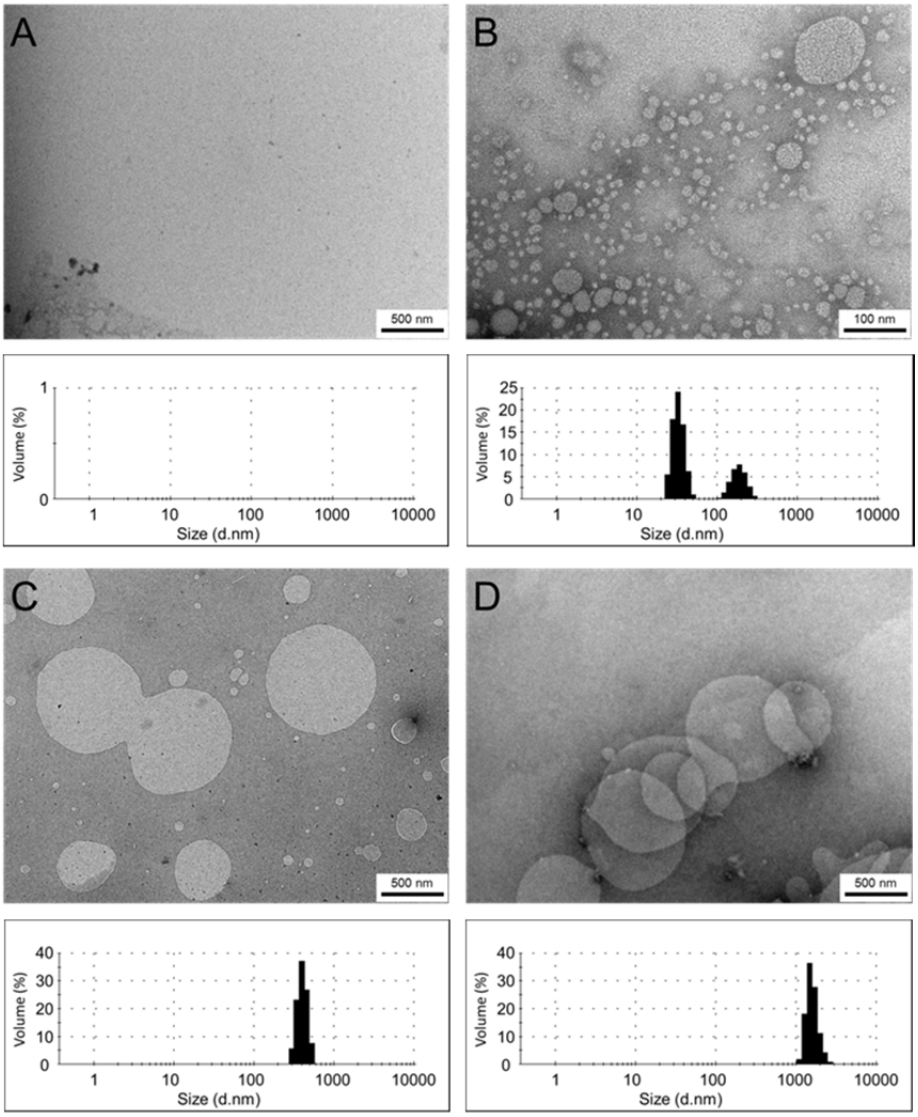


Figure 3-11. Transmission electron micrographs along with a representative histogram of volume-based particle size distribution of PGM_2 compounds in PBS at 0.4 mg mL^{-1}. TEM samples were prepared by negative staining with 1% PTA. **(A)** PGM_2 (0:0) (scale bar= 500 nm) **(B)** PGM_2 (10:10) (scale bar= 100 nm), **(C)** PGM_2 (16:16) (scale bar= 500 nm), **(D)** PGM_2 (18:18) (scale bar= 500 nm).

The likely explanation for this is that the molecules may organise in micellar rather than bilayer structures[253]. DLS measurements of PGM_2 (10:10) in solution resulted in two peaks (**Figure 3-11 B**), the first with a mean diameter of 40.0 ± 5.9 nm (62.8 ± 7.6%), which can also be seen in the TEM sample. Again large aggregates were seen as a minor peak at 193.97 ± 12.57 nm (37.2 ± 7.6%). The average size of PGM_2 (16:16) particles in solution was 503.5 ± 85.5 nm and a

distribution width of 77.1 ± 15.4 nm. TEM, shown in **Figure 3-11 C**, confirmed the formation of round shaped aggregates although from the image the particle sizes are slightly smaller than those detected by DLS. **Figure 3-11 D** shows the aggregates formed by PGM_2 (18:18) were regular spherical structures with relatively large average diameters of 1874.0 ± 380.4 nm and a distribution width of 383.1 ± 146.1 nm.

As anticipated, the charge of the phosphatidyl moiety resulted in a negative zeta potential with values between -18 and -23 mV (**Table 3-3**). The charge did not appear to be affected by the changes in the head groups or lipids. This study provided strong evidence that the acylated PIM_2 and PGM_2 are able to self-assemble in aqueous solution to form organised structures. Furthermore, it appears that acyl chain length plays a significant role in determining the size of the particles formed.

Table 3-3. Zeta potential measurements (ZP in mV) of PIM_2 and PGM_2 compounds in PBS at a concentration of 0.4 mg mL^{-1}. Measurements were carried out at 25°C (mean ± SD, n=3).

Lipid	ZP
PIM_2 (16:16)	-18.9 ± 0.84
PIM_2 (18:18)	-22.9 ± 0.48
PGM_2 (0:0)	-
PGM_2 (10:10)	-24.3 ± 0.66
PGM_2 (16:16)	-20.8 ± 1.42
PGM_2 (18:18)	-22.7 ± 0.99

3.4.4 Suppression of airway eosinophilia

In earlier studies phosphatidylinositol mannoside extracts from mycobacteria and synthetic analogues have been shown to suppress allergic airway inflammation in mice[70,96,227,236,248]. To help determine the effect of varied lipophilicity and head group structure on biological activity, the different compounds were tested in a mouse model of allergic asthma. Here a modified protocol of an airway inflammation model[248] was utilised, with the aim of investigating the effect of the treatment on the cellular immune responses as well as the lung inflammatory response. To assess the effect of synthetic PIM_2 and PGM_2 compounds on lung eosinophilia, groups of OVA-sensitised C57BL/6 mice were treated with the different compounds, PBS or dexamethasone. Following a bronchoalveolar lavages (BALs), differential cell counts were performed on stained cytospins. **Figure 3-12** shows representative samples of microscope investigation of cytospin samples.

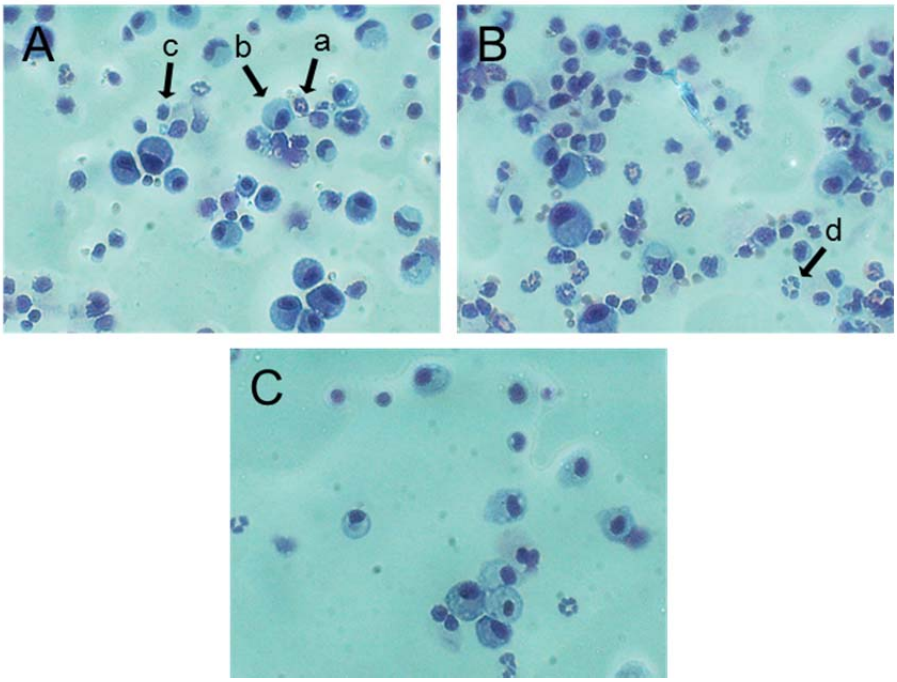


Figure 3-12. Cytospin samples for mice treated with **(A)** PGM_2 (16:16), **(B)** PBS and **(C)** dexamethasone. On day 11 of the study bronchoalveolar lavages (BALs) were performed and BAL cells spun onto slides. Following staining, the percentages of different cell types were determined microscopically. Arrows indicate different cell types: (a) eosinophils, (b) macrophages, (c) lymphocytes and (d) neutrophils.

As expected, the PBS treated control group had an influx of eosinophils into the BAL as well as high total cell numbers (**Figure 3-13**). Both the frequency (6 ± 3, $p \leq 0.001$) and total number (9 ± 5, $p \leq 0.01$) of eosinophils in the BAL were reduced by treatment with dexamethasone. Treatment with the acylated PIM_2 and PGM_2 compounds appeared to suppress the airway eosinophila. However, this reduction in eosinophil frequency (12 ± 3, $p \leq 0.05$) and total eosinophils (19 ± 4, $p \leq 0.05$) was only significant in mice treated with PGM_2 (16:16). All remaining compounds had a subtle effect on the eosinophil percentage. Consistent with early results from a purified extract[236], the deacylated PGM_2 (0:0) was possibly the least effective in suppressing the influx of eosinophils concerning the total eosinophil numbers (**Figure 3-13 B**).

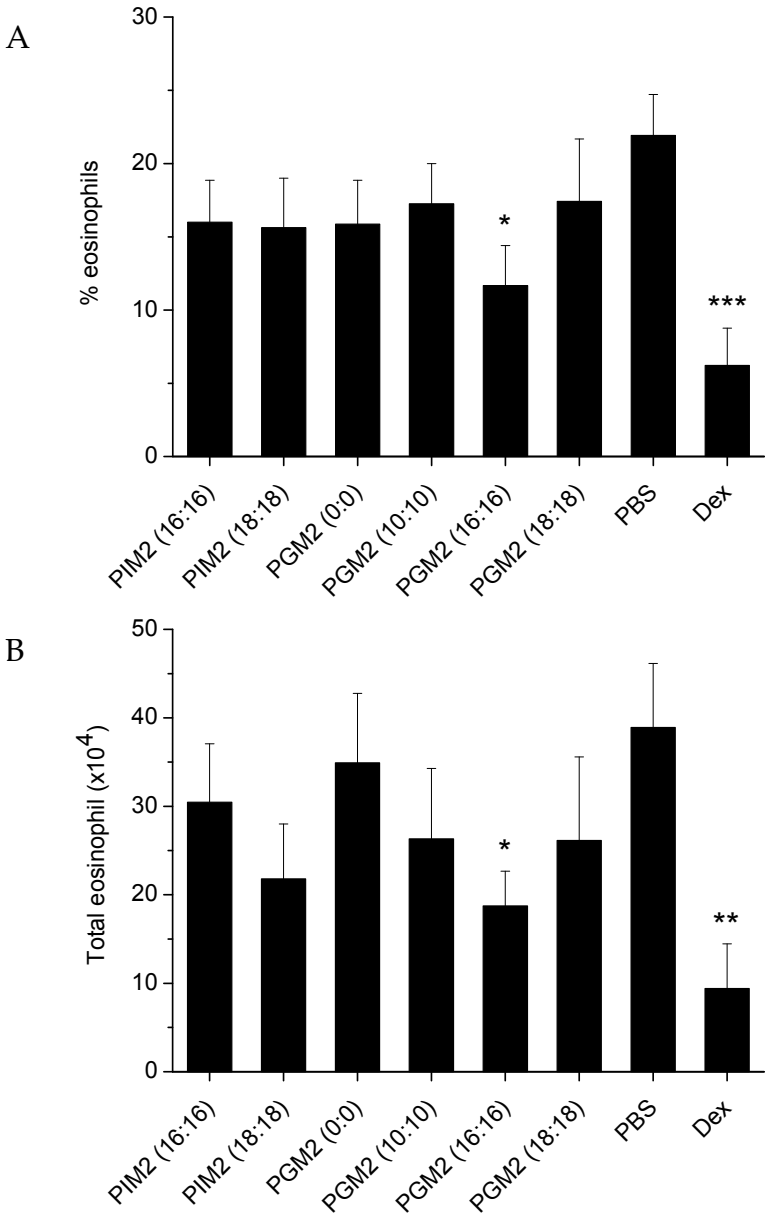


Figure 3-13. Airway eosinophilia in OVA-sensitised mice. **(A)** Percent **(B)** total number of airway eosinophils in BAL fluid. C57BL/6 mice were immunised i.p. with OVA/alum on day 0. On day 6 mice were treated i.n. with various PIM_2 and PGM_2 in 50 μL of PBS or PBS alone. Mice were challenged intranasally with OVA on day 7. Four days post-OVA challenge lungs were flushed and differential cell count performed on stained cytospins. Bars depict mean + SE from n=3 mice per group from four independent experiments. * denotes $p \leq 0.05$, ** $p \leq 0.01$, and *** describes $p \leq 0.001$ relative to PBS group.

3.4.5 Expansion of transgenic $CD4^+$ and $CD8^+$ T cells

Next, the ability of PIM_2 and PGM_2 to suppress cellular OVA-specific immune responses was analysed. To do this, OVA-specific $CD4^+$ and $CD8^+$ transgenic cells were adoptively transferred into the recipient mice prior to OVA sensitisation on day 0. These cells provide a population of tracer cells that can be specifically identified by flow cytometry, and can be used to measure antigen-specific cell frequencies. Expansion of antigen specific $CD4^+$ and $CD8^+$ Vα2Vβ5 T cells in the mediastinal lymph nodes and spleens harvested from treatment groups was investigated. As shown in **Figure 3-14**, a decrease in the percentage of OVA-specific $CD4^+$ T cells in lymph nodes was observed in mice treated with the PIM_2 and PGM_2 compounds or dexamethasone. This decrease was significant in the case of mice treated with PIM_2 (16:16) (7.5 ± 0.8, $p \leq 0.05$), PIM_2 (18:18) (7.3 ± 1.0, $p \leq 0.05$), PGM_2 (16:16) (7.7 ± 0.9, $p \leq 0.05$) and PGM_2 (0:0) (6.7 ± 0.7, $p \leq 0.01$), dexamethasone (5.7 ± 1.1, $p \leq 0.01$). However, when the total number of Vα2Vβ5 $CD4^+$ T cells was examined the decrease was significant only in mice treated with dexamethasone (0.1 ± 0.05, $p \leq 0.01$) (**Figure 3-14 B**). The frequency (5.5 ± 1.0, $p \leq 0.001$) and total number (0.2 ± 0.06, $p \leq 0.001$) of Vα2Vβ5 $CD8^+$ T cells was only significantly reduced in the dexamethasone control group.

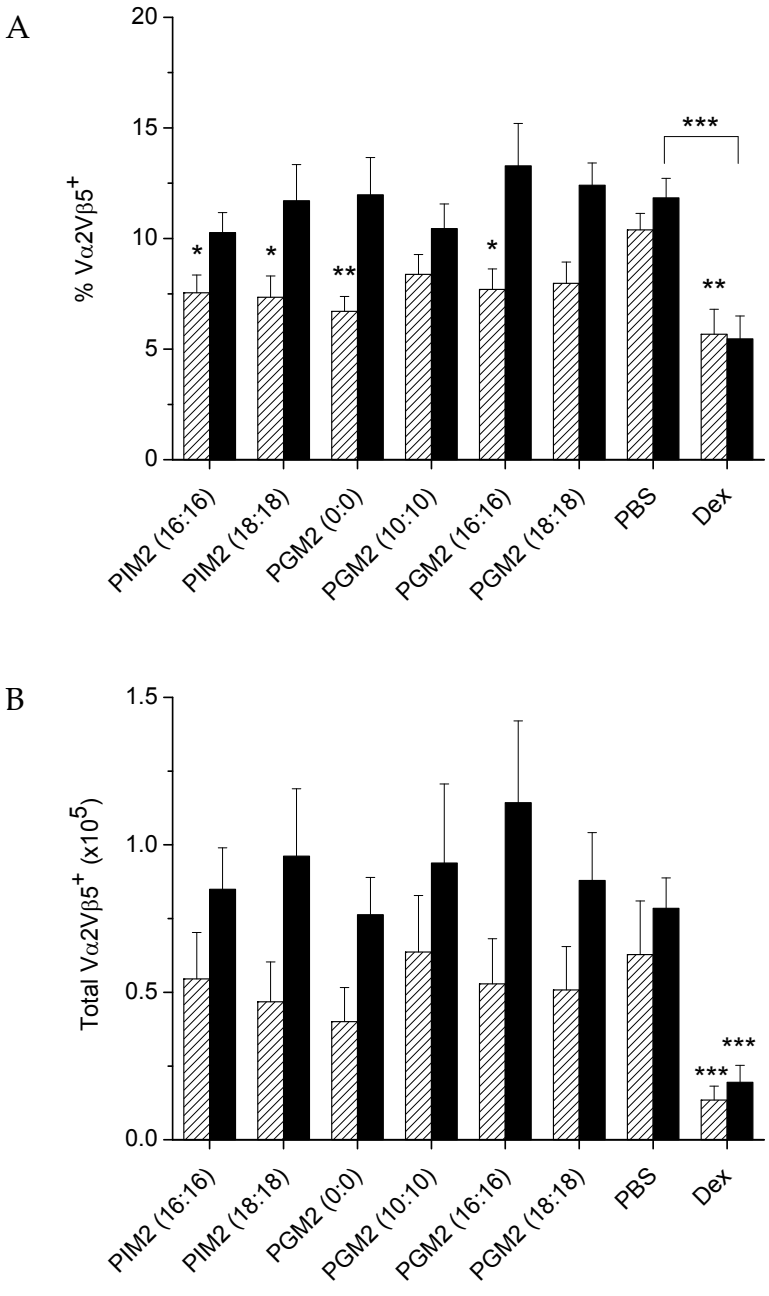


Figure 3-14. OVA-specific expansion of Vα2Vβ5 T cells. **(A)** Percent and **(B)** total number of $CD4^+$ (striped bars) and $CD8^+$ (black bars) Vα2Vβ5 T cells in the mediastinal lymph nodes. Graphs depict mean + SE from n=3 mice per group from four independent experiments, * denotes $p \leq 0.05$, ** $p \leq 0.01$, and *** describes $p \leq 0.001$ relative to PBS treatment group.

The expansions of antigen specific $CD4^+$ and $CD8^+$ Vα2Vβ5 T cells in spleens were comparable between treatment groups and PBS control (**Figure 3-15**). A significant reduction in percentage of T cells could only be detected in mice treated with dexamethasone for both $CD4^+$ (2.5 ± 0.2, $p \leq 0.01$) and $CD8^+$

(3.4 ± 0.4, $p \leq 0.01$). As it can be seen from **Figure 3-15 B**, there was a similar trend for decreased total numbers of $CD4^+$ and $CD8^+$ for dexamethasone, however this trend was not significant ($p > 0.05$). All remaining treatment groups showed similar total numbers to PBS control group.

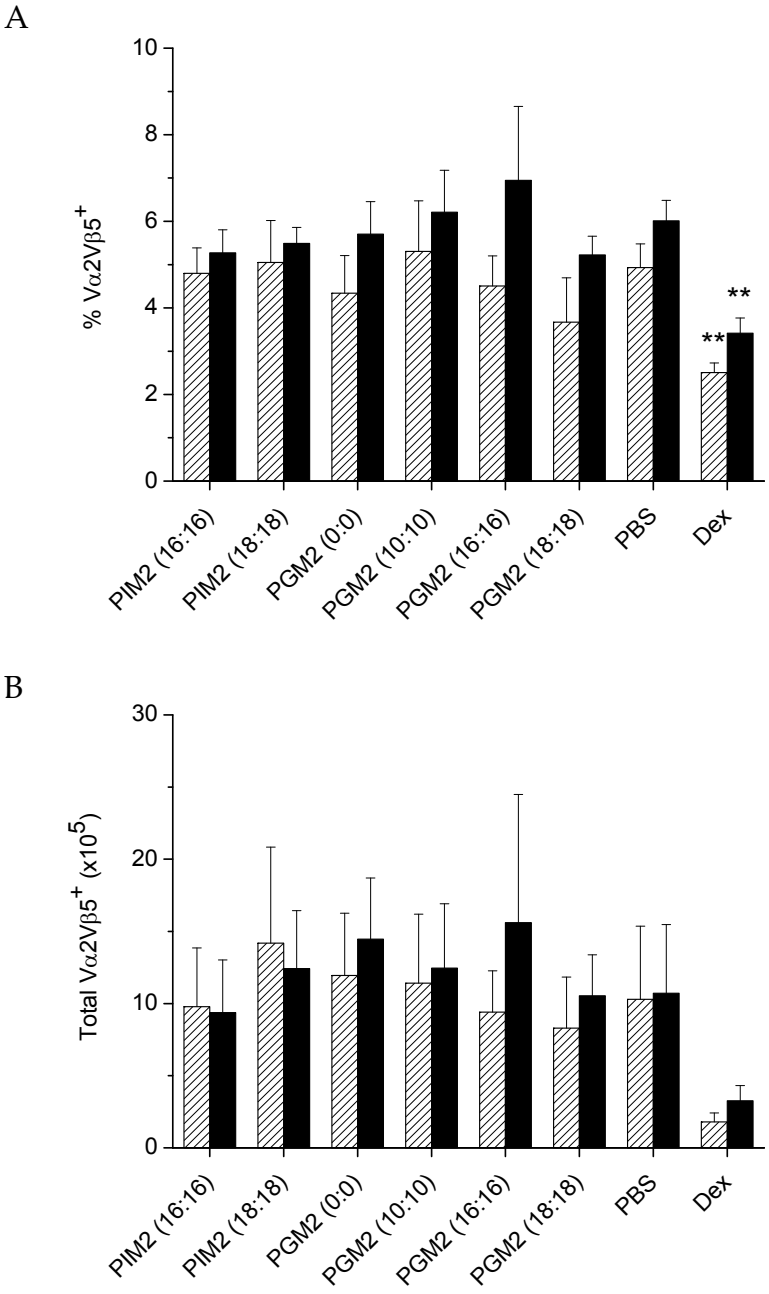


Figure 3-15. OVA-specific expansion of Vα2Vβ5 T cells. **(A)** Percent and **(B)** total number of $CD4^+$ (striped bar) and $CD8^+$ (black bar) Vα2Vβ5 T cells in spleens. Spleens were pooled within each treatment group. Graphs depict mean + SE from n=3 mice per group from four independent experiments, **denotes $p \leq 0.01$ relative to PBS treatment group.

3.4.6 T cell proliferation after *in vitro* restimulation with OVA

The extent of mediastinal lymph node and spleen cell division, in response to OVA, was determined utilising a standard thymidine incorporation assay. This method is based on the strategy wherein the radiolabeled nucleoside, ^{3}H-thymidine, is incorporated into cells during cell division. Quantification of the radioactivity is then used to determine the extent of cell proliferation. The results are presented as stimulation index (SI), the ratio between OVA-stimulated (foreground) and non-stimulated cells (background) (**Figure 3-16**).

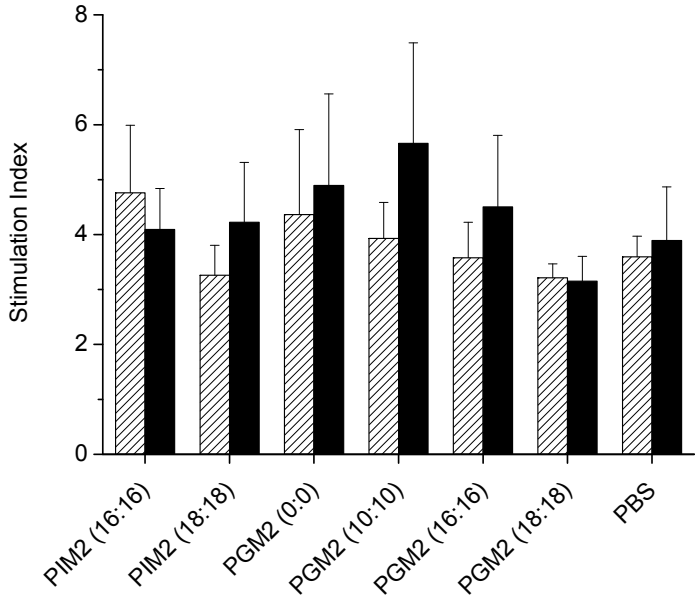


Figure 3-16. Proliferation of T cells isolated from mediastinal lymph nodes (striped bars) and spleens (black bars) of each study group after *in vitro* restimulation with OVA and media. Results are expressed as stimulation indices (SI= OVA/media). Bars depict mean + SE from n=3 mice per group from three independent experiments.

No significant differences in proliferative responses of the isolated lymphocytes could be detected between the treatment groups and PBS control group. All count rates measured for the spleen samples were found to be similar and no significant differences in proliferation were observed between the treatment groups ($p > 0.05$).

3.4.7 OVA-specific production of cytokines

To further investigate the underlying mechanism of airway eosinophilia suppression, the capacity of mediastinal lymph node to produce INF-γ, IL-4, IL-5 and IL-13 was assessed. The mediastinal lymph nodes were collected. If sufficient cells were available, they were restimulated *in vitro* and OVA-specific cytokine responses analysed. No IL-4 or IL-5 were detected (data not shown) and the levels of INF-γ and IL-13 in mediastinal lymph nodes were generally reduced in mice treated with PIM_2 and PGM_2 (**Figure 3-17**). However, this reduction was significant only for INF-γ in mice treated with PIM_2 (16:16) (442 ± 104, $p \leq 0.01$) and PGM_2 (18:18) (600 ± 122, $p \leq 0.05$). It was not possible to assess the effect of dexamethasone on cytokine production or proliferation due to the low numbers of cells able to be harvested from the mediastinal lymph nodes of these mice.

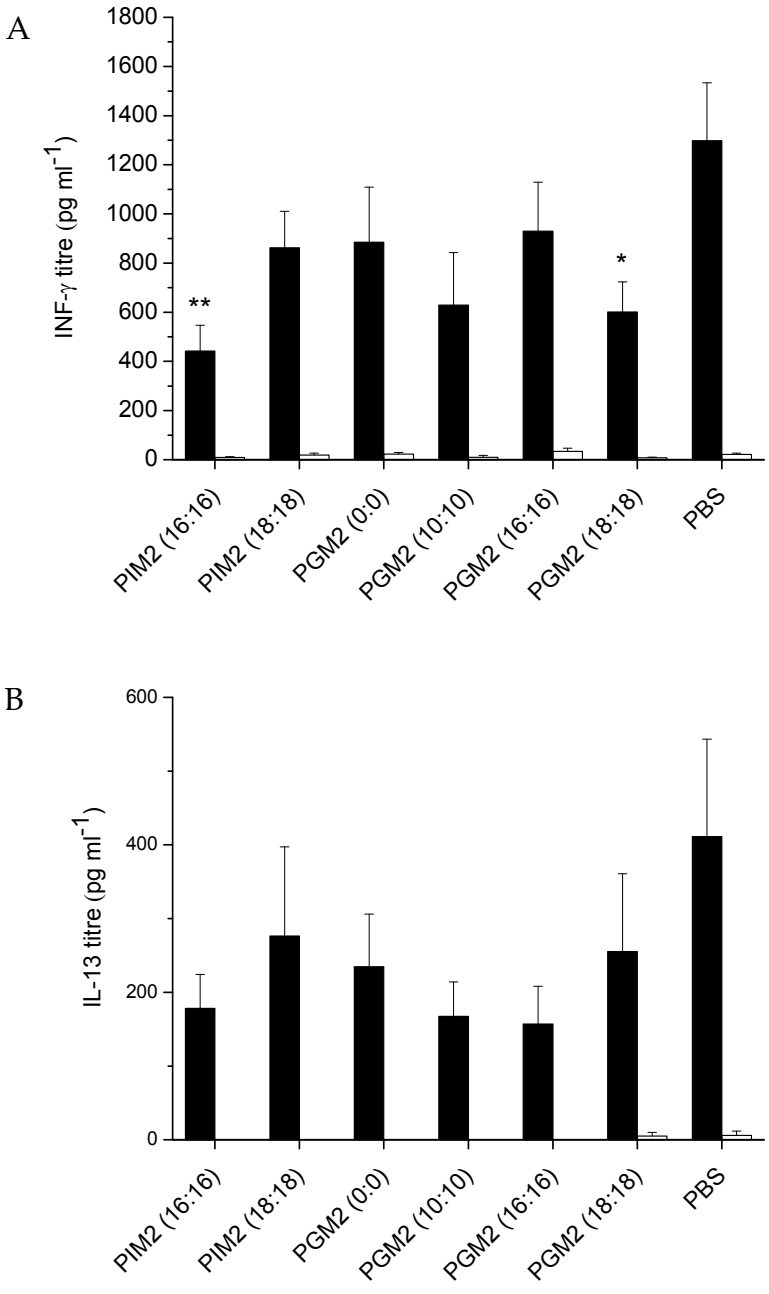


Figure 3-17. Production of **(A)** IFN-γ and **(B)** IL-13 by T-cells isolated from mediastinal lymph nodes of each study group. Titres of cytokine responses were determined after *in vitro* restimulation with OVA (black bars) or medium (white bars, negative control). Bars depict mean + SE from n=3 mice per group from four independent experiments. * denotes $p \leq 0.02$, while ** denotes $p \leq 0.002$ relative to PBS treatment group.

3.5 Discussion

To date, little research has focussed on the physical characterisation of PIM_2 and PGM_2 compounds at a molecular level, and how this impacts on biological activity. To obtain information on the interfacial behaviour of these phosphoglycolipids, their arrangement at the air/water interface was investigated using the Langmuir trough technique[301]. This technique is commonly used to obtain information about the structure and dynamics of phospholipid and glycolipid monolayers[253,282,312]. Distinct phase transitions and the profile of the π-A isotherms indicate the physical state of monolayers and the degree of ordering of molecules at the air/water interface.

Since these monolayers are considered to be model systems[302], data gained from these studies was used to provide insight into how the molecular assembly of the PIM_2 and PGM_2 compounds in aqueous media was influenced by acyl chain length and the dimension and flexibility of the head group[193]. The π-A isotherms of the compounds in pure monolayers differed significantly. The long-chain phosphoglycolipids formed insoluble monolayers with obvious phase transitions (G→LE→LC). Stronger hydrophobic attractive forces between the longer fatty acid chains promoted molecular orientation in the interface, resulting in closer packing of the molecules and a more stable monolayer[253]. Those intermolecular interactions led to the formation of less expanded films compared to short-chain analogues, characterised by decreased limiting areas per molecule A_0. The reasoning that there were more Van der Waals interactions between the long-chain phosphoglycolipids is further supported by larger $C_s^{-1}{}_{max}$ values, as it was seen for PGM_2 (18:18), indicating dense monolayers[281,282,309]. PIM_2 compounds showed higher A_0 when compared to PGM_2, which could be related to steric hindrance caused by the inositol head

group. Replacement of the inositol core with the glycerol unit appeared to increase the overall conformational flexibility of the hydrophilic group, allowing a closer arrangement of the molecules. The glycerol head group impacted positively on the packing behaviour and further stabilised the monolayer. This was evident by higher collapse pressures which are linearly correlated to stability[284]. In contrast to the interfacial behaviour of the long-chain PGM_2 molecules, PGM_2 (10:10) showed detergent-like characteristics. The π-A isotherm indicated the formation of an unstable monolayer, in which molecules were continuously exchanged between the interface and bulk-phase, due to weak hydrophobic interactions between the short acyl chains[258,280].

These monolayer findings compare well with the reported interfacial behaviours of other components of the cell wall of *M. tuberculosis*[223,271]. Langmuir monolayers of various mycolic acids have been thoroughly analysed, in order to clarify the role of mycolate layers in the mycobacterial cell envelope[267,268,271]. As part of the cell wall, mycolic acids can be bound to arabinogalactan via an ester-linkage or be part of the glycolipid trehalose-6,6-dimycolate (TDM). Their structure is specified by a hydrophilic head group and long fatty acids (meromycolate chains) which varies greatly depending on bacterial species and strains[268]. For instance, keto-mycolic acid was reported to form solid-condensed monolayers with a high collapse pressure of 57 mN m^{-1} and an A_0 of around 80 $Å^2$ where the hydrocarbon chains are thought to be densely packed[271]. More recent work on a synthetic analogue (MMG-1) of the mycobacterial lipid monomycoloyl glycerol demonstrated how the two saturated C14 and C15 alkyl chains arrange in the air/water interface to forma condensed monolayer[223]. This was characterised by an A_0 of 37.1 ± 0.7 $Å^2$ and a collapse pressure of 54.7 ± 0.5 mN m^{-1}.

Investigations, such as the evaluation of anti-inflammatory activities of purified mycobacterial PIMs or synthetic analogues, are mainly conducted using solutions of PIMs[96,224,227,248]. However, the chemical structures of PIM_2 and PGM_2 show features typical of amphiphilic molecules leading to the hypothesis that these compounds may self-assemble upon dispersion in aqueous solutions. This theory has been supported by studies that report the self-aggregation of mannosylated LAM (ManLAM) in water[69], and the formation of liposome vesicles from total polar lipids (comprising phosphoglycolipids and phospholipids) extracted from *M. bovis* BCG[225]. Based on these findings, it has been postulated that PIMs also organise into aggregates in an aqueous environment[313]. Indeed, the work presented in this chapter provides strong evidence that individual acylated PIM_2 and PGM_2 molecules show self-aggregation upon dispersion in an aqueous solution. The obtained data confirmed the formation of aggregates in response to spontaneous orientation of hydrophobic and hydrophilic groups. The deacylated PGM_2 (0:0) showed no particle formation as anticipated based on the monolayer behaviour, which is in agreement with previously published work[69]. Fatty acids play a crucial role in the aggregation process and hydrophobic interactions are most likely the main driving force for self-assembly. Unlike ManLAM molecules, which associated into relatively small structures, the size of the phosphoglycolipid structures examined here was dependent on the length of the fatty acid chains, with the longer chain forming larger particles. Amphiphiles with a large head and a small tail usually form micelles in aqueous environment[292], as it was seen with PGM_2 (10:10), because the hydrophobic interactions are not strong enough to allow self-assembly into vesicles. This was in good agreement with findings from the Langmuir monolayer study. Interestingly, the same concept may be applicable to explain the aggregation behaviour of PIM_2 (16:16), with the molecules associating mainly into spherical structures of relatively small size

(about 15 nm in diameter). Different size populations could be attributed to aggregation of smaller particles.

The formation of aggregates is likely to impact dramatically on the biological activity of these compounds. It is known from the literature that recognition and uptake of biologically active agents by cells of the immune system, and subsequent cell activation depends on the way such compounds are delivered and presented. When active agents are delivered in soluble form, only a small amount may actually reach the cells due to rapid degradation and excretion of the molecules[314]. The ability of molecules to self-aggregate can provide advantages including protection from extracellular degradation and a prolonged circulation time[314]. Also, interactions between crucial domains of molecules and receptors can be enhanced leading to increased binding efficacy and receptor valency. Nigou *et al.*[65] found that the ability of native ManLAMs to interact with the C-type lectins depended on their ability to form clusters in water, as this was thought to improve the presentation of mannosyl residues to mannose receptors on dendritic cells. ManLAMs capable of forming aggregates (total ManLAMs) induced inhibition of IL-12 production, whereas deacylated ManLAMs showed no activity. In a similar study, *M. bovis* BCG ManLAM aggregates exerted stronger binding to human pulmonary surfactant protein A (a C-type lectin receptor) than did poorly aggregated monomers[69]. The removal of the lipid moiety of PIM has been shown to abolish immunosuppressive activity[236]. Loss of activity was similarly found for a deacylated natural PIM (*M. bovis* BCG) and a related synthetic deacylated PIM_2 mimetic did not inhibit LPS-induced cytokine release *in vitro*[96]. It is possible that this loss of activity is at least in part related to an inability to form aggregates.

The biological function examined in this chapter was the ability of the PIMs to suppress airway inflammation. This assay was chosen due to the wealth of data supporting a role for mycobacterial cell wall extracts, and related compounds, in immunosuppression[19,70,224,236,248]. While the physical analyses carried out, determined that the structure of the PIM_2 and PGM_2 compounds impacted on how the compounds behaved at an air/water interface, little impact on biological activity could be detected, with all compounds appearing to have a slight immunosuppressive phenotype. Recruitment of airway eosinophils occurs as a result of the differentiation of $CD4^+$ T helper cells into $CD4^+$ Th2 cells which secrete cytokines such as IL-4, IL-5 and IL-13[315]. IL-5 is the main cytokine associated with influx of eosinophil into the lungs. In this particular model many parameters may influence the activity of biologically active compounds, for example dose, timing and route of delivery (local versus systemic) of the immunomodulatory compound. The effect observed for PIM_2 and PGM_2 was subtle compared to dexamethasone; an effective glucocorticoid with strong anti-inflammatory properties, which involve the non-specific down-regulation of the immune response. Interestingly, while the PIM_2 and PGM_2 compounds appeared to modify the eosinophil and CD4 response, the CD8 response did not appear to be effected.

This study confirmed that replacement of the inositol ring with the glycerol unit maintained biological activity in PGM_2 compounds[96]. This was in agreement with previous work by Harper *et al.*[248], in which PGM_2 (18:18) showed suppressive activity in a similar mouse model of OVA-induced allergic airway inflammation. In the work described here deacylated PGM_2 was not able to suppress airway eosinophilia but did decrease the proportion of antigen specific $CD4^+$ cells in the mediastinal lymph node. The previously discussed importance of acylation and/or the ability to form aggregates may not apply to

all biological responses as recognition of PIM_2 by DC-SIGN was independent of the degree of acylation[27]. The exact mechanism by which PIMs and related compounds cause immune modulation has yet to be elucidated. Until recently, these mycobacterial molecules were believed to indirectly modulate the function and response of adaptive T cells via interactions with APCs. However, recent studies demonstrated that mycobacteria[95] as well as infected macrophages excrete vesicles containing immunomodulatory agents such as TLR-2 ligands (lipoprotein LprA and LprG)[316] and mycobacterial lipids[95]. These compounds directly affect $CD4^+$ T cells and may induce cytokine secretion and T cell proliferation. Direct interaction with $CD4^+$ T cells independently of APCs was reported for lipoproteins[316,317] and PIMs[97] mediated by TLR-2 or integrin binding on T cells.

In conclusion, the work presented in this chapter provided a detailed physicochemical characterisation of PIM_2 and PGM_2 compounds varying in the length of the fatty acid and type of polar head group. Particularly, the interfacial behaviour of these phosphoglycolipids could be described at the air/water interface in which the arrangement of molecules was significantly affected by number of hydrocarbons in the acyl chains and the steric flexibility of the polar head group. Aggregation behaviour reported here may help to further elucidate receptor interactions of PIM_2 and PGM_2 compounds.

While this chapter addressed evaluating molecular properties of pure compounds and the effect of these characteristics on immunosuppression, the following chapter focusses on behaviour of PIM_2 and PGM_2 in binary Langmuir monolayers with a common phospholipid. The aim was to formulate particulate systems which could be further tested for their immunoactivating abilities *in vitro* and *in vivo*.

Chapter Four

Physical characterisation of PIM_2/PGM_2 and PC in binary systems and immunostimulatory investigations

4 Physical characterisation of PIM_2/PGM_2 and PC in binary systems and immunostimulatory investigations

4.1 Introduction

Particulate delivery systems have proven to be a powerful approach for vaccine delivery, as discussed in detail in **Chapter One**. Co-delivery of immunoadjuvant and antigen via a delivery system is an attractive strategy. Incorporation into carrier vehicles prevents extracellular degradation and ensures delivery of the antigen to APCs, while the immunostimulant activates targeted immune cells[314]. A review of the current literature reveals a lack of studies in which the adjuvant properties of individual PIMs are investigated using suitable particulate formulations.

This chapter explores the possibility of constructing delivery systems containing PIM_2 and PGM_2. Based on their ability to form lipid monolayers (**Chapter Three**), the compounds were incorporated into liposome-based delivery systems prepared using phosphatidylcholine (PC). Prior to liposome preparation, molecular interactions between PC and the phosphoglycolipids were examined in mixed Langmuir monolayers. Interfacial behaviour in binary mixtures provided information on mutual interactions and miscibility of the different components. These findings allowed conclusions to be drawn regarding the successful insertion of these lipids into PC bilayers. Investigations of the immunostimulatory activities of the developed delivery systems were conducted using both *in vitro* and *in vivo* models.

4.1.1 Mixed monolayers

The method to investigate lipid monolayers using the Langmuir trough technique has been detailed in **Chapter Three**. Briefly, this technique is used to prepare monomolecular films of lipids at the air/water interface. From these compressed monolayers, information can be obtained about structures, dynamics and the packing characteristics of lipid molecules. They are widely used as a model system to study molecular interactions or arrangements in an organised system[302]. While **Chapter Three** investigated the interfacial behaviour of individual monolayers, the work presented in this chapter focussed on intermolecular interactions in monolayers containing binary lipid mixtures.

Two-component monolayers can be prepared by co-spreading a lipid mixture at the air/water interface[255]. Surface behaviour of the lipids depends on the composition of the mixture. Interactions may be investigated by evaluating the effect of composition on the area occupied by the binary system. According to Gaines[318], the relationship between composition and molecular area can be described through the addition of molecular areas obtained from pure monolayers:

$$A_{\text{ideal}} = X_1(A_1) + (1 - X_1)(A_2) \qquad \textbf{Equation 4-1}$$

Whereby X_1 refers to molar fraction of compound 1 in the mixture, and the limiting molecular area A_1 obtained from one-component monolayer, while A_2 is denoted to compound 2. The ideal area, A_{ideal}, is a theoretical value which describes the linear relation between composition and area. If experimental areas are consistent with predicted A_{ideal} values, compounds either show ideal mixing behaviour with no interactions present[319], or molecules are immiscible

and phase separated[320]. Deviations from the theoretical values give insight into the nature of any interactions occurring[321]. While attractive interactions cause negative deviations from ideality, repulsive forces between the molecules result in positive deviations[255,321]. Sterols such as cholesterol are well known for their "condensing effects" on lipid monolayers[322-324]. The π-A isotherm of pure cholesterol shows an almost linear increase in surface pressure which indicates a solid film formation[322,323]. When mixed with phospholipids, cholesterol can be accommodated in film cavities; it then improves the packing of phospholipid chains by limiting their degree of movement and making the film more rigid[284]. As major parts of bilayer membranes, cholesterol[284,310,324,325] as well as phosphoplipids[310,326] are often studied in combination with other membrane components, to understand interactions and distribution within membrane structures or cellular processes.

Many studies have investigated the interfacial behaviour of PC in mixed systems[258,301,327]. For instance, mixed films comprising PC and glyceryl mono-oleate showed non-ideal behaviour when compressed at an interface. Molecular areas of the binary mixture negatively deviated from ideality throughout the composition range, and decreased gradually with an increasing mole fraction of glyceryl mono-oleate[327].

Repulsive forces are mainly attributed to head group interactions. They significantly affect interactions within monolayers and the stability of the system. As shown in earlier studies on mixed PC films, repulsive interactions between head groups led to expanded films. These were characterised by increased mean molecular areas[320] and reduced stability[284]. It should be noted that this phenomenon greatly depends on the pH and ionic strength of the sub-

phase, as these factors determine the net charge of the monolayer and the extent of electrostatic interactions[328].

Other studies have analysed the miscibility of components in mixed monolayers based on film collapse pressures. The incorporation of varied molar ratios of PC into cholesterol monolayers led to increased collapse pressures[320], which according to Crisp *et al.*[329] are indicative of mutual interactions. The mixed cholesterol/PC films had a single collapse points which was detected between those of the pure components[320]. In contrast to this, Seoane *et al.*[330] observed two collapse points for a mixed cholesterol/stearic acid monolayer. No interactions existed within the binary system and each component was forced out of the interface at its own collapse pressure[329,330].

A variety of biologically relevant molecules from *Mycobacterium* have been investigated in mixed monolayers. Trehalose-6,6-dimycolate (TDM, also known as cord factor), a glycolipid found in the mycobacterial cell wall, has been studied in mixtures with phospholipids in order to elucidate possible interactions with the mitochondrial membrane of infected cells[331]. Other researchers have studied the role of mycobacterial lipids in the development of tuberculosis infections using model surfactant systems; in particular the underlying mechanism of lung surfactant dysfunction as a result of interactions between mycolic acid and host lipids has been investigated[332,333]. Dipalmitoylphosphatidylcholine (DPPC) is the main component of the pulmonary surfactant system and has been utilised in pure and binary monolayers to model the pulmonary air/aqueous interface. Incorporation of mycolic acid promoted destabilisation of lung surfactant-like films, most probably by altering the orientation of DPPC molecules in the interface and preventing tight lipid packing[332]. In patients with pulmonary tuberculosis, this

obstructive effect of mycolic acid on DPPC monolayers may have dramatic effects, such as collapse of the alveoli and reduced gas exchange[332]. Similar expanded DPPC/mycolic acid monolayers were reported by Pénzes *et al.*[334], when they studied the penetration ability of an antituberculotic drug conjugate. The behaviours of PI (a component of biological membranes) and synthetic derivatives, were assessed in mixture with various phospholipids including DPPC[263,265] and distearoylphosphatidylethanolamine (DSPE)[266], in order to gain information about membrane distribution and the role of PI in cellular processes. Mixed monolayers of PI/DSPE showed non-ideal behaviour, and were found to be in the condensed phases at low PI concentrations, while increased molar fractions of PI induced film expansion[266]. PI was immiscible with distearoylphosphatidylcholine (DSPC) and both compounds were phase separated in mixed monolayers[264].

4.1.2 Mixed monolayers and their relationship to lipid bilayers

Due to their molecular organisation, lipid monomolecular films can be considered as half a bilayer structure (**Figure 4-1**). Consequently, data gained from these studies can provide insight into lipid packing, and reveal information on how molecular assembly is influenced by such parameters as acyl chain length and the dimension of the head group[193]. As mentioned above, several research groups have used mixed monolayers to model membrane structures. These studies allowed detection of interactions between membrane components and additives such as surface-active agents[335] or mycobacterial derivatives[331-334].

Additionally, studying single layered structures can provide information on the physicochemical behaviour of molecules in bilayered liposomal constructs[193,310]. **Figure 4-1** illustrates the relationship between monolayers,

bilayers and liposome structures. It has been demonstrated that mixed monolayer studies can be a useful approach to establish pharmaceutical properties, such as lipid-lipid interactions in mixed monolayers in order to formulate liposome-based delivery systems[223]. Lipid packing alongside stability of liposomal bilayers can be assessed[223,272] and drug-lipid interactions[336,337] investigated. Modelling membrane structures using monolayer studies is a suitable approach to obtain insight into such characteristics as those mentioned above. However, there are limitations which need to be considered. Because monolayers represent half a membrane, their utility is limited to modelling molecular interactions, occurring at the membrane surface[256].

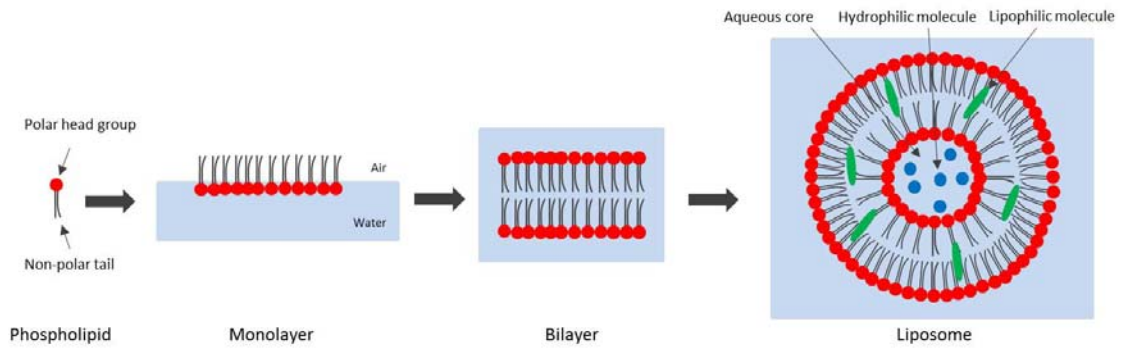


Figure 4-1. Schematic illustration of the relationship between monolayers, bilayer structures and bilayer vesicles (liposomes). Following spreading onto water, surface active agents orientate at the air/water interface. Amphiphilic molecules such as phospholipids spontaneously associate into bilayers upon dispersion in aqueous media which bend round to form closed compartment vesicles termed liposomes. The orientation of the phospholipid molecules allows for incorporation of hydrophilic and lipophilic molecules in the aqueous core and lipid bilayer, respectively.

To investigate transmembrane processes such as ion transport, bilayer lipid membranes models are recommended[338]. In monolayer approaches, the film formation and molecular packing are controlled by physical barriers (for set-up of a Langmuir trough see **Chapter Three**, **Figure 3-3**). This limits hydrogen bonding between head groups and with the aqueous medium. While in

liposomal structures, the area occupied by the each molecule is determined by the extent of hydration[259].

4.1.3 Liposomes as vaccine delivery systems

The various approaches for the preparation and use of liposomes were outlined in **Chapter One**. It was highlighted that phospholipid molecules are commonly used to produce liposomes possessing diverse characteristics. Their amphiphilic structures allow entrapment of hydrophilic and lipophilic molecules[187] (**Figure 4-1**). For instance, soluble hydrophilic agents (such as the model antigen OVA) can be encapsulated into the aqueous core or aqueous regions of uni- or multilamellar vesicles[195]; whereas glycolipids or bacterial cell wall components are incorporated into lipidic bilayer structures (**Figure 4-1**). Moreover, surface modifications enable control of physicochemical properties such as aggregation[195] and liposome fate *in vivo*[190]. Egg-PC, also known as L-α-lecithin, is commonly utilised for vesicle preparation[339], and was used to prepare liposomes in this work. PC is zwitterionic and generally comprises a mixture of different fatty acid residues (R) such as palmitic, stearic, oleic and linoleic acid[339] (**Figure 4-2 A**).

Liposomes present well-studied vaccine delivery systems for effective protection of soluble antigens and adjuvant compounds from degradation and for enhancement of pharmacokinetic profiles[190]. A study by White *et al.*[206] investigated the incorporation of the adjuvant Quil A into liposomes containing lipid core peptides. It was shown that the elicited immune response *in vivo* was significantly increased when Quil A was included into liposome formulations[206]. Other studies have found that a C32 analogue of the mycobacterial compound monomycoloyl glycerol (MMG, **Figure 4-2 B**) was able to improve immune responses when it was included into liposomes at

very low concentrations[221,222]. Based on those findings, for the present study, PIM_2 and PGM_2 molecules were incorporated into PC-based liposomes at concentrations of 2% w/w of total lipid.

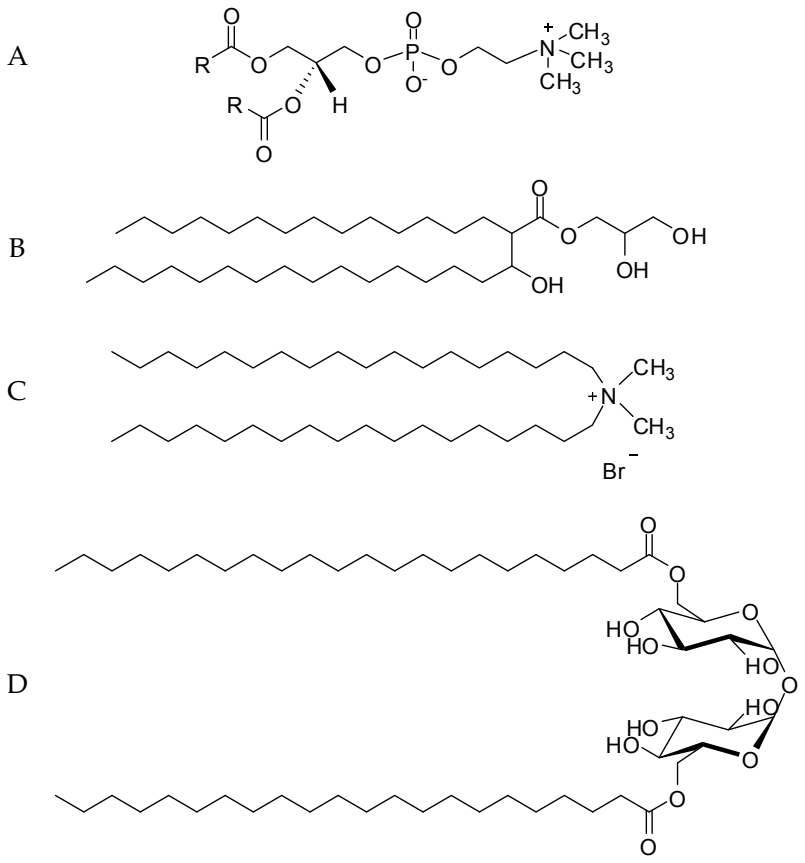


Figure 4-2. Chemical structures of **(A)** PC whereby R can be a mixture of palmitic, stearic, oleic and linoleic acid, **(B)** C32 monomycoloyl glycerol analogue (MMG), **(C)** dimethyldioctadecylammonium bromide (DDA) and **(D)** trehalose-6,6-dibehenate (TDB).

Several mycobacterial cell wall derivatives have been investigated in liposomal delivery systems. A synthetic monomycoloyl glycerol (MMG-1) was included into dimethyldioctadecylammonium (DDA, **Figure 4-2 C**) liposomes via a conventional preparation method[223]. The cationic liposomes were heterogeneous in size with diameters of approximately 400 nm. MMG-1 was found to stabilise DDA liposomes when more than 18 mol% was incorporated into the bilayer. Nordly *et al.*[223] explained the MMG-1 stabilising effect as

improved hydrogen bonding with aqueous media and enhanced hydration of DDA head groups in the bilayer. Also, the combination of MMG-1 and DDA molecules weakened repulsive interactions between the positively charged DDA head groups, and allowed for increased packing of the molecules[223]. In this particular study the negatively charged antigen was adsorbed to liposome surfaces via electrostatic interactions. Although a thorough characterisation of the delivery system was provided, the adsorption efficacy was not discussed. Other studies investigated liposomes constructed from total lipid extracts from *M. bovis BCG* alone[225,340] or in combination with other lipids such as cholesterol[293] and DDA[340]. The total lipid extract was identified to include PIMs as major components[225]. More recently, novel liposomes were developed in which glycolipid trehalose-6,6-dibehenate (TDB, **Figure 4-2 D**), a synthetic analogue of trehalose-6,6-dimycolate, was incorporated into DDA liposome bilayers[149,211].

4.1.4 Thermotropic behaviour of lipid bilayer

Lipid bilayers and liposomes undergo characteristic order-disorder thermotropic transitions. At the main phase transition temperature, the lipids change from the tightly ordered crystalline gel structure to the liquid-crystalline phase. Above the transition temperature, the lipid chains are 'melted' and the overall movement of the molecules is increased. The phase behaviour (gel or liquid-crystalline) of lipids determines characteristics such as permeability of the membrane, fluidity, packing and stability of the liposomes[185,195]. The phase transition temperature is mainly influenced by the length of the hydrocarbon chain[195]. Nevertheless, many other parameters, including the degree of chain saturation, the extent of attractive Van der Waals interactions between the lipid chains and the type of the polar head group, can affect the transition temperature[189]. Determining the phase transition

temperature of lipids is important for liposome preparation. Due to the increased movement of lipid chains in the fluid phase, preparation above the phase transitions of the lipid ensures fusion of lipids and uniform distribution within the bilayers. However, phospholipids with T_m below ambient temperature exhibit a considerable amount of bilayer flexibility due to their liquid-crystalline phase, potentially causing membrane instability. Therefore, lipids with higher T_m are preferred as these would exist in the gel phase at ambient temperature and have an increased rigidity of liposomal bilayers. For the purpose of controlled drug release or targeted release into certain tissues, the desired phase transition temperatures can be achieved by using combinations of lipids[195].

4.1.5 PIMs as immunostimulatory agents

Mycobacteria are known to modulate host immune responses. Particularly their abilities to induce immune responses have been employed in the well-known adjuvant CFA which contains inactivated mycobacteria. However, due to severe side effects, it has not been approved for use in humans[153]. Many of the immunological activities have been attributed to the lipids embedded in the mycobacterial cell envelope, including LAMs, LMs and PIMs[19,55,295,296]. Due to the need for co-administration of adjuvants with subunit vaccines, much research has been focussed on establishing their mode of action. Amongst the promising adjuvant candidates are native and synthetic PIMs. Beneficially, PIM molecules can be prepared using synthetic strategies providing well-defined chemical structures. The purity of synthetic molecules ensures the absence of contaminants, including other mycobacterial products, thereby decreasing the side effects associated with these by-products.

In addition to their potential as immunosuppressive agents, as detailed in **Chapter Three**, PIMs have been identified to exert a number of immunostimulatory activities. Various mechanisms of action have been suggested for these. Mycobacterial PIM_2 and PIM_4 have been shown to activate NK T cells mediated by CD1d receptor-dependent mechanism[90,107]. NK T cells enhance cellular immunity by producing INF-γ and are known to contribute greatly to the granuloma response typical in tuberculosis infections[90,107]. Other researchers have suggested immune activation occurs via TLR signalling. PIM extracts[91] and also fractionated natural PIM_2 and PIM_6[21] activated TNF-α secretion by macrophages in a TLR-2 dependent manner. The agonist activity was found to be independent of PIM acylation state[21]. This indicates potential adjuvant properties of this class of compounds.

In addition to these *in vitro* experiments, several studies have investigated the adjuvant activity of native PIM[341] (containing PIM_2 and PIM_6) from *M. bovis* and synthetic PIMs (PIM_2 and PIM_4)[224,341] using a mouse model. PIMs elicited Th1-type immune responses with increased secretion of INF-γ rather than IL-4[341]. The immune activation of synthetic PIMs was comparable to native PIMs. However, synthetic PIM_4 was less effective in comparison to synthetic PIM_2[224,341]. An evaluation of various delivery routes revealed efficient vaccination via the intranasal and oral routes, suggesting that PIMs may be potent mucosal adjuvants, providing a possible alternative to invasive vaccination methods[341]. The fact that synthetic molecules maintain activity was further supported by a study in which a synthetic PIM_2, similar in its acyl residues to the PIM_2 reported earlier[341], was more potent than natural PIMs and other derivatives[226]. When combined with the model antigen Ag85B-ESAT-6 (mycobacterial fusion protein), the synthetic PIM_2 provoked high levels of Th1-phenotype cytokines, decreased lesions in lung tissue as well as reduced

bacterial numbers in airways following *M. bovis* airway challenge. These findings are in good concordance with other reports, in which the addition of synthetic PIM_2 to a vaccine formulation containing the BCG vaccine, *M. bovis* culture filtrate (CFP) and DDA enhanced protection against *M. bovis* infection in cattle[342]. Furthermore, a synthetic PIM analogue (PIM_2ME), where the acyl linkage at the *sn*-2 glycerol position was replaced by an ether linkage, was shown to be active *in vitro*[343,344] and *in vivo* when used in combination with a hepatitis C viral antigen[344]. Adjuvant activity of the modified compound was evident by enhanced titres of INF-γ and IL-12 and reduced levels of IL-10. Despite these findings, a study by Parlane *et al.*[226] could not confirm the immune stimulation of PIM_2ME characterised by high levels of INF-γ *in vivo*, however, the results were similar with respect to the low titres of IL-10.

A number of groups have demonstrated the capacity of modified lipid vesicles to target key immune cells such as macrophages. Liposomes prepared by mixing mannosylated phospholipids extracted from *M. bovis* BCG and cholesterol (2:1 w/w), were found to be taken up by murine inflammatory macrophages in a manner, dependent on liposome size and lipid concentration[293]. Larger particles were taken up faster (1.4 μm compared to 400 – 700 nm diameter) and the uptake rate was saturated at high liposome concentrations (400 μg mL^{-1})[293]. Following uptake of the mannosylated phospholipids/cholesterol liposomes by thioglycolate-activated macrophages, nitric oxide (NO) synthase was upregulated[294]. Sprott *et al.*[225] prepared liposomes using a total polar lipid (TPL) extract from *M. bovis* BCG without addition of further lipids. In contrast to findings by Tenu *et al.*[294], TPL liposomes and liposomes containing TPL and other lipids (1:1 w/w) activated DCs to secrete IL-12 without additional stimulators[225].

4.2 Chapter aims

Several research groups have investigated the immunostimulatory activities of different compounds derived from the mycobacterial cell wall. However, limited work has been carried out exploring the incorporation of individual PIM lipids into particulate delivery systems such as liposomes.

The aim of this chapter was to characterise the effect of synthetic PIM_2 and PGM_2 on the PC monolayer formed at the air/water interface. Characterisations of these mixed systems at varied molar ratios were conducted to evaluate potential lipid-lipid interactions. Intermolecular interactions were verified by deviations from the ideal molecular areas and collapse pressures of the binary systems. For this purpose, ideal mixed molecular areas were calculated on the basis of molecular areas obtained from one-component monolayers. Furthermore, PC-based liposomes were prepared using the thin lipid film method[183]. PIMs were incorporated into liposomes at concentrations of 2% w/w of total lipid. The model antigen FITC-OVA was entrapped at a concentration of 10 mg mL^{-1}. The particulate delivery systems were characterised in terms of particle size, zeta potential, encapsulation capacity and membrane stability. Following physical characterisation of the liposomes, the formulations were investigated in an *in vitro* model for their ability to be taken up by and consequently stimulate DCs. Finally, the immunostimulatory activities of the modified liposomes were tested *in vivo* where their ability to elicit cell-mediated and humoral immune responses in comparison to unmodified PC liposomes was determined.

4.3 Experimental section

4.3.1 Materials

Fluorescein isothiocyanate (FITC, isomer 1, minimum purity of 90% by HPLC) and ovalbumin (OVA, albumin from chicken egg, grade V, minimum purity of 98% by agarose electrophoresis) used for the preparation of fluorescently-labelled OVA, were purchased from Sigma Aldrich (St. Louis, MO, USA).

Chloroform (purity 99-99.4%) and methanol (purity > 99.8%) used for lipid stock solutions and vesicle formation, were obtained from Merck (Darmstadt, Germany). Distilled water de-ionised with a Milli-Q Continental Water System (Millipore Corporations, Bedford, MA, USA) and a resistivity of 18.2 MΩcm, served as the sub-phase for Langmuir trough experiments.

L-α-phosphatidylcholine (PC, lyophilized powder), concanavalin A (ConA, from Jack Bean, Type VI, lyophilized powder) and Triton®-X 100 were obtained from Sigma Aldrich (St. Louis, MO, USA).

Phosphate buffered saline (PBS, DulbeccoA, Oxoid, UK) was prepared in Milli-Q water with a pH of 7.5.

Research grade alum was purchased from Serva (Alu-gel-S, suspension in water, Serva electrophoresis GmbH, Heidelberg, Germany).

Antibodies (anti-CD16/CD32, primary antibodies, secondary reagents) and propidium iodide (PI) used or flow cytometry were all supplied by BD Pharmingen (Franklin Lakes, NJ, USA).

4.3.1.1 Preparation of fluorescently-labelled ovalbumin

The fluorescent marker fluorescein isothiocyanate (FITC) was conjugated to ovalbumin (OVA) according to a method previously described[345]. Briefly, 100 mg FITC and 500 mg OVA were dissolved in 50 mL carbonate buffer (220 mM, pH 9.5) (**Appendix A**) and the mixture was stirred gently in the dark at 4°C. After 18 h the unbound FITC was removed by ultrafiltration. To do this, the solution was transferred into an ultrafiltration cell (Amicon, Beverly MA, USA) containing a cellulose membrane (molecular weight cut-off 10 000, Amicon Bioseparations, Millipore Corporations, Bedford, MA, USA). The solution was continuously flushed with Milli-Q water and unbound FITC was removed by filtration under (nitrogen atmosphere) gas pressure. This procedure was performed protected from light and repeated until the filtrate appeared colourless. Subsequent lyophilisation (Freezone 6 freeze-dryer, Labconco, MO, USA) gave a fluffy orange powder which was stored at 4°C protected from light.

4.3.2 Langmuir trough technique and mixed monolayer conditions

Lipid stock solutions of PIM_2 (16:16), PIM_2 (18:18), PGM_2 (10:10), PGM_2 (16:16), PGM_2 (18:18) and PC were prepared at a concentration of 0.5 mg mL^{-1} in chloroform/methanol (4:1, v/v). To prepare binary lipid mixtures, aliquots of the phosphoglycolipid stock solutions were combined with PC to obtain the desired ratios of 2, 25, 50 mol% of PIM_2 or PGM_2. The binary solutions had a total lipid concentration of 0.5 mg mL^{-1}. Lipid films were produced at the air/water interface from pure PC and PC in combination with each of the phosphoglycolipids. Monolayer formation and compression experiments were further conducted, as described in **Chapter Three**, using the same instrumental set-up.

4.3.2.1 Analysis of π-A isotherm for binary systems

As described in **Chapter Three**, the isotherm for one-component films was obtained by plotting surface pressure versus molecular area. However, for mixed monolayers the occupied area at the air/water interface was expressed as average area per molecule, whereby the total area was divided by the total number of PC and phosphoglycolipid molecules. The total number of molecules (N) per lipid in the applied volume was calculated by **Equation 4-2**:

$$N = \frac{N_A \times C \times V}{MW} \qquad \textbf{Equation 4-2}$$

Where N_A is the Avogadro constant, C the concentration (g l^{-1}), V the volume applied onto surface (l) and MW the molecular weight of the corresponding lipid. Limiting area per molecule (Å^2) or average area per molecule (Å^2), both at zero pressure, and collapse pressure (mN m^{-1}) of the appropriate film were further determined according to the method used in **Chapter Three**.

4.3.2.2 Ideal areas of binary systems

To help understand interactions between the lipids in a mixture, a theoretical ideal area occupied by the binary mixture at the interface can be predicted[318]. The ideal average molecular area of the mixed monolayers was calculated using **Equation 4-1**:

$$A_{\text{ideal}} = X_1(A_1) + (1 - X_1)(A_2) \qquad \textbf{Equation 4-1}$$

Where X_1 is the molar fraction of PC and X_2 (equals 1 - X_1) denotes PIM_2 or PGM_2. A_1 and A_2 represent the limiting molecular areas of pure PC and the corresponding phosphoglycolipid, respectively.

4.3.3 Determination of phase transition temperature

Differential scanning calorimetry (DSC) is commonly used to characterise thermal events such as the phase transition temperature of lipids. Briefly, the sample and the reference pan are maintained at the same temperature throughout the experiment, and the energy required (i.e. heat flow) to keep both pans at equal temperature is measured. Thus, a thermogram obtained by DSC shows the heat flow as a function of temperature. By measuring the difference in heat flow between the sample and reference, the amount of heat absorbed (endothermic) or released (exothermic) during a thermal event can be studied[346]. The area under the curve is directly proportional to the heat flow and integration of the peak area yields the enthalpy. In the current work, experiments were performed using a TA-DSC Q100 (V8.2 Build 268, TA-Instruments-Waters LLC, New Castle, USA). Thermograms of each phosphoglycolipid were obtained under a nitrogen gas flow of 50 mL min^{-1}. Calibration of the DSC was carried out using indium as a standard. Dry samples (1 to 2 mg) were crimped in an aluminium pan and the thermal behaviour of the samples was studied at a heating rate of 10 K min^{-1} from 0°C to 120°C. Phase transition temperatures were determined as the onset temperatures using TA-Universal Analysis 2000 software (version 4.7A).

4.3.4 Preparation of liposomes by the thin film method

The liposome formulations were prepared according to a method by Bangham *et al.*[183]. A total lipid amount of 50 mg, composed of either pure PC or PC with 2% w/w of PIM_2 (16:16), PIM_2 (18:18), PGM_2 (10:10), PGM_2 (16:16) or PGM_2 (18:18) was dissolved in chloroform/methanol (4:1, v/v). The solvent was evaporated under vacuum at 45°C (Rotavapor R110, Büchi Labortechnik AG, Switzerland) and the resultant dry lipid film was purged with nitrogen gas to

ensure complete removal of the organic solvents. To generate loaded vesicles, the lipid film was rehydrated in 1 mL phosphate-buffered saline (PBS, pH 7.5) containing 10 mg mL^{-1} FITC-OVA at 60˚C (above lipid phase transition temperatures). Glass beads were added to facilitate rehydration and the flask vigorously shaken. PGM_2 (0:0) was dissolved in PBS along with FITC-OVA and added during liposome rehydration. The preparations were incubated under constant shaking for 2 h at 60˚C, followed by three freeze-thaw cycles to improve entrapment. The lipid dispersions were bath sonicated for 5 min at 60˚C and for size homogenisation extruded 10 times through stacked 800 - 400 nm polycarbonate membranes (Nucleopore®, Whatman Ltd., USA), using a 10 mL extruder (Lipex Biomembranes Inc., Vancouver, Canada). Unentrapped protein was separated by three washing cycles with PBS (5 mL) and ultracentrifugation (L-80 Ultracentrifuge, Optima, Beckman, USA) at 38 000 rpm for 30 min at 25˚C. The liposomes were redispersed in PBS and stored at 4˚C.

4.3.5 Physicochemical characterisation of liposomes

4.3.5.1 Vesicle size and zeta potential measurements

Particle size distribution and zeta potential were determined by dynamic light scattering (DLS) and electrophoretic mobility, respectively. Both measurements were carried out at 25°C using a Zetasizer NanoZS (Malvern Instruments). Particle sizes were measured in triplicates (each run for 100 seconds) and are presented as intensity based mean sizes (Z-average size). The corresponding polydispersity index (PDI) is a width parameter and indicates the homogeneity of the sample. Zeta potential values (mV) were derived from the measured electrophoretic mobility using the Smoluchowski equation[303]. Three replicate measurements were performed for each sample with a number of sub-runs

which was automatically selected by the instrument. Prior to measurements, aliquots which had been stored at 4°C were allowed to equilibrate at room temperature. For consistency between the different experiments, all formulations were prepared at 300-fold dilutions in PBS (pH 7.5).

4.3.5.2 Lectin binding assay

To examine incorporation of the phosphoglycolipids into the liposomes, the availability of mannosyl residues on the liposome surface was investigated using a Concanavalin A (ConA) agglutination assay. This assay was modified from earlier reports[206,347]. A stock solution of ConA at a concentration of 10 mg mL^{-1} in 10 mM HEPES buffer (**Appendix A**) was prepared. ConA-mediated aggregation of the liposomes was assessed by adding 10 μL of the ConA solution to 10 μL of liposome dispersion (50 mg mL^{-1}) in 3 mL of 10 mM HEPES buffer containing 1 mM $CaCl_2$ and $MnCl_2$ (**Appendix A**). Size measurements were performed every five minutes (Zetasizer NanoZS, Malvern Instruments). Following the addition of ConA, the change in the size of the liposomes was monitored for further 40 min.

4.3.5.3 Determination of FITC-OVA entrapment efficiency

Aliquots (100 μL) of the liposome formulations were washed several times with PBS (1 mL) followed by centrifugation at 14 000 rpm for 30 min at 25˚C (5417 C Centrifuge, Eppendorf, Hamburg, Germany) to remove unentrapped protein. PBS containing 5% (w/v) Triton-X 100 (900 μL) (**Appendix A**) was then added to lyse the liposomes and FITC-OVA quantified by fluorimetry (excitation 485 nm, emission 520 nm; Polarstar Omega Microplate Reader, BMG Labtech, Ortenberg, Germany) against appropriate standards.

4.3.5.4 Liposome stability

The liposome dispersions were investigated with regards to membrane stability by measuring size and FITC-OVA entrapment upon storage in PBS (pH 7.5) at 4˚C over a period of 21 days.

4.3.6 Experimental mice

Male C57BL/6, OT-I and OT-II mice were maintained as described in **Chapter Three**, **Section 3.3.3.1**. All experiments were performed with the approval of the University of Otago Animal Ethics Committee (AEC D46/11).

4.3.7 Testing of transgenic mice

OT-I and OT-II mice were tested for their transgenic status by a method described in **Chapter Three**, **Section 3.3.3.2**.

4.3.8 *In vitro* immunological methods

4.3.8.1 Preparation of murine bone marrow-derived dendritic cells

Male C57BL/6 mice were sacrificed by cervical dislocation and the hind limbs removed and cleaned of tissue. Using sterile scissors, both ends of the femur and tibias were cut off and the marrow flushed out with cIMDM using a 26 gauge needle. The extracted marrow was filtered through a cell strainer into a 50 mL Falcon tube. In order to prepare a single cell suspension, cells were washed with cIMDM and spun down (1200 rpm, 8 min). The supernatant was discarded and cell pellet resuspended by vortexing. Collected cells were treated with sterile lysis buffer to lyse the red blood cells (incubation at room temperature for 10 min). Cells were then subjected to repeated washing steps,

and resuspended in cIMDM containing 20 ng mL^{-1} granulocyte macrophage colony stimulating factor (GM-CSF, recombinant mouse GM-CSF, carrier-free, BioLegend, San Diego, CA, USA). An aliquot was diluted with trypan blue dye and total cell numbers were determined using phase-contrast microscopy. Cells were then resuspended at 1 x 10^6 cells mL^{-1} in cIMDM + 20 ng mL^{-1} GM-CSF and cultured at 5 mL per well in six well tissue culture plates. Culture plates were incubated at 37°C with 5% CO_2 for differentiation into murine bone marrow-derived dendritic cells (BMDCs).

After four days supernatants were carefully removed and replaced with 5 mL of cIMDM + 10 ng mL^{-1} GM-CSF. The culture plates were placed back in the incubator for further two days (37°C, 5% CO_2). On day six, cells were harvested by gentle pipetting media several times and washed with cIMDM by centrifugation (1200 rpm, 8 min).

4.3.8.2 Dendritic cell activation

To investigate uptake of liposome formulations and subsequent activation of BMDCs, harvested cells were resuspended at 1 x 10^6 cells mL^{-1} in cIMDM + 10 ng mL^{-1} GM-CSF. BMDCs (aliquots of 500 μL) were seeded on 24 well plates and incubated with 500 μL of the different liposome formulations described above. Prior to this, liposome aliquots (100 μL) were washed several times with PBS (1 mL), followed by centrifugation at 14 000 rpm for 30 min at 25°C to remove unentrapped FITC-OVA. Pellets were resuspended in 100 μL sterile PBS. Aliquots were further diluted with cIMDM and added to the wells to obtain concentrations 10, 50 and 250 μg mL^{-1} of total lipid. Culture plates were incubated for 48 hours at 37°C with 5% CO_2. For comparison MPL (10 ng mL^{-1} and 1 μg mL^{-1}), cIMDM and FITC-OVA in cIMDM (concentration according to liposome entrapment) were added to additional wells.

4.3.9 *In vivo* vaccine model

4.3.9.1 Preparation of liposome formulations for immunological investigations

The various liposomes composed of either PC or PC with 2% w/w of a PIM_2 or PGM_2 lipid were prepared according to the method described in **Section 4.3.4**. As part of the immunological protocol outlined below, test animals would receive standardised amounts of PIM_2/PGM_2 (50 μg) and FITC-OVA (10 μg) per dose (200 μL). In order to achieve this, the amount of FITC-OVA loaded into the liposomes was adjusted due to different entrapment efficiency. Accordingly, PC and PC PGM_2 (0:0) liposomes were rehydrated in 1 mL PBS containing 2 mg mL^{-1} FITC-OVA, whereas all remaining formulations were loaded with 4 mg mL^{-1} FITC-OVA. Formulations were characterised as described in **Section 4.3.5**. Prior to administration, liposome aliquots were washed several times with PBS (1 mL) by centrifugation (14 000 rpm, 30 min, 25°C, 5417 C Centrifuge, Eppendorf, Hamburg, Germany) to remove unentrapped FITC-OVA followed by resuspension in sterile PBS. Protein entrapments were determined on day 0 and 14 of vaccine study. All formulations were stored at 4°C until day 14.

Control mice received FITC-OVA in alum. Therefore, a stock solution of FITC-OVA in sterile PBS was prepared (5 mg mL^{-1}). The solution was further diluted at 1:100 in alum and thoroughly mixed by vortexing prior to administration.

4.3.9.2 Adoptive T cell transfer

Transgenic OT-I and OT-II T cells were adoptively transferred into the study animals on day −1 according to protocol described in **Chapter Three**, **Section 3.3.3.3**.

4.3.9.3 Immunisation protocol

On day 0 of the study, mice (male C57Bl/6) were immunised subcutaneously in the dorsal skinfold with 200 μL PBS, containing 50 μL of each liposome formulation (50 mg mL^{-1}), loaded with standardised amounts of FITC-OVA (10 μg). The different formulations used for vaccinations are described in **Table 4-1**. Control groups were given 200 μL of FITC-OVA in alum (50 μg mL^{-1}). All groups received booster immunisations (s.c.) on day 14 and were sacrificed on day 17.

Table 4-1. Various liposome formulations used for the vaccination of mice and the amount of FITC-OVA (μg) delivered in a total volume of 200 μL on day 0 and 14. Data is shown as mean ± SD for three independent vaccine studies.

Formulation	Immunisation day 0 FITC-OVA (μg)	Boost immunisation day 14 FITC-OVA (μg)
PC PIM_2 (16:16)	14 ± 3	14 ± 3
PC PIM_2 (18:18)	12 ± 2	12 ± 1
PC PGM_2 (0:0)	9	11 ± 7
PC PGM_2 (10:10)	22 ± 10	20 ± 6
PC PGM_2 (16:16)	12 ± 3	11 ± 5
PC PGM_2 (18:18)	13 ± 3	13 ± 2
PC	9 ± 4	9 ± 3

4.3.9.4 Harvesting cells from vaccinated mice

Mice were euthanised on day 17 of the study with an intraperitoneal lethal dose of anaesthetic (1 mL), consisting of ketamine (10 mg mL^{-1}) and xylazine (300 μg mL^{-1}). Draining (axillary and brachial) lymph nodes and spleens were harvested from each mouse and stored on ice in cIMDM. The combined lymph nodes were analysed individually for each mouse whilst harvested spleens

were pooled for each vaccination group. Preparation of single cell suspensions was conducted as described in **Chapter Three**, **Section 3.3.3.6**.

4.3.9.5 *In vitro* T cell restimulation

Single cell suspensions were prepared from collected tissue (2×10^6 cells mL^{-1}) and cells were restimulated with α-CD3 (10 μg mL^{-1}, BD Biosciences), OVA (200 μg mL^{-1}) or media alone, each in conjunction with IL-2 (10 IU mL^{-1}, R&D Systems) at 37°C and 5% CO_2 for 72 hours. The extent of T cell proliferation was determined following the method in **Chapter Three**, **Section 3.3.3.7**.

4.3.9.6 Cytokine production

After three days, culture supernatants were collected (see **Section 4.3.9.5**) and IFN-γ levels measured using BD CBA Mouse IFN-γ Flex Set (BD Biosciences). Samples were analysed on BD FACSCanto II (Becton Dickinson, Franklin Lakes, USA). Cytokine concentrations were calculated against standards using FCAP Array software (v1.0, Soft Flow) with the lowest detection level being 10.35 pg mL^{-1}.

4.3.9.7 OVA IgG enzyme-linked immunosorbent assay

On day 17 of the vaccine study, blood samples were collected from each mouse. Samples were centrifuged at 14 000 rpm for 10 min (5417 C Centrifuge, Eppendorf, Hamburg, Germany) in order to enable separation of serum. All serum samples were then stored at -20°C until further analysis.

Enzyme-linked immunosorbent assay (ELISA) plates (Microtest® 96 well ELISA plates, BD Biosciences, Bedford, MA, USA) were coated with 100 μL per well of

10 μg mL^{-1} OVA in coating buffer (**Appendix A**) and incubated overnight at 4°C. The plates were then washed four times with wash buffer (**Appendix A**) and subsequently 150 μL of blocking buffer (**Appendix A**) was added to each well. Following incubation for an hour at room temperature, the blocking buffer was discarded. No further washing steps were required. Serum samples were diluted in assay buffer (**Appendix A**), added to corresponding wells as 1:10 dilution and continuously diluted (1:2 in assay buffer) across the plate. Plates were again incubated for two hours at room temperature and then washed six times in wash buffer. A volume of 50 μL of the secondary antibody, a goat-anti-mouse IgG conjugated to Horseradish Peroxidase (HRP, Zymax®, Zymed, San Francisco, CA, USA), diluted in assay buffer (1:4000), was added to each well and the plates were incubated at room temperature for two hours. After washing the plates six times with washing buffer, 100 μL of the HRP substrate ABTS (2,2'-azino-bis(3-ethylbenzthiazoline-6-sulphonic acid, Sigma-Aldrich, Steinheim, Germany), containing 1 μL mL^{-1} of 30% hydrogen peroxide, was added to each well. Plates were incubated in the dark for 10 min. To stop the reaction, 50 μL of a 2 mM sodium azide solution was added to each well. Finally, the absorbance of the samples was measured using a Polarstar Omega Microplate Reader (BMG Labtech, Ortenberg, Germany) at a wavelength of 414 nm.

4.3.10 Cell staining and flow cytometry analysis

After 48 hours incubation time, BMDCs (see **Section 4.3.7.2**) were isolated for the analysis of formulation uptake and surface cell marker expression by FACS. Cell staining and FACS analysis were detailed previously in **Chapter Three, Section 3.3.3.9**. Briefly, BMDCs pulsed with various formulations were harvested from culture plates and washed twice with FACS buffer followed by incubation with anti-CD16/CD32 (2.4G2 Fc Block) in order to block non-specific

binding. Samples were stained with the antibodies CD11c-APC (N418), CD86–PE-Cy7 (B7-2), CD80-biotin (16-10A1), and major histocompatibility complex (MHC) class II-biotin (2G9). The secondary reagent streptavidin-APC-Cy7 was added to visualise CD80-biotin and MHC class II-biotin. Cells were resuspended in approximately 100 μL FACS buffer for FACS analysis.

Staining and FACS analysis of lymph node and spleen cell samples obtained for the *in vivo* vaccine study (see **Section 4.3.8.4**) were conducted as described in **Chapter Three, Section 3.3.3.9**.

4.3.11 Statistical analysis

Where applicable, results are expressed as mean ± standard deviation (SD) unless otherwise stated. Statistical analyses were carried out using an unpaired Student's t-test (two-tailed) or one-way analysis of variance (ANOVA) followed by post hoc analysis using Tukey's pairwise comparison, as appropriate. In all instances, statistical analyses were conducted using IBM SPSS Statistics 20 (SPSS Inc., Chicago, IL, USA).

4.4 Results

4.4.1 Interfacial behaviour in mixed monolayers

In the work presented in this chapter, the Langmuir trough technique was used to investigate intermolecular interactions in mixed monolayers. π-A isotherms were analysed for pure PC monolayers and for mixed PC PIM_2 or PC PGM_2 monolayers. PC is a widely used lipid in Langmuir monolayer studies[258,327,328], while PIM_2 or PGM_2 are synthetic analogues of mycobacterial derivatives. The isotherms of mixed systems containing increasing concentrations of PIM_2 or

PGM_2 provide an opportunity to investigate the effect of these phosphoglycolipids (with different head and acyl groups) on PC monolayer behaviour. Interactions were assessed by measuring deviations of experimentally determined average molecular areas from ideality and changes in collapse pressures.

Investigation of the interfacial behaviour of PC in pure monolayers, as shown in **Figure 4-3**, gave values of 73.7 ± 5.9 $Å^2$ and 41.6 ± 0.2 mN m^{-1} for the limiting molecular area and collapse pressure, respectively (**Table 4-2**). The measured values for the PC isotherm were comparable to data (54 - 61 $Å^2$ and 40 - 45 mN m^{-1}) published by other groups with consideration of varied composition of egg-PC due to different sources[327,328]. To examine interactions between different lipids, binary mixtures of PC and 2, 25 or 50 mol% of each of the phosphoglycolipids were compressed at the air/water interface. Specific characteristics of each of the mixed monolayers, such as the experimental average molecular area, deviation from ideal molecular area and collapse surface pressure were determined.

π-A Isotherms for PC PIM_2 (16:16) and PC PIM_2 (18:18) at different ratios are shown in **Figure 4-3**. The corresponding monolayer characteristics are summarised in **Table 4-2**. The average molecular areas of the investigated mixtures were found to differ negatively from the predicted values, but these differences were not significant ($p > 0.05$). The collapse pressures of each two-component films were higher than the collapse of pure PC. However, this increase was only significant for PC with 25% PIM_2 (16:16) (42.4 ± 0.4 compared to 41.6 ± 0.2 mN m^{-1}, $p \leq 0.05$). Other mixed systems showed an correlation of lipid ratio and isotherm characteristics such as collapse pressure[193,223]. While for instance an increasing MMG-1 content led to higher collapse pressures of a

DDA lipid film[223] this effect was not observed by adding the phosphoglycolipid to PC films.; i.e. adding 2% or 50% of the PIM_2 compounds had a similar effect on the molecular area and collapse pressure.

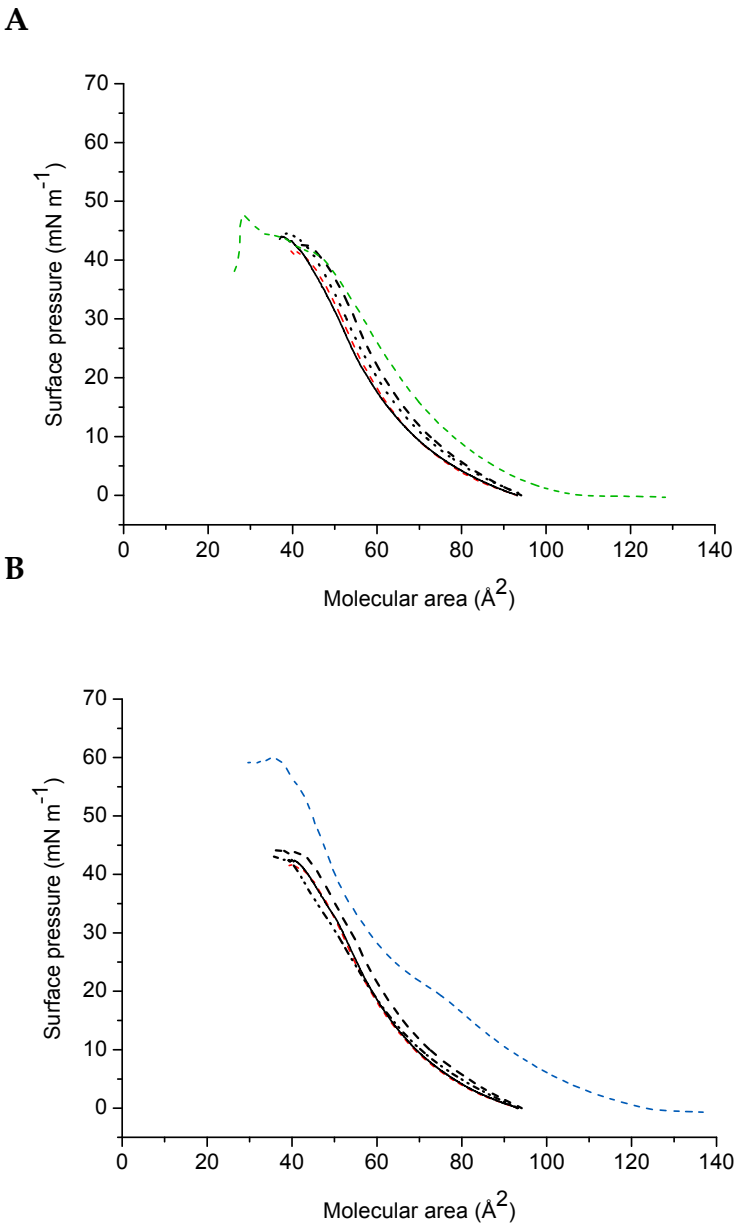


Figure 4-3. Monolayer compression at the air/water interface: π-A isotherms for mixtures of PC (---) with 2 (—), 25 (---), 50 (-··) and 100 mol% **(A)** PIM_2 (16:16) (---) and **(B)** PIM_2 (18:18) (---).

Table 4-2. Monolayer characteristics of PC and PIM_2 lipids mixed at various ratios (mol%): Experimental average area per molecule (A_{exp}, $Å^2$), ideal average area per molecule (A_{ideal}, $Å^2$), deviation from ideality (Dev, %) and collapse pressure (π_{coll}, mN m^{-1}). Results are displayed as mean ± SD of three independent measurements, * denotes $p \leq 0.05$ relative to PC.

Lipid and binary mixtures	$\mathbf{A_{exp}}$	$\mathbf{A_{ideal}}^{\#}$	**Dev**	$\boldsymbol{\pi_{coll}}$
PC	73.7 ± 5.9	-	-	41.6 ± 0.2
PIM_2 (16:16)	81.0 ± 3.2	-	-	43.7 ± 1.0
PC PIM_2 (16:16) (98:2%)	70.7 ± 2.8	73.8	-4.2	43.7 ± 1.6
PC PIM_2 (16:16) (75:25%)	76.5 ± 4.7	75.5	1.3	42.4 ± 0.4*
PC PIM_2 (16:16) (50:50%)	73.7 ± 2.6	77.4	-4.8	43.4 ± 1.2
PIM_2 (18:18)	69.9 ± 3.0	-	-	55.3 ± 0.7
PC PIM_2 (18:18) (98:2%)	72.4 ± 2.1	73.6	-1.6	43.1 ± 1.2
PC PIM_2 (18:18) (75:25%)	76.6 ± 0.1	72.7	5.4	42.5 ± 2.6
PC PIM_2 (18:18) (50:50%)	73.3 ± 4.2	71.7	2.2	43.0 ± 1.5

$^{\#}$calculated using **Equation 4-1**.

The deacylated PGM_2 (0:0) was not included in this study as it possesses no amphiphilic properties and molecules would not be able to orientate at the air/water interface (**Chapter Three**). Incorporation of PGM_2 (10:10) into the PC monolayers dramatically affected the π-A isotherms. As shown in **Figure 4-4 A**, the isotherms recorded for the mixed monolayers were found to be between those of the pure compounds. No ideal molecular areas could be calculated for the PC PGM_2 (10:10) mixtures, as limiting area per molecule $Å_0$ and the collapse pressure π_{coll} could not be determined for pure PGM_2 (10:10) monolayers (**Table 4-3**). The effect of the addition of PGM_2 (10:10) to the PC monolayer became more obvious with increased molar fractions, and caused a shift to smaller molecular areas compared to that of pure PC (**Table 4-3**). When the

lipids were mixed in an equimolar ratio, the average molecular area was significantly reduced to 56.6 ± 0.2 Å^2 ($p \leq 0.01$). Interestingly, the collapse pressures decreased with increasing concentrations of PGM_2 (10:10), with the collapse pressure of the 1:1 molar ratio being significantly decreased (37.3 ± 1.4 mN m^{-1} compared to 41.6 ± 0.2 mN m^{-1}, $p \leq 0.01$). This indicated that this mixture was the least stable.

Isotherms recorded for PC PGM_2 (16:16) and PC PGM_2 (18:18) monolayers are shown in **Figure 4-4 B** and **C**. The experimental areas for the mixed films showed negative deviations from the additive rule (**Table 4-3**). Tendencies to smaller average molecular areas were observed with incorporation of an increased molar fraction of PGM_2 lipids into PC films. In particular, increasing the concentrations of PGM_2 (16:16) resulted in significantly decreased A_{exp} (72.0 ± 0.4 Å^2 and 70.0 ± 0.9 Å^2 $p \leq 0.001$ compared to 75.1 ± 0.3 Å^2, and 72.0 ± 0.4 Å^2 $p \leq 0.05$ compared to 70.0 ± 0.9 Å^2). All investigated mixtures showed single collapse points, which were increased compared to that of the pure PC films. Collapse pressures were significantly higher for PC with 25 mol% ($p \leq 0.001$) and 50 mol% PGM_2 (16:16) ($p \leq 0.05$). Similarly, the mixed monolayers of PC PGM_2 (18:18) with 2 mol% and 50 mol% of PGM_2 (18:18) collapsed at significantly higher surface pressures, when compared to PC (42.7 ± 0.3 mN m^{-1} $p \leq 0.01$ and 50.2 ± 1.8 mN m^{-1} $p \leq 0.001$ compared to 41.6 ± 0.2 mN m^{-1}).

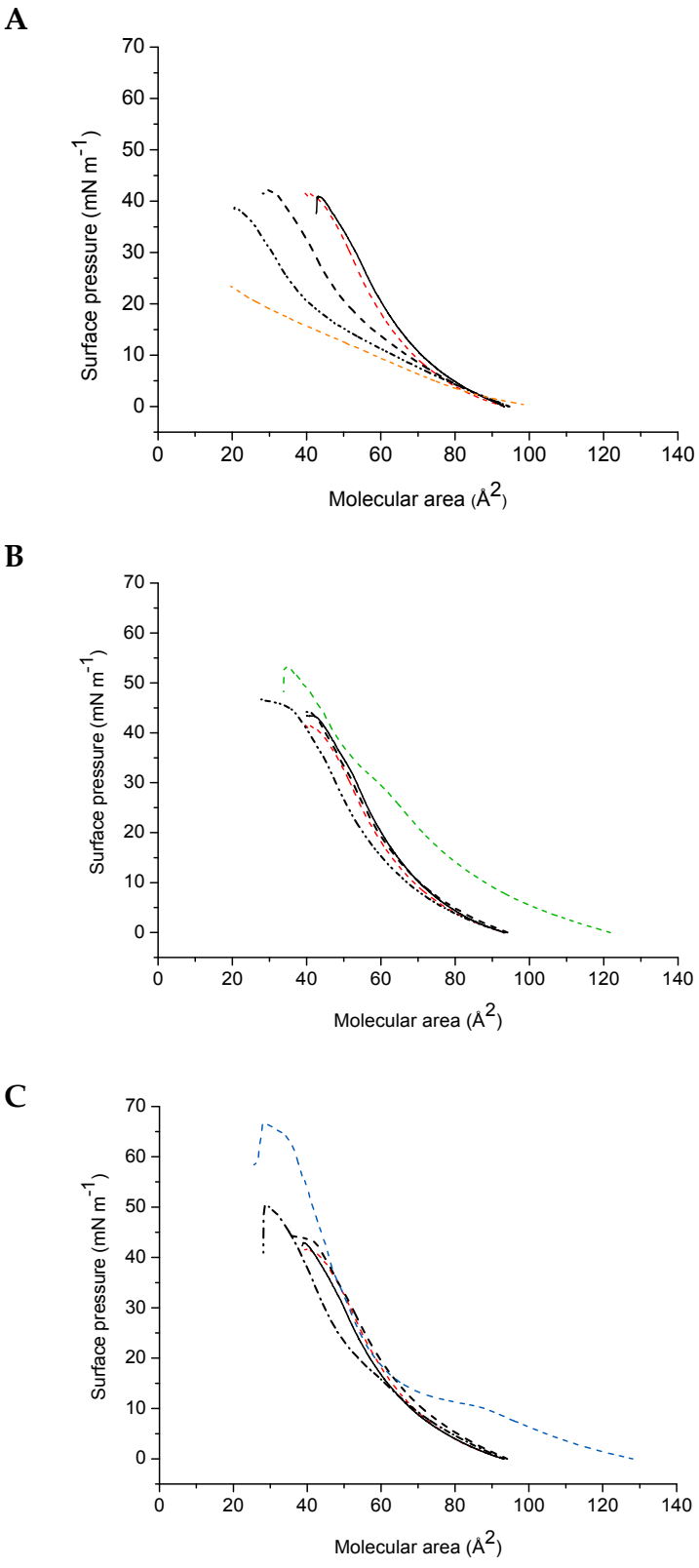


Figure 4-4. Monolayer compression at the air/water interface: π-A isotherms for mixtures of PC (---) with 2 (—), 25 (---), 50 (-··) and 100 mol% **(A)** PGM_2 (10:10) (---), **(B)** PGM_2 (16:16) (---) and **(C)** PGM_2 (18:18) (---).

Table 4-3. Monolayer characteristics of PC and PGM_2 lipids mixed at various ratios (mol%): Experimental average area per molecule (A_{exp}, $Å^2$), ideal average area per molecule (A_{ideal}, $Å^2$), deviation from ideality (Dev, %) and collapse pressure (π_{coll}, mN m^{-1}). Results are displayed as mean ± SD of three measurements, * denotes $p \leq 0.05$, ** $p \leq 0.01$ and *** describes $p \leq 0.001$ relative to PC.

Lipid and binary mixtures	$\mathbf{A_{exp}}$	$\mathbf{A_{ideal}}^{\#}$	**Dev**	$\boldsymbol{\pi_{coll}}$
PC	73.7 ± 5.9	-	-	41.6 ± 0.2
PGM_2 (10:10)	-	-	-	-
PC PGM_2 (10:10) (98:2%)	76.3 ± 5.6	NA	NA	39.7 ± 1.1
PC PGM_2 (10:10) (75:25%)	66.6 ± 2.4	NA	NA	41.9 ± 0.9
PC PGM_2 (10:10) (50:50%)	56.6 ± 0.2**	NA	NA	37.3 ± 1.4**
PGM_2 (16:16)	79.5 ± 1.4	-	-	52.7 ± 1.0
PC PGM_2 (16:16) (98:2%)	75.1 ± 0.3	73.8	1.8	42.4 ± 1.1
PC PGM_2 (16:16) (75:25%)	72.0 ± 0.4	75.2	-4.3	44.0 ± 0.0***
PC PGM_2 (16:16) (50:50%)	70.0 ± 0.9	76.6	-8.6	43.9 ± 1.1*
PGM_2 (18:18)	63.2 ± 2.2	-	-	60.7 ± 2.1
PC PGM_2 (18:18) (98:2%)	70.2 ± 1.7	73.5	-1.6	42.7 ± 0.3**
PC PGM_2 (18:18) (75:25%)	74.3 ± 3.3	71.1	5.5	43.2 ± 1.1
PC PGM_2 (18:18) (50:50%)	66.8 ± 3.9	68.5	2.3	50.2 ± 1.8***

$^{\#}$calculated using **Equation 4-1**, NA denotes where no ideal molecular A_{ideal} could be calculated.

The influence of the phosphoglycolipid head group on mixed monolayer formation was further evaluated. Incorporation of PGM_2 (18:18) into PC films resulted in greater shift to smaller experimental areas compared to PIM_2 (18:18) at all investigated ratios. These mixtures also showed significantly higher

collapse pressures. Similar results were found for PC monolayers containing PGM_2 (16:16) or PIM_2 (16:16).

4.4.2 Thermal phase behaviour of PIM_2 and PGM_2 lipids

The thermotropic phase behaviour of PIM_2 and PGM_2 was investigated using differential scanning calorimetry (DSC). The transition from gel (crystalline) to liquid-crystalline phases for dry samples was monitored and the calorimetric transition curves obtained are displayed in **Figure 4-5**.

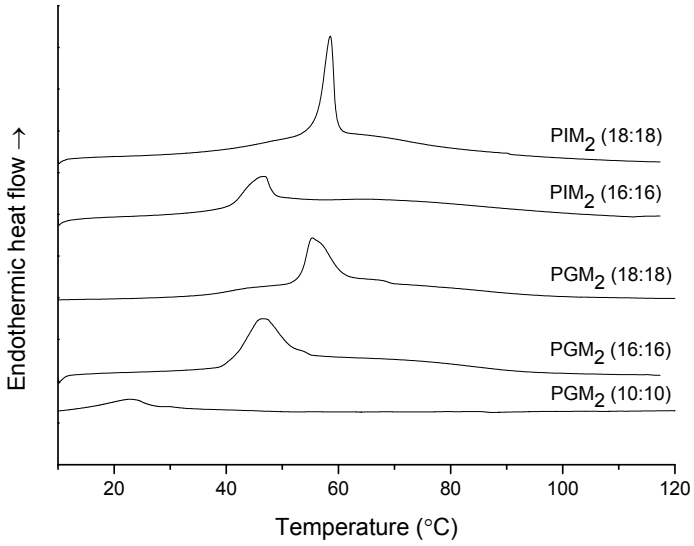


Figure 4-5. DSC scans of PIM_2 and PGM_2 lipids. The measurements of the dry samples were performed at a heating rate of 10 K min^{-1}.

The corresponding calculated transition temperatures (T_ms, as onset temperatures) for each lipid are summarised in **Table 4-4**. The acyl chain length was found to have a major impact on the T_m of PIM_2, whereby longer C18 fatty acid residues resulted in significantly higher phase transition temperatures compared to PIM_2 (16:16) ($p \leq 0.05$). These findings agreed with other studies which reported increased phase transition temperatures for lipids with varied

lengths of their hydrocarbon chains: dimyristoylphosphatidylcholine (DMPC, 24°C), DPPC (42°C) and DPSC (55°C) [189,348]. Thermograms recorded for PGM_2s showed the same tendency and the T_m increased with an increased number of hydrocarbons. Significant differences in T_ms were found between all PGM_2 compounds ($p \leq 0.05$). While literature suggests an impact of the polar head group, particularly the degree of hydration, on transition temperature[189,349], the comparison of T_ms of PIM_2 and PGM_2 compounds with the same acyl chain length (C16 or C18), indicated a minor effect of the head group with non-significant differences between corresponding T_ms.

Table 4-4. Phase transition temperatures (T_ms) of various lipids, T_ms as onset temperatures (mean ± SD, n=3).

Lipid	**T_m (°C)**
PIM_2 (16:16)	42.1 ± 1.3
PIM_2 (18:18)	55.9 ± 0.5
PGM_2 (0:0)	-
PGM_2 (10:10)	23.2 ± 0.8
PGM_2 (16:16)	40.1 ± 1.3
PGM_2 (18:18)	54.9 ± 1.7

4.4.3 Characterisation of liposome formulations

4.4.3.1 Vesicle size and zeta potential

Physical characteristics of the investigated liposome formulations are summarised in **Table 4-5.** PC liposomes had an average diameter of 321 ± 45 nm after extrusion through stacked 800 - 400 nm polycarbonate membranes. As discussed earlier, 2% PGM_2 (0:0) was incorporated into the aqueous liposomes core due its hydrophilic character. The resultant liposomes had comparable

particle sizes to PC liposomes of 336 ± 29 nm. Integration of 2% lipidated PIM_2 and PGM_2 into the PC liposomal bilayer led to a notable decrease in particle size (**Table 4-5**). The average diameters were found to be significantly smaller for liposomes containing PIM_2 (16:16) and PGM_2 (10:10) ($p \leq 0.05$) in comparison to PC formulations. All dispersions showed a polydispersity index (PDI) smaller than 0.3 on the day of preparation, indicating a moderately homogeneous size distribution for all samples.

Table 4-5. Physical characterisation of liposome formulations. Average particle size shown as z-average (d.nm), polydispersity index (PDI) and zeta potential (mV) of PC liposomes ± 2% (w/w) of different incorporated phosphoglycolipids. Results are displayed as mean ± SD of three independent formulations.

Formulation	Z-average	PDI	Zeta potential
PC PIM_2 (16:16)	234 ± 30	0.23 ± 0.06	-3.0 ± 0.5
PC PIM_2 (18:18)	257 ± 18	0.22 ± 0.01	-3.5 ± 0.6
PC PGM_2 (0:0)	336 ± 29	0.27 ± 0.00	-0.8 ± 0.0
PC PGM_2 (10:10)	235 ± 14	0.26 ± 0.04	-1.8 ± 0.5
PC PGM_2 (16:16)	252 ± 15	0.21 ± 0.03	-3.5 ± 0.4
PC PGM_2 (18:18)	258 ± 15	0.23 ± 0.06	-2.9 ± 0.4
PC	321 ± 45	0.25 ± 0.06	-0.7 ± 0.1

Zeta potential measurements of PC and PC PGM_2 (0:0) liposomes gave particle surface charges of -0.7 ± 0.1 mV and -0.8 mV, respectively. A zeta potential close to 0 mV was expected due to the neutral head group charge of PC at the investigated pH 7.5. Negative shifts of the zeta potential recorded for PC PIM_2 or PC PGM_2 liposomes were attributed to the negative charge of the ionised phosphatidyl moiety. This shift was statistically significant for liposomes with PIM_2 (16:16), PIM_2 (18:18), PGM_2 (16:16) and PGM_2 (18:18) ($p \leq 0.05$) compared to PC based liposomes.

4.4.3.2 ConA agglutination assay

To confirm the successful incorporation of the glycolipids into the bilayer, the availability of mannosyl residues on the liposome surface was investigated using a ConA agglutination assay[350,351]. ConA is a lectin that binds to carbohydrates such as mannose and glucose, resulting in aggregation of vesicles containing glycolipids[352]. DLS measurements were performed to monitor vesicle sizes before and after the addition of ConA. The data is expressed as the relative increase in the particle diameter and was calculated by dividing the measured diameter by the initial value. In **Figure 4-6** the arrow illustrates the addition time of the ConA solution to the liposomes after 20 min.

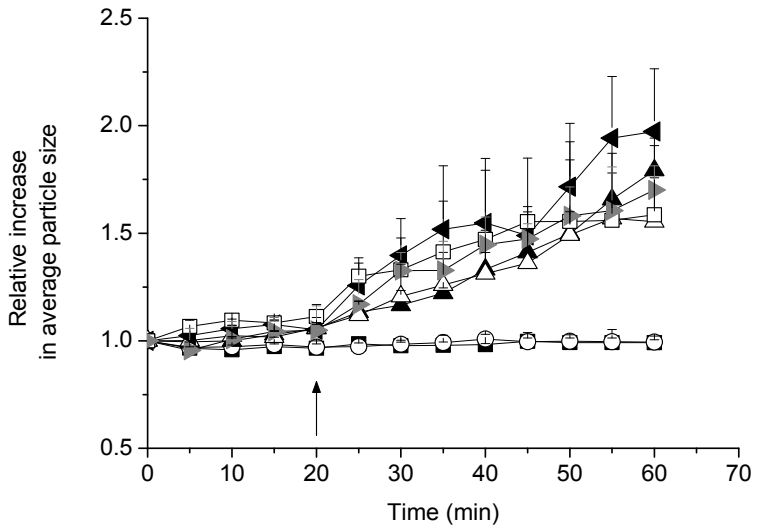


Figure 4-6. ConA-induced agglutination of liposome formulation PC PIM_2 (16:16) (□), PC PIM_2 (18:18) (►), PC PGM_2 (0:0) (○), PC PGM_2 (10:10) (▲), PC PGM_2 (16:16) (Δ), PC PGM_2 (18:18) (◄) and PC (■). The aggregation was monitored by measuring the particle size every 5 min. Addition of the ConA solution is indicated by the arrow. Values are expressed as mean + SD (n=2).

An increase in average particle sizes for liposomes containing acylated glycolipids in their bilayers was recorded instantly. Particle sizes increased

gradually and after 60 min the extent of aggregation was comparable between the different formulations. In contrast, the PC and PC PGM_2 (0:0) liposomes, both acting as controls, showed no increase in particle size.

4.4.3.3 Entrapment of FITC-OVA and membrane stability

Following preparation, the amount of incorporated FITC-OVA was determined to obtain the initial entrapment on day 0 (**Table 4-6**). Extruded PC liposomes had a protein entrapment of 1.11 ± 0.20 mg mL^{-1}. PC PGM_2 (0:0) liposomes had a similar amount of protein incorporated (1.2 ± 0.36 mg mL^{-1}), while the presence of acylated lipid in the PC bilayer was seen to result in decreased protein amounts entrapped within the liposomes (**Table 4-6**). A significantly reduced entrapment was found for PC PGM_2 (16:16) liposomes ($p \leq 0.05$).

Stability studies revealed that the investigated formulations had different abilities to retain the encapsulated protein. After 21 days, PC and PC PGM_2 (0:0) liposomes showed a similar loss of FITC-OVA of around 0.23 mg mL^{-1} and 0.29 mg mL^{-1}, respectively. PC PIM_2 or PC PGM_2 liposomes containing C16 acyl chains, maintained the same amount of protein entrapped upon storage, whereas small amounts of protein leaked from liposomes containing C18 analogues (**Table 4-6**).

Table 4-6. Entrapment of fluorescently-labelled OVA in liposome formulations. Amount of protein incorporated (mg mL^{-1}) on day 0 and after 21 days following storage at 4°C in PBS (pH 7.5). Results are shown for PC liposomes ± 2% of different phosphoglycolipids incorporated. Values represent mean ± SD of three independent formulations.

Formulation	Entrapment Day 0	Entrapment Day 21
PC PIM_2 (16:16)	0.52 ± 0.30	0.52 ± 0.23
PC PIM_2 (18:18)	0.74 ± 0.27	0.61 ± 0.19
PC PGM_2 (0:0)	1.20 ± 0.36	0.91 ± 0.30
PC PGM_2 (10:10)	0.70 ± 0.18	0.46 ± 0.18
PC PGM_2 (16:16)	0.43 ± 0.09	0.43 ± 0.09
PC PGM_2 (18:18)	0.65 ± 0.14	0.54 ± 0.06
PC	1.11 ± 0.20	0.89 ± 0.21

Interestingly, the membrane stability of PC PGM_2 (10:10) liposomes was comparable to PC and PC PGM_2 (0:0) liposomes. PC and PC PGM_2 (0:0) liposomes lost more than twice as much entrapped protein during storage, in comparison to formulations containing acylated phosphoglycolipids (C16 and C18). This indicated that the membrane stability of the liposomes was affected by the incorporation of these phosphoglycolipids into the bilayer. These findings suggested that the length of the hydrocarbon chains played an important role in membrane stability.

Stability studies suggested that the dispersions remained in the nanometer size range over the investigated period of 21 days (**Figure 4-7**), with the PDI being consistently smaller than 0.3 over the time of storage. No increase in vesicle size was detected, indicating that no particle aggregation occurred upon storage. Zeta potential measurements showed no significant variations and maintained their values over 21 days.

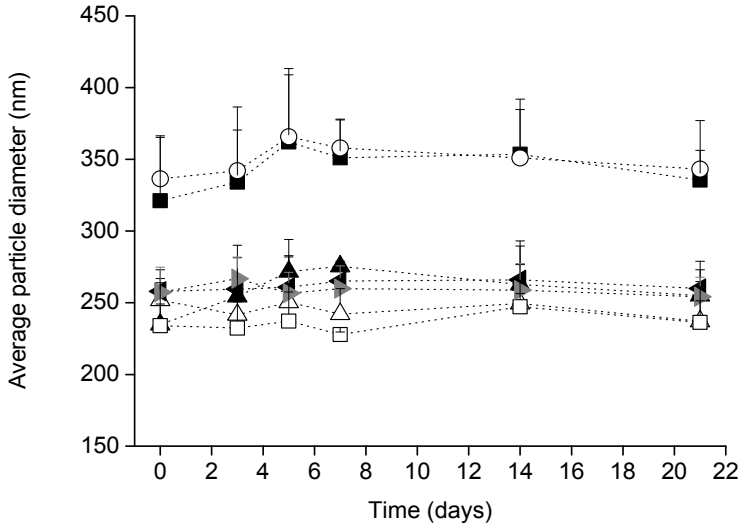


Figure 4-7. Effect of storage on average particle size (z-average) of liposome formulations PC PIM_2 (16:16) (□), PC PIM_2 (18:18) (►), PC PGM_2 (0:0) (○), PC PGM_2 (10:10) (▲), PC PGM_2 (16:16) (Δ), PC PGM_2 (18:18) (◄) and PC (■). Liposomes were stored at 4°C in PBS (pH 7.5). Results are shown as mean + SD of three independent experiments.

4.4.4 *In vitro* liposome immunogenicity- Formulation uptake and DC activation

This *in vitro* experiment evaluated the uptake of various liposome formulations by BMDCs and their subsequent stimulation. For this purpose, BMDCs were incubated at 37°C with liposomes containing FITC-OVA or media as a negative control. Following incubation for 48 hours, cells were washed to remove excess formulation and stained with PI and antibodies against the BMDC marker CD11c for FACS analysis, as outlined in **Section 4.3.9**. Following appropriate gating on size (forward scatter), granularity (side scatter) and cell viability (PI^{low}), cell-associated FITC fluorescence of CD11c-positive cells was determined. The percentage of viable cells in response to treatment with formulations was comparable to untreated cells (media), with no significant differences found (**Appendix C**). The effect of varied total lipid concentrations (10, 50 and 250 μg mL^{-1}) on liposome uptake was investigated. The results are

presented as fold increase of FITC mean fluorescence intensity (MFI) of live, CD11c-positive cells over media (**Figure 4-8**). While there were relatively large within group variations for FITC MFI, there was a trend towards an increase in uptake with increased total lipid concentrations of each formulation. However, comparison of modified formulations to PC liposomes showed that the uptake was not affected by incorporation of PIM_2 and PGM_2. No significant differences to unmodified PC liposomes were detected at any concentration.

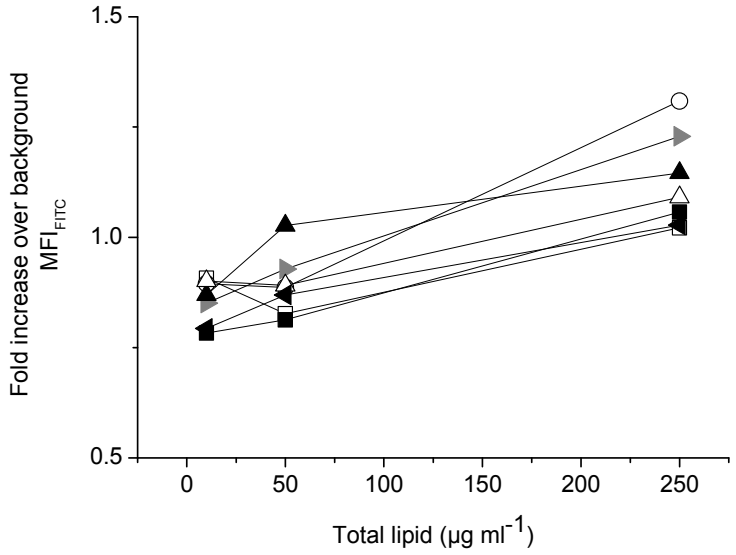


Figure 4-8. Uptake of FITC-OVA containing liposome formulations by BMDC *in vitro*. BMDC were pulsed at 37°C for 48 hours with different amounts of total lipid of PC PIM_2 (16:16) (□), PC PIM_2 (18:18) (►), PC PGM_2 (0:0) (○), PC PGM_2 (10:10) (▲), PC PGM_2 (16:16) (Δ), PC PGM_2 (18:18) (◄) and PC (■). Results are expressed as fold increase of CD11c-positive cells incubated with liposomes over CD11c-positive cells pulsed with media (background). The data is shown for one experiment. The results of two other replicates are shown in **Appendix C**.

Furthermore, activation of BMDCs was determined after incubation with various formulations, with and without the adjuvant MPL (10 ng mL^{-1}), for 48 hours at 37°C. Cells were pulsed with a combination of MPL and liposome in order to assess if any synergistic effects could be detected.

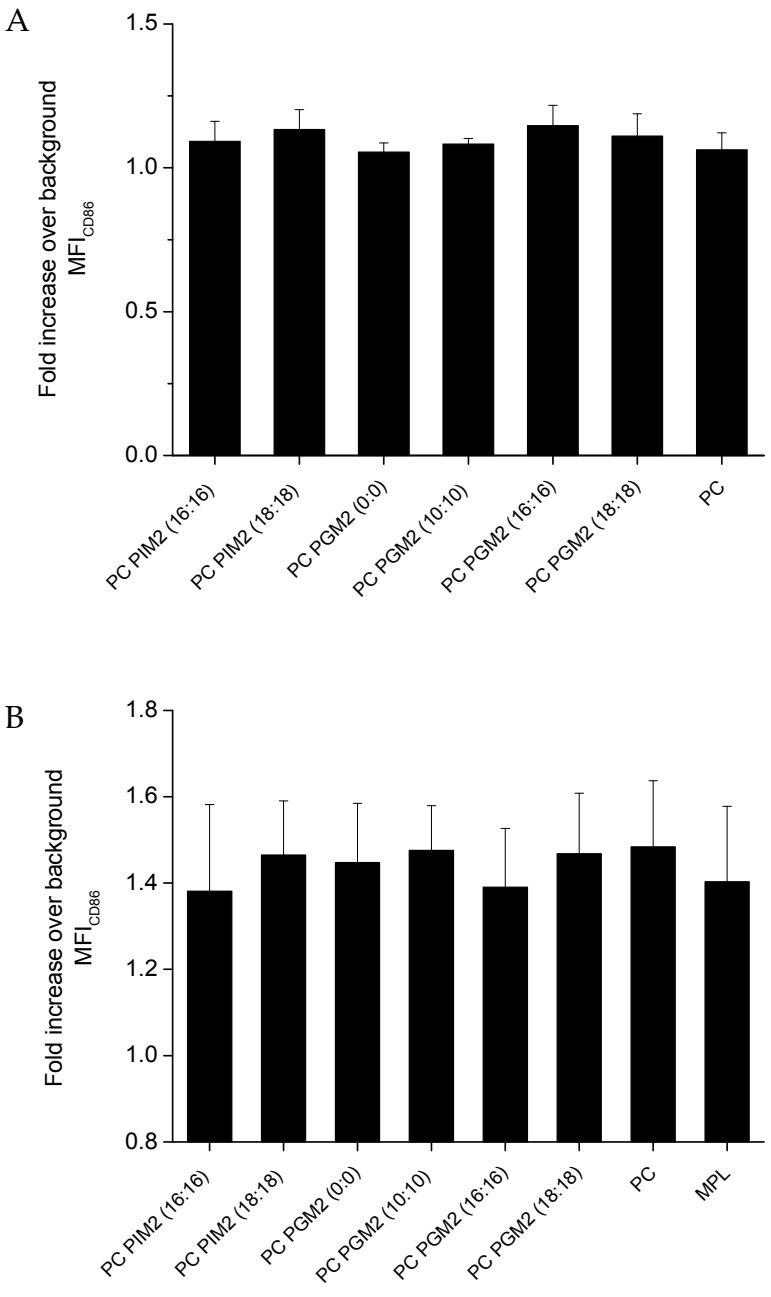


Figure 4-9. Expression of BMDC surface activation marker CD86 following *in vitro* incubation with various formulations at 37°C for 48 hours. **(A)** BMDC were incubated with FITC-OVA containing liposome formulations (250 μg mL^{-1} total lipid). **(B)** BMDC were pulsed with FITC-OVA containing liposome formulations (250 μg mL^{-1} total lipid) + MPL (10 ng mL^{-1}) and MPL (10 ng mL^{-1}). Results are expressed as fold increase of CD11c-positive cells incubated with various formulations over CD11c-positive cells pulsed with media (background). Data represent mean of three independent experiments + SD.

The extent of DC activation was determined by assessing the expression of the activation surface markers CD86, CD80 and MHC class II on CD11c-positive

DC. As shown in **Figure 4-9 A**, treatment of BMDCs with various liposome formulations (250 μg mL^{-1} total lipid) resulted in similar levels of the activation marker CD86. No increase in expression of CD80 and MHC class II surface markers was detected (**Appendix C**). The extent of BMDC activation by liposome formulations with MPL was comparable to MPL (10 ng mL^{-1}) alone (**Figure 4-9 B**). Expression of surface markers CD80 and MHC class II remained unchanged (**Appendix C**).

4.4.5 *In vivo* vaccine model

4.4.5.1 Expansion of transgenic $CD4^+$ and $CD8^+$ T cells

In order to analyse the ability of various liposome formulations to induce an OVA-specific helper T cell response as well as a cellular immune response, the expansion of both $CD4^+$ and $CD8^+$ antigen-specific T cells was determined. With the aim of providing a population of tracer cells that could be specifically identified by flow cytometry, OVA-specific $CD4^+$ and $CD8^+$ transgenic cells were adoptively transferred into the recipient mice prior to immunisation on day 0. Alum was included as a control, as this is the most commonly used adjuvant in human vaccines. This adjuvant is known to be a potent inducer of humoral immunity[145].

Expansions of antigen specific $CD4^+$ and $CD8^+$ Vα2Vβ5 T cells in the lymph nodes and spleens harvested from vaccination groups were assessed on day 17, following boosting of test animals on day 14. As shown in **Figure 4-10 A**, an increase in the percentage of OVA-specific $CD4^+$ T cells in lymph nodes was observed in mice vaccinated with modified liposomes, compared to PC liposomes. However, this increase was only significant in the case of mice vaccinated with PC PGM_2 (10:10) liposomes (1.7 ± 0.2, $p \leq 0.05$).

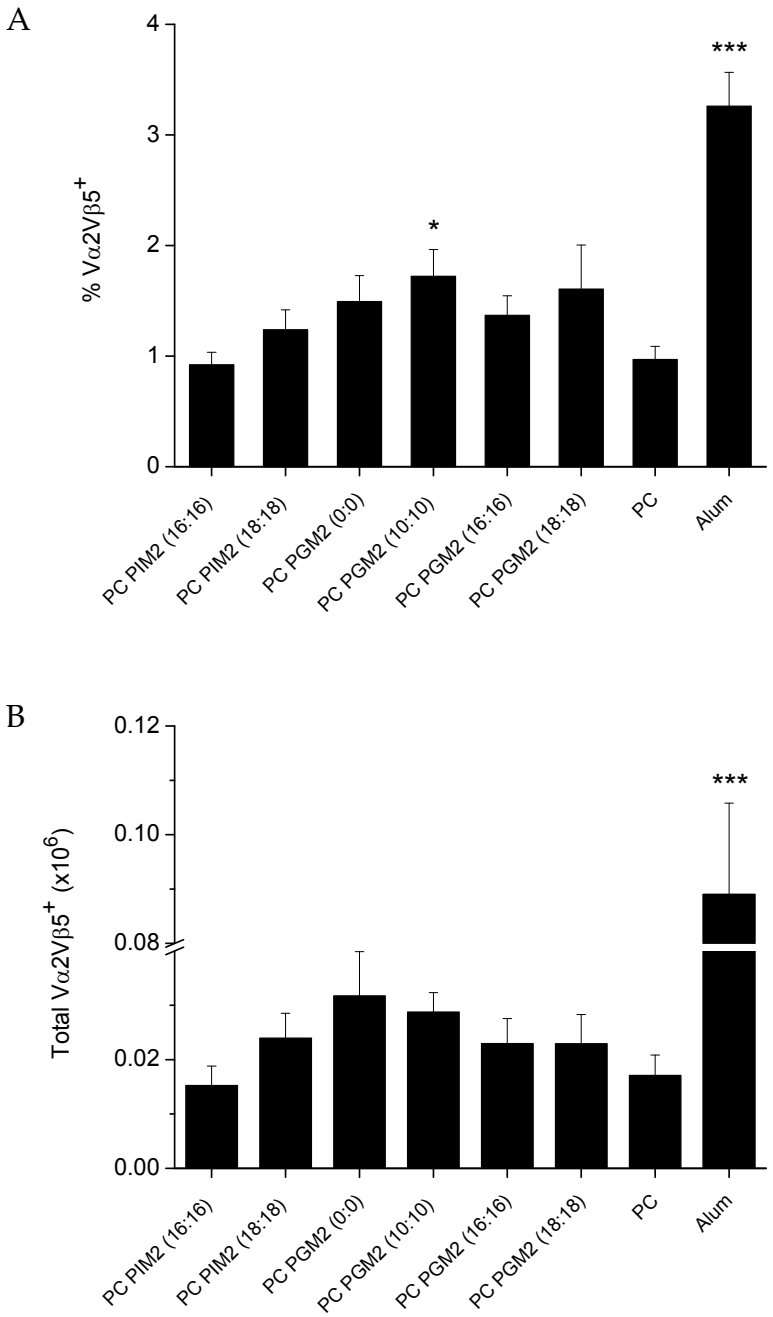


Figure 4-10. OVA-specific expansion of Vα2Vβ5 T cells. **(A)** Percent and **(B)** total number of CD4+ Vα2Vβ5 T cells in lymph nodes of each vaccination group. Bars depict mean + SE from n=3 mice per group from three independent experiments, * describes $p \leq 0.05$ and *** $p \leq 0.001$ relative to PC vaccination group.

The same trend was observed for total number of Vα2Vβ5 CD4+ T cells, although these were not found to be significantly different when compared to unmodified liposomes (**Figure 4-10 B**). Both frequency (3.3 ± 0.3, $p \leq 0.001$) and total number (0.09 ± 0.02, $p \leq 0.001$) of CD4+ Vα2Vβ5 T cells in the draining

lymph nodes of alum-vaccinated mice were significantly increased compared to the PC vaccination group, suggesting a greater ability to induce T helper cell immunity. Vα2Vβ5 $CD4^+$ T cells in spleen samples were comparable between different liposome formulations and no significant differences were observed. Mice immunised with alum showed a greater expansion in percentages of splenic $CD4^+$ T cells compared to PC (0.99 ± 0.02, $p \leq 0.001$) (**Appendix C**).

The expansion of antigen specific $CD8^+$ Vα2Vβ5 T cells in lymph nodes showed similar trends for percentages and total cell numbers, as it was previously shown for $CD4^+$ (**Figure 4-11**). Again, a significant increase in percentage of $CD8^+$ Vα2Vβ5 T cells could only be detected in mice vaccinated with PC PGM_2 (10:10) liposomes (5.8 ± 0.7, $p \leq 0.05$) and alum (6.3 ± 0.3, $p \leq 0.001$), in comparison to PC liposomes (**Figure 4-11 A**). Splenic T cells harvested from vaccination groups showed similar activation profiles in percentage and total numbers of $CD8^+$ Vα2Vβ5 T cells, with no significant differences notable (**Appendix C**). $CD8^+$ T cell proliferation resulting from alum vaccination was seen to be similar to that induced by different liposome formulations.

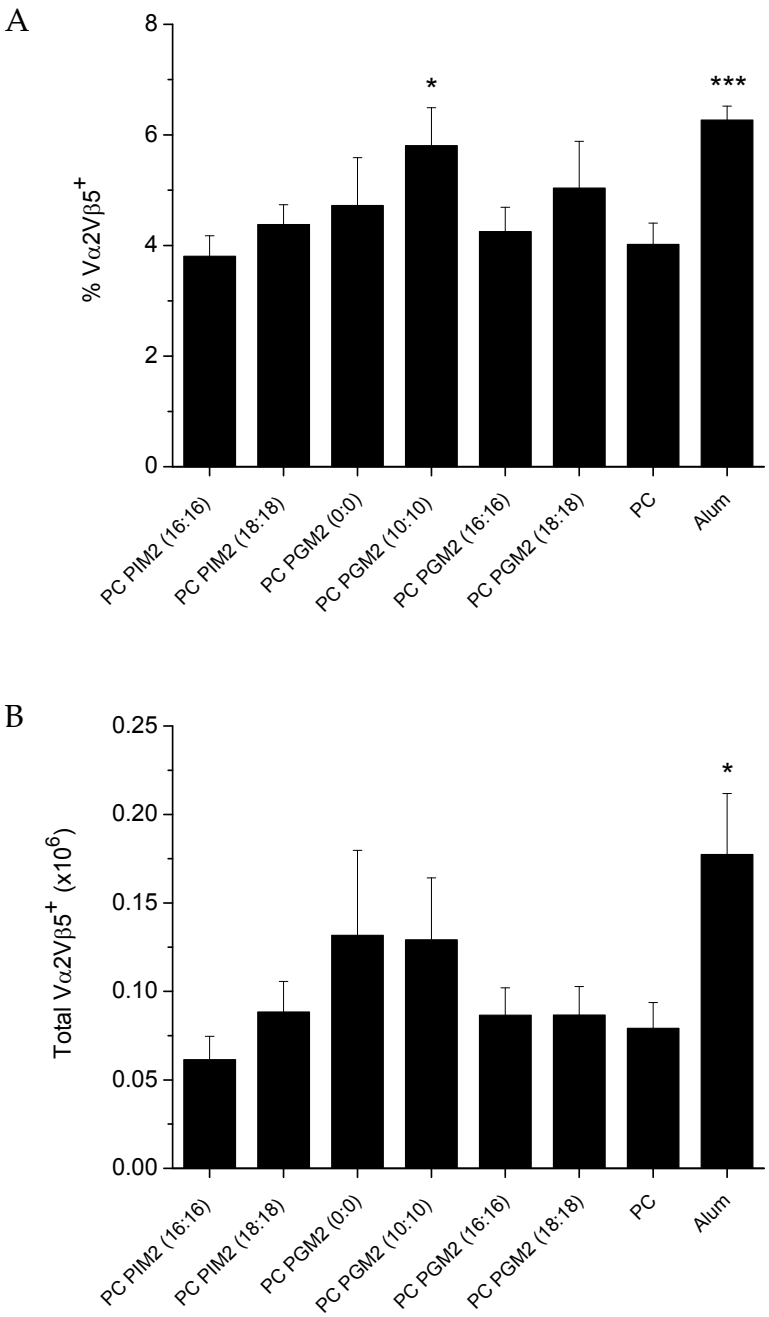


Figure 4-11. OVA-specific expansion of Vα2Vβ5 T cells. **(A)** Percent and **(B)** total number of $CD8^+$ Vα2Vβ5 T cells in lymph nodes. Bars depict mean + SE from n=3 mice per group from three independent experiments, * denotes $p \leq 0.05$ and *** $p \leq 0.001$ relative to PC vaccination group.

4.4.5.2 T cell proliferation after *in vitro* restimulation with OVA

Next, the extent of lymph node and spleen cell division in response to restimulation *in vitro* with OVA was determined. This was done using a

standard thymidine incorporation assay, as previously described in **Chapter Three**. The amount of radiolabeled ^{3}H-thymidine which was incorporated into cells during cell division was measured. The proliferation of T cells was presented as stimulation index (SI = OVA-stimulated/non-stimulated cells) in **Figure 4-12**. Proliferative responses of the lymphocytes isolated from the draining lymph nodes were higher for all vaccination groups, as compared to the alum control group. However, this difference was only found to be significant for PC PIM_2 (18:18) liposomes (14.3 ± 1.8, $p \leq 0.05$) and PC PGM_2 (0:0) liposomes (15.6 ± 1.6, $p \leq 0.01$). PC PGM_2 (0:0) liposomes also showed a higher stimulation index in comparison to PC liposomes ($p \leq 0.05$). Stimulation indices of splenic T cells showed no significant differences in proliferation between the vaccination groups.

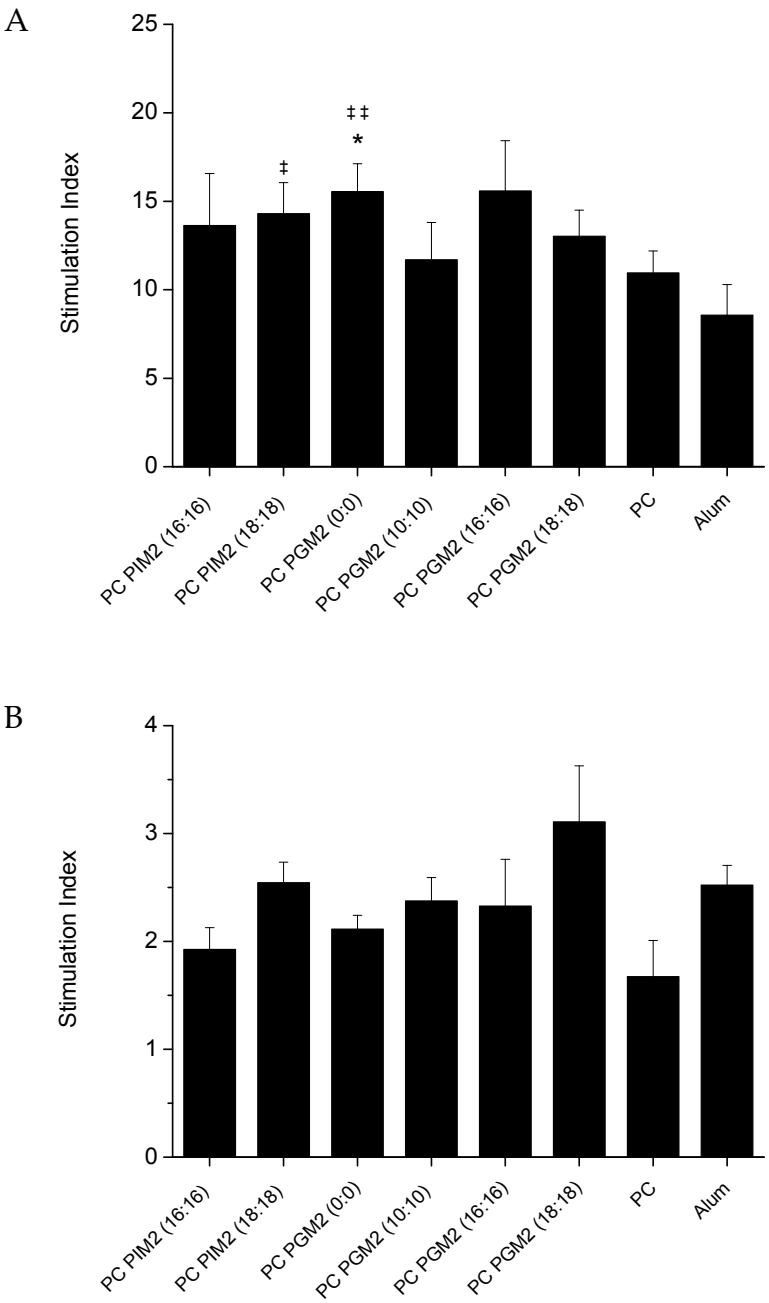


Figure 4-12. Proliferation of T cells isolated from **(A)** lymph nodes and **(B)** spleens of each study group after *in vitro* restimulation with OVA and media. Results are expressed as stimulation indices (SI= OVA/media). Bars depict mean + SE from n=3 mice per group from three independent experiments, * denotes $p \leq 0.05$ relative to PC group, ‡ denotes $p \leq 0.05$, ‡‡ $p \leq 0.01$ relative to alum vaccination group.

4.4.5.3 OVA-specific production of cytokines

Furthermore, the capacity of lymph node and splenic T cells to produce INF-γ following *in vitro* restimulation with OVA was investigated (**Figure 4-13**).

IFN-γ levels were measured so as to probe the ability of liposome formulations to induce an antigen-specific Th1 immune response. The results revealed no obvious trend in increased IFN-γ titres in comparison to unmodified liposomes and alum control. No statistically significant differences in these cytokine levels were detected. Results for splenic T cells are presented in **Appendix C**.

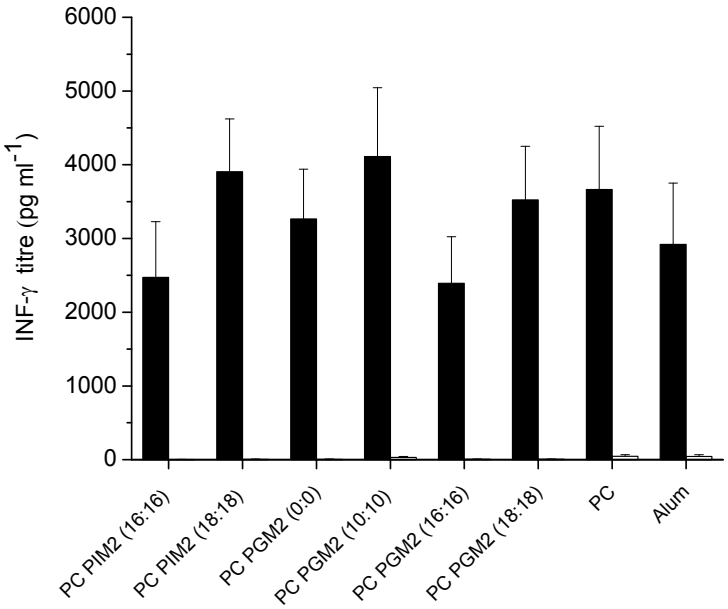


Figure 4-13. Production of IFN-γ by T-cells isolated from lymph nodes of each study group. Titres of cytokine responses were determined after *in vitro* restimulation with OVA (black bars) or medium (white bars, negative control). Bars depict mean + SE from n=3 mice per group from three independent experiments.

4.4.5.4 Production of OVA-specific antibody

To further evaluate the ability to generate humoral immune responses, the levels of OVA-specific IgG antibody in the serum of vaccinate mice was assessed (**Figure 4-14**). Serum samples were collected from study mice on day 17 and antibody titres determined using ELISA. No Ova specific IgG could be detected in mice immunised with liposomes.

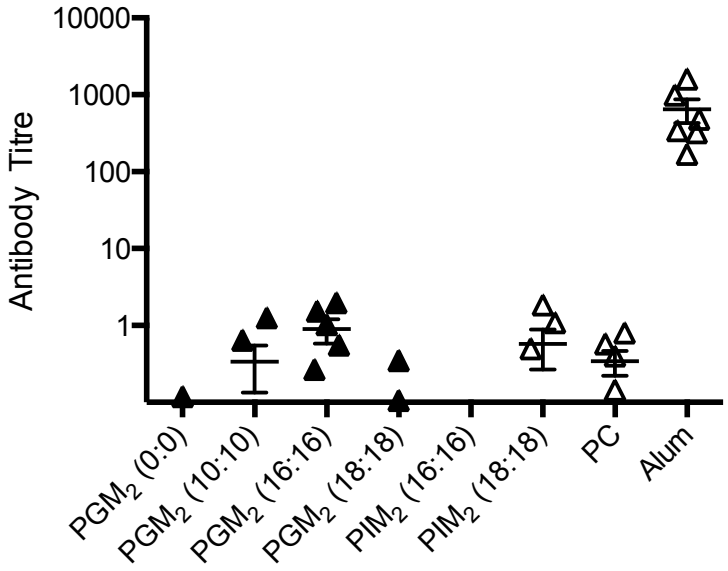


Figure 4-14. Production of OVA-specific IgG antibody as determined by ELISA. The symbols depict results from individual mice, whereas bars represent the mean values within a vaccination group. Data is presented for two independent experiments, with each experiment consisting of n = 3 mice per group.

4.5 Discussion

The ability of PIM_2 and PGM_2 to suppress immune responses was demonstrated in **Chapter Three**. To investigate the immunostimulatory activity of these compounds, the PIM_2 and PGM_2 compounds were incorporated into delivery systems to ensure co-delivery of the model FITC-OVA. Therefore, the overall aim of the work in this chapter was to design modified liposomes containing the PIM_2 and PGM_2 molecules as delivery systems, and to assess their physical (particle size, entrapment of model antigen and membrane stability) and immunological characteristics.

Mixed monolayer studies provided an insight into interactions that occurred between PIM_2/PGM_2 and PC. Analysis of interactions was conducted according to previously published methods that examined the collapse pressures of the binary systems and deviations of experimentally determined molecular areas

from theoretical ideal areas[329]. The mixed monolayers investigated in the current study showed non-ideal behaviour at all ratios of PC to phosphoglycolipid examined. In case of PIM_2 lipids, there was no obvious trend in the effect of incorporating increasing amounts of PIM_2 on experimental molecular areas. While the molecular areas of PC PIM_2 mixtures deviated from ideality, these were not significantly different from A_{exp} for the pure PC monolayer.

However, when PGM_2 were incorporated into PC monolayer, experimental molecular areas shifted towards smaller values with increased molar fractions of PGM_2 (16:16) and PGM_2 (18:18). The results obtained for the PC PGM_2 mixed isotherms suggested that the strength of the lipid-lipid interaction was dependent on the length of the acyl chain, whereby the longer C18 chains showed decreased A_{exp} when compared to PC PGM_2 (16:16) at the same ratios (70.2 ± 1.7 compared to 75.1 ± 0.3, $p \leq 0.01$; 66.8 ± 3.9 compared to 70.0 ± 0.9, $p > 0.05$). It has been shown for mixtures of phosphatidylcholines and sterols that the longer the acyl chains (C16 versus C18), the stronger the interactions between lipids as mediated through increased Van der Waals forces[310]. This was further shown to lead to smaller molecular areas. These findings are comparable with those reported for different mixed monolayers, where PC was mixed with several lipids in order to investigate membrane fusion[327]. The behaviour of PC was evaluated in binary systems with glyceryl mono-oleate[327], oleic acid[353] and palmitoleic acid[327]. Deviations from predicted molecular areas suggested miscibility of the components and the presence of interactions between lipids[327]. Non-ideal behaviour was also detected for mixed monolayers comprising PC and di- and tri-sialogangliosides[354]. Furthermore, PC has also been reported to strongly interact with a natural derivative of mycobacterial trehalose-6,6-dimycolate (cord factor)[331]. This study was conducted in order to

understand the ability of these mycobacterial glycolipids to interact with membrane phospholipids of infected cells. Interactions between glycolipid and PC were already found with a low molar fraction of 0.1% of the glycolipid, suggesting that interactions with mitochondrial membranes after internalisation by immune cells is possible[331]. Similar evidence for interactions were demonstrated for mixtures of trehalose-6,6-dimycolate and DPPC. DPPC is known to be poorly hydrated due to its neutral charge. Thus, in addition to chain-chain interactions, condensing effects on the monolayer may be caused by improved hydrogen-bonding between the phosphate of the DPPC and hydroxyl groups of the glycolipids[331].

The PC monolayers investigated here displayed single collapse pressures in the presence of PIM_2/PGM_2 molecules, which verified the miscibility of these two-component films[329]. Higher collapse pressures have further been suggested to indicate existing stabilising interactions between PC and the incorporated lipids[355]. In agreement with findings by other research groups was that the collapse pressures of the PC- PIM_2/PGM_2 mixed monolayers were intermediate to the ones of the corresponding pure components[320].

The influence of PGM_2 (10:10) was noteworthy, in that it significantly affected the behaviour of the PC monolayer. PGM_2 (10:10) molecules can be retained at the air/water interface when mixed with PC up to an equimolar ratio. The formation of insoluble monolayers was seen in all of the PGM_2 (10:10) binary mixtures, as evidenced by the presence of film collapse pressure. This is most likely mediated by strong synergistic interactions between components[255,356]. These findings are comparable to a mixed surfactant system in which a surfactant mixture, with chain lengths of C16/C12, showed more condensed

films, rather than the unstable monolayers formed by a C12/C12 system[356]. This was due to enhanced attractive forces between molecules[356].

When PC is co-spread with PGM_2 (10:10), its long-chain fatty acids[339] exert strong hydrophobic interactions between molecules. Thus promoting the orientation of the shorter chains of PGM_2 (10:10) at the air/water interface. Similar interfacial behaviours have been reported for mixed monolayers of cationic and anionic surfactants. In this case, strong synergistic electrostatic interactions between head groups of the water-soluble surfactants, together with hydrophobic interactions, enabled film formation[357]. It is likely that here hydrophobic interactions enabled mixed film formation, since higher PGM_2 (10:10) concentrations led to a decreased stability, as evidenced by significantly decreased collapse pressure values. This may be explained by weaker interactions between the short acyl chains of PGM_2 (10:10) and PC, which at higher PGM_2 (10:10) concentrations, would destabilise mixed monolayers[356].

The nature of the polar head group had significant effects on the interactions of the phosphoglycolipids with PC in the mixed monolayers. Comparisons of mixed monolayers containing PIM_2 and PGM_2 with the same acyl chain length, provided insight into the effects of the head group on interactions with PC. Decreased molecular areas were observed in the present study for the glycerol based compounds. For instance, PGM_2 (18:18) showed a decreased molecular area compared to PIM_2 (18:18) at equimolar ratios with PC, although this difference was not significant. However, the collapse pressure of PC PGM_2 (18:18) (50:50%) mixed monolayers was significantly increased in comparison to PC PIM_2 (18:18) (50:50%) monolayers (50.2 ± 1.8 versus 43.0 ± 1.5, $p \leq 0.01$). Overall, the effect of PIM_2 lipids on PC monolayers were less pronounced as compared to PGM_2, which could be attributed to the bulkier head group. As

previously shown in **Chapter Three**, the steric constraints of the inositol group determined the lipid packing in pure monolayers. Likewise, this hindrance of the head group had a significant impact on mixed monolayers with PC. Another possible explanation arises from the consideration of the structural differences between the head groups. The additional hydroxyl groups in the inositol core may allow for increased hydrogen-bonding with surrounding water molecules but also intermolecular PIM_2-PIM_2 hydrogen-bonding in pure monolayers. When PIM_2 molecules are mixed with PC, these intermolecular bonds are disrupted, which is not energetically favourable and may result in less stable monolayers compared to PGM_2 mixed systems[310].

Varied concentrations of PIM_2 and PGM_2 combined with PC were investigated in the monolayer study. Lipid interactions could be detected with as little as 2 mol% of any of the phosphoglycolipids. Based on findings from earlier studies, PIM_2 and PGM_2 were incorporated into PC-based lipid vesicles at 2 mol%. A dose of 50 μg of the PIM_2 and PGM_2 compounds, respectively was administered to mice to allow for comparison with other published studies[225,226]. As highlighted in **Chapter One**, important structural features of PIM molecules required for bioactivity, are fatty acids and mannose residues[96,227,236,248]. PIMs are known to interact with a number of receptors expressed on DCs such as MRs[26,27]. In light of this, following liposome preparation, the presence of mannosyl residues on the particle surface, was confirmed using a lectin (ConA) binding assay. Addition of ConA to liposome formulations, where phosphoglycolipids had been incorporated into bilayers, resulted in an increase in average particle diameter. No increase in size could be detected when no mannose residues were present in the bilayer (PC and PC PGM_2 (0:0) liposomes). These findings indicated that mannosylated lipids were positioned within the bilayer, such that the mannose residues oriented towards

the vesicle surface, making them accessible for interaction with receptors such as MRs. ConA-induced aggregation is a convenient method to confirm the presence of mannosyl residues, but it has not been reported by other groups for mixed vesicles containing PIMs[225,293].

Physical characterisation revealed reduced particle diameters for liposomes containing PIM_2 and PGM_2 lipids in their bilayer. The smaller size of the modified liposomes may be ascribed to a different packing morphology. The bulkier carbohydrate head group present on both PIM_2 and PGM_2 would lead to a more conical packing as opposed to the cylindrical packing found in PC bilayers[292]. Observations from the mixed monolayers suggested that lipid interactions occurred with very low concentrations of phosphoglycolipids. This may be reflected in reduced sizes of PC liposomes when PIM_2 or PGM_2 were incorporated into bilayers. Similar findings were reported by Nordly *et al.*[223], where the synthetic monomycoloyl glycerol (MMG-1) was incorporated at various ratios into DDA bilayers. According to molecular areas obtained from mixed monolayer investigations, molecular areas decreased with increased amount of MMG-1 incorporated. Correlations between molecular areas of mixed monolayers and liposomes size were also found when MPL was incorporated into DDA/TDB liposomes[358]. Results presented here also compare well with a study on mannosylated liposomes by White *et al.*[206]. They incorporated mono- or tri-mannosylated dipalmitoylphosphatidyl-ethanolamine (M_1-DPPE and M_3-DPPE) at various concentrations into PC bilayers. At concentration as low as 1 and 5% (w/w) of either M_1-DPPE or M_3-DPPE, liposome diameters were decreased as compared to PC liposomes.

Even though slightly increased molecular areas were determined for some combinations, in general the sizes of liposomes containing acylated PIM_2 or

PGM_2 compounds, showed decreased diameters. The lack of correlation between molecular area and size (as measured by DLS) for some combinations, may be due to the fact that monolayer studies are performed under restricted and controlled conditions, and the overall arrangement of molecules may be different in a monolayer compared to bilayered liposomal constructs[193,259]. While findings from monolayer studies can be extrapolated to bilayers and may help to understand lipid interactions, there is no absolute concordance[259].

In **Chapter Three**, surface charges of approximately -20 mV were observed for particles formed by acylated PIM_2 and PGM_2 lipids, upon dispersion in aqueous media. This surface charge was caused by the negatively charged phosphatidyl moiety. However, even the low PIM_2 and PGM_2 content in the liposomes (2%) had an effect on the overall charge, increasing it from -0.7 mV measured for pure zwitterionic PC liposomes to around -3 mV for the modified liposomes. As anticipated, liposomes containing PGM_2 (0:0) had neutral zeta potential with measurements similar to PC liposomes. Furthermore, consistent zeta potential values over a period of 21 days suggested that no loss of PIM_2 or PGM_2 from the bilayer occurred, in which case a shift towards zero would have been recorded.

The amount of FITC-OVA entrapped within the liposome formulations was comparable to earlier studies[206,359]. White *et al.*[206] prepared PC-liposomes with various percentages of mannosylated lipid incorporated into the bilayer. The entrapments of these formulations ranged from 0.54 - 0.68 mg mL^{-1}. PC-based formulations modified with M_3-DPPE, investigated by Copland *et al.*[359] encapsulated an average amount of 1.37 ± 0.22 mg mL^{-1} FITC-OVA. It could be demonstrated that liposome stability was affected by incorporation of acylated PIM_2 and PGM_2. Leakage of FITC-OVA over a period of 21 days was reduced

in the presence of lipids containing C16 and C18 acyl chains. This correlates well with the findings from the mixed monolayer study, where PC mixtures containing 2 mol% long-chain PIM_2/PGM_2 showed increased collapse points. In comparison, integration of PGM_2 (10:10) did not decrease vesicle stability, as it was implied by the decreased collapse pressure found for PC PGM_2 (10:10) monolayer at a ratio of 98:2 mol%. Leakage of entrapped protein from these liposomes occurred to the same extent as with unmodified PC liposomes. Again, this shows that there is no absolute accordance between lipid packing in monolayers and corresponding bilayers[259]. As suggested earlier, the increased stability of the bilayer structure containing long-chain phosphoglycolipids, is most likely due to strong hydrophobic interactions occurring between the components resulting in improved lipid packing[193,255,310]. In a study by Yamauchi *et al.*[360], the stability of various DPPC/steroid (7:3 mol%) liposomes was described using the Langmuir method. Among the steroids investigated, stigmasterol was found to form the least stable mixed monolayer with DPPC, characterised by the lowest collapse pressure. Decreased interactions in binary monolayer systems were reflected by reduced stability of liposome bilayers, showing the highest leakage. Furthermore, the bilayer stability of DDA liposomes could be improved by incorporation of TDB, characterised by less leakage from these liposomes[211]. Christensen *et al.*[361] demonstrated the stabilising effect of TDB on the DDA bilayer in mixed monolayers. An increase in collapse pressure was reported with an increased concentration of TDB.

Following physicochemical characterisation of the different liposome formulations, their ability to be taken up by murine bone-marrow derived DCs (BMDCs) was investigated *in vitro*. In order to address the effect of lipid concentration on cell uptake, BMDCs were incubated with varied quantities of total lipid (10, 50, 250 $\mu g\ mL^{-1}$). At the investigated lipid concentrations, none of

the liposome formulations affected cell viability. A general trend was found that uptake was increased with an increased lipid concentration. This concentration dependence of formulation uptake is in agreement with an earlier study, examining liposomes prepared from mycobacterial extract (*M. bovis* BCG) and cholesterol (2:1 w/w)[293]. The *in vitro* uptake by murine inflammatory macrophages increased up to 400 μg of phospholipid and was saturable at high lipid amounts.

However, in the study presented here there was no increase in uptake of modified formulations as compared to unmodified liposomes. These findings are similar to reports by White *et al.*[206], where M_1-DPPE and M_3-DPPE containing liposomes showed similar uptake rates compared to PC liposomes. However, Barrat *et al.*[293] demonstrated a 2-fold increase in uptake by murine macrophages of the BCG extract/cholesterol (2:1 w/w) liposomes, in comparison with PC/phosphatidylserine liposomes, where no mycobacterial lipids were included. Uptake of mycobacterial compounds including PIMs into cells is mediated by C-type lectins, mainly MRs but also by DC-SIGN receptors[75,362]. MRs are known to act as phagocytic receptors on APCs and induce endocytosis of pathogenic components. In comparison, TLRs generally stimulate immune cells following pathogen binding[75]. Important for binding to MRs are properties of mannosylated ligands such as composition, carbohydrate valency and density and conformation of mannose motifs[67]. ManLAMs from various *M. tuberculosis* strains differed in their MR binding affinity, due to differences in mannosylation and acylation[27]. MRs comprise eight carbohydrate recognition domains (CRDs) which interact to bind multi-valent ligands with high affinity[67]. While more mannose residues (as are found in higher-order PIMs such as Ac_1PIM_6 and Ac_1PIM_5) promote higher affinity, a lower degree of acylation improved receptor binding[27]. The fact that inclusion of mannosylated

glycolipids into the liposomal bilayer did not enhance internalisation by BMDC may reflect the complexity of mannose recognition. The results presented here imply that the conformation of the mannose moieties, when presented in the prepared liposomes, was not optimal for MR binding. In contrast, the BCG extract/cholesterol (2:1 w/w) liposomes investigated by Barrat *et al.*[293] were prepared at a 2:1 (w/w) ratio with cholesterol. The higher content of BCG phospholipids in the lipid bilayer provides a higher density of mannose residues available to interact with MRs. Additionally, the BCG extract was found to consist mainly of mannosylated phosphatidylinositols substituted with 1 to 6 mannose residues. This may enhance binding to MRs, as they are known to bind multi-valent ligands with high affinity[67]. Furthermore, the available data on the DC-SIGN binding affinity of PIMs is conflicting[27,101,228]. This may be due to different assays and emphasizes the issue of using cell lines with unknown and/or differing receptor specificities. For instance, White *et al.*[206] showed differences when they compared uptake of M_3-DPPE/PC liposomes by murine BMDCs and human monocyte derived dendritic cells (Mo-DC). Whilst no differences in uptake could be detected in BMDCs, there was an obvious trend that with increasing M_3-DPPE content, uptake by Mo-DCs was increased.

Investigation of expression of the DC surface activation markers CD86, CD80 and MHC class II revealed no significant increase for modified formulations, in comparison to PC liposomes. Although no difference was found, these results are in accordance with the inability of M_1-DPPE- and M_3-DPPE-containing liposomes to activate DCs[206]. Incubation of BMDCs with liposomes containing various amounts of M_1-DPPE and M_3-DPPE did not result in a significant upregulation of co-stimulatory molecules, compared to the PC liposome control. A study by Sprott *et al.*[225] investigated the upregulation of DC surface

markers *in vitro* after incubation with liposomes prepared from mycobacterial phosphoglycolipids TPL BCG (total polar lipids (TPL) extracted from *M. bovis* BCG). A non-significant increase in the expression of CD80 was found (1 – 2-fold over unstimulated cells) after incubation with TPL BCG liposomes, di-palmitoylated PIM liposomes and BCG-PI liposomes (as the control). Similar trends were reported for MHC class II and CD86. However, the upregulation was even less pronounced.

BMDC were additionally co-incubated with sub-optimal amounts of MPL, as well as the liposome formulations. However, again no activation was detected. A study by Tenu *et al.*[294] utilising liposomes composed of mannosylated phospholipids extracted from *M. bovis* BCG, mixed with cholesterol (2:1, w/w) or PE/cholesterol/oleic acid (1:7:5:3, w/w/w/w), found that stimulation of primed macrophages only occurred in the presence of INF-γ as an activation signal. The extent of induction of NO synthase was comparable to the LPS control for both liposome formulations. However, only BCG lipids mixed with PE/cholesterol/oleic acid induced significantly higher levels of TNF-α, compared to the LPS control.

Various mechanisms have been proposed for the immunostimulatory effects of mycobacterial PIMs *in vitro*[21,90,91,107]. Signalling through TLRs, resulting in activation of transcription factor NF-κB (nuclear factor-kappaB), and subsequent cytokine secretion has been partially resolved[363]. While the TLR-signalling pathway has been mostly understood, signalling through C-type lectins remains unclear. This is further complicated by the fact that these receptors are known to interfere with TLR signalling[75]. Furthermore, synthetic PIMs may be processed differently than native compounds. With the use of natural purified PIMs, there remains a possibility of contamination with other

compounds or that mixtures of PIMs are obtained with varied degrees of mannosylation, which may affect bioactivity.

In the *in vivo* vaccine model, the ability of antigen-loaded modified liposomes to elicit humoral and cellular immune responses, was tested 17 days following vaccination. As expected, a large expansion of $CD4^+$ T cells was induced by vaccination with OVA + alum. Alum is an established adjuvant and is known to polarise immune responses towards a Th2 phenotype immune response[145]. Modified liposomes appeared to promote slightly greater $CD4^+$ T cell responses, in comparison to PC liposomes, for both the percentage and total numbers of antigen specific $CD4^+$ T cells in lymph nodes. Similar trends were noted for $CD8^+$ T cell expansion, although the trends were less pronounced. However, due to large interindividual variations, only percentages of $CD4^+$ T cells and $CD8^+$ T cells for the PC PGM_2 (10:10) vaccination group were statistically different ($p \leq 0.05$). Even though PC PGM_2 (10:10) liposomes induced significantly increased percentages of $CD4^+$ and $CD8^+$ T cells, these findings are biologically insignificant, as these liposomes were unable to elicit immune responses comparable to alum.

Furthermore, the effector response of isolated T cells was evaluated. T cells harvested from the lymph nodes of animals vaccinated with modified liposomes showed increased *in vitro* T cell proliferations compared to alum and PC liposome control groups (statistically different for PC PIM_2 (18:18) ($p \leq 0.05$), PC PGM_2 (0:0) ($p \leq 0.01$) versus alum and PC PGM_2 (0:0) ($p \leq 0.05$) versus PC). Even though an increase in T cell proliferation was observed, INF-γ levels remained unchanged. Similarly, no OVA-specific production of IgG was detected, suggesting that no humoral immune responses were elicited. However, the time point examined (only three days post boost), while

appropriate for examining T cell responses, was not optimal for examining antibody titres. Other studies also reported a lack of strong activation of humoral responses. Sprott *et al.*[225] investigated the adjuvant effect of mannosylated liposomes *in vivo*. They demonstrated that incorporation of 10 mol% TLP BCG into PC/phosphatidylglycerol/cholesterol (1.8:0.2:1.5 mol%) liposomes (equivalent to 50 μg per mouse) evoked significantly reduced antibody responses, as compared to those induced by alum + OVA. Only when the amount of TLP BCG was increased to 50 and 100 mol% (equivalent to 250 and 500 μg per mouse, respectively) did the antibody titres increase, and were comparable to alum + OVA control group. Similarly, another study investigated the adjuvant effect of PIMs (each vaccination contained 35 μg of the PIM compound) in combination with model antigen Ag85B-ESAT-6 and mixed with Emulsigen® (20% v/v)[226]. Emulsigen® is an oil and water adjuvant which prolongs antigen stability and presentation to immune cells via a depot effect[364]. None of the PIM-containing formulations tested showed increased antibody production as compared to antigen + Emulsigen®. Similar results were reported for INF-γ production, which was found to be significantly increased compared to PBS treatment, but not to antigen + Emulsigen®[226]. Interestingly, a study conducted in cattle showed potent humoral and cellular immune responses following vaccination with a formulation containing the BCG vaccine, tuberculosis culture filtrate proteins (CFP), DDA and the synthetic PIM_2 (250 μg PIM_2 per dose)[342]. Furthermore, the extent of the activation by the vaccine combination BCG-CFP-DDA-PIM_2 was comparable to a formulation containing the adjuvant MPL (BCG-CFP-DDA-MPL).

The data obtained from the *in vivo* vaccine study does not suggest an immunostimulatory activity of the investigated formulations. Despite trends,

there was no obvious consistency for any of the modified formulations to stimulate a humoral or cellular immune response.

The available literature indicates an immunoactivating effect of PIM molecules. However, there are inconsistencies in findings from these studies, likely due to the different sources of PIMs used in the studies, differences in formulation and delivery and the assay model used. More research needs to focus on elucidating the effects of synthetic and native PIMs, when delivered in particulate formulations, which are necessary for protection and co-delivery with antigens. For instance, results obtained by Sprott *et al.*[225] suggested that antigen inclusion into delivery system is a requirement to elicit immune responses, as TLP liposomes admixed with OVA prior to vaccination were found to be incapable of inducing humoral responses. Similarly, several groups demonstrated that TDB was more potent when delivered in a particulate system like an emulsion[365], as compared to soluble TDB[366].

In conclusion, the present study is novel in presenting a thorough physicochemical characterisation of mixed PC phosphoglycolipid systems, utilising phosphoglycolipids varying in the length of the fatty acid chains, and in the nature of the polar head groups. Results gained from the mixed monolayer studies provided valuable information on interactions between PC and PIM_2 or PGM_2, and confirmed their miscibility in binary systems. Furthermore, PC liposomes containing 2% (w/w) PIM_2 or PGM_2 were successfully prepared and were shown to be stable upon storage, with regards to particle aggregation and bilayer composition (21 days). The membrane stability of the liposomes was found to be dependent on incorporation of phosphoglycolipids. However, all formulations retained an adequate amount of protein over 21 days, which could be available for delivery. Despite these

findings, which indicated that PC liposomes carrying PIM_2 and PGM_2 could be employed to deliver these phosphoglycolipids, only minor immunological effects were determined *in vitro* and *in vivo*. The uptake of antigen by BMDC *in vitro* could not be enhanced through the incorporation of PIM_2 or PGM_2 into liposomes. In accordance with the unaffected uptake rate, was the inability of PIM_2/PGM_2-containing liposomes to stimulate BMDC activation to a greater extent than BMDC incubated with PC liposomes. Vaccination of mice with modified formulations did not cause significantly stronger immune responses compared to PC liposomes. The lack of immunostimulatory activity may be attributed to a combination of factors including, perhaps a less efficient configuration of mannose groups resulting in decreased receptor affinities.

Chapter Five

General discussion and future directions

5 General discussion and future directions

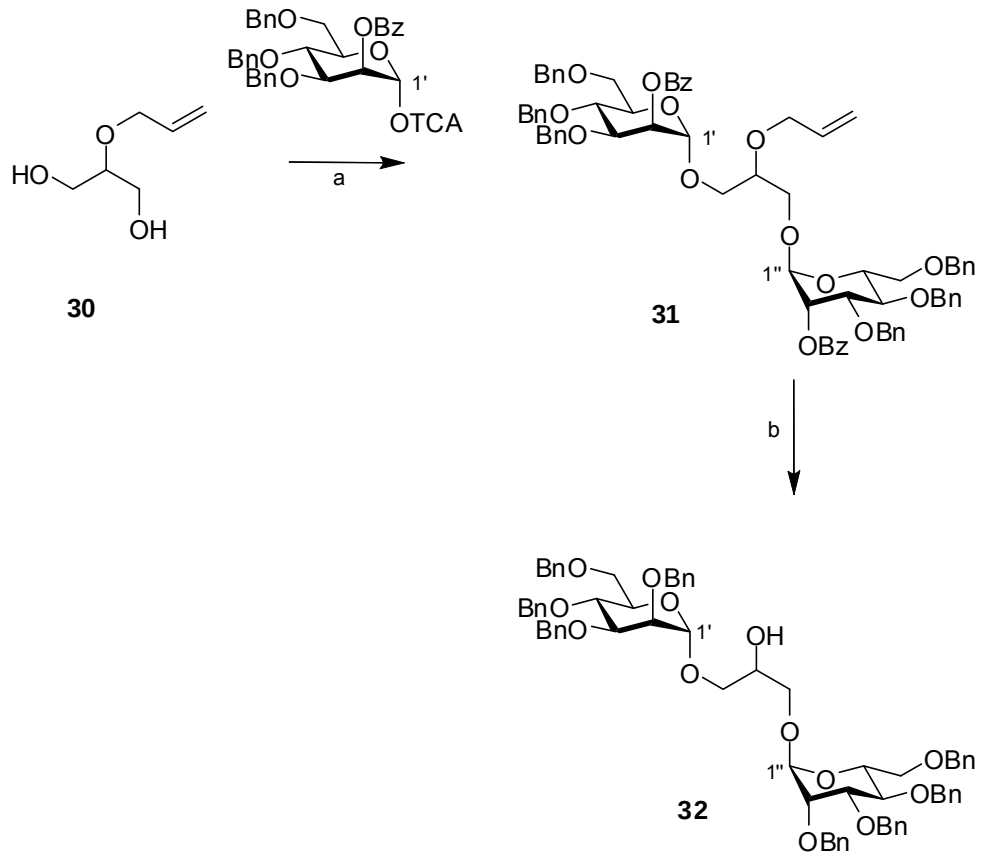
Mycobacteria are aerobic, non-motile Gram-positive Actinobacteria[367]. However, unlike most Gram positive bacteria, they have a thick, complex and waxy cell wall[368]. A diverse array of proteins, polysaccharides, glycolipids and unusual, long hydrocarbon chains (mycolic acids) give mycobacterial cell walls their characteristic asymmetric structure[368]. A result of this complex arrangement is low permeability, which is likely to contribute to the resistance of mycobacteria to drug treatments including antibiotics and chemotherapeutics. Furthermore, mycobacteria are resistant to dehydration, alkali, acids and extreme environmental conditions in soil, where most of the non-virulent species are found[368]. The properties are attributed to the unusual cell wall structure making mycobacteria resilient pathogens.

In addition, many of the cell wall components have been shown to be key factors in the virulence and the pathogenicity of mycobacteria. A crucial role in the successful evasion of host immune responses has been ascribed to glycolipids such as LAMs, LMs and PIMs. These glycolipids have heterogeneous structures and vary in their composition between different species. Their structural variations generate a complexity with regard to the immunomodulatory activities of these compounds, and particular structural requirements leading to suppressive or activatory effects, have yet to be defined.

Various extraction methods have been utilised to provide specific cell wall components for structure-function-analysis. However, purification processes are complicated by the diversity of these glycolipids, and PIMs extracted from natural sources are not homogeneous. Another major drawback arising from

these techniques is the potential presence of impurities. Therefore, synthetic strategies have been developed to provide PIMs with well-defined structures.

The preparation of synthetic PIM compounds is challenging, particularly due to the stereochemistry of the *myo*-inositol core. Many of the reported approaches for PIM syntheses are lengthy and may result in low yields of the desired products[230-234]. The presence of the stereochemical centres in the *myo*-inositol limits approaches to shorten the synthesis of these molecules. However, several studies[96,248] including the allergic asthma model presented in this thesis, have shown that the phosphatidylglycerol mannosides (PGMs) maintain bioactivity. Their preparation is facilitated by the lack of asymmetric centres. Recently, additional research has been undertaken to further simplify the synthetic scheme utilised in this thesis, by reducing the number of steps required (personal communication, David Larsen). An alternative strategy to the one presented in **Chapter Two**, is shown in **Scheme 5-1**. The synthesis of the PGM_2 head group **32** can be accomplished from 2-*O*-allylglycerol **30**. Mannosylation of compound **30** can be achieved in multiple-gram amounts in a research laboratory. Access to large quantities of **32**, would allow the preparation of gram-scale quantities of PGM_2 compounds (5 - 10 g).



Reagents and conditions: (a) TMSOTf, toluene; (b) (i) $NaOCH_3$, MeOH, (ii) NaH, BnBr, (iii) iridium (I) catalyst.

Scheme 5-1. Modified approach for the preparation of the PGM_2 head group **32**.

Physicochemical characterisation provided information on how the behaviour of phosphoglycolipids in an aqueous environment was influenced by the acyl chain length and the flexibility of the head group. Using the Langmuir trough technique, it was shown that the lipid packing of the long-chain phosphoglycolipids was comparable to that of typical phospholipids. Strong intermolecular interactions, such as hydrophobic forces and Van der Waals interactions, promoted a tight packing of these molecules at the air/water interface. A number of reports have shown a role for self-aggregation of ManLAM[65,69]. Here, this concept was further extended to demonstrate, that individual acylated PIM_2 and PGM_2 molecules self-assemble in an aqueous solution. Aggregation behaviour was mainly driven by hydrophobic

interactions and the size of the aggregates was affected by the length of the hydrocarbon chains. The phosphoglycolipids were found either to self-aggregate into vesicles, or possibly micelles, depending on acyl chain length and the overall geometry of the molecules.

Biological activity of PIMs[96,236] and ManLAM[65] is known to be dependent on the presence of acyl residues. Furthermore, the investigation of the physicochemical properties of the PIM_2 and PGM_2 molecules, presented in **Chapters Three** and **Four,** revealed that acyl residues are crucial structural features and influence these characteristics. The acyl chains determined their behaviour at the interface between two dissimilar phases and their self-aggregation in aqueous environment. Similar to reports concerning ManLAM[65,69], the ability of PIMs to form aggregates may at least in part contribute to biological activity.

To further understand the contribution of the acylation state (number of acyl residues), as opposed to the acyl chain length, on the observed physical properties, the effect of additional acylation should be assessed. Doz *et al.*[96] demonstrated a reduced immunosuppressive activity for a natural PIM with only one fatty acid at the phosphatidyl moiety (lyso-PIM_6), or when this compound was acylated with four fatty acids (Ac_2PIM_6). These observations raise the possibility of extending the physicochemical characterisation performed here, and to further investigate the effect of the acylation status of PIMs. The work presented earlier suggested Ac_1PIM_6, containing three fatty acids, as an effective inhibitor of TNF release *in vitro*[96]. With regards to this, the impact of the position of these fatty acid residues should be evaluated, to see whether there is a difference, if the third acyl residue is attached at the inositol core (C-3) or at the mannosyl residue attached to the C-2 position of the inositol

core (**Chapter One**, **Figure 1-4**). Future work could potentially focus on the influence of the nature of the fatty acids, particularly the effect of chain unsaturation, or the incorporation of branched fatty acids such as the naturally occurring tuberculostearic acid. Monolayer behaviour is known to be affected by the presence of double or triple bonds, with less compact films being formed due to restricted rotation of the acyl chains[253,282].

Subtle modifications of the PIM structure can strikingly impact the type of immune response generated[226]. For instance, PIM_2 (16:16)[224,226,341] and PIM_2 (18:18)[227], two related compounds which only differ in their acyl chain by two carbons, were found to either stimulate or suppress immune responses, respectively. However, in the OVA-induced allergic asthma model utilised in **Chapter Three**, both compounds exhibited some suppressive activity. The adjuvant activity of PIM_2 (16:16) could not be verified after incorporation into liposomes (**Chapter Four**). This may possibly be attributed to the assay protocol and the administration of PIMs in a particulate system, although as shown by the aggregation studies it is likely that PIMs spontaneously form particles when dispersed in an aqueous media. A study by Parlane *et al.*[226] further modified the PIM_2 (16:16) structure by exchanging one ester with an ether linkage (PIM_2ME), introducing an extra lipid chain ($AcPIM_2$) or replacing the inositol core by a three carbon glycerol unit (PGM_2 (16:16)). In a vaccination model, these modified compounds were shown to be less effective in inducing immune responses, or even resulted in adverse immune responses[226].

It is still not fully understood through which receptors specific biological effects of PIMs are mediated. Two independent studies reported mycobacterial PIM_2 and PIM_6 (*M. bovis*) as having inflammatory[21] and anti-inflammatory[96] activities. In both studies, the PIMs were extracted utilising identical methods[90].

TLR-2-agonist activity was proposed as the mechanism for immune activation by PIM_2 and PIM_6, which again was found to be independent of the acylation state[21]. On the other hand, a study by Doz *et al.*[96] found that PIM_2 and PIM_6 inhibited activation of primary bone marrow-derived macrophages and subsequent release of the cytokines TNF, IL-12 and IL-10 in a TLR-2 independent manner[96]. This immunosuppressive ability was dependent on acylation. Interestingly, activity of PIM_2 and PIM_6 was enhanced in the absence of TLR-2 signalling. This difference in activity was ascribed to the removal of the simultaneous agonist activity. It is likely that PIMs interact with a number of different receptors. The different signals received by ligation of these receptors may together determine if immune activation or suppression occurs. The results of Doz *et al.*[96] suggested that the adjuvant activity of PIMs, may potentially be weaker than their ability to suppress immune responses. This presumption is further supported by reports where activation of TLRs, resulting in production of IL-12 which further stimulates INF-γ and TNF-α, can be inhibited by C-type lectin signalling[28,66,74].

Inconsistency in the published literature may additionally come from the source of the compounds being tested and whether they are purified from extracts or synthetically prepared. The assay used to measure biological activity must also be considered, including such variables as concentration (dose of the active), cell line or type of test animal used, timing of treatments and administration route. The interplay of all these variables makes it difficult to fully clarify structure-function relationships. This highlights the need for further systematic studies such as the one presented here. In the airway model used in this thesis (**Chapter Three**), one i.n. treatment with the phosphoglycoplid was given 6 days post OVA-sensitisation. Increasing the

numbers of treatments, changing the dosages of PIM_2 and PGM_2 or changing the timing of treatments might alter therapeutic efficacy.

PIMs were incorporated into liposomes to create a particulate delivery system whereby the mannose residues would be available for receptor interaction (as confirmed by the lectin agglutination assay). However, the results in **Chapter Four** showed that modified liposomes, containing 2% phosphoglycolipid did not enhance uptake by and activation of murine BMDC. Moreover, PIMs were unable to stimulate significant immune responses in mice. Investigation of the ability of PIMs and analogues in eliciting cell-mediated immune responses, measured as production of Th1-type cytokines[224,226,341,343,344], is conflicting. This possibly correlates with the density and availability of mannose residues for receptor interactions. With an increased amount of incorporated mannose, the binding affinity to C-type lectin receptors may be enhanced. Sprott *et al.*[225] found that incorporation of low concentrations of TPL BCG into liposomes (10% w/w) generated poor humoral immunity. Whereas increased amounts of mannosylated lipids (BCG TPL) led to increased antibody production[225].

In light of these findings, future studies could investigate the incorporation of higher molar fractions of PIMs into liposome bilayer. This would potentially increase density of mannose on the vesicle surface, and may enhance affinity to C-type lectin receptors. It has been suggested that the high avidity binding of ManLAM[65,69] and LM[92] to MRs is mediated through their numerous mannose residues (**Chapter One**, **Figure 1-3**). Due to its eight carbohydrate recognition domains (CRDs), MRs preferentially bind multi-valent ligands with high amounts of mannose[67]. The number of mannosyl residues was also found to affect interactions of PIMs with TLRs[92]. The signalling of PIM_2 through TLR-2 was considerably reduced in comparison to LM[92]. Therefore an alternative

method for improving the immunological activity of PIMs may be to lengthen the oligosaccharide chain. The binding affinity to MRs may be enhanced by the addition of more mannosyl units. Synthetic approaches are currently being developed to provide modified PIMs, where five mannosyl residues are attached to the C-2 and C-6 of the *myo*-inositol core (personal communication, David Larsen). Furthermore, the higher binding affinity of LM has been attributed to its distinct mannose chain, typically linear oligosaccharides of 1,6-α-D-linked mannopyranoside bearing 1,2-α-D-mannopyranosides[92]. By mimicking the composition of the mannose residues in LM, the binding affinity of PIMs to TLRs may be improved. This could further be extended by evaluating the effect of a branched mannose domain, similar to the arabinan domain in LAMs. Investigation of these modified compounds could provide more insight into the effect of the length and dimension of the carbohydrate structures of PIMs on biological activity (**Figure 5-1**).

In addition to TLRs and C-type lectins, PIMs are known to interact with a number of other different receptors. The particular requirements for each receptor interaction and the biological consequences of these interactions still need to be better elucidated. While the degree of mannosylation may affect the binding to C-type lectins and TLRs, the nature of the sugar moiety itself may promote binding to different receptors. Mycobacterial PIMs are known to be presented via CD1b and CD1d[105-107] to αβ NK T cells, leading to the production of INF-γ[107]. However, in a comparative study, the synthetic glycolipid α-galactosylceramide (α-GalCer) was shown to be more effective in stimulation of αβ NK T cells than a mycobacterial PIM_4[107]. α-GalCer, which was initially purified from a sea sponge[369], comprises an α-anomeric galactose carbohydrate and a ceramide lipid unit with a fatty acyl chain and a sphingosine chain of different lengths[370]. The α-anomeric conformation of the sugar moiety is

essential for binding and the long fatty acids promote higher binding affinity to the hydrophobic groove of CD1 receptors[369,371]. Interestingly, α-mannosyl ceramide (α-ManCer) was found to be less effective in stimulating proliferation of NK T cells[369]. This was attributed to the altered configuration of the C-2 hydroxyl group at the sugar moiety, which is axially orientated in the mannose, rather than equatorially, as it is found in galactosyl residue[369].

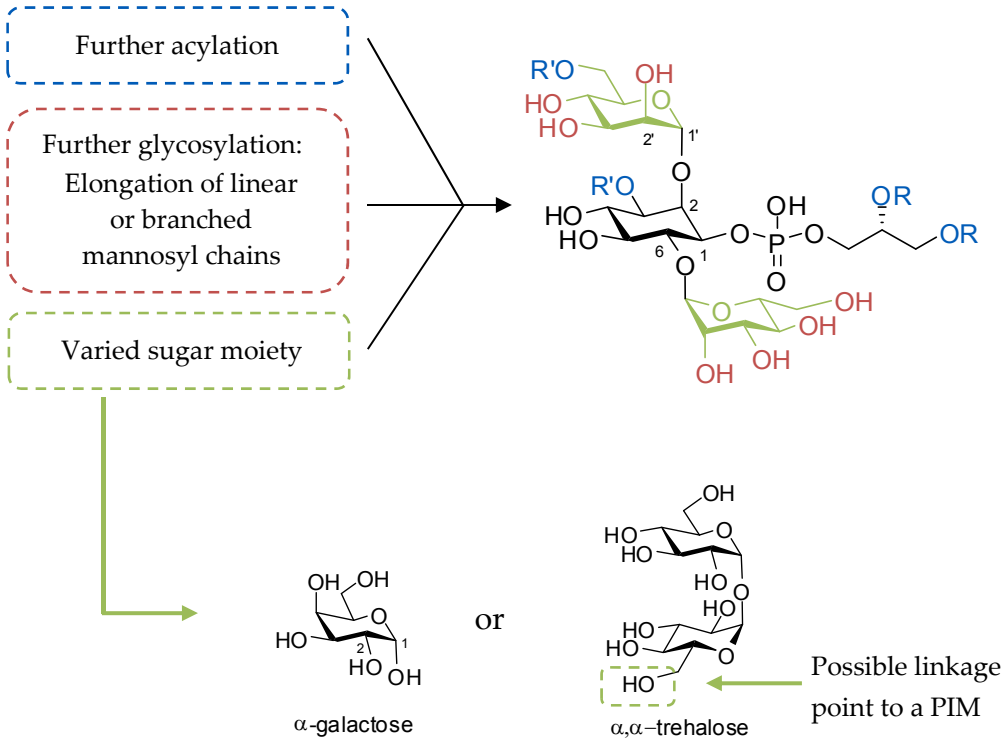


Figure 5-1. General structure of phosphatidylinositol mannosides (PIMs). Possible structural modifications are described in the left panels. PIMs can have two acyl residues (R) at the phosphatidyl moiety and can be further acylated, indicated as R'. Potential carbohydrates could be used to create a new PIM scaffold, e.g. α-galactose or α,α-trehalose.

In consideration of these results, the replacement of mannosyl residues in the current PIM structure with α-D-galactosides, should be evaluated in further synthetic approaches (**Figure 5-1**). The design of a new PIM scaffold, may lead

to improvements in immunostimulatory activity through recognition by NK T cells.

Further attention should be given to the carbohydrate α,α-trehalose, contained in trehalose-6,6-dimycolate (TDM). The mycobacterial glycolipid TDM and synthetic analogues are strong Th1 adjuvants[149,211,372]. However, the pathways by which these compounds induce inflammatory immune responses are not yet fully understood. Signalling through Mincle, a C-type lectin receptor, has been proposed as a potential mode of action[373], while other researchers suggested immunoactivation in a Syk–Card9-dependent fashion[209,220]. Binding to Mincle has been described to be mediated by the symmetric structure of these molecules (chemical structure of TDM, **Chapter Four**, **Figure 4-2**). Each of the carbohydrate/fatty acid units in TDM acts as receptor epitope, and upon binding, every TDM molecule links two Mincle receptors[373]. This concept may be of interest as part of future studies and PIM structures may be modified in a way to mimic the acylated trehalose head groups in TDM (**Figure 5-1**).

In addition to the carbohydrate moieties in PIMs, fatty acids are known to have a crucial impact on receptor recognition and the type of the immune responses induced. The purified lipopolysaccharide derivative MPL, is a widely known adjuvant used in combinations with various human vaccines[181,182]. Its inflammatory activity is mediated through TLR-4[148,180]. A criterion for immunstimulatory activity of MPL, is the presence of long-chain fatty acids attached to the two glucosamine units[374] (chemical structure of MPL, **Chapter One**, **Figure 1-7**). Similarly, PIMs are known to be agonists at TLR-2 and TLR-4[21,91,96,297]. Future work could focus on the inclusion of additional fatty acids into the PIM structures. Besides the common positions for acylation, indicated as R and R' in **Figure 5-1**, further potential sides of acylation may be at the hydroxyl

groups. These modifications could result in enhanced biological activity of PIM compounds.

Due to the versatility of liposomes, there are various ways to enhance the immunogenicity of PIMs. As discussed in **Chapter One**, combinations of different adjuvants are commonly used to enhance immune responses to particular antigens, and to ensure the stimulation of humoral and cell-mediated immunity. PIMs may be combined with established activatory ligands such as TLR agonists (MPL, immunostimulatory nucleic acids) or non-TLR dependent adjuvants (Quil A), which could provide additional co-stimulatory signals. Synergistic effects between the adjuvants may direct the immune response in order to generate protective immune responses.

However, liposomes may be prone to rapid degradation of the lipid bilayer by plasma proteins and enzymes depending on their bilayer composition. This results in the loss of the incorporated active agents[196,198]. Subsequent work could also evaluate alternative approaches for the co-delivery of PIM adjuvants and antigens to targeted cells. Promising results were obtained when immunostimulatory deoxynucleotides (ODNs) were chemically conjugated to antigens[375]. These conjugate vaccine formulations elicited high levels of antibodies, a cytokine profile typical for Th1-type immune responses as well as cytotoxic T cells. In a similar way, enhanced immunogenic efficacy may be achieved when PIMs are covalently attached to the appropriate antigens.

In conclusion, the work conducted in this thesis has provided insight into how physiochemical properties of various PIM_2 molecules and analogues can be affected by structural modifications. Their behaviour in pure, as well as binary systems, was described in aqueous environments. However, only minor effects

of these changes on immunomodulatory activities were determined, and no correlations between these characteristics and bioactivity could be established. Future work needs to be conducted to gain a better understanding of the role of PIMs as immunomodulating agents, in particular focussing on the specific mechanisms by which these immunological activities are mediated. Strategies need to be established to improve the inflammatory and anti-inflammatory activities of PIM_2 and PGM_2 molecules, by structural modifications and/or through the addition of further immunomodulatory signals.

6 References

1. Dheda K, Schwander SK, Zhu B, van Zyl-Smit RN, Zhang Y. The immunology of tuberculosis: From bench to bedside. *Respirology* **2010**; 15: 433-450.
2. Leung AN. Pulmonary Tuberculosis: The Essentials. *Radiology* **1999**; 210: 307-322.
3. *Global tuberculosis control* WHO report 2011, World Health Organization, Geneva, Switzerland **2011**.
4. Herzog H. History of tuberculosis. *Respiration* **1998**; 65 5-15.
5. Wang J, Xing Z. Tuberculosis vaccines: the past, present and future. *Expert Review of Vaccines* **2002**; 1: 341-354.
6. Ayele WY, Neill SD, Zinsstag J, Weiss MG, Pavlik I. Bovine tuberculosis: an old disease but a new threat to Africa. *The International Journal of Tuberculosis and Lung Disease* **2004**; 8: 924-937.
7. Fine PEM. Variation in protection by BCG: implications of and for heterologous immunity. *The Lancet* **1995**; 346: 1339-1345.
8. *Trial of BCG vaccines in south India for tuberculosis prevention: first report*. Tuberculosis Prevention Trial, Bulletin of the World Health Organization, **1979**, 57, 819-827.
9. Saltini C. Chemotherapy and diagnosis of tuberculosis. *Respiratory Medicine* **2006**; 100: 2085-2097.
10. Onozaki I, Raviglione M. Stopping tuberculosis in the 21st century: Goals and strategies. *Respirology* **2010**; 15: 32-43.
11. Kaufmann SHE, Hussey G, Lambert P-H. New vaccines for tuberculosis. *The Lancet* **2010**; 375: 2110-2119.
12. Kochi A. Tuberculosis: Distribution, Risk Factors, Mortality. *Immunobiology* **1994**; 191: 325-336.
13. World Health Organization, Accessed on 2nd August 2012 from http://www.who.int/gho/tb/en/index.html
14. McShane H, Rowland R. Tuberculosis vaccines in clinical trials. *Expert Review of Vaccines* **2011**; 10: 645-658.
15. Barker LF, Brennan MJ, Rosenstein PK, Sadoff JC. Tuberculosis vaccine research: the impact of immunology. *Current Opinion in Immunology* **2009**; 21: 331-338.
16. Brennan MJ, Thole J. Tuberculosis vaccines-A strategic blueprint for the next decade. *Tuberculosis* **2012**; 92: S1-S35.
17. Nicol MP, Wilkinson RJ. The clinical consequences of strain diversity in Mycobacterium tuberculosis. *Transactions of the Royal Society of Tropical Medicine and Hygiene* **2008**; 102: 955-965.
18. Pozos TC, Ramakrishan L. New models for the study of Mycobacterium–host interactions. *Current Opinion in Immunology* **2004**; 16: 499-505.
19. Barnes P, Chatterjee D, Abrams J, Lu S, Wang E, Yamamura M, Brennan P, Modlin R. Cytokine production induced by Mycobacterium tuberculosis lipoarabinomannan. Relationship to chemical structure. *Journal of Immunology* **1992**; 149: 541-547.

20. Gilleron M, Bala L, Brando T, Vercellone A, Puzo G. Mycobacterium tuberculosis H37Rv Parietal and Cellular Lipoarabinomannans. *Journal of Biological Chemistry* **2000**; 275: 677-684.
21. Gilleron M, Quesniaux VFJ, Puzo G. Acylation state of the phosphatidylinositol hexamannosides from Mycobacterium bovis bacillus Calmette Guerin and Mycobacterium tuberculosis H37Rv and its implication in toll-like receptor response. *Journal of Biological Chemistry* **2003**; 278: 29880-29889.
22. Harding CV, Boom WH. Regulation of antigen presentation by Mycobacterium tuberculosis: a role for Toll-like receptors. *Nature Reviews Microbiology* **2010**; 8: 296-307.
23. Quesniaux V, Fremond C, Jacobs M, Parida S, Nicolle D, Yeremeev V, Bihl F, Erard F, Botha T, Drennan M, Soler M-N, Le Bert M, Schnyder B, Ryffel B. Toll-like receptor pathways in the immune responses to mycobacteria. *Microbes and Infection* **2004**; 6: 946-959.
24. Villeneuve C, Gilleron M, Maridonneau-Parini I, Daffé M, Astarie-Dequeker C, Etienne G. Mycobacteria use their surface-exposed glycolipids to infect human macrophages through a receptor-dependent process. *Journal of Lipid Research* **2005**; 46: 475-483.
25. Park S-H, Bendelac A. CD1-restricted T-cell responses and microbial infection. *Nature* **2000**; 406: 788-792.
26. Pitarque S, Herrmann JL, Duteyrat JL, Jackson M, Stewart GR, Lecointe F, Payre B, Schwartz O, Young DB, Marchal G, Lagrange PH, Puzo G, Gicquel B, Nigou J, Neyrolles O. Deciphering the molecular bases of Mycobacterium tuberculosis binding to the lectin DC-SIGN reveals an underestimated complexity. *Biochemical Journal* **2005**; 392: 615–624.
27. Torrelles JB, Azad AK, Schlesinger LS. Fine Discrimination in the Recognition of Individual Species of Phosphatidyl-myo-Inositol Mannosides from Mycobacterium tuberculosis by C-Type Lectin Pattern Recognition Receptors. *Journal of Immunology* **2006**; 177: 1805-1816.
28. Maeda N, Nigou J, Herrmann J-L, Jackson M, Amara A, Lagrange PH, Puzo G, Gicquel B, Neyrolles O. The Cell Surface Receptor DC-SIGN Discriminates between Mycobacterium Species through Selective Recognition of the Mannose Caps on Lipoarabinomannan. *Journal of Biological Chemistry* **2003**; 278: 5513-5516.
29. Barral DC, Brenner MB. CD1 antigen presentation: how it works. *Nature Reviews Immunology* **2007**; 7: 929-941.
30. Peyron P, Vaubourgeix J, Poquet Y, Levillain F, Botanch C, Bardou F, Daffé M, Emile J-F, Marchou B, Cardona P-J, de Chastellier C, Altare F. Foamy Macrophages from Tuberculous Patients' Granulomas Constitute a Nutrient-Rich Reservoir for M. tuberculosis Persistence. *PLoS Pathogens* **2008**; 4: 1-14.
31. Davis JM, Ramakrishnan L. The Role of the Granuloma in Expansion and Dissemination of Early Tuberculous Infection. *Cell* **2009**; 136: 37-49.
32. Bean AGD, Roach DR, Briscoe H, France MP, Korner H, Sedgwick JD, Britton WJ. Structural Deficiencies in Granuloma Formation in TNF Gene-Targeted Mice Underlie the Heightened Susceptibility to Aerosol Mycobacterium tuberculosis Infection, Which Is Not Compensated for by Lymphotoxin. *Journal of Immunology* **1999**; 162: 3504-3511.

33. Flynn JL, Goldstein MM, Chan J, Triebold KJ, Pfeffer K, Lowenstein CJ, Schrelber R, Mak TW, Bloom BR. Tumor necrosis factor-α is required in the protective immune response against mycobacterium tuberculosis in mice. *Immunity* **1995**; 2: 561-572.
34. Cooper AM, Magram J, Ferrante J, Orme IM. Interleukin 12 (IL-12) Is Crucial to the Development of Protective Immunity in Mice Intravenously Infected with Mycobacterium tuberculosis. *The Journal of Experimental Medicine* **1997**; 186: 39-45.
35. Altare F, Jouanguy E, Lamhamedi S, Döffinger R, Fischer A, Casanova J-L. Mendelian susceptibility to mycobacterial infection in man. *Current Opinion in Immunology* **1998**; 10: 413-417.
36. Russell DG. Who puts the tubercle in tuberculosis? *Nature Reviews Microbiology* **2007**; 5: 39-47.
37. Schwander SK, Torres M, Sada E, Carranza C, Ramos E, Tary-Lehmann M, Wallis RS, Sierra J, Rich EA. Enhanced Responses to Mycobacterium tuberculosis Antigens by Human Alveolar Lymphocytes during Active Pulmonary Tuberculosis. *Journal of Infectious Diseases* **1998**; 178: 1434-1445.
38. Taha RA, Kotsimbos TC, Song YL, Menzies D, Hamid Q. IFN-gamma and IL-12 are increased in active compared with inactive tuberculosis. *American Journal of Respiratory and Critical Care Medicine* **1997**; 155: 1135-1139.
39. Herrera MT, Torres M, Nevels D, Perez-Redondo CN, Ellner JJ, Sada E, Schwander SK. Compartmentalized bronchoalveolar IFN-γ and IL-12 response in human pulmonary tuberculosis. *Tuberculosis* **2009**; 89: 38-47.
40. Flynn JL, Chan J, Triebold KJ, Dalton DK, Stewart TA, Bloom BR. An essential role for interferon γ in resistance to Mycobacterium tuberculosis infection. *Journal of Experimental Medicine* **1993**; 178: 2249-2254.
41. Chan J, Fujiwara T, Brennan P, McNeil M, Turco SJ, Sibille JC, Snapper M, Aisen P, Bloom BR. Microbial glycolipids: possible virulence factors that scavenge oxygen radicals. *Proceedings of the National Academy of Sciences* **1989**; 86: 2453-2457.
42. Haas A, Goebel W. Microbial Strategies to Prevent Oxygen-Dependent Killing by Phagocytes. *Free Radical Research* **1992**; 16: 137-157.
43. Ribeiro-Rodrigues R, Resende Co T, Rojas R, Toossi Z, Dietze R, Boom WH, Maciel E, Hirsch CS. A role for CD4+CD25+ T cells in regulation of the immune response during human tuberculosis. *Clinical & Experimental Immunology* **2006**; 144: 25-34.
44. Chen X, Zhou B, Li M, Deng Q, Wu X, Le X, Wu C, Larmonier N, Zhang W, Zhang H, Wang H, Katsanis E. CD4+CD25+FoxP3+ regulatory T cells suppress Mycobacterium tuberculosis immunity in patients with active disease. *Clinical Immunology* **2007**; 123: 50-59.
45. Mills KHG. Regulatory T cells: friend or foe in immunity to infection? *Nature Reviews Immunology* **2004**; 4: 841-855.
46. Jacobs M, Brown N, Allie N, Gulert R, Ryffel B. Increased resistance to mycobacterial infection in the absence of interleukin-10. *Immunology* **2000**; 100: 494-501.
47. Korbel DS, Schneider BE, Schaible UE. Innate immunity in tuberculosis: myths and truth. *Microbes and Infection* **2008**; 10: 995-1004.

48. Wolf AJ, Linas B, Trevejo-Nuñez GJ, Kincaid E, Tamura T, Takatsu K, Ernst JD. Mycobacterium tuberculosis Infects Dendritic Cells with High Frequency and Impairs Their Function In Vivo. *Journal of Immunology* **2007**; 179: 2509-2519.
49. Fortune SM, Solache A, Jaeger A, Hill PJ, Belisle JT, Bloom BR, Rubin EJ, Ernst JD. Mycobacterium tuberculosis Inhibits Macrophage Responses to IFN-γ through Myeloid Differentiation Factor 88-Dependent and -Independent Mechanisms. *Journal of Immunology* **2004**; 172: 6272-6280.
50. Pai RK, Convery M, Hamilton TA, Henry Boom W, Harding CV. Inhibition of IFN-γ-induced class II transactivator expression by a 19-kDa lipoprotein from Mycobacterium tuberculosis: A potential mechanism for immune evasion. *Journal of Immunology* **2003**; 171: 175-184.
51. Noss EH, Pai RK, Sellati TJ, Radolf JD, Belisle J, Golenbock DT, Boom WH, Harding CV. Toll-Like Receptor 2-Dependent Inhibition of Macrophage Class II MHC Expression and Antigen Processing by 19-kDa Lipoprotein of Mycobacterium tuberculosis. *Journal of Immunology* **2001**; 167: 910-918.
52. Cáceres N, Tapia G, Ojanguren I, Altare F, Gil O, Pinto S, Vilaplana C, Cardona P-J. Evolution of foamy macrophages in the pulmonary granulomas of experimental tuberculosis models. *Tuberculosis* **2009**; 89: 175-182.
53. Brennan PJ. Structure, function, and biogenesis of the cell wall of Mycobacterium tuberculosis. *Tuberculosis* **2003**; 83: 91-97.
54. Hunter SW, Brennan PJ. Evidence for the presence of a phosphatidylinositol anchor on the lipoarabinomannan and lipomannan of Mycobacterium tuberculosis. *Journal of Biological Chemistry* **1990**; 265: 9272-9279.
55. Chatterjee D, Khoo K-H. Mycobacterial lipoarabinomannan: An extraordinary lipoheteroglycan with profound physiological effects. *Glycobiology* **1998**; 8: 113-120.
56. Chatterjee D, Hunter SW, McNeil M, Brennan PJ. Lipoarabinomannan. Multiglycosylated form of the mycobacterial mannosylphosphatidylinositols. *Journal of Biological Chemistry* **1992**; 267: 6228-6233.
57. Jozefowski S, Sobota A, Kwiatkowska K. How Mycobacterium tuberculosis subverts host immune responses. *Bioessays* **2008**; 30: 943-954.
58. Chatterjee D, Lowell K, Rivoire B, McNeil MR, Brennan PJ. Lipoarabinomannan of Mycobacterium tuberculosis. Capping with mannosyl residues in some strains. *Journal of Biological Chemistry* **1992**; 267: 6234-6239.
59. Hunter SW, Gaylord H, Brennan PJ. Structure and antigenicity of the phosphorylated lipopolysaccharide antigens from the leprosy and tubercle bacilli. *Journal of Biological Chemistry* **1986**; 261: 12345-12351.
60. Nigou J, Gilleron M, Rojas M, García LF, Thurnher M, Puzo G. Mycobacterial lipoarabinomannans: modulators of dendritic cell function and the apoptotic response. *Microbes and Infection* **2002**; 4: 945-953.
61. Adams LB, Fukutomi Y, Krahenbuhl JL. Regulation of murine macrophage effector functions by lipoarabinomannan from mycobacterial strains with different degrees of virulence. *Infection and Immunity* **1993**; 61: 4173-4181.
62. Chatterjee D, Roberts AD, Lowell K, Brennan PJ, Orme IM. Structural basis of capacity of lipoarabinomannan to induce secretion of tumor necrosis factor. *Infection and Immunity* **1992**; 60: 1249-1253.

63. Yoshida A, Koide Y. Arabinofuranosyl-terminated and mannosylated lipoarabinomannans from Mycobacterium tuberculosis induce different levels of interleukin-12 expression in murine macrophages. *Infection and Immunity* **1997**; 65: 1953-1955.
64. Means TK, Lien E, Yoshimura A, Wang S, Golenbock DT, Fenton MJ. The CD14 Ligands Lipoarabinomannan and Lipopolysaccharide Differ in Their Requirement for Toll-Like Receptors. *Journal of Immunology* **1999**; 163: 6748-6755.
65. Nigou J, Zelle-Rieser C, Gilleron M, Thurnher M, Puzo G. Mannosylated Lipoarabinomannans Inhibit IL-12 Production by Human Dendritic Cells: Evidence for a Negative Signal Delivered Through the Mannose Receptor. *Journal of Immunology* **2001**; 166: 7477-7485.
66. Geijtenbeek TBH, van Vliet SJ, Koppel EA, Sanchez-Hernandez M, Vandenbroucke-Grauls CMJE, Appelmelk B, van Kooyk Y. Mycobacteria Target DC-SIGN to Suppress Dendritic Cell Function. *The Journal of Experimental Medicine* **2003**; 197: 7-17.
67. Taylor ME, Drickamer K. Structural requirements for high affinity binding of complex ligands by the macrophage mannose receptor. *Journal of Biological Chemistry* **1993**; 268: 399-404.
68. Schlesinger LS, Kaufman TM, Iyer S, Hull SR, Marchiando LK. Differences in mannose receptor-mediated uptake of lipoarabinomannan from virulent and attenuated strains of Mycobacterium tuberculosis by human macrophages. *Journal of Immunology* **1996**; 157: 4568-4575.
69. Rivière M, Moisand A, Lopez A, Puzo G. Highly Ordered Supra-Molecular Organization of the Mycobacterial Lipoarabinomannans in Solution. Evidence of a Relationship Between Supra-Molecular Organization and Biological Activity. *Journal of Molecular Biology* **2004**; 344: 907-918.
70. Doz E, Rose S, Nigou J, Gilleron M, Puzo G, Erard F, Ryffel B, Quesniaux VFJ. Acylation determines the toll-like receptor (TLR)-dependent positive versus TLR2-, Mannose receptor-, and SIGNR1-independent negative regulation of pro-inflammatory cytokines by mycobacterial lipomannan. *Journal of Biological Chemistry* **2007**; 282: 26014-26025.
71. Geijtenbeek TBH, Gringhuis SI. Signalling through C-type lectin receptors: shaping immune responses. *Nature Reviews Immunology* **2009**; 9: 465-479.
72. Ishikawa E, Ishikawa T, Morita YS, Toyonaga K, Yamada H, Takeuchi O, Kinoshita T, Akira S, Yoshikai Y, Yamasaki S. Direct recognition of the mycobacterial glycolipid, trehalose dimycolate, by C-type lectin Mincle. *The Journal of Experimental Medicine* **2009**; 206: 2879-2888.
73. Rothfuchs AG, Bafica A, Feng CG, Egen JG, Williams DL, Brown GD, Sher A. Dectin-1 Interaction with Mycobacterium tuberculosis Leads to Enhanced IL-12p40 Production by Splenic Dendritic Cells. *Journal of Immunology* **2007**; 179: 3463-3471.
74. Tailleux L, Schwartz O, Herrmann J-L, Pivert E, Jackson M, Amara A, Legres L, Dreher D, Nicod LP, Gluckman JC, Lagrange PH, Gicquel B, Neyrolles O. DC-SIGN Is the Major Mycobacterium tuberculosis Receptor on Human Dendritic Cells. *The Journal of Experimental Medicine* **2003**; 197: 121-127.

75. Cambi A, Figdor CG. Dual function of C-type lectin-like receptors in the immune system. *Current Opinion in Cell Biology* **2003**; 15: 539-546.
76. Quesniaux VJ, Nicolle DM, Torres D, Kremer L, Guerardel Y, Nigou J, Puzo G, Erard F, Ryffel B. Toll-Like Receptor 2 (TLR2)-Dependent-Positive and TLR2-Independent-Negative Regulation of Proinflammatory Cytokines by Mycobacterial Lipomannans. *Journal of Immunology* **2004**; 172: 4425-4434.
77. Chan J, Fan XD, Hunter SW, Brennan PJ, Bloom BR. Lipoarabinomannan, a possible virulence factor involved in persistence of Mycobacterium tuberculosis within macrophages. *Infection and Immunity* **1991**; 59: 1755-1761.
78. Gilleron M, Nigou J, Nicolle D, Quesniaux V, Puzo G. The acylation state of mycobacterial lipomannans modulates innate immunity response through Toll-like receptor 2. *Chemistry & Biology* **2006**; 13: 39-47.
79. Zhang Y, Broser M, Cohen H, Bodkin M, Law K, Reibman J, Rom WN. Enhanced interleukin-8 release and gene expression in macrophages after exposure to Mycobacterium tuberculosis and its components. *Journal of Clinical Investigation* **1995**; 95: 586-592.
80. Anderson RJ. The chemistry of the lipoids of tubercle bacilli. XIV. The occurrence of inosite in the phosphatide from human tubercle bacilli 1. *Journal of the American Chemical Society* **1930**; 52: 1607-1608.
81. Ballou CE, Vilkas E, Lederer E. Structural Studies on the Myo-inositol Phospholipids of Mycobacterium tuberculosis (var. bovis, strain BCG). *Journal of Biological Chemistry* **1963**; 238: 69-76.
82. Lee YC, Ballou CE. Structural Studies on the Myo-inositol Mannosides from the Glycolipids of Mycobacterium tuberculosis and Mycobacterium phlei. *Journal of Biological Chemistry* **1964**; 239: 1316-1327.
83. Lee YC, Ballou CE. Complete Structures of the Glycophospholipids of Mycobacteria*. *Biochemistry* **1965**; 4: 1395-1404.
84. Severn WB, Furneaux RH, Falshaw R, Atkinson PH. Chemical and spectroscopic characterisation of the phosphatidylinositol manno-oligosaccharides from Mycobacterium bovis AN5 and WAg201 and Mycobacterium smegmatis mc2 155. *Carbohydrate Research* **1998**; 308: 397-408.
85. Brennan P, Ballou CE. Biosynthesis of Mannophosphoinositides by Mycobacterium phlei. *Journal of Biological Chemistry* **1967**; 242: 3046-3056.
86. Pangborn MC, McKinney JA. Purification of serologically active phosphoinositides of Mycobacterium tuberculosis. *Journal of Lipid Research* **1966**; 7: 627-633.
87. Khoo K-H, Dell A, Morris HR, Brennan PJ, Chatterjee D. Structural definition of acylated phosphatidylinositol mannosides from Mycobacterium tuberculosis: definition of a common anchor for lipomannan and lipoarabinomannan. *Glycobiology* **1995**; 5: 117-127.
88. Kremer L, Gurcha SS, Bifani P, Hitchen PG, Baulard A, Morris HR, Dell A, Brennan PJ, Besra GS. Characterization of a putative alpha-mannosyltransferase involved in phosphatidylinositol trimannoside biosynthesis in Mycobacterium tuberculosis. *Biochemical Journal* **2002**; 363: 437-447.
89. Gilleron M, Nigou J, Cahuzac B, Puzo G. Structural study of the LipoMannans from Mycobacterium bovis BCG: characterisation of multiacylated forms of the

phosphatidyl-myo-inositol anchor. *Journal of Molecular Biology* **1999**; 285: 2147-2160.

90. Gilleron M, Ronet C, Mempel M, Monsarrat B, Gachelin G, Puzo G. Acylation state of the phosphatidylinositol mannosides from Mycobacterium bovis bacillus Calmette Guerin and ability to induce granuloma and recruit natural killer T cells. *Journal of Biological Chemistry* **2001**; 276: 34896-34904.
91. Jones BW, Means TK, Heldwein KA, Keen MA, Hill PJ, Belisle JT, Fenton MJ. Different Toll-like receptor agonists induce distinct macrophage responses. *Journal of Leukocyte Biology* **2001**; 69: 1036-1044.
92. Vignal C, Guérardel Y, Kremer L, Masson M, Legrand D, Mazurier J, Elass E. Lipomannans, But Not Lipoarabinomannans, Purified from Mycobacterium chelonae and Mycobacterium kansasii Induce TNF-α and IL-8 Secretion by a CD14-Toll-Like Receptor 2-Dependent Mechanism. *Journal of Immunology* **2003**; 171: 2014-2023.
93. Beatty WL, Rhoades ER, Ullrich H-J, Chatterjee D, Heuser JE, Russell DG. Trafficking and Release of Mycobacterial Lipids from Infected Macrophages. *Traffic* **2000**; 1: 235-247.
94. Rhoades E, Hsu FF, Torrelles JB, Turk J, Chatterjee D, Russell DG. Identification and macrophage-activating activity of glycolipids released from intracellular Mycobacterium bovis BCG. *Molecular Microbiology* **2003**; 48: 875-888.
95. Prados-Rosales R, Baena A, Martinez LA, Luque-Garcia J, Kalscheuer R, Veeraraghavan U, Camara C, Nosanchuk JD, Besra GS, Bing C, Jimenez J, Glatman-Freedman A, Jacobs Jr WR, Porcelli SA, Casadevall A. Mycobacteria release active membrane vesicles that modulate immune responses in a TLR2-dependent manner in mice. *Journal of Clinical Investigation* **2011**; 121: 1471-1483.
96. Doz E, Rose S, Court N, Front S, Vasseur V, Charron S, Gilleron M, Puzo G, Fremaux I, Delneste Y, Erard Fo, Ryffel B, Martin OR, Quesniaux VFJ. Mycobacterial Phosphatidylinositol Mannosides Negatively Regulate Host Toll-like Receptor 4, MyD88-dependent Proinflammatory Cytokines, and TRIF-dependent Co-stimulatory Molecule Expression. *Journal of Biological Chemistry* **2009**; 284: 23187-23196.
97. Rojas RE, Thomas JJ, Gehring AJ, Hill PJ, Belisle JT, Harding CV, Boom WH. Phosphatidylinositol Mannoside from Mycobacterium tuberculosis Binds {alpha}5beta1 Integrin (VLA-5) on CD4+ T Cells and Induces Adhesion to Fibronectin. *Journal of Immunology* **2006**; 177: 2959-2968.
98. Mahon RN, Rojas RE, Fulton SA, Franko JL, Harding CV, Boom WH. Mycobacterium tuberculosis Cell Wall Glycolipids Directly Inhibit CD4+ T-Cell Activation by Interfering with Proximal T-Cell-Receptor Signaling. *Infection and Immunity* **2009**; 77: 4574-4583.
99. Ainge GD, Martin WJ, Compton BJ, Hayman CM, Larsen DS, Yoon S-i, Wilson IA, Harper JL, Painter GF. Synthesis and Toll-like Receptor 4 (TLR4) Activity of Phosphatidylinositol Dimannoside Analogues. *Journal of Medicinal Chemistry* **2011**; 54: 7268-7279.
100. Boonyarattanakalin S, Liu X, Michieletti M, Lepenies B, Seeberger PH. Chemical Synthesis of All Phosphatidylinositol Mannoside (PIM) Glycans from

Mycobacterium tuberculosis. *Journal of the American Chemical Society* **2008**; 130: 16791-16799.
101. Driessen NN, Ummels R, Maaskant JJ, Gurcha SS, Besra GS, Ainge GD, Larsen DS, Painter GF, Vandenbroucke-Grauls CMJE, Geurtsen J, Appelmelk BJ. Role of Phosphatidylinositol Mannosides in the Interaction between Mycobacteria and DC-SIGN. *Infection and Immunity* **2009**; 77: 4538-4547.
102. Sada-Ovalle I, Chiba A, Gonzales A, Brenner MB, Behar SM. Innate Invariant NKT Cells Recognize Mycobacterium tuberculosis-Infected Macrophages, Produce Interferon-γ, and Kill Intracellular Bacteria. *PLoS Pathogens* **2008**; 4: 1-9.
103. Moody DB, Porcelli SA. Intracellular pathways of CD1 antigen presentation. *Nature Reviews Immunology* **2003**; 3: 11-22.
104. Zeng Z-H, Castaño AR, Segelke BW, Stura EA, Peterson PA, Wilson IA. Crystal Structure of Mouse CD1: An MHC-Like Fold with a Large Hydrophobic Binding Groove. *Science* **1997**; 277: 339-345.
105. Sieling P, Chatterjee D, Porcelli S, Prigozy T, Mazzaccaro R, Soriano T, Bloom B, Brenner M, Kronenberg M, Brennan P. CD1-restricted T cell recognition of microbial lipoglycan antigens. *Science* **1995**; 269: 227-230.
106. Ernst WA, Maher J, Cho S, Niazi KR, Chatterjee D, Moody DB, Besra GS, Watanabe Y, Jensen PE, Porcelli SA, Kronenberg M, Modlin RL. Molecular Interaction of CD1b with Lipoglycan Antigens. *Immunity* **1998**; 8: 331-340.
107. Fischer K, Scotet E, Niemeyer M, Koebernick H, Zerrahn J, Maillet S, Hurwitz R, Kursar M, Bonneville M, Kaufmann SHE, Schaible UE. Mycobacterial phosphatidylinositol mannoside is a natural antigen for CD1d-restricted T cells. *Proceedings of the National Academy of Sciences of the United States of America* **2004**; 101: 10685-10690.
108. To T, Stanojevic S, Moores G, Gershon A, Bateman E, Cruz A, Boulet L-P. Global asthma prevalence in adults: findings from the cross-sectional world health survey. *BMC Public Health* **2012**; 12: 204.
109. Larche M, Akdis CA, Valenta R. Immunological mechanisms of allergen-specific immunotherapy. *Nature Reviews Immunology* **2006**; 6: 761-771.
110. Barnes PJ. Immunology of asthma and chronic obstructive pulmonary disease. *Nature Reviews Immunology* **2008**; 8: 183-192.
111. Lukacs NW. Role of chemokines in the pathogenesis of asthma. *Nature Reviews Immunology* **2001**; 1: 108.
112. Wills-Karp M, Santeliz J, Karp CL. The germless theory of allergic disease: revisiting the hygiene hypothesis. *Nature Reviews Immunology* **2001**; 1: 69-75.
113. Del Prete G, Maggi E, Parronchi P, Chretien I, Tiri A, Macchia D, Ricci M, Banchereau J, De Vries J, Romagnani S. IL-4 is an essential factor for the IgE synthesis induced in vitro by human T cell clones and their supernatants. *Journal of Immunology* **1988**; 140: 4193-4198.
114. Wills-Karp M. Interleukin-13 in asthma pathogenesis. *Immunological Reviews* **2004**; 202: 175-190.
115. Takatsu K, Nakajima H. IL-5 and eosinophilia. *Current Opinion in Immunology* **2008**; 20: 288-294.
116. Strachan DP. Hay fever, hygiene, and household size. *British Medical Journal* **1989**; 299: 1259-1260.

117. Holgate ST, Polosa R. Treatment strategies for allergy and asthma. *Nature Reviews Immunology* **2008**; 8: 218-230.
118. Dahl R. Systemic side effects of inhaled corticosteroids in patients with asthma. *Respiratory Medicine* **2006**; 100: 1307-1317.
119. Valenta R, Niederberger V. Recombinant allergens for immunotherapy. *Journal of Allergy and Clinical Immunology* **2007**; 119: 826-830.
120. Pauli G, Larsen TH, Rak S, Horak F, Pastorello E, Valenta R, Purohit A, Arvidsson M, Kavina A, Schroeder JW, Mothes N, Spitzauer S, Montagut A, Galvain S, Melac M, André C, Poulsen LK, Malling H-J. Efficacy of recombinant birch pollen vaccine for the treatment of birch-allergic rhinoconjunctivitis. *Journal of Allergy and Clinical Immunology* **2008**; 122: 951-960.
121. Jutel M, Jaeger L, Suck R, Meyer H, Fiebig H, Cromwell O. Allergen-specific immunotherapy with recombinant grass pollen allergens. *Journal of Allergy and Clinical Immunology* **2005**; 116: 608-613.
122. Simon HU, Seelbach H, Ehmann R, Schmitz M. Original article Clinical and immunological effects of low-dose IFN-α treatment in patients with corticosteroid-resistant asthma. *Allergy* **2003**; 58: 1250-1255.
123. Bryan SA, O'Connor BJ, Matti S, Leckie MJ, Kanabar V, Khan J, Warrington SJ, Renzetti L, Rames A, Bock JA, Boyce MJ, Hansel TT, Holgate ST, Barnes PJ. Effects of recombinant human interleukin-12 on eosinophils, airway hyper-responsiveness, and the late asthmatic response. *The Lancet* **2000**; 356: 2149-2153.
124. Krieg AM. CpG motifs: the active ingredient in bacterial extracts? *Nature Medicine* **2003**; 9: 831-835.
125. Simons FER, Shikishima Y, Van Nest G, Eiden JJ, HayGlass KT. Selective immune redirection in humans with ragweed allergy by injecting Amb a 1 linked to immunostimulatory DNA. *Journal of Allergy and Clinical Immunology* **2004**; 113: 1144-1151.
126. Tulic MK, Fiset P-O, Christodoulopoulos P, Vaillancourt P, Desrosiers M, Lavigne F, Eiden J, Hamid Q. Amb a 1–immunostimulatory oligodeoxynucleotide conjugate immunotherapy decreases the nasal inflammatory response. *Journal of Allergy and Clinical Immunology* **2004**; 113: 235-241.
127. Creticos PS, Schroeder JT, Hamilton RG, Balcer-Whaley SL, Khattignavong AP, Lindblad R, Li H, Coffman R, Seyfert V, Eiden JJ, Broide D. Immunotherapy with a Ragweed–Toll-Like Receptor 9 Agonist Vaccine for Allergic Rhinitis. *New England Journal of Medicine* **2006**; 355: 1445-1455.
128. Klimek L, Willers J, Hammann-Haenni A, Pfaar O, Stocker H, Mueller P, Renner WA, Bachmann MF. Assessment of clinical efficacy of CYT003-QbG10 in patients with allergic rhinoconjunctivitis: a phase IIb study. *Clinical & Experimental Allergy* **2011**; 41: 1305-1312.
129. Shirakawa T, Enomoto T, Shimazu S-i, Hopkin JM. The Inverse Association Between Tuberculin Responses and Atopic Disorder. *Science* **1997**; 275: 77-79.
130. Strannegård IL, Larsson LO, Wennergren G, Strannegård Ö. Prevalence of allergy in children in relation to prior BCG vaccination and infection with atypical mycobacteria. *Allergy* **1998**; 53: 249-254.

131. Erb KJ, Holloway JW, Sobeck A, Moll H, Le Gros G. Infection of Mice with Mycobacterium bovis–Bacillus Calmette-Guérin (BCG) Suppresses Allergen-induced Airway Eosinophilia. *The Journal of Experimental Medicine* **1998**; 187: 561-569.
132. Herz U, Gerhold K, Grüber C, Braun A, Wahn U, Renz H, Paul K. BCG infection suppresses allergic sensitization and development of increased airway reactivity in an animal model. *Journal of Allergy and Clinical Immunology* **1998**; 102: 867-874.
133. Hopfenspirger MT, Agrawal DK. Airway Hyperresponsiveness, Late Allergic Response, and Eosinophilia Are Reversed with Mycobacterial Antigens in Ovalbumin-Presensitized Mice. *Journal of Immunology* **2002**; 168: 2516-2522.
134. Major Jr T, Wohlleben G, Reibetanz B, Erb KJ. Application of heat killed Mycobacterium bovis-BCG into the lung inhibits the development of allergen-induced Th2 responses. *Vaccine* **2002**; 20: 1532-1540.
135. Wang C-C, Rook GAW. Inhibition of an established allergic response to ovalbumin in BALB/c mice by killed Mycobacterium vaccae. *Immunology* **1998**; 93: 307-313.
136. Zuany-Amorim C, Sawicka E, Manlius C, Le Moine A., Brunet LR, Kemeny DM, Bowen G, Rook G, Walker C. Suppression of airway eosinophilia by killed Mycobacterium vaccae-induced allergen-specific regulatory T-cells. *Nature Medicine* **2002**; 8: 625-629.
137. Hansen G, Yeung VP, Berry G, Umetsu DT, DeKruyff RH. Vaccination with Heat-Killed Listeria as Adjuvant Reverses Established Allergen-Induced Airway Hyperreactivity and Inflammation: Role of CD8+ T Cells and IL-18. *Journal of Immunology* **2000**; 164: 223-230.
138. KuoLee R, Zhou H, Harris G, Zhao X, Qiu H, Patel GB, Chen W. Inhibition of airway eosinophilia and pulmonary pathology in a mouse model of allergic asthma by the live vaccine strain of Francisella tularensis. *Clinical & Experimental Allergy* **2008**; 38: 1003-1015.
139. Plotkin SA. Vaccines: past, present and future. *Nature Medicine* **2005**; 11: S5 - S11.
140. O'Hagan DT, De Gregorio E. The path to a successful vaccine adjuvant – 'The long and winding road'. *Drug Discovery Today* **2009**; 14: 541-551.
141. Huang DB, Wu JJ, Tyring SK. A review of licensed viral vaccines, some of their safety concerns, and the advances in the development of investigational viral vaccines. *Journal of Infection* **2004**; 49: 179-209.
142. Hilleman MR. Vaccines in historic evolution and perspective: a narrative of vaccine discoveries. *Vaccine* **2000**; 18: 1436-1447.
143. Perrie Y, Mohammed AR, Kirby DJ, McNeil SE, Bramwell VW. Vaccine adjuvant systems: Enhancing the efficacy of sub-unit protein antigens. *International Journal of Pharmaceutics* **2008**; 364: 272-280.
144. Hesseling AC, Marais BJ, Gie RP, Schaaf HS, Fine PEM, Godfrey-Faussett P, Beyers N. The risk of disseminated Bacille Calmette-Guerin (BCG) disease in HIV-infected children. *Vaccine* **2007**; 25: 14-18.
145. Marrack P, McKee AS, Munks MW. Towards an understanding of the adjuvant action of aluminium. *Nature Reviews Immunology* **2009**; 9: 287-293.

146. Morel S, Didierlaurent A, Bourguignon P, Delhaye S, Baras B, Jacob V, Planty C, Elouahabi A, Harvengt P, Carlsen H, Kielland A, Chomez P, Garçon N, Van Mechelen M. Adjuvant System AS03 containing α-tocopherol modulates innate immune response and leads to improved adaptive immunity. *Vaccine* **2011**; 29: 2461-2473.
147. O'Hagan DT. MF59 is a safe and potent vaccine adjuvant that enhances protection against influenza virus infection. *Expert review of vaccines* **2007**; 6: 699-710.
148. Baldridge JR, Cluff CW, Evans JT, Johnson DA, Lacy MJ, Persing DH. Enhancement of antigen-specific immunity via the TLR4 ligands MPL adjuvant and Ribi.529. *Expert Review of Vaccines* **2003**; 2: 219-229.
149. Holten-Andersen L, Doherty TM, Korsholm KS, Andersen P. Combination of the Cationic Surfactant Dimethyl Dioctadecyl Ammonium Bromide and Synthetic Mycobacterial Cord Factor as an Efficient Adjuvant for Tuberculosis Subunit Vaccines. *Infection and Immunity* **2004**; 72: 1608-1617.
150. Pulendran B, Ahmed R. Immunological mechanisms of vaccination. *Nature Immunology* **2011**; 12: 509-517.
151. Allison AC, Gregoriadis G. Liposomes as immunological adjuvants. *Nature* **1974**; 252: 252-252.
152. Morein B, Sundquist B, Hoglund S, Dalsgaard K, Osterhaus A. Iscom, a novel structure for antigenic presentation of membrane proteins from enveloped viruses. *Nature* **1984**; 308: 457-460.
153. Gupta RK, Relyveld EH, Lindblad EB, Bizzini B, Ben-Efraim S, Gupta CK. Adjuvants — a balance between toxicity and adjuvanticity. *Vaccine* **1993**; 11: 293-306.
154. Petrovsky N, Aguilar JC. Vaccine adjuvants: Current state and future trends. *Immunology & Cell Biology* **2004**; 82: 488-496.
155. Hawkins LD, Ishizaka ST. E6020: a synthetic Toll-like receptor 4 agonist as a vaccine adjuvant. *Expert Review of Vaccines* **2007**; 6: 773-784.
156. Mbow ML, De Gregorio E, Valiante NM, Rappuoli R. New adjuvants for human vaccines. *Current Opinion in Immunology* **2010**; 22: 411-416.
157. O'Hagan DT, MacKichan ML, Singh M. Recent developments in adjuvants for vaccines against infectious diseases. *Biomolecular Engineering* **2001**; 18: 69-85.
158. Reed SG, Bertholet S, Coler RN, Friede M. New horizons in adjuvants for vaccine development. *Trends in Immunology* **2009**; 30: 23-32.
159. Glenny AT, G. PC, Waddington H, Wallace U. The antigenic value of toxoid precipitated by potassium alum. *The Journal of Pathology and Bacteriology* **1926**; 29:
160. Clements CJ, Griffiths E. The global impact of vaccines containing aluminium adjuvants. *Vaccine* **2002**; 20, Supplement 3: S24-S33.
161. Eisenbarth SC, Colegio OR, O'Connor W, Sutterwala FS, Flavell RA. Crucial role for the Nalp3 inflammasome in the immunostimulatory properties of aluminium adjuvants. *Nature* **2008**; 453: 1122-1126.
162. Li H, Nookala S, Re F. Aluminum Hydroxide Adjuvants Activate Caspase-1 and Induce IL-1β and IL-18 Release. *Journal of Immunology* **2007**; 178: 5271-5276.
163. Kool M, Pétrilli V, De Smedt T, Rolaz A, Hammad H, van Nimwegen M, Bergen IM, Castillo R, Lambrecht BN, Tschopp J. Cutting Edge: Alum

Adjuvant Stimulates Inflammatory Dendritic Cells through Activation of the NALP3 Inflammasome. *Journal of Immunology* **2008**; 181: 3755-3759.

164. Franchi L, Núñez G. The Nlrp3 inflammasome is critical for aluminium hydroxide-mediated IL-1β secretion but dispensable for adjuvant activity. *European Journal of Immunology* **2008**; 38: 2085-2089.
165. Freund J, Cascals J, Hosmer EP. Sensitization and antibody formation after injection of tubercle bacilli and paraffin oil *Proceedings of the Society for Experimental Biology and Medicine* **1937**; 37: 509-513.
166. Degen WGJ, Jansen T, Schijns VEJC. Vaccine adjuvant technology: from mechanistic concepts to practical applications. *Expert Review of Vaccines* **2003**; 2: 327-335.
167. Salk JE, Laurent AM, Bailey ML. Direction of Research on Vaccination against Influenza-New Studies with Immunologic Adjuvants *American Journal of Public Health and the Nation's Health* **1951**; 41: 669-677.
168. Stuart-Harris CH. Adjuvant influenza vaccines. *Bulletin of the World Health Organization* **1969**; 41: 617-621.
169. Keefer MC, Graham BS, McElrath MJ, Matthews TJ, Stablein DM, Corey L, Wright PF, Lawrence D, Fast PE, Weinhold K, Hsieh RH, Chernoff D, Dekker C, Dolin R. Safety and immunogenicity of Env 2-3, a human immunodeficiency virus type 1 candidate vaccine, in combination with a novel adjuvant, MTP-PE/MF59. NIAID AIDS Vaccine Evaluation Group. *AIDS Research and Human Retroviruses* **1996**; 12: 683-693.
170. Keitel W, Couch R, Bond N, Adair S, Van Nest G, Dekker C. Pilot evaluation of influenza virus vaccine (IVV) combined with adjuvant. *Vaccine* **1993**; 11: 909-913.
171. Ott G, Barchfeld GL, Nest GV. Enhancement of humoral response against human influenza vaccine with the simple submicron oil/water emulsion adjuvant MF59. *Vaccine* **1995**; 13: 1557-1562.
172. Dupuis M, Denis-Mize K, LaBarbara A, Peters W, Charo IF, McDonald DM, Ott G. Immunization with the adjuvant MF59 induces macrophage trafficking and apoptosis. *European Journal of Immunology* **2001**; 31: 2910-2918.
173. Mosca F, Tritto E, Muzzi A, Monaci E, Bagnoli F, Iavarone C, O'Hagan D, Rappuoli R, De Gregorio E. Molecular and cellular signatures of human vaccine adjuvants. *Proceedings of the National Academy of Sciences* **2008**; 105: 10501-10506.
174. Dupuis M, Murphy TJ, Higgins D, Ugozzoli M, van Nest G, Ott G, McDonald DM. Dendritic Cells Internalize Vaccine Adjuvant after Intramuscular Injection. *Cellular Immunology* **1998**; 186: 18-27.
175. Aucouturier J, Ascarateil S, Dupuis L. The use of oil adjuvants in therapeutic vaccines. *Vaccine* **2006**; 24, Supplement 2: S44-S45.
176. Scalzo AA, Elliott SL, Cox J, Gardner J, Moss DJ, Suhrbier A. Induction of protective cytotoxic T cells to murine cytomegalovirus by using a nonapeptide and a human-compatible adjuvant (Montanide ISA 720). *Journal of Virology* **1995**; 69: 1306-1309.
177. Quintilio W, Kubrusly FS, Iourtov D, Miyaki C, Sakauchi MA, Lúcio F, de Cássia Dias S, Takata CS, Miyaji EN, Higashi HG, Leite LCC, Raw I. Bordetella

pertussis monophosphoryl lipid A as adjuvant for inactivated split virion influenza vaccine in mice. *Vaccine* **2009**; 27: 4219-4224.
178. Tapping RI, Akashi S, Miyake K, Godowski PJ, Tobias PS. Toll-Like Receptor 4, But Not Toll-Like Receptor 2, Is a Signaling Receptor for Escherichia and Salmonella Lipopolysaccharides. *Journal of Immunology* **2000**; 165: 5780-5787.
179. Mata-Haro V, Cekic C, Martin M, Chilton PM, Casella CR, Mitchell TC. The Vaccine Adjuvant Monophosphoryl Lipid A as a TRIF-Biased Agonist of TLR4. *Science* **2007**; 316: 1628-1632.
180. Didierlaurent AM, Morel S, Lockman L, Giannini SL, Bisteau M, Carlsen H, Kielland A, Vosters O, Vanderheyde N, Schiavetti F, Larocque D, Van Mechelen M, Garçon N. AS04, an Aluminum Salt- and TLR4 Agonist-Based Adjuvant System, Induces a Transient Localized Innate Immune Response Leading to Enhanced Adaptive Immunity. *Journal of Immunology* **2009**; 183: 6186-6197.
181. Harper DM. Currently approved prophylactic HPV vaccines. *Expert Review of Vaccines* **2009**; 8: 1663-1679.
182. Thoelen S, Van Damme P, Mathei C, Leroux-Roels G, Desombere I, Safary A, Vandepapeliere P, Slaoui M, Meheus A. Safety and immunogenicity of a hepatitis B vaccine formulated with a novel adjuvant system. *Vaccine* **1998**; 16: 708-714.
183. Bangham AD, Standish MM, Watkins JC. Diffusion of univalent ions across the lamellae of swollen phospholipids. *Journal of Molecular Biology* **1965**; 13: 238-252.
184. Gregoriadis G, Ryman BE. Fate of Protein-Containing Liposomes Injected into Rats. *European Journal of Biochemistry* **1972**; 24: 485-491.
185. New RRC. *Liposomes: a practical approach*, ed. Oxford: IRL Press, **1990**.
186. Gregoriadis G, Perrie Y. *Liposomes*. In eLS. Chichester: John Wiley & Sons, Ltd, http://www.els.net/WileyCDA/ElsArticle/refId-a0002656.html, **2010**.
187. Gregoriadis G. Drug entrapment in liposomes. *FEBS Letters* **1973**; 36: 292-296.
188. Gregoriadis G. Immunological adjuvants: a role for liposomes. *Immunology Today* **1990**; 11: 89-97.
189. Ulrich AS. Biophysical Aspects of Using Liposomes as Delivery Vehicles. *Bioscience Reports* **2002**; 22: 129-150.
190. Henriksen-Lacey M, Korsholm KS, Andersen P, Perrie Y, Christensen D. Liposomal vaccine delivery systems. *Expert Opinion on Drug Delivery* **2011**; 8: 505-519.
191. Gregoriadis G, Davis C. Stability of liposomes in vivo and in vitro is promoted by their cholesterol content and the presence of blood cells. *Biochemical and Biophysical Research Communications* **1979**; 89: 1287-1293.
192. Demel RA, De Kruyff B. The function of sterols in membranes. *Biochimica et Biophysica Acta (BBA) - Reviews on Biomembranes* **1976**; 457: 109-132.
193. Moghaddam B, Ali MH, Wilkhu J, Kirby DJ, Mohammed AR, Zheng Q, Perrie Y. The application of monolayer studies in the understanding of liposomal formulations. *International Journal of Pharmaceutics* **2011**; 417: 235-244.
194. Samad A, Sultana Y, Aqil M. Liposomal drug delivery systems: an update review. *Current Drug Delivery* **2007**; 4: 297-305.
195. Lian T, Ho RJY. Trends and developments in liposome drug delivery systems. *Journal of Pharmaceutical Sciences* **2001**; 90: 667-680.

196. Semple SC, Chonn A, Cullis PR. Interactions of liposomes and lipid-based carrier systems with blood proteins: Relation to clearance behaviour in vivo. *Advanced Drug Delivery Reviews* **1998**; 32: 3-17.
197. Brewer JM, Tetley L, Richmond J, Liew FY, Alexander J. Lipid Vesicle Size Determines the Th1 or Th2 Response to Entrapped Antigen. *Journal of Immunology* **1998**; 161: 4000-4007.
198. Gregoriadis G. Overview of liposomes. *Journal of Antimicrobial Chemotherapy* **1991**; 28: 39-48.
199. Gregoriadis G. *Liposome technology*, 3rd ed. New York: Informa Healthcare, **2006**.
200. Castile JD, Taylor KMG. Factors affecting the size distribution of liposomes produced by freeze–thaw extrusion. *International Journal of Pharmaceutics* **1999**; 188: 87-95.
201. Szoka F, Papahadjopoulos D. Procedure for preparation of liposomes with large internal aqueous space and high capture by reverse-phase evaporation. *Proceedings of the National Academy of Sciences* **1978**; 75: 4194-4198.
202. Olson F, Hunt CA, Szoka FC, Vail WJ, Papahadjopoulos D. Preparation of liposomes of defined size distribution by extrusion through polycarbonate membranes. *Biochimica et Biophysica Acta* **1979**; 557: 9-23.
203. Kirby C, Gregoriadis G. Dehydration-Rehydration Vesicles: A Simple Method for High Yield Drug Entrapment in Liposomes. *Nature Biotechnology* **1984**; 2: 979-984.
204. Langer R. New methods of drug delivery. *Science* **1990**; 249: 1527-1533.
205. Park YS. Tumor-Directed Targeting of Liposomes. *Bioscience Reports* **2002**; 22: 267-281.
206. White KL, Rades T, Furneaux RH, Tyler PC, Hook S. Mannosylated liposomes as antigen delivery vehicles for targeting to dendritic cells. *Journal of Pharmacy and Pharmacology* **2006**; 58: 729-737.
207. Foged C, Arigita C, Sundblad A, Jiskoot W, Storm G, Frokjaer S. Interaction of dendritic cells with antigen-containing liposomes: effect of bilayer composition. *Vaccine* **2004**; 22: 1903-1913.
208. Moser C, Metcalfe IC, Viret J-F. Virosomal adjuvanted antigen delivery systems. *Expert Review of Vaccines* **2003**; 2: 189-196.
209. Christensen D, Korsholm KS, Andersen P, Agger EM. Cationic liposomes as vaccine adjuvants. *Expert Review of Vaccines* **2007**; 10: 513-521.
210. Christensen D, Agger EM, Andreasen LV, Kirby D, Andersen P, Perrie Y. Liposome-based cationic adjuvant formulations (CAF): Past, present, and future. *Journal of Liposome Research* **2009**; 19: 2-11.
211. Davidsen J, Rosenkrands I, Christensen D, Vangala A, Kirby D, Perrie Y, Agger EM, Andersen P. Characterization of cationic liposomes based on dimethyldioctadecylammonium and synthetic cord factor from M. tuberculosis (trehalose 6,6′-dibehenate)—A novel adjuvant inducing both strong CMI and antibody responses. *Biochimica et Biophysica Acta (BBA) - Biomembranes* **2005**; 1718: 22-31.
212. Press JB, Reynolds RC, May RD, Marciani DJ. *Structure/function relationships of immunostimulating saponins*. In Studies in Natural Products Chemistry, pp. 131-174: Elsevier, **2000**.

213. Sun H-X, Xie Y, Ye Y-P. Advances in saponin-based adjuvants. *Vaccine* **2009**; 27: 1787-1796.
214. Sjölander A, Drane D, Maraskovsky E, Scheerlinck J-P, Suhrbier A, Tennent J, Pearse M. Immune responses to ISCOM® formulations in animal and primate models. *Vaccine* **2001**; 19: 2661-2665.
215. Schellack C, Prinz K, Egyed A, Fritz JH, Wittmann B, Ginzler M, Swatosch G, Zauner W, Kast C, Akira S, von Gabain A, Buschle M, Lingnau K. IC31, a novel adjuvant signaling via TLR9, induces potent cellular and humoral immune responses. *Vaccine* **2006**; 24: 5461-5472.
216. Fritz JH, Brunner S, Birnstiel ML, Buschle M, Gabain Av, Mattner F, Zauner W. The artificial antimicrobial peptide KLKLLLLLKLK induces predominantly a TH2-type immune response to co-injected antigens. *Vaccine* **2004**; 22: 3274-3284.
217. Hemmi H, Takeuchi O, Kawai T, Kaisho T, Sato S, Sanjo H, Matsumoto M, Hoshino K, Wagner H, Takeda K, Akira S. A Toll-like receptor recognizes bacterial DNA. *Nature* **2000**; 408: 740-745.
218. Agger EM, Rosenkrands I, Olsen AW, Hatch G, Williams A, Kritsch C, Lingnau K, von Gabain A, Andersen CS, Korsholm KS, Andersen P. Protective immunity to tuberculosis with Ag85B-ESAT-6 in a synthetic cationic adjuvant system IC31. *Vaccine* **2006**; 24: 5452-5460.
219. van Dissel JT, Arend SM, Prins C, Bang P, Tingskov PN, Lingnau K, Nouta J, Klein MR, Rosenkrands I, Ottenhoff THM, Kromann I, Doherty TM, Andersen P. Ag85B–ESAT-6 adjuvanted with IC31® promotes strong and long-lived Mycobacterium tuberculosis specific T cell responses in naïve human volunteers. *Vaccine* **2010**; 28: 3571-3581.
220. Werninghaus K, Babiak A, Groß O, Hölscher C, Dietrich H, Agger EM, Mages J, Mocsai A, Schoenen H, Finger K, Nimmerjahn F, Brown GD, Kirschning C, Heit A, Andersen P, Wagner H, Ruland J, Lang R. Adjuvanticity of a synthetic cord factor analogue for subunit Mycobacterium tuberculosis vaccination requires FcRγ–Syk–Card9–dependent innate immune activation. *The Journal of Experimental Medicine* **2009**; 206: 89-97.
221. Andersen CAS, Rosenkrands I, Olsen AW, Nordly P, Christensen D, Lang R, Kirschning C, Gomes JM, Bhowruth V, Minnikin DE, Besra GS, Follmann F, Andersen P, Agger EM. Novel Generation Mycobacterial Adjuvant Based on Liposome-Encapsulated Monomycoloyl Glycerol from Mycobacterium bovis Bacillus Calmette-Guérin. *Journal of Immunology* **2009**; 183: 2294-2302.
222. Bhowruth V, Minnikin DE, Agger EM, Andersen P, Bramwell VW, Perrie Y, Besra GS. Adjuvant properties of a simplified C32 monomycolyl glycerol analogue. *Bioorganic & Medicinal Chemistry Letters* **2009**; 19: 2029-2032.
223. Nordly P, Korsholm KS, Pedersen EA, Khilji TS, Franzyk H, Jorgensen L, Nielsen HM, Agger EM, Foged C. Incorporation of a synthetic mycobacterial monomycoloyl glycerol analogue stabilizes dimethyldioctadecylammonium liposomes and potentiates their adjuvant effect in vivo. *European Journal of Pharmaceutics and Biopharmaceutics* **2011**; 77: 89-98.
224. Ainge GD, Parlane NA, Denis M, Hayman CM, Larsen DS, Painter GF. Phosphatidylinositol mannosides: Synthesis and adjuvant properties of phosphatidylinositol di- and tetramannosides. *Bioorganic & Medicinal Chemistry* **2006**; 14: 7615-7624.

225. Sprott GD, Dicaire CJ, Gurnani K, Sad S, Krishnan L. Activation of Dendritic Cells by Liposomes Prepared from Phosphatidylinositol Mannosides from Mycobacterium bovis Bacillus Calmette-Guérin and Adjuvant Activity In Vivo. *Infection and Immunity* **2004**; 72: 5235-5246.
226. Parlane NA, Compton BJ, Hayman CM, Painter GF, Basaraba RJ, Heiser A, Buddle BM. Phosphatidylinositol di-mannoside and derivates modulate the immune response to and efficacy of a tuberculosis protein vaccine against Mycobacterium bovis infection. *Vaccine* **2012**; 30: 580-588.
227. Ainge GD, Hudson J, Larsen DS, Painter GF, Gill GS, Harper JL. Phosphatidylinositol mannosides: Synthesis and suppression of allergic airway disease. *Bioorganic & Medicinal Chemistry* **2006**; 14: 5632-5642.
228. Boonyarattanakalin S, Liu XY, Michieletti M, Lepenies B, Seeberger PH. Chemical Synthesis of All Phosphatidylinositol Mannoside (PIM) Glycans from Mycobacterium tuberculosis. *Journal of the American Chemical Society* **2008**; 130: 16791-16799.
229. Dyer BS, Jones JD, Ainge GD, Denis M, Larsen DS, Painter GF. Synthesis and Structure of Phosphatidylinositol Dimannoside. *The Journal of Organic Chemistry* **2007**; 72: 3282-3288.
230. Elie CJJ, Dreef CE, Verduyn R, Van Der Marel GA, Van Boom JH. Synthesis of 1-O-(1,2-Di-O-palmitoyl-SN-glycero-3-phosphoryl)-2-O-α-D-mannopyranosyl-D-MYO-inositol: a fragment of mycobacterial phospholipids. *Tetrahedron* **1989**; 45: 3477-3486.
231. Pietrusiewicz KM, Salamończyk GM, Bruzik KS, Wieczorek W. The synthesis of homochiral inositol phosphates from myo-inositol. *Tetrahedron* **1992**; 48: 5523-5542.
232. Lindberg J, Öhberg L, Garegg PJ, Konradsson P. Efficient routes to glucosamine-myo-inositol derivatives, key building blocks in the synthesis of glycosylphosphatidylinositol anchor substances. *Tetrahedron* **2002**; 58: 1387-1398.
233. Wewers W, Gillandt H, Schmidt Traub H. Advances in analysis and synthesis of myo-inositol-derivatives through resolution by crystallisation. *Tetrahedron: Asymmetry* **2005**; 16: 1723-1728.
234. Bender SL, Budhu RJ. Biomimetic synthesis of enantiomerically pure D-myo-inositol derivatives. *Journal of the American Chemical Society* **1991**; 113: 9883-9885.
235. Singh-Gill G, Larsen DS, Jones JD, Severn WB, Harper JL. **2005**, *Patent No. European Patent Number WO 2005049631*.
236. Sayers I, Severn W, Scanga CB, Hudson J, Le Gros G, Harper JL. Suppression of allergic airway disease using mycobacterial lipoglycans. *Journal of Allergy and Clinical Immunology* **2004**; 114: 302-309.
237. Yamazaki F, Sato S, Nukada T, Ito Y, Ogawa T. Synthesis of α-d-Manp-(1→3)-[β-d-GlcpNAc-(1→4)]-[α-d-Manp-(1→6)]-β-d-Manp-(1→4)-β-d-GlcpNAc-(1→4)-[α-l-Fucp-(1→6)]-d-GlcpNAc, a core glycoheptaose of a "bisected" complex-type glycan of glycoproteins. *Carbohydrate Research* **1990**; 201: 31-50.
238. Sowden JC, Fischer HOL. Optically Active α,β-Diglycerides. *Journal of the American Chemical Society* **1941**; 63: 3244-3248.

239. Schmidt RR. Facile Synthesis of α- and β-O-Glycosyl Imidates; Preparation of Glycosides and Disaccharides. *Angewandte Chemie International Edition* **1980**; 19: 731-732.
240. Galonic DP, Gin DY. Chemical glycosylation in the synthesis of glycoconjugate antitumour vaccines. *Nature* **2007**; 446: 1000-1007.
241. Podlasek CA, Wu J, Stripe WA, Bondo PB, Serianni AS. [13C]Enriched Methyl Aldopyranosides: Structural Interpretations of 13C-1H Spin-Coupling Constants and 1H Chemical Shifts. *Journal of the American Chemical Society* **1995**; 117: 8635-8644.
242. Nifantyev EE, Predvoditelev DA, Fursenko IV, Smirnova LI. Synthesis of Alkyl Carboxylates by Acylation of Acetals. *Synthesis* **1982**; 1982: 132,134.
243. Ainge GD. *The synthesis of phosphatidylinositol mannans and their analogues* Thesis submitted for Doctor of Philosophy, University of Otago, Dunedin, New Zealand, **2008**.
244. Johns MK, Yin M-X, Conway SJ, Robinson DEJE, Wong LSM, Bamert R, Wettenhall REH, Holmes AB. Synthesis and biological evaluation of a novel cardiolipin affinity matrix. *Organic & Biomolecular Chemistry* **2009**; 7: 3691-3697.
245. Sawada T, Shirai R, Iwasaki S. Efficient asymmetric synthesis of phosphatidyl-D-myo-inositol 3,4,5-trisphosphate. *Chemical and Pharmaceutical Bulletin* **1997**; 45: 1521-1523.
246. Dreef CE, Schiebler W, van der Marel GA, van Boom JH. Synthesis of 5-phosphonate analogues of myo-inositol 1,4,5-trisphosphate: possible intracellular calcium antagonists. *Tetrahedron Letters* **1991**; 32: 6021-6024.
247. Jayaprakash KN, Lu J, Fraser-Reid B. Synthesis of a key Mycobacterium tuberculosis biosynthetic phosphoinositide intermediate. *Bioorganic & Medicinal Chemistry Letters* **2004**; 14: 3815-3819.
248. Harper JL, Hayman CM, Larsen DS, Painter GF, Singh-Gill G. A PIM_2 analogue suppresses allergic airway disease. *Bioorganic & Medicinal Chemistry* **2011**; 19: 917-925.
249. Franklin B, Brownrigg W, Farish M. Of the Stilling of Waves by means of Oil. Extracted from Sundry Letters between Benjamin Franklin, LL. D. F. R. S. William Brownrigg, M. D. F. R. S. and the Reverend Mr. Farish. *Philosophical Transactions* **1774**; 64: 445-460.
250. Pockels A. Surface tension [4]. *Nature* **1891**; 43: 437-439.
251. Rayleigh L. XXXVI. Investigations in Capillarity:—The size of drops.—The liberation of gas from supersaturated solutions.—Colliding jets.—The tension of contaminated water-surfaces. *Philosophical Magazine Series 5* **1899**; 48: 321-337.
252. Langmuir I. The constitution and fundamental properties of solids and liquids. II. Liquids. *Journal of the American Chemical Society* **1917**; 39: 1848-1906.
253. Dynarowicz-Latka P, Dhanabalan A, Oliveira ON. Modern physicochemical research on Langmuir monolayers. *Advances in Colloid and Interface Science* **2001**; 91: 221-293.
254. Erbil HY. *Surface Chemistry of Solid and Liquid Interfaces*, ed. Oxford Blackwell Publishing Ltd., **2006**.
255. Dynarowicz-Latka P, Kita K. Molecular interaction in mixed monolayers at the air/water interface. *Advances in Colloid and Interface Science* **1999**; 79: 1-17.

256. Brezesinski G, Möhwald H. Langmuir monolayers to study interactions at model membrane surfaces. *Advances in Colloid and Interface Science* **2003**; 100–102: 563-584.
257. Miñones J, Rodríguez Patino JM, Conde O, Carrera C, Seoane R. The effect of polar groups on structural characteristics of phospholipid monolayers spread at the air-water interface. *Colloids and Surfaces A: Physicochemical and Engineering Aspects* **2002**; 203: 273-286.
258. Ali S, Smaby JM, Momsen MM, Brockman HL, Brown RE. Acyl Chain-Length Asymmetry Alters the Interfacial Elastic Interactions of Phosphatidylcholines. *Biophysical Journal* **1998**; 74: 338-348.
259. Phillips MC, Chapman D. Monolayer characteristics of saturated 1,2-diacyl phosphatidylcholines (lecithins) and phosphatidylethanolamines at the air-water interface. *Biochimica et Biophysica Acta (BBA) - Biomembranes* **1968**; 163: 301-313.
260. Möhwald H. Phospholipid and Phospholipid-Protein Monolayers at the Air/Water Interface. *Annual Review of Physical Chemistry* **1990**; 41: 441-476.
261. McConnell HM. Structures and Transitions in Lipid Monolayers at the Air-Water Interface. *Annual Review of Physical Chemistry* **1991**; 42: 171-195.
262. von Tscharner V, McConnell HM. An alternative view of phospholipid phase behavior at the air-water interface. Microscope and film balance studies. *Biophysical Journal* **1981**; 36: 409-419.
263. Cordoba J, Jackson SM, Jones MN. Mixed monolayers of phosphatidylinositol and dipalmitoylphosphatidylcholine and their interaction with liposomes. *Colloids and Surfaces* **1990**; 46: 85-94.
264. DeWolf C, Leporatti S, Kirsch C, Klinger R, Brezesinski G. Phase separation in phosphatidylinositol/phosphatidylcholine mixed monolayers. *Chemistry and Physics of Lipids* **1999**; 97: 129-138.
265. Mansour H, Wang D-S, Chen C-S, Zografi G. Comparison of Bilayer and Monolayer Properties of Phospholipid Systems Containing Dipalmitoylphosphatidylglycerol and Dipalmitoylphosphatidylinositol. *Langmuir* **2001**; 17: 6622-6632.
266. Patil-Sen Y, Tiddy GJT, Brezesinski G, DeWolf C. A monolayer phase behaviour study of phosphatidylinositol, phosphatidylinositol 4-monophosphate and their binary mixtures with distearoylphosphatidylethanolamine. *Physical Chemistry Chemical Physics* **2004**; 6: 1562-1565.
267. Hasegawa T, Nishijo J, Watanabe M, Funayama K, Imae T. Conformational Characterization of α-Mycolic Acid in a Monolayer Film by the Langmuir−Blodgett Technique and Atomic Force Microscopy. *Langmuir* **2000**; 16: 7325-7330.
268. Hasegawa T, Leblanc RM. Aggregation properties of mycolic acid molecules in monolayer films: a comparative study of compounds from various acid-fast bacterial species. *Biochimica et Biophysica Acta (BBA) - Biomembranes* **2003**; 1617: 89-95.
269. Hasegawa T, Nishijo J, Watanabe M, Umemura J, Ma Y, Sui G, Huo Q, Leblac RM. Characteristics of long-chain fatty acid monolayers studied by infrared external-reflection spectroscopy. *Langmuir* **2002**; 18: 4758-4764.

270. Zhang Z, Pen Y, Edyvean RG, Banwart SA, Dalgliesh RM, Geoghegan M. Adhesive and conformational behaviour of mycolic acid monolayers. *Biochimica et Biophysica Acta (BBA) - Biomembranes* **2010**; 1798: 1829-1839.
271. Villeneuve M, Kawai M, Kanashima H, Watanabe M, Minnikin DE, Nakahara H. Temperature dependence of the Langmuir monolayer packing of mycolic acids from Mycobacterium tuberculosis. *Biochimica et Biophysica Acta (BBA) - Biomembranes* **2005**; 1715: 71-80.
272. Demel RA, Geurts van Kessel WSM, van Deenen LLM. The properties of polyunsaturated lecithins in monolayers and liposomes and the interactions of these lecithins with cholesterol. *Biochimica et Biophysica Acta (BBA) - Biomembranes* **1972**; 266: 26-40.
273. Kita-Tokarczyk K, Junginger M, Belegrinou S, Taubert A. Amphiphilic polymers at interfaces. *Advances in Polymer Science* **2011**; 242: 151-201.
274. Dennison SR, Harris F, Phoenix DA. A Langmuir approach using monolayer interactions to investigate surface active peptides. *Protein and Peptide Letters* **2010**; 17: 1363-1375.
275. Schwarz G, Taylor SE. Thermodynamic Analysis of the Surface Activity Exhibited by a Largely Hydrophobic Peptide. *Langmuir* **1995**; 11: 4341-4346.
276. Haefele T, Kita-Tokarczyk K, Meier W. Phase Behavior of Mixed Langmuir Monolayers from Amphiphilic Block Copolymers and an Antimicrobial Peptide. *Langmuir* **2005**; 22: 1164-1172.
277. Pakalns T, L. Haverstick K, Fields GB, McCarthy JB, L. Mooradian D, Tirrell M. Cellular recognition of synthetic peptide amphiphiles in self-assembled monolayer films. *Biomaterials* **1999**; 20: 2265-2279.
278. Schenning APHJ, Elissen-Román C, Weener JW, Baars MWPL, Van Der Gaast SJ, Meijer EW. Amphiphilic dendrimers as building blocks in supramolecular assemblies. *Journal of the American Chemical Society* **1998**; 120: 8199-8208.
279. Tao A, Kim F, Hess C, Goldberger J, He R, Sun Y, Xia Y, Yang P. Langmuir−Blodgett Silver Nanowire Monolayers for Molecular Sensing Using Surface-Enhanced Raman Spectroscopy. *Nano Letters* **2003**; 3: 1229-1233.
280. Yun H, Choi Y-W, Kim NJ, Sohn D. Physicochemical Properties of Phosphatidylcholine (PC) Monolayers with Different Alkyl Chains, at the Air/Water Interface. *Bulletin of the Korean Chemical Society* **2002**; 24: 377-383.
281. Mattjus P, Hedström G, Slotte JP. Monolayer interaction of cholesterol with phosphatidylcholines: effects of phospholipid acyl chain length. *Chemistry and Physics of Lipids* **1994**; 74: 195-203.
282. Kim S-R, Choi S-A, Kim J-D. The monolayer behavior and transfer characteristics of phospholipids at the air/water interface. *Korean Journal of Chemical Engineering* **1996**; 13: 46-53.
283. Bouffioux O, Berquand A, Eeman M, Paquot M, Dufrêne YF, Brasseur R, Deleu M. Molecular organization of surfactin-phospholipid monolayers: Effect of phospholipid chain length and polar head. *Biochimica et Biophysica Acta (BBA) - Biomembranes* **2007**; 1768: 1758-1768.
284. Dynarowicz-Latka P, Hac-Wydro K. Interactions between phosphatidylcholines and cholesterol in monolayers at the air/water interface. *Colloids and Surfaces B: Biointerfaces* **2004**; 37: 21-25.

285. Möhwald H. Direct characterization of monolayers at the air-water interface. *Thin Solid Films* **1988**; 159: 1-15.
286. Anders M, Chi LF, Fuchs H, Johnston RR, Ringsdorf H. Domain structures in Langmuir-Blodgett films investigated by atomic force microscopy. *Science* **1993**; 259: 213-216.
287. Binnig G, Quate CF, Gerber C. Atomic Force Microscope. *Physical Review Letters* **1986**; 56: 930-933.
288. Hoenig D, Moebius D. Direct visualization of monolayers at the air-water interface by Brewster angle microscopy. *The Journal of Physical Chemistry* **1991**; 95: 4590-4592.
289. Hénon S, Meunier J. Microscope at the Brewster angle: Direct observation of first-order phase transitions in monolayers. *Review of Scientific Instruments* **1991**; 62: 936-939.
290. Israelachvili JN. *Intermolecular and surface forces* 2nd ed. London; San Diego Academic Press, **1991**.
291. Kauzmann W. Some factors in the interpretation of protein denaturation. *Advances in Protein Chemistry* **1959**; 14: 1-63.
292. Israelachvili JN, Mitchell DJ, Ninham BW. Theory of self-assembly of hydrocarbon amphiphiles into micelles and bilayers. *Journal of the Chemical Society, Faraday Transactions 2* **1976**; 72: 1525-1568.
293. Barratt G, Tenu J-P, Yapo A, Petit J-F. Preparation and characterisation of liposomes containing mannosylated phospholipids capable of targetting drugs to macrophages. *Biochimica et Biophysica Acta (BBA) - Biomembranes* **1986**; 862: 153-164.
294. Tenu JP, Sekkai D, Yapo A, Petit JF, Lemaire G. Phosphatidylinositolmannoside-Based Liposomes Induce No Synthase in Primed Mouse Peritoneal-Macrophages. *Biochemical and Biophysical Research Communications* **1995**; 208: 295-301.
295. Flynn JL, Chan J. Immunology of Tuberculosis. *Annual Review of Immunology* **2001**; 19: 93-129.
296. Geisel RE, Sakamoto K, Russell DG, Rhoades ER. In vivo activity of released cell wall lipids of Mycobacterium bovis bacillus Calmette-Guérin is due principally to trehalose mycolates. *Journal of Immunology* **2005**; 174: 5007-5015.
297. Trinchieri G, Sher A. Cooperation of Toll-like receptor signals in innate immune defence. *Nature Reviews Immunology* **2007**; 7: 179-190.
298. Akbari O, Stock P, DeKruyff RH, Umetsu DT. Role of regulatory T cells in allergy and asthma. *Current Opinion in Immunology* **2003**; 15: 627-633.
299. Zuany-Amorim C, Hailé S, Leduc D, Dumarey C, Huerre M, Vargaftig BB, Pretolani M. Interleukin-10 inhibits antigen-induced cellular recruitment into the airways of sensitized mice. *The Journal of Clinical Investigation* **1995**; 95: 2644-2651.
300. Front S, Court N, Bourigault ML, Rose S, Ryffel B, Erard F, Quesniaux VFJ, Martin OR. Phosphatidyl myo-inositol mannosides mimics built on an acyclic or heterocyclic core: Synthesis and anti-inflammatory properties. *ChemMedChem* **2011**; 6: 2081-2093.
301. Bos MA, Nylander T. Interaction between Î²-Lactoglobulin and Phospholipids at the Air/Water Interface. *Langmuir* **1996**; 12: 2791-2797.

302. Martin P, Szablewski M. *Langmuir-Blodgett Troughs Operating Manual*, 6th ed. Coventry: Nima Technology Ltd, **2002**.
303. Hunter RJ. *Electrophoresis and electro-osmosis measurements*. In Introduction to Modern Colloid Science, pp. 241-249. London: Oxford University Press Inc., **1993**.
304. Barnden MJ, Allison J, Heath WR, Carbone FR. Defective TCR expression in transgenic mice constructed using cDNA-based α- and β-chain genes under the control of heterologous regulatory elements. *Immunology & Cell Biology* **1998**; 76: 34-40.
305. Hogquist KA, Jameson SC, Heath WR, Howard JL, Bevan MJ, Carbone FR. T cell receptor antagonist peptides induce positive selection. *Cell* **1994**; 76: 17-27.
306. Hook S, Prout M, Camberis M, Konig M, Zimmer A, Van Heeke G, Le Gros G. Th2-dependent airway eosinophilia is regulated by preproenkephalin. *Journal of Neuroimmunology* **2000**; 107: 59-65.
307. Colqui Quiroga MV, Monzón LMA, Yudi LM. Interaction of triflupromazine with distearoylphosphatidylglycerol films studied by surface pressure isotherms and cyclic voltammetry at a 1,2-dichloroethane/water interface. *Electrochimica Acta* **2010**; 55: 5840-5846.
308. Davies JT, Rideal EK. *Interfacial phenomena*, 2nd ed. New York Academic Press, **1963**.
309. Brown R, Brockman H. Using Monomolecular Films to Characterize Lipid Lateral Interactions. *Methods in Molecular Biology* **2007**; 398: 41-58.
310. Hac-Wydro K, Wydro P, Jagoda A, Kapusta J. The study on the interaction between phytosterols and phospholipids in model membranes. *Chemistry and Physics of Lipids* **2007**; 150: 22-34.
311. Maniti O, Cheniour M, Marcillat O, Vial C, Granjon T. Morphology modifications in negatively charged lipid monolayers upon mitochondrial creatine kinase binding. *Molecular Membrane Biology* **2009**; 26: 171-185.
312. Leblanc RM. Molecular recognition at Langmuir monolayers. *Current Opinion in Chemical Biology* **2006**; 10: 529-536.
313. Court N, Rose S, Bourigault M-L, Front S, Martin OR, Dowling JK, Kenny EF, O'Neill L, Erard F, Quesniaux VFJ. Mycobacterial PIMs Inhibit Host Inflammatory Responses through CD14-Dependent and CD14-Independent Mechanisms. *PLoS ONE* **2011**; 6: e24631.
314. Ahsan F, Rivas IP, Khan MA, Torres Suárez AI. Targeting to macrophages: role of physicochemical properties of particulate carriers—liposomes and microspheres—on the phagocytosis by macrophages. *Journal of Controlled Release* **2002**; 79: 29-40.
315. Walsh ER, August A. Eosinophils and allergic airway disease: there is more to the story. *Trends in Immunology* **2010**; 31: 39-44.
316. Li Q, Ding X, Thomas JJ, Harding CV, Pecora ND, Ziady AG, Shank S, Boom WH, Lancioni CL, Rojas RE. Rv2468c, a novel Mycobacterium tuberculosis protein that costimulates human CD4+ T cells through VLA-5. *Journal of Leukocyte Biology* **2012**; 91: 311-320.
317. Lancioni CL, Li Q, Thomas JJ, Ding X, Thiel B, Drage MG, Pecora ND, Ziady AG, Shank S, Harding CV, Boom WH, Rojas RE. Mycobacterium tuberculosis

Lipoproteins Directly Regulate Human Memory CD4+ T Cell Activation via Toll-Like Receptors 1 and 2. *Infection and Immunity* **2011**; 79: 663-673.
318. Gaines GL. *Insoluble monolayers at liquid-gas interfaces / by George L. Gaines*, ed. New York Interscience Publishers, **1966**.
319. Maget-Dana R, Ptak M. Interactions of surfactin with membrane models. *Biophysical Journal* **1995**; 68: 1937-1943.
320. Gálvez Ruiz MJ, Cabrerizo Vilchez MA. A study of the miscibility of bile components in mixed monolayers at the air-liquid interface I. Cholesterol, lecithin, and lithocholic acid. *Colloid & Polymer Science* **1991**; 269: 77-84.
321. Costin IS, Barnes GT. Two-component monolayers. II. Surface pressure-area relations for the octadecanol-docosyl sulphate system. *Journal of Colloid and Interface Science* **1975**; 51: 106-121.
322. Demel RA, Van Deenen LLM, Pethica BA. Monolayer interactions of phospholipids and cholesterol. *Biochimica et Biophysica Acta (BBA) - Biomembranes* **1967**; 135: 11-19.
323. Chapman D, Owens NF, Phillips MC, Walker DA. Mixed monolayers of phospholipids and cholesterol. *Biochimica et Biophysica Acta (BBA) - Biomembranes* **1969**; 183: 458-465.
324. Smaby JM, Brockman HL, Brown RE. Cholesterol's Interfacial Interactions with Sphingomyelins and-Phosphatidylcholines: Hydrocarbon Chain Structure Determines the Magnitude of Condensation. *Biochemistry* **1994**; 33: 9135-9142.
325. Ali S, Smaby JM, Brockman HL, Brown RE. Cholesterol's interfacial interactions with galactosylceramides. *Biochemistry* **1994**; 33: 2900-2906.
326. Smaby JM, Kulkarni VS, Momsen M, Brown RE. The interfacial elastic packing interactions of galactosylceramides, sphingomyelins, and phosphatidylcholines. *Biophysical Journal* **1996**; 70 868-877.
327. Maggio B, Lucy JA. Studies on Mixed Monolayers of Phospholipids and Fusogenic Lipids. *Biochem. J.* **1975**; 149: 597-608.
328. Rojas E, Tobias JM. Membrane model: Association of inorganic cations with phospholipid monolayers. *Biochimica et Biophysica Acta (BBA) - Biophysics including Photosynthesis* **1965**; 94: 394-404.
329. Crisp DJ. *Surface Chemistry*, ed. London: Butterworth, **1949**.
330. Seoane R, Miñones J, Conde O, Casas M, Iribarnegaray E. Thermodynamic and Brewster Angle Microscopy Studies of Fatty Acid/Cholesterol Mixtures at the Air/Water Interface. *The Journal of Physical Chemistry B* **2000**; 104: 7735-7744.
331. Durand E, Welby M, Laneelle G, Tocanne J-F. Phase Behavior of Cord Factor and Related Bacterial Glycolipid Toxins. *European Journal of Biochemistry* **1979**; 93: 103-112.
332. Chimote G, Banerjee R. Lung surfactant dysfunction in tuberculosis: Effect of mycobacterial tubercular lipids on dipalmitoylphosphatidylcholine surface activity. *Colloids and Surfaces B: Biointerfaces* **2005**; 45: 215-223.
333. Chimote G, Banerjee R. Effect of mycolic acid on surface activity of binary surfactant lipid monolayers. *Journal of Colloid and Interface Science* **2008**; 328: 288-298.
334. Pénzes CB, Schnöller D, Horváti K, Bősze S, Mező G, Kiss É. Membrane affinity of antituberculotic drug conjugate using lipid monolayer containing mycolic

acid. *Colloids and Surfaces A: Physicochemical and Engineering Aspects* **2012**; In Press: Corrected Proof.

335. Ah-Fat NMW, Craig DQM, Taylor KMG. An investigation into the effects of surfactants on phospholipid monolayers using a Langmuir-Blodgett film balance. *International Journal of Pharmaceutics* **1994**; 107: 239-242.
336. Chou T-H, Chu IM, Chang C-H. Interaction of paclitaxel with DSPC in monolayers at the air/water interface at different temperatures. *Colloids and Surfaces B: Biointerfaces* **2002**; 25: 147-155.
337. Zhao L, Feng S-S. Effects of lipid chain length on molecular interactions between paclitaxel and phospholipid within model biomembranes. *Journal of Colloid and Interface Science* **2004**; 274: 55-68.
338. Ti Tien H, Ottova-Leitmannova A. *Membrane Biophysics: As Viewed from Experimental Bilayer Lipid Membranes (Planar Lipid Bilayers and Spherical Liposomes)*, 1st ed. Amsterdam Elsevier Science B.V., **2000**.
339. Vemuri S, Rhodes CT. Preparation and characterization of liposomes as therapeutic delivery systems: a review. *Pharmaceutica Acta Helvetiae* **1995**; 70: 95-111.
340. Rosenkrands I., Agger E. M., Olsen A. W., Korsholm K. S., Swtman Andersen C., Jensen K. T., P. A. Cationic Liposomes Containing Mycobacterial Lipids: a New Powerful Th1 Adjuvant System. *Infection and Immunity* **2005**; 73: 5817–5826.
341. Parlane NA, Denis M, Severn WB, Skinner MA, Painter GF, La Flamme AC, Ainge GD, Larsen DS, Buddle BM. Phosphatidylinositol Mannosides are Efficient Mucosal Adjuvants. *Immunological Investigations* **2008**; 37: 129-142.
342. Wedlock DN, Denis M, Painter GF, Ainge GD, Vordermeier HM, Hewinson RG, Buddle BM. Enhanced protection against bovine tuberculosis after coadministration of Mycobacterium bovis BCG with a mycobacterial protein vaccine-adjuvant combination but not after coadministration of adjuvant alone. *Clinical and Vaccine Immunology* **2008**; 15: 765-772.
343. Ainge GD, Parlane NA, Denis M, Dyer BS, Härer A, Hayman CM, Larsen DS, Painter GF. Phosphatidylinositol Mannoside Ether Analogues: Syntheses and Interleukin-12-Inducing Properties. *The Journal of Organic Chemistry* **2007**; 72: 5291-5296.
344. Denis M, Ainge GD, Larsen DS, Severn WB, Painter GF. A synthetic analogue of phosphatidylinositol mannoside is an efficient adjuvant. *Immunopharmacology and Immunotoxicology* **2009**; 31: 577-582.
345. Koennings S, Copland MJ, Davies NM, Rades T. A method for the incorporation of ovalbumin into immune stimulating complexes prepared by the hydration method. *International Journal of Pharmaceutics* **2002**; 241: 385-389.
346. Brittain HG. *Physical characterization of pharmaceutical solids*, ed. New York: M. Dekker, **1995**.
347. Engel A, Chatterjee SK, Al-Arifi A, Nuhn P. Influence of spacer length on the agglutination of glycolipid-incorporated liposomes by ConA as model membrane. *Journal of Pharmaceutical Sciences* **2003**; 92: 2229-2235.
348. Mabrey S, Sturtevant JM. Investigation of phase transitions of lipids and lipid mixtures by sensitivity differential scanning calorimetry. *Proceedings of the National Academy of Sciences* **1976**; 73: 3862-3866.

349. Jacobson K, Papahadjopoulos D. Phase transitions and phase separations in phospholipid membranes induced by changes in temperature, pH, and concentration of bivalent cations. *Biochemistry* **1975**; 14: 152-161.
350. Orr GA, Rando RR, Bangerter FW. Synthetic glycolipids and the lectin-mediated aggregation of liposomes. *J. Biol. Chem.* **1979**; 254: 4721-4725.
351. Rando RR, Bangerter FW. Threshold effects on the lectin-mediated aggregation of synthetic glycolipid-containing liposomes. *Journal of Supramolecular Structure* **1979**; 11: 295-309.
352. Vyas SP, Sihorkar V, Jain S. Mannosylated liposomes for bio-film targeting. *International Journal of Pharmaceutics* **2007**; 330: 6-13.
353. Torosian G, Lemberger AP. Surface films of soybean lecithin II. Interactions between lecithin and lipid substances in mixed monomolecular films. *Journal of Pharmaceutical Sciences* **1968**; 57: 17-22.
354. Maggio B, Cumar FA, Caputto R. Interactions of gangliosides with phospholipids and glycosphingolipids in mixed monolayers. *Biochemical Journal* **1978**; 175: 1113-1118.
355. Phillips MC, Joos P. The collapse pressures and miscibilities of mixed insoluble monolayers. *Colloid & Polymer Science* **1970**; 238: 499-505.
356. Chou T-H, Lin Y-S, Li W-T, Chang C-H. Phase behavior and morphology of equimolar mixed cationic-anionic surfactant monolayers at the air/water interface: Isotherm and Brewster angle microscopy analysis. *Journal of Colloid and Interface Science* **2008**; 321: 384-392.
357. Gonçalves da Silva AM, Viseu MI. Synergism in mixed monolayers of cationic and anionic surfactants: A thermodynamic analysis of miscibility at the air-water interface. *Colloids and Surfaces A: Physicochemical and Engineering Aspects* **1998**; 144: 191-200.
358. Nordly P, Agger E, Andersen P, Nielsen H, Foged C. Incorporation of the TLR4 Agonist Monophosphoryl Lipid A Into the Bilayer of DDA/TDB Liposomes: Physico-Chemical Characterization and Induction of CD8+ T-Cell Responses In Vivo. *Pharmaceutical Research* **2011**; 28: 553-562.
359. Copland MJ, Baird MA, Rades T, McKenzie JL, Becker B, Reck F, Tyler PC, Davies NM. Liposomal delivery of antigen to human dendritic cells. *Vaccine* **2003**; 21: 883-890.
360. Yamauchi H, Takao Y, Abe M, Ogino K. Molecular interactions between lipid and some steroids in a monolayer and a bilayer. *Langmuir* **1993**; 9: 300-304.
361. Christensen D, Kirby D, Foged C, Agger EM, Andersen P, Perrie Y, Nielsen HM. α,α'-trehalose 6,6′-dibehenate in non-phospholipid-based liposomes enables direct interaction with trehalose, offering stability during freeze-drying. *Biochimica et Biophysica Acta (BBA) - Biomembranes* **2008**; 1778: 1365-1373.
362. Engering A, Geijtenbeek TBH, Van Vliet SJ, Wijers M, Van Liempt E, Demaurex N, Lanzavecchia A, Fransen J, Figdor CG, Piguet V, Van Kooyk Y. The dendritic cell-specific adhesion receptor DC-SIGN internalizes antigen for presentation to T cells. *Journal of Immunology* **2002**; 168: 2118-2126.
363. Akira S, Takeda K, Kaisho T. Toll-like receptors: critical proteins linking innate and acquired immunity. *Nature Immunology* **2001**; 2: 675-680.
364. EMULSIGEN® (Oil-in-Water Emulsified Adjuvant) Technical Bulletin, 7th September 2012 from http://www.mvplabs.com/copy/adjuvant/Emulsigen.pdf

365. Pimm MV, Baldwin RW, Polonsky J, Lederer E. Immunotherapy of an ascitic rat hepatoma with cord factor (trehalose-6,6′-dimycolate) and synthetic analogues. *International Journal of Cancer* **1979**; 24: 780-785.
366. Yarkoni E, Rapp HJ, Polonsky J, Lederer E. Immunotherapy with an intralesionally administered synthetic cord factor analogue. *International Journal of Cancer* **1978**; 22: 564-569.
367. Russell DG. Mycobacterium tuberculosis: here today, and here tomorrow. *Nature Reviews Molecular Cell Biology* **2001**; 2: 569-586.
368. Brennan PJ, Nikaido H. The Envelope of Mycobacteria. *Annual Review of Biochemistry* **1995**; 64: 29-63.
369. Kawano T, Cui J, Koezuka Y, Toura I, Kaneko Y, Motoki K, Ueno H, Nakagawa R, Sato H, Kondo E, Koseki H, Taniguchi M. CD1d-Restricted and TCR-Mediated Activation of Vα14 NKT Cells by Glycosylceramides. *Science* **1997**; 278: 1626-1629.
370. Kaer LV. α-Galactosylceramide therapy for autoimmune diseases: prospects and obstacles. *Nature Reviews Immunology* **2005**; 5: 31-42.
371. Brossay L, Naidenko O, Burdin N, Matsuda J, Sakai T, Kronenberg M. Cutting Edge: Structural Requirements for Galactosylceramide Recognition by CD1-Restricted NK T Cells. *Journal of Immunology* **1998**; 161: 5124-5128.
372. Koike Y, Yoo YC, Mitobe M, Oka T, Okuma K, Tono-oka S, Azuma I. Enhancing activity of mycobacterial cell-derived adjuvants on immunogenicity of recombinant human hepatitis B virus vaccine. *Vaccine* **1998**; 16: 1982-1989.
373. Matsunaga I, Moody DB. Mincle is a long sought receptor for mycobacterial cord factor. *The Journal of Experimental Medicine* **2009**; 206: 2865-2868.
374. Marciani DJ. Vaccine adjuvants: role and mechanisms of action in vaccine immunogenicity. *Drug Discovery Today* **2003**; 8: 934-943.
375. Datta SK, Cho HJ, Takabayashi K, Horner AA, Raz E. Antigen–immunostimulatory oligonucleotide conjugates: mechanisms and applications. *Immunological Reviews* **2004**; 199: 217-226.

7 Appendices

7.1 Appendix A

Solutions used in this thesis

Formulation and physicochemical characterisation

10 mM Hydroxyethyl piperazineethanesulfonic acid (HEPES) buffer

Hydroxyethyl piperazineethanesulfonic acid	0.24 g
Milli-Q water to	100 mL
Adjust pH to 7.5	

10 mM HEPES buffer containing 1 mM $CaCl_2$ and $MnCl_2$

(A) Prepare stock solution in Milli-Q water

Calcium chloride dihydrate	1.47 g
Manganese chloride tetrahydrate	1.98 g
Milli-Q water to	100 mL

(B) Dilute stock solution 1:100 in 10 mM HEPES buffer

Phosphate Buffered Saline (PBS) containing 5% (w/v) Triton-X 100

Triton-X 100	5.0 g
PBS	100 mL
Adjust pH to 7.5	

Preparation of fluorescently-labelled model antigen (FITC-OVA)

220 mM Carbonate buffer

Sodium carbonate (Na_2CO_3)	2.65 g
Sodium hydrogen carbonate ($NaHCO_3$)	2.1 g
Milli-Q water to	100 mL
Adjust pH to 9.5	

Cell culture work

Alseviers Solution

Dextrose (D-Glucose)	20.5 g
Sodium chloride (NaCl)	4.2 g
Sodium citrate ($Na_3C_6H_5O_7$)	8.0 g
Milli-Q water to	1000 mL

Lysis Buffer

(A) 0.16 M Ammonium chloride (NH_4Cl) solution

Ammonium chloride	8.29 g
Milli-Q water to	1000 mL
Adjust pH to 7.4	

(B) 0.17 M Tris hydrochloride (Tris-HCl) solution

Tris-HCl	20.6 g
Milli-Q water to	1000 mL
Adjust pH to 7.65	

Mix 9 parts of solution A with 1 part of solution B, filter sterilise through a 0.22 μm filter prior to use.

Fluorescence-activated cell sorting (FACS) buffer

Sodium azide (NaN_3)	0.1 g
Bovine serum albumin (BSA)	10.0 g
PBS (pH 7.5) to	1000 mL

Complete Iscove's Modified Dulbecco's Medium (cIMDM)

Penicillin/Streptomycin solution	10.0 mL
2-mercaptoethanol	1.0 mL
Foetal calf serum (FCS)	50.0 mL
Glutamax	10.0 mL
IMDM to	1000 mL

Ovalbumin enzyme-linked immunosorbent assays (OVA ELISAs)

0.1 M Carbonate-bicarbonate buffer (coating buffer)

Sodium carbonate (Na_2CO_3)	0.318 g
Sodium hydrogen carbonate ($NaHCO_3$)	0.586 g
Milli-Q water to	200 mL

Adjust pH to 9.6

(This buffer was also for coating of plates for *in vitro* T cell restimulation)

Wash buffer

Tween 20	0.5 mL
PBS to	1000 mL

Adjust pH to 7.4

Blocking buffer

Bovine serum albumin (BSA)	4.0 g
PBS to	200 mL
Adjust pH to 7.4	

Assay buffer

Bovine serum albumin (BSA)	1.0 g
Wash buffer to	200 mL
Adjust pH to 7.4	

7.2 Appendix B

Optimisation of the Langmuir trough technique using a model phospholipid

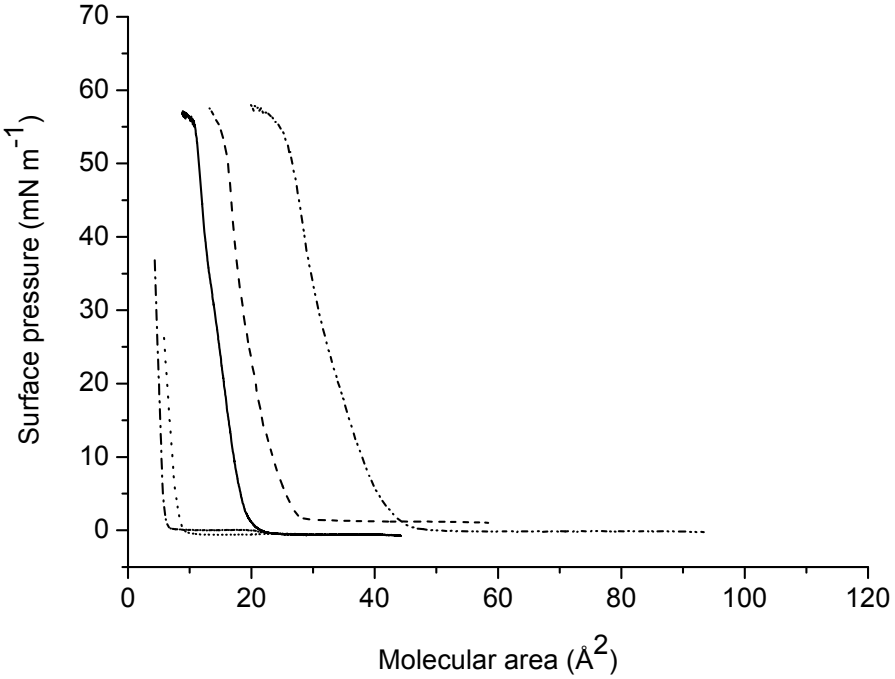


Figure B-1. Effect of lipid concentration on DSPG monolayer formation at the air/water interface: Lipid stock solutions were prepared at concentrations of 1.0 mg mL^{-1} (**-··**), 0.84 mg mL^{-1} (1.0 mM) (**···**) and 0.5 mg mL^{-1} (**—**). A volume of 50 μL was spread on sub-phase. To further investigate the effect of the applied volume, two additional volumes of DSPG stock solution (0.5 mg mL^{-1}) were applied on sub-phase: 40 μL (**---**), 25 μL (**··**). All lipid solutions were prepared in chloroform. Lipid monolayers were compressed at constant barrier speed (5 cm^2 min^{-1}).

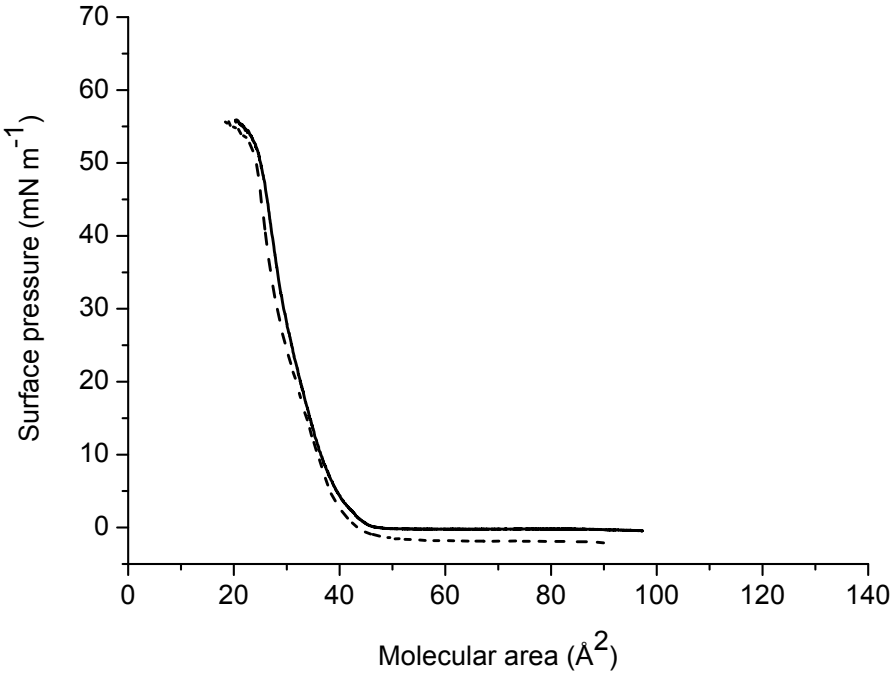


Figure B-2. Monolayer compression of DSPG at the air/water interface: Lipid solutions (0.5 mg mL^{-1}) were prepared in either chloroform (**—**) or chloroform/methanol (4:1, v/v) (**---**). In all experiments 25 μL were deposited onto water surface and the isotherms were recorded at constant compression rate (5 cm^2 min^{-1}). The curves are each a representative of three independent experiments.

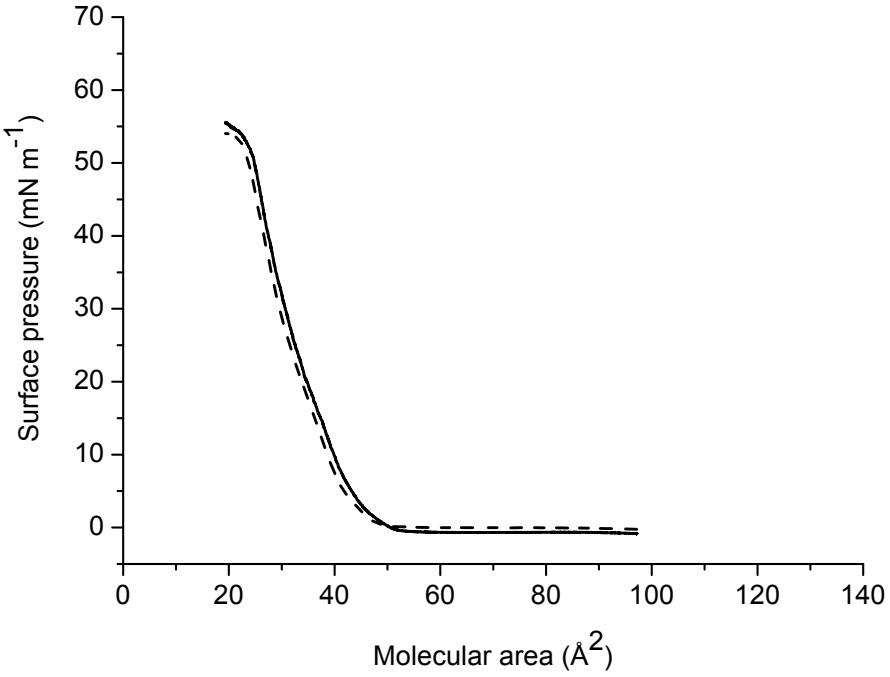


Figure B-3. Effect of compression rate on DSPG monolayer formation: DSPG molecules (0.5 mg mL^{-1} in chloroform) were compressed at a barrier speed of 5 cm^2 min^{-1} (**—**) or 10 cm^2 min^{-1} (**---**). A volume of 25 μL was applied in all experiments. The curves are each a representative of three independent measurements.

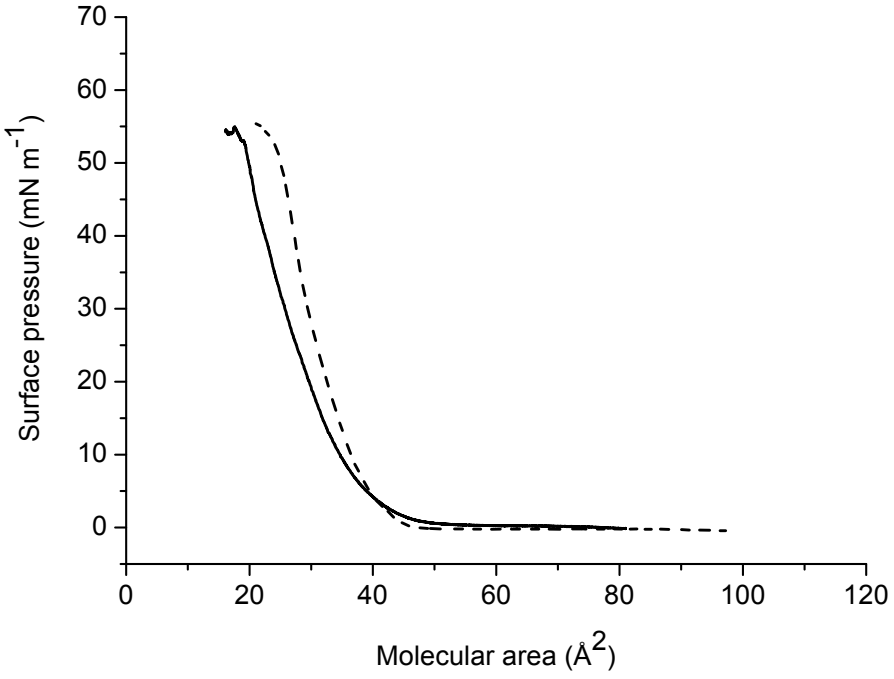


Figure B-4. Monolayer compression of DSPG at the air/liquid interface: A volume of 25 μL of DSPG in chloroform (5 mg mL^{-1}) was spread onto different sub-phases. π-A isotherms compressed (barrier speed 5 cm^2 min^{-1}) on Milli-Q water (**---**) or PBS buffer, pH 7.4 (**—**). The curves are each a representative of three independent measurements.

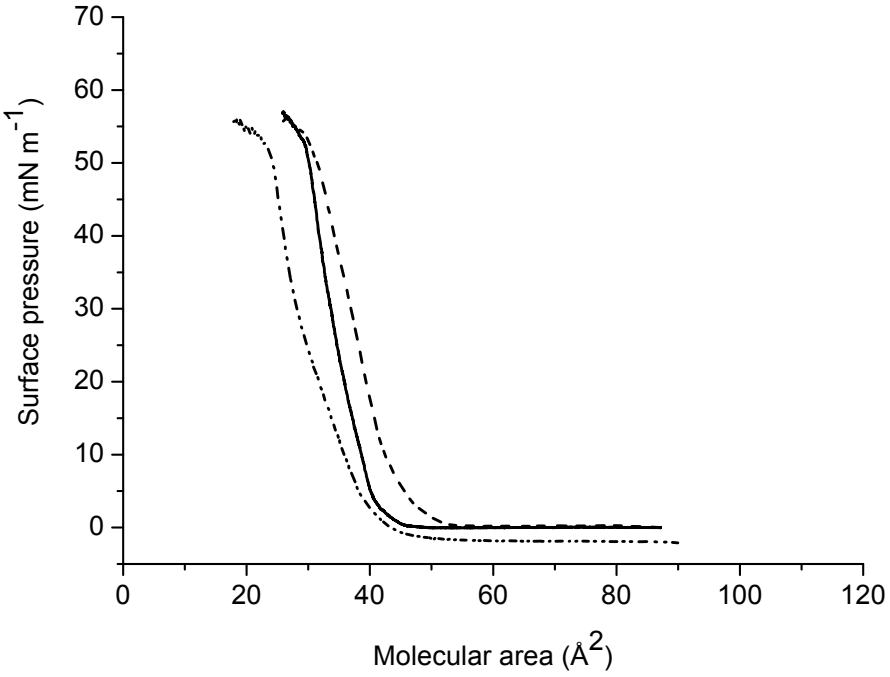


Figure B-5. Reproducibility of DSPG monolayer compression: Lipid films were compressed at a rate of 5 cm^2 min^{-1}. DSPG was dissolved at 0.5 mg mL^{-1} in chloroform and a volume of 25 μL was added on Milli-Q water sub-phase. Each π-A isotherm is a representative of a triplicate which was measured in independent experiments.

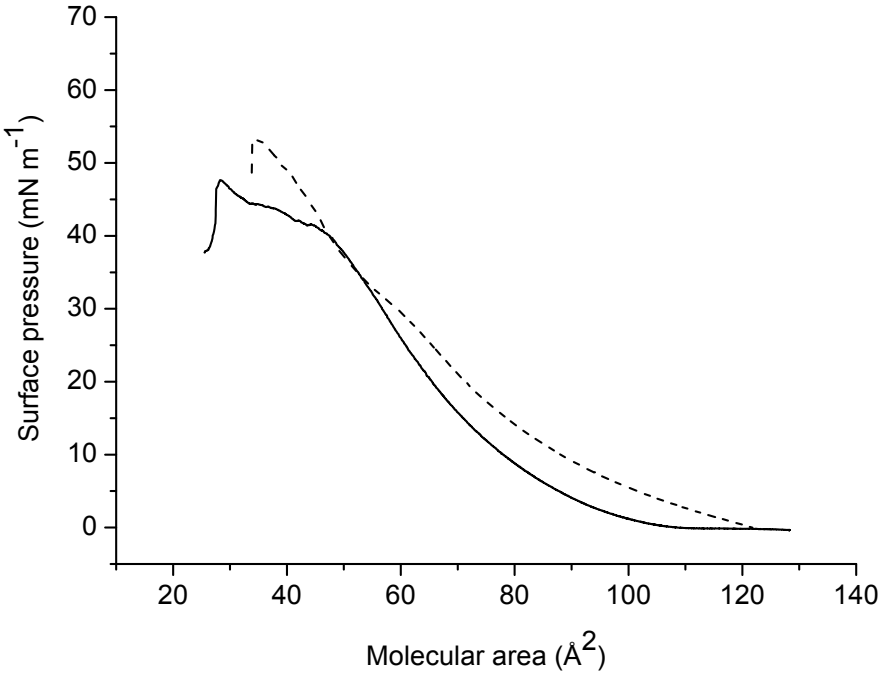


Figure B-6. Effect of head group on monolayer formation: π-A isotherms of PIM_2 (16:16) (**---**) and PGM_2 (16:16) (**—**) at the air/water interface. The curves are each a representative of three independent experiments.

7.3 Appendix C

In vitro liposome immunogenicity - Formulation uptake and DC activation

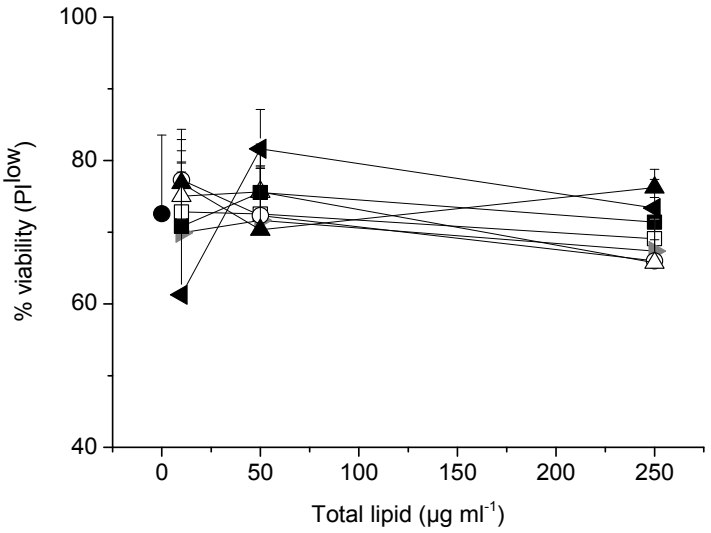


Figure C-1. Viability of BMDC after incubation (37°C for 48 hours) with different amounts of total lipid of PC PIM_2 (16:16) (□), PC PIM_2 (18:18) (►), PC PGM_2 (0:0) (○), PC PGM_2 (10:10) (▲), PC PGM_2 (16:16) (Δ), PC PGM_2 (18:18) (◄) and PC (■). Cells were stained with propidium iodide (PI) to exclude dead cell. Data represent mean of three independent experiments + SD.

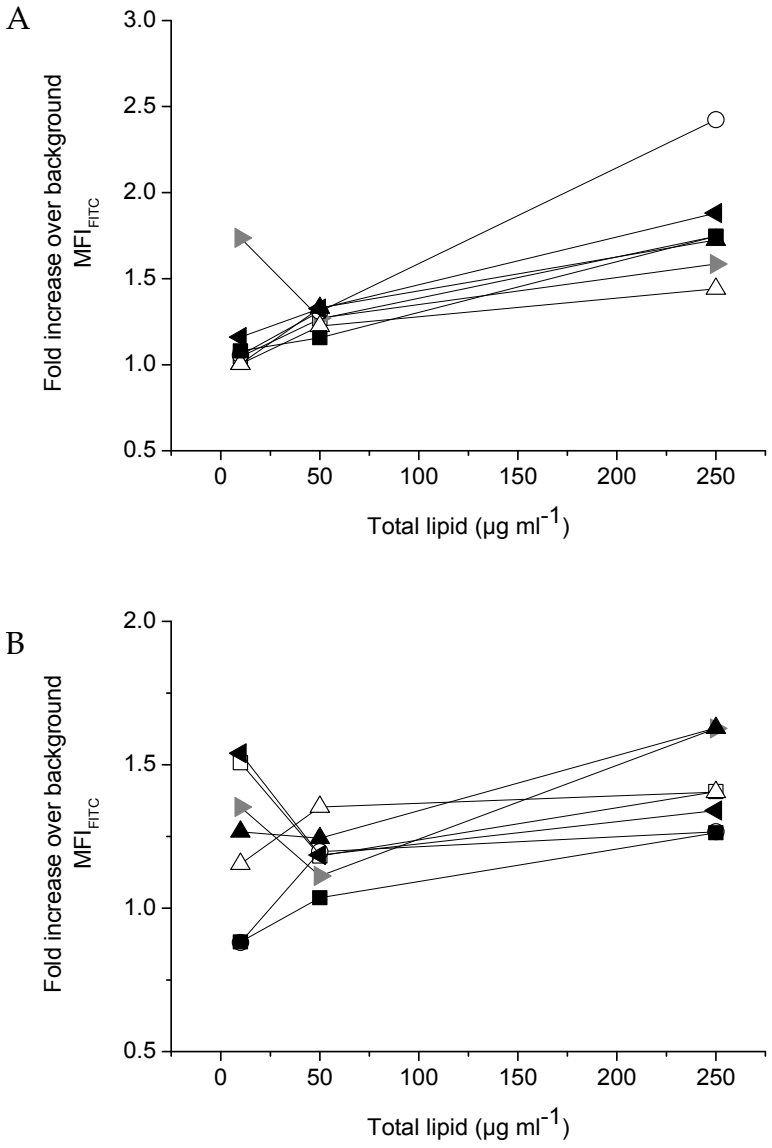


Figure C-2. Uptake of FITC-OVA containing liposome formulations by BMDC *in vitro*. BMDC were pulsed at 37°C for 48 hours with different amounts of total lipid of PC PIM_2 (16:16) (□), PC PIM_2 (18:18) (►), PC PGM_2 (0:0) (○), PC PGM_2 (10:10) (▲), PC PGM_2 (16:16) (Δ), PC PGM_2 (18:18) (◄) and PC (■). Results are expressed as fold increase of CD11c-positive cells incubated with liposomes over CD11c-positive cells pulsed with media (background). The data shows representative results for **(A)** experiment 2 and **(B)** experiment 3.

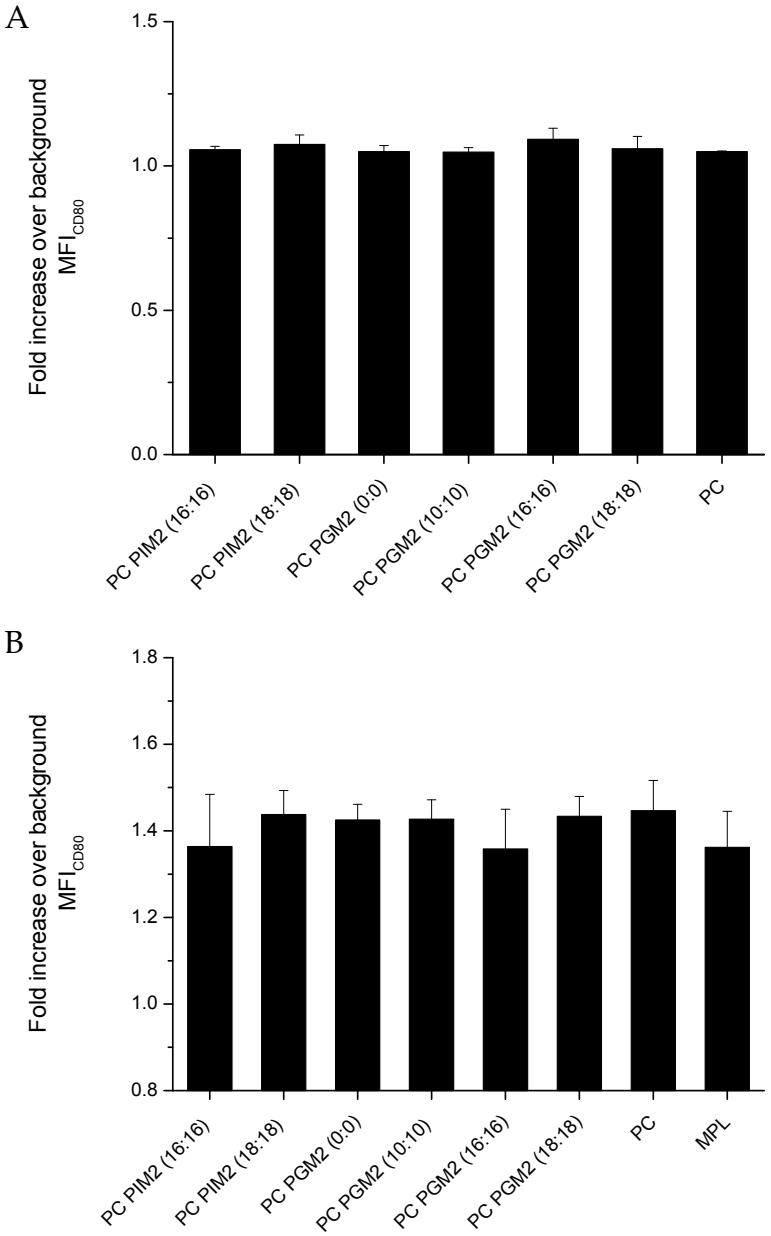


Figure C-3. Expression of BMDC surface activation marker CD80 following *in vitro* incubation with various formulations at 37°C for 48 hours. **(A)** BMDC were incubated with FITC-OVA containing liposome formulations (250 μg mL^{-1} total lipid). **(B)** BMDC were pulsed with FITC-OVA containing liposome formulations (250 μg mL^{-1} total lipid) + MPL (10 ng mL^{-1}) and MPL (10 ng mL^{-1}). Results are expressed as fold increase of CD11c-positive cells incubated with various formulations over CD11c-positive cells pulsed with media (background). Data represent mean of three independent experiments + SD.

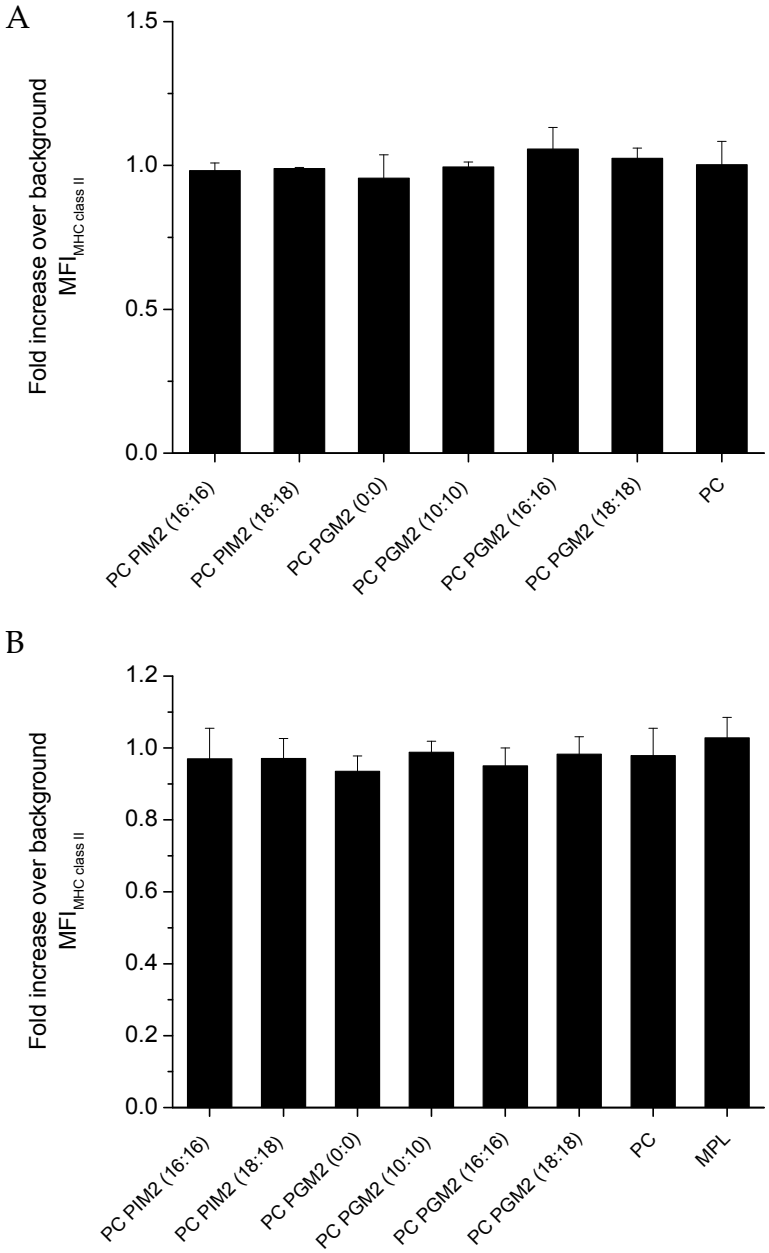


Figure C-4. Expression of BMDC surface activation marker MHC class II following *in vitro* incubation with various formulations at 37°C for 48 hours. **(A)** BMDC were incubated with FITC-OVA containing liposome formulations (250 μg mL^{-1} total lipid). **(B)** BMDC were pulsed with FITC-OVA containing liposome formulations (250 μg mL^{-1} total lipid) + MPL (10 ng mL^{-1}) and MPL (10 ng mL^{-1}). Results are expressed as fold increase of CD11c-positive cells incubated with various formulations over CD11c-positive cells pulsed with media (background). Data represent mean of three independent experiments + SD.

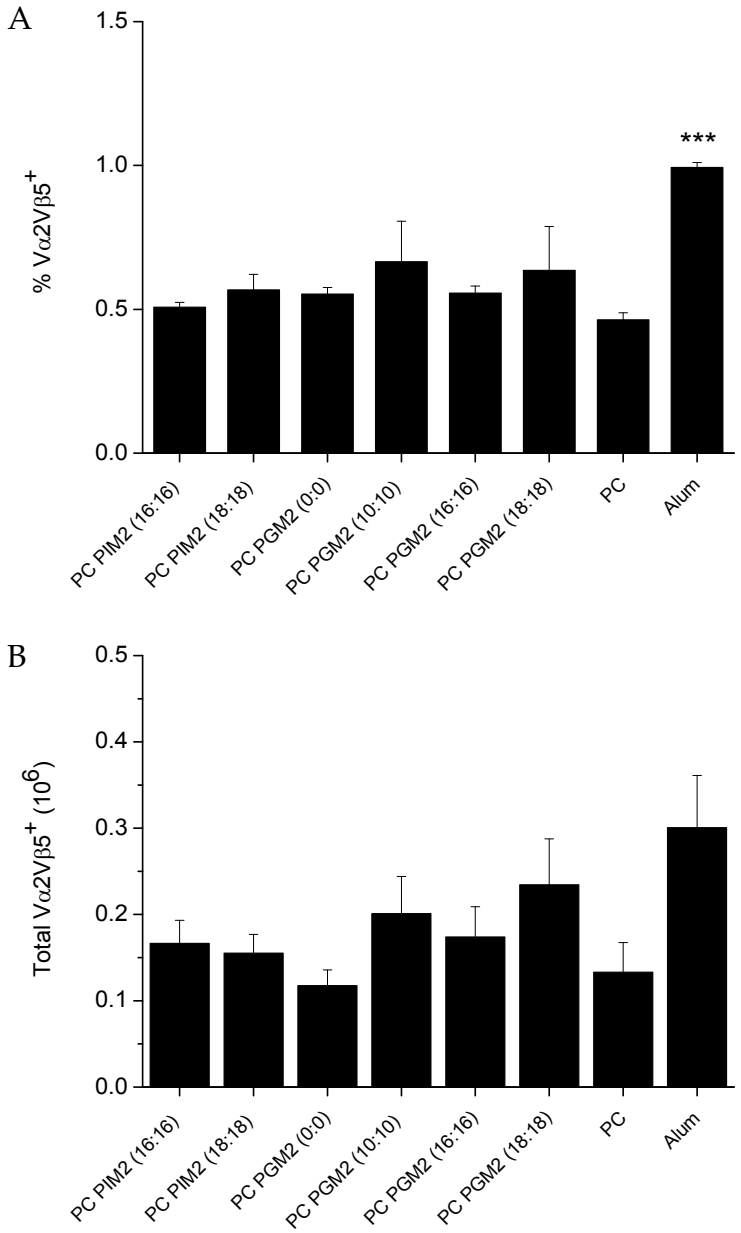


Figure C-5. OVA-specific expansion of Vα2Vβ5 T cells. **(A)** Percent and **(B)** total number of $CD4^+$ Vα2Vβ5 T cells in spleens. Spleens were pooled within each vaccination group. Graphs depict mean + SE from n=3 mice per group from three independent experiments.

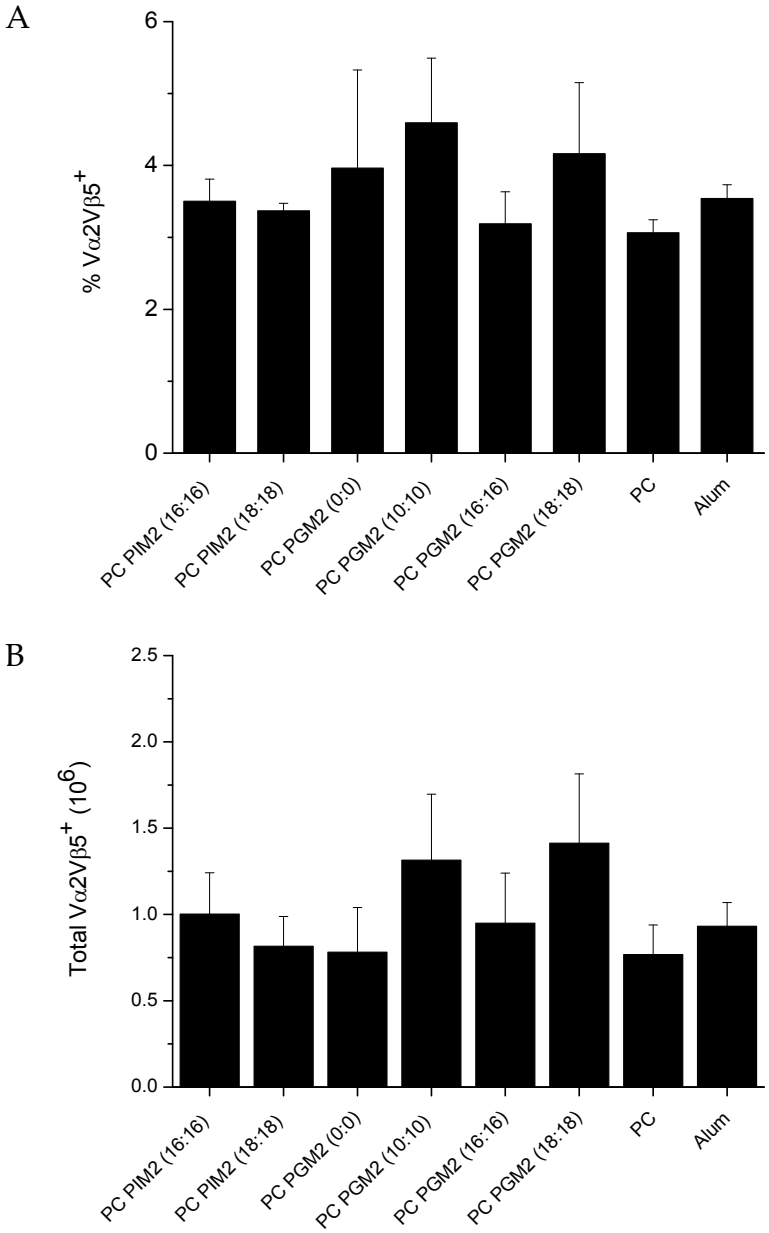


Figure C-6. OVA-specific expansion of Vα2Vβ5 T cells. **(A)** Percent and **(B)** total number of $CD8^+$ Vα2Vβ5 T cells in spleens. Spleens were pooled within each vaccination group. Graphs depict mean + SE from n=3 mice per group from three independent experiments.

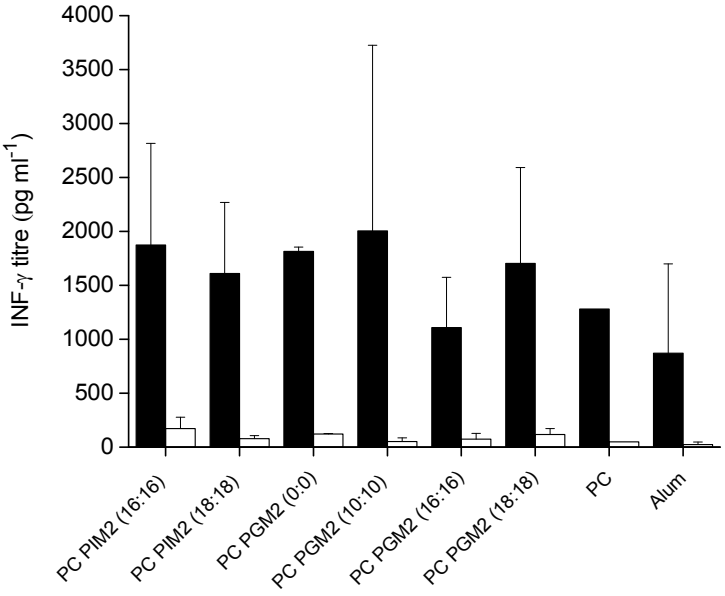


Figure C-7. Production of IFN-γ by T-cells isolated from spleen samples of each study group. Spleens were pooled within each vaccination group. Titres of cytokine responses were determined after *in vitro* restimulation with OVA (black bars) or medium (white bars, negative control). Bars depict mean + SE from n=3 mice per group from three independent experiments.